5-2015

Early host response and immune signaling to 2009 pandemic influenza A (H1N1) viruses in primary cell culture models.

Rachael Lask Gerlach
University of Louisville

EARLY HOST RESPONSES AND IMMMUNE SIGNALING TO 2009 PANDEMIC INFLUENZA A (H1N1) VIRUSES IN PRIMARY CELL CULTURE MODELS

By

Rachael Lask Gerlach

B.S., Murray State University, 2007

M.S.P.H., George Washington University, 2009

A Dissertation

Submitted to the Faculty of the

School of Medicine of the University of Louisville

In Partial Fulfillment of the Requirements

for the Degree of

Doctor of Philosophy

In Microbiology and Immunology

Department of Microbiology and Immunology

University of Louisville

Louisville, KY

May 2015

EARLY HOST RESPONSES AND IMMMUNE SIGNALING TO 2009 PANDEMIC INFLUENZA A (H1N1) VIRUSES IN PRIMARY CELL CULTURE MODELS

By

Rachael Lask Gerlach

B.S., Murray State University, 2007

M.S.P.H., George Washington University, 2009

A Dissertation Approved on

March 18, 2015

By the following Dissertation Committee Members:

Colleen Jonsson Ph.D. _____
(Dissertation Director)

Haribabu Bodduluri, Ph.D. _____

Michele Kosiewicz Ph.D. _____

Igor Lukashevich, MD _____

Haval Shirwan Ph.D. _____

Jill Suttles Ph.D. _____

DEDICATION

This dissertation is dedicated to

my husband Hunter Gerlach

and to my parents George and Amy Lask

who have given me invaluable support and love throughout the pursuit of my degree.

ACKNOWLEDGEMENTS

I first want to thank my mentor, Dr. Colleen Jonsson, for giving me the opportunity to work in her laboratory and for her guidance, support and encouragement. I am very grateful for her teaching me to become a better scientist, through improving my laboratory techniques, giving oral presentations, and writing. I am fortunate to have a strong, female mentor whom I look up to and will continue to learn from for many years to come.

I am very thankful to my committee members Dr. Igor Lukashevich, Dr. Jill Suttles, Dr. Michelle Kosiewicz, Dr. Haval Shirwan, and Dr. Haribabu Bodduluri for their support, guidance and time. Your endless support and encouragement throughout my time at UofL have meant so much to me.

A special thanks also to Department of Microbiology and Immunology faculty, staff, and students, as well as the Center for Predictive Medicine for providing me excellent support to pursue my PhD.

I would also like to thank all the members of the Jonsson Lab and our collaborators. I would like to specifically thank Mawadda Alnaeeli for her support and valuable discussions, Dr. Donghoon Chung for his assistance with molecular techniques and general virology discussion and Dr. Yong-Kyu Chu for his continued support throughout my years in the lab.

I especially would like to thank Jeremy Camp for his endless support in and out of the lab. He was instrumental in my laboratory training and has been the best laboratory teammate I could have ever wished for. Words cannot express my gratitude for his help and encouragement over the years and I know he will be an excellent PI one day.

I would also like to thank my fellow lab mates Ryan McAllister and Scott Adcock for their endless support over the years. Whether it was helping me find reagents or helping me with experiments, these two were always there for me and I am forever grateful for their support.

Lastly, I want to thank my family. To my best friend, tech support, and husband Hunter, I could not have done this without you. Thank you for always being my

biggest fan and my cheerleader. I could not have asked for a better companion. To my parents, George and Amy, I can never thank you enough for all you have done for me. Thank you for giving me the best educational opportunities and insisting that no goal is too high. Thank you cooking dinners and taking care of my dog when I so busy with work. I could not have made it through this program without you.

ABSTRACT

EARLY HOST RESPONSES AND IMMMUNE SIGNALING TO 2009 PANDEMIC INFLUENZA A (H1N1) VIRUSES IN PRIMARY CELL CULTURE MODELS

Rachael Lask Gerlach

March 18, 2015

Influenza A virus (IAV) subtypes and even genotypes within subtypes can show differences in tropism (host, cell type), magnitude of infection, immune response and progression of illness. My dissertation focused on the development and use of two *in vitro* physiologically-relevant human cell culture models, well-differentiated normal human bronchial epithelial (wdNHBE) cells and human monocyte-derived macrophages (MDM) for the study of early IAV-host interactions. These models have given new insight into early host responses to seasonal H1N1 (BN59) and two pandemic A(H1N1)2009 viruses or H1N1pdm herein. The H1N1pdm are clinical isolates from a fatal (A/KY/180/10) and nonfatal (A/KY/136/09) case. In the wdNHBE model, KY180 showed a significantly higher titer as compared to the other two viruses at 24 hpi (hours post-infection). Interestingly, by microarray analysis, there were no significant differences in the host genome-wide expression intensity profiles of each virus following infection. Soluble cytokine measurements revealed increased apical and basal pro-inflammatory cytokine secretion overtime. A key finding from our

data was greater basolateral secretion of cytokines (IL6, CCL5, CCL4 and CCL2) by KY180-infected wdNHBE cells. This finding suggests that the basolateral signals from infected epithelial cells may differ in their potential for recruitment and responses elicited by recruited monocytes/macrophages.

In the second model, I used an *in vitro* model of recruited “resting” MDMs to study virus-host interactions of the clinical H1N1pdm isolates. These viruses replicated in MDM albeit inefficiently. While titers were similar and remained relatively low for all isolates, pro- and anti-inflammatory expression levels differed markedly between KY180 as compared to KY136 and BN59. KY180 had delayed expression at 8 hpi of pro-inflammatory genes (CCL5, TNF, IFN, CXCL10). This apparent delay in response to KY180 depended on the mode of viral entry. For KY180, this occurred primarily through macropinocytosis, mapping to the HA1 gene. In summary, my studies reveal subtle, yet important differences in IAV-host interactions that result in alterations of immune signaling in epithelial and macrophage cell culture models. Continued advancement of the *in vitro* human cell culture models for the study of IAV is important as they will allow mechanistic insight into the intricate biology of these viruses.

TABLE OF CONTENTS

DEDICATION iii
ACKNOWLEDGEMENTS iv
ABSTRACT vi
LIST OF TABLES ix
LIST OF FIGURES x
CHAPTER 1 1
INTRODUCTION 1
INFLUENZA A VIRUS LIFE CYCYLE 5
HOST IMMUNE RESPONSE TO IAV INFECTION 20
EMERGENCE OF NEW INFLUENZA VIRUSES 22
H1N1 INFLUENZA ISOLATE SPECIFIC DIFFERENCES 26
OBJECTIVE OF DISSERTATION 28

CHAPTER 2 46
OVERVIEW 46
INTRODUCTION 47
METHODS 51
RESULTS 55
DISCUSSION 61

CHAPTER 3 84
INTRODUCTION 84
METHODS 88
RESULTS 93
DISCUSSION 98

CHAPTER 4 112
OVERVIEW 112
INTRODUCTION 113
METHODS 117
RESULTS 127
DISCUSSION 139

CHAPTER 5 167
CONCLUSIONS 167
PRELIMINARY STUDIES AND FUTURE DIRECTIONS 180

REFERENCES 190
APPENDIX 219
CURRICULUM VITAE 222

LIST OF TABLES

CHAPTER 1

1. Description of influenza A virus proteins 33
2. Description of influenza A subtypes resulting from antigenic shift which have historically caused pandemics 41
3. Panel of H1N1pdm clinical isolates obtained from hospitalized patients in Louisville, KY 45

CHAPTER 2

4. Seasonal and pandemic IAV isolates used in this study 67
5. Differentially expressed genes in IAV–infected wdNHBE cells at 36 hpi . 74
6. Notable genes upregulated in wdNHBE cells infected with seasonal and pandemic IAV isolates at 36 hpi 77
7. Fold change of significantly differentially expressed genes 79
8. Top five significant canonical pathways in IAV-infected NHBE cells at 36 hpi relative to mock 82

CHAPTER 3

9. Primers utilized for RT-PCR and cDNA synthesis 103

CHAPTER 4

10. Description of mutations within the HA gene of KY180 165
11. Percent inhibition of viral entry in the presence of macropinocytosis inhibitor EIPA (data from figure 38) 166

LIST OF FIGURES

CHAPTER 1:

1. Schematic of influenza A virion and nomenclauture 34
2. Life cycle of influenza A virus in cells..... 35
3. Schematic of the human respiratory tract and distribution of influenza A virus receptors 37
4. Schematic of two of the known entry pathways utilized by influenza A viruses 38
5. Cryo-EM micrographs of influenza A virus structure..... 39
6. Current model of the activation of pattern-recognition receptors (PRRs) after influenza A infection..... 40
7. Phylogenetic tree demonstrating the variation in NS proteins of influenza A, B, and C 42
8. Emergence of the 2009 pandemic H1N1 Influenza A virus..... 44

CHAPTER 2:

9. Virus titer detected in supernatant from cells infected seasonal and pandemic influenza A viruses 68
10. Immunohistochemical microscopy of wdNHBE cells after influenza A infection 69
11. Apical cytokine and chemokine production by wdNHBE cells infected with seasonal and pandemic influenza A viruses 70
12. Basal cytokine and chemokine production by wdNHBE cells infected with seasonal and pandemic influenza A viruses 71
13. Apical and basal secretion of cytokines and chemokines from wdNHBE cells infected with seasonal and pandemic influenza A viruses at 36h after infection 73
14. Summary of wdNHBE microarray analysis 75
15. Pathways significantly represented by all isolates as compared to mock 80
16. Changes in epithelial layer integrity in infected wdNHBE cells at 36h after infection 83

CHAPTER 3:

17. Schematic of recruitment of macrophages to site of infection..... 101

18. Schematic of approach used to culture and characterize the 'resting' human monocyte-derived macrophages (MDM) model by RT-PCR and flow cytometry 106
19. Characterization of 'resting' human monocyte-derived macrophages model by microscopy and RT-PCR 108
20. Evaluation cell morphology and permissibility of MDM infection to egg-derived and cell-derived viral stocks 109
21. Cell Viability at different MOIs 24h post-infection 110
22. Infection of MDM by H1N1pdm isolates 111

CHAPTER 4:

23. Subsets of macrophages and their associated markers 144
24. Balance of pro-inflammatory and anti-inflammatory response to influenza A viruses 145
25. Approach used to recover reverse genetics recombinant NL602 viruses with KY180 HA gene and NL602 virus with specific mutations in the HA gene 146
26. Pandemic and seasonal influenza A viruses infect primary human monocyte-derived macrophages 147
27. Replication of seasonal and pandemic influenza A viruses in MDM cells 148
28. Differential expression of macrophage activation genes in MDM after infection by KY180, KY136, and BN59 150
29. Influenza virus-mediated mRNA expression of cytokines and chemokines in MDM 151
30. Influenza virus-mediated mRNA expression of pattern recognition receptor genes 152
31. TNF protein production in the presence or absence of secondary signal, LPS in IAV-infected cells 153
32. Innate immune response gene expression (with UV) and apoptosis 154
33. Requirement for low pH for entry and determination of the threshold pH of fusion for KY180 and KY136 by syncytia assay in MDCK cells 156
34. Effects of macropinocytosis and clathrin-mediated endocytosis inhibitors on viral entry into MDM 158
35. Expression of immune response genes in the presence or absence of inhibitor 159
36. Cryo-EM pictures of KY180 and KY136 160
37. Sensitivity to macropinocytosis inhibitors can be mapped to the HA protein of KY180 161
38. Sensitivity to macropinocytosis inhibitors can be mapped to specific mutations within the HA1 protein in KY180 162

39. Gene expression of innate signaling and pro-inflammatory genes with recombinant viruses in the presence of absence of inhibitors..... 164

CHAPTER 5:

40. Schematic of Influenza Virus in Humans 176
41. Results and hypothesis generated from wdNHBE studies..... 177
42. Hypothesis generated from MDM studies..... 178
43. Proposed model of the interaction between macrophages and epithelial cells based on data presented in this dissertation 179
44. Timeline of co-culture experiment including description of all treatment and control groups..... 184
45. Preliminary results from co-culture of infected 16HBE cells with MDM.. 185
46. Human airway nicotine (environmental) exposure and susceptibility to IAV infection 189

CHAPTER 1

INTRODUCTION

INFLUENZA VIRUSES, PAST, PRESENT, AND FUTURE

Influenza viruses, family *Orthomyxoviridae*, are important respiratory pathogens in humans that circulate in a variety of hosts including humans, birds, water mammals, horses, dogs and pigs [1-4]. Influenza viruses are transmitted between and across species primarily by respiratory secretions and fomites [5]. Annual seasonal influenza virus epidemics in humans present a significant public health burden resulting in millions of infections and hospitalizations each year. Moreover, the highly associated morbidity and mortality impose an extensive, annual economic impact resulting from illness amounting to 10-16 billion dollars [6-10]. The annual global attack rate of seasonal influenza is estimated at 5 – 10% in adults and 20 – 30% in children, with more than 200,000 hospitalizations and 41,000 deaths each year in the United States alone [7, 11]. Secondary bacterial pneumonia is a frequent complication of influenza infection [12, 13]. Co-infections occur in approximately 25% of all influenza-related deaths with the highest incidence in elderly people and individuals with certain chronic diseases [14-18].

The 2013 report from the International Committee on Taxonomy of Viruses show the *Orthomyxoviridae* comprise of five genera of which three are influenza viruses (*influenzavirus A*, *influenzavirus B* and *influenzavirus C*). Each genus has one viral species, respectively, *Influenza A virus* (IAV), *Influenza B virus* (IBV) and *Influenza C virus* (ICV). All three genera cause human disease, with the best recognized and most pathogenic being IAV. The viruses are grouped according to their antigenic relatedness which is driven from differences between the two main surface glycoproteins hemagglutinin (HA) and neuraminidase (NA) (Figure 1A) [19, 20]. IAV are the most common of the *Orthomyxoviridae* genera. IAV infect a range of mammalian and avian species and can cause pandemics, whereas, IBV circulate among in human populations and have not been associated with any pandemic [4, 20]. Similar to IBV, ICV has a limited host range and has been isolated from humans, pigs and dogs. Cases of ICV each year are very rare and have a minimal public health impact [21].

In 1936, Smith, Andrews and Laidlaw isolated IBV from patients by infection of human nasal secretions in the ferret [22]. Subsequently, in 1983 IBVs diverged into two antigenically and genetically distinct lineages B/Victoria/2/87-like and B/Yamagata/16/88-like viruses [23-26]. IBV resembles IAV when evaluated by electron microscopy [27]; however, there are key differences between the two viruses. First, the antigenic properties, which describe the immune response triggered by antigens on a virus, were shown to be different by serological assays (Figure 1A) [20, 28]. Where IAV has three membrane proteins, IBV has four proteins in the envelope: HA, NA, NB, and B

matrix protein 2 (BM2) [20, 29]. NB and BM2 are integral membrane proteins that are unique to IBV and function proton channels important for viral entry but are not necessarily important for viral replication [30, 31].

Secondly, they differ in the length of the open reading frames and non-coding regions [20, 32, 33]. As mentioned previously, the reservoir of IBV is humans, however, water mammals such as seals can become infected via human sewage released into the ocean [4, 26]. IBV can cause severe disease in humans and are responsible for an average of 24% of all laboratory-confirmed influenza cases annually [20, 34].

Compared to IAV and IBV, ICV infections cause a mild respiratory illness and are not thought to cause epidemics or pose any public health concern to humans [35]. From 1997-1998, two cases of ICV were reported throughout the entire season highlighting the rarity of these cases occurring during yearly outbreaks of IAV/IBV [36]. In contrast to IAV and IBV, ICV has only one surface glycoprotein, giving it only seven genomic vRNAs [20]. Further, while IAV and IBV have two major surface glycoproteins, HA and NA, ICV has only one, HEF (hemagglutinin-esterase fusion) [37]. Based on comparative sequencing studies using the HA protein, it was estimated that IAV HA gene diverged from the IBV HA gene more recently than from HEF gene (HA equivalent) in ICV [19].The seven vRNA segments encode three RNA dependent RNA polymerase (RdRp) proteins (PB2, PB1, PA), hemagglutinin esterase-fusion (HEF) glycoprotein, nucleoprotein (NP), matrix (M1) and CM2 (membrane protein), and the

nonstructural proteins (NS1 and NS2) [20]. Like IBV, ICV does not have an animal reservoir minimizing the chance for reassortment across species.

In this introduction, I review the current state-of the IAV structure and life cycle, the host immune response to infection in humans, and what is currently known regarding the historical emergence of new epidemic and pandemic influenza strains.

INFLUENZA A VIRUS STRUCTURE

Classified as enveloped viruses, the IAV virion is formed from a lipid bilayer derived from the host plasma membrane during assembly and budding (Figure 1A) [38]. The envelope consists of two glycoproteins, HA and NA, and a tetrameric proton channel protein matrix 2 M2 (Figure 1A). The HA and NA are commonly referred to as spike proteins based on their shape. Underneath the lipid bilayer of the viral envelope is a structural layer composed of matrix protein (M1) (Figure 1A). The virion contains eight vRNA segments which are single-stranded and in the negative-sense; hence these viruses are further classified as negative-strand, single-stranded RNA viruses. The genomic segments are coated with NP (Figure 1A). The NP encapsidated vRNAs and the polymerase proteins form the viral ribonucleoprotein (vRNP) complex (Figure 1A). IAVs are primarily spherical viruses but some filamentous forms have been reported [39]. The filamentous phenotype has been mapped to specific genomic segments and genotypic differences in amino acid sequences within HA, NA, M1, and M2 [39-44].The functions of each of the viral proteins are summarized in Table 1. The viral morphology will be described in further detail in the section on the life cycle.

NOMENCLATURE

IAVs are divided into subtypes based on antigenic variations of their surface glycoproteins HA and NA [20]. At present, 18 different HA subtypes and 11 different NA subtypes have been identified (H1 through H18 and N1 through N11 respectively) [3, 45]. Of those HA subtypes, six are associated with human disease (H1, H2, H3, H5, H7, and H9). The standard nomenclature system for IAV includes the following information: genus, host of origin, geographic origin, case/strain number and year of isolation (Figure 1B). Additionally, the subtype for each of the glycoproteins is given in parentheses for type A.

INFLUENZA A VIRUS LIFE CYCYLE

ATTACHMENT AND BINDING

The respiratory epithelium is a primary target for influenza virus infection and replication [20, 46]. The infectious cycle (Figure 2) begins with the binding and penetration of the plasma membrane, which is mediated by the HA [47]. This surface glycoprotein is translated as a precursor, HA0, which is cleaved into HA1 and HA2 subunits by extracellular host cell proteases. Cleavage is required for HA1 to bind sialic acid (SA) receptors and HA2 to fuse with susceptible cells within the host respiratory tract [48]. HA2 is a transmembrane subunit that mediates membrane fusion between viral and endosomal membranes during endocytosis [20, 49, 50]. The cleavage (or activation) site lies close to the external face of the virion membrane and mutations within this site are a key determinant of IAV pathogenesis [51, 52]. Mutations within the HA cleavage of

H5 and H7 avian influenza viruses have been linked to pathogenicity of IAVs [53, 54].

Changes in the external loop of the HA0 cleavage site, which links the HA1 and HA2 together, alters the structure of HA molecules and can alter their sensitivity to host extracellular proteases [55]. Specifically, the HAO cleavage site has either a single or several Lys or Arg forming either a monobasic or multi-basic cleavage site [55]. IAVs having a monobasic HAO cleavage site can utilize trypsin (or other trypsin-like serine proteases) for activation, with the tissue distribution of these protease typically restricted to the respiratory tract [56, 57]. IAVs having multi-basic HAO cleavage sites can be cleaved by ubiquitous host proteases, such as furin, which can result in viruses that are able to infect and replicate systemically, and ultimately lead to more severe disease [48, 58].

For IAV, the HA show differences in their binding specificity for different two main SA receptors within the respiratory tract, alpha-2,3 and alpha-2,6 SA (Figure 3A) [20]. These binding preferences drive the location for virus replication in the upper and/or lower tract epithelial [59-61]. Further, the receptor-binding specificity of the HA is a major determinant of the host range, tissue tropism, pathogenicity, and transmissibility [62-64]. SA was first identified as being responsible for binding of influenza viruses more than 50 years ago [65]. In humans, the epithelial cells lining the respiratory tract have different distributions of alpha-2,6-SA (mainly upper) and alpha-2,3-SA (mainly lower) receptors (Figure 3A) [66]. Therefore, IAVs vary in their ability to infect upper or lower respiratory tract as depending on the binding affinity for the receptors. For

example, the HA of the avian H5N1 influenza viruses preferentially bind to alpha-2,3-SA [67, 68], while H1N1 preferentially bind to alpha-2,6-SA that predominate in the human upper respiratory tract [69-71]. Amino acids mutations that switch binding specificity from alpha-2,3-SA to alpha-2,6-SA are generally thought to be necessary, but not a completely sufficient requirement for the adaptation of IAVs for efficient growth in the upper respiratory tracts of mammals and permit airborne transmissibility [63, 72, 73].

Most seasonal IAV strains infect the upper respiratory tract with limited lower respiratory tract involvement. Patients hospitalized due to the recent 2009 pandemic influenza A (H1N1) virus (H1N1pdm) showed both upper and lower respiratory tract involvement [74]. While a number of the adult patients had pre-existing comorbidities, many did not. Moreover a large percentage of children without pre-existing comorbidities presented with upper and lower respiratory tract involvement. This led some researchers in the influenza field to ask whether the HA had a broader specificity for human receptors since the HA of this virus had an avian origin [66, 74-76]. One avian signature of the HA is at the G position 222 in the HA [77, 78]. In the context of H1N1pdm, this specific mutation in the HA1 shows dual receptor specificity for both alpha-2,3-SA and alpha-2,6-SA, with an affinity to macrophages and type II pneumocytes in the alveoli and to both ciliated and goblet cells in both the tracheal and bronchial portions of the respiratory tract [79, 80].

The respiratory epithelium is a highly complex environment composed of a heterogeneous cell population, including secretory (Clara), goblet (mucus),

ciliated, and basal cells that differ in frequency and distribution depending on location in the lung (Figure 3B) [81]. In the small airways, additional cell types, alveolar type 1 and 2, dominate. These cell types differ in their expression of alpha-2,3-SA and alpha-2,6-SA receptors (Figure 3B) [66, 82]. Currently there are mixed conclusions reported regarding what cell type is preferred by seasonal IAV with data supporting binding to ciliated and/or non-ciliated (goblet) cells [61, 66]. Seasonal and H1N1pdm IAVs enter and replicate efficiently in ciliated cells that line the epithelial cell layer in the large and small airways of the respiratory tract, while H5N1 enters and replicates more efficiently in non-ciliated cells (type II pneumocytes) within the small lower airways (Figure 3B) [74, 75, 83-87]. Hence, the spatial distribution and concentration of potential receptors associated within different areas of the respiratory tract and/or different cell types are integral in the study of IAV infection and disease [75, 88-91].

INTERNALIZATION

Once bound to the SA receptor, IAV may enter via clathrin-dependent endocytosis however internalization of IAV also may occur via caveolae, non-clathrin and non-caveolae pathways and by macropinocytosis (Figure 4) [92-96]. However, clathrin-mediated endocytosis has long been identified as the major route of IAV cell entry [95, 96]; and is by far, the best characterized endocytic pathway. Early insights into the pathways of entry of IAV in a susceptible cell line, Madin-Darby Canine Kidney Epithelial Cells (MDCK) were conducted by electron microscopy showing IAV pH-independent internalization into coated pits on the cell surface and coated vesicles in the cell cytoplasm within 7 minutes after viral

binding [95, 97]. These results provide evidence that IAV enter by clathrin-mediated endocytosis; however, IAV was also observed to be within uncoated vesicles inside the cell suggesting an alternative, clathrin-independent, pathway of entry [97, 98].

In clathrin-dependent endocytosis, IAV attachment to its SA receptor induces the binding of the adaptor protein clathrin to the cytoplasmic tail. The accumulations of clathrin on the inside face of the plasma membrane all the receptor. The accumulation of clathrin on the inside face of the plasma membrane allows clathrin to multimerize to form characteristic invaginations or clathrin-coated pits. These pits are then pinched off from the plasma membrane by membrane scission proteins DNM1/Dynamin-1 or DNM2/Dynamin-2 pinch which releases the virus inside the cell within the clathrin-coated vesicle (CCV) (Figure 4A) [99-103].

Macropinocytosis or clathrin-independent endocytosis, is characterized by actin-dependent reorganizations of the plasma membrane forming protrusions of the plasma membrane that bring the virus into the cell through an invagination of the plasma membrane (Figure 4B, step 2) [104-106]. Macropinosomes are formed after fission events separate the invagination from the extracellular space, characterized morphologically as heterogenic vesicles that lack coat structures (Figure 4). Characterization of the early events of IAV infection by this route are very limited with only a few studies using inhibitors to show these viruses can actually enter via this route [104, 107]. Clathrin-coated vesicles and macropinosomes traffic and mature in a parallel manner (Figure 4) [108]. Both

are transported towards and fuse with early endosomes (EE), regulated by associated Rab5 GTPases [109]. Over the course of maturation the endosomes are acidified by membrane bound V-type proton ATPases and Rab5 GTPases are exchanged for Rab7, which then surrounds the late endosomes (LE) [109]. The endosomes travel along microtubules mediated by the motor protein dynein and once the pH within the LE undergoes acidification, the IAV virus escapes by membrane fusion [92, 110].

Macropinosomes are formed after fission events separate the invagination from the extracellular space, characterized morphologically as heterogenic vesicles that lack coat structures. Clathrin-coated vesicles and macropinosomes traffic and mature in a parallel manner. Both are transported towards and fuse with early endosomes (EE), regulated by associated Rab5 GTPases. Over the course of maturation the endosomes are acidified by membrane bound V-type proton ATPases and Rab5 GTPases are exchanged for Rab7, which then surrounds the late endosomes (LE). The endosomes travel along microtubules mediated by the motor protein dynein. When the pH decreases, the virus fuses and its genome is released into the cytoplasm.

ENTRY/FUSION

In order for the virion to be released from the endosomal vesicle within the cell, it must fuse and undergo a pH-induced, conformational change [20]. Fusion of the virus particle with endosomal membranes and uncoating of viral ribonucleoprotein is mediated by the HA and M2 proteins [20, 111]. As mentioned before, once the HA0 is cleaved, the HA1 and HA2 become

functional. The HA1 subunit is responsible for binding of sialic acid receptor and then, once bound and internalized, the HA2 protein mediates the fusion and release of viral nucleic acid into the cellular cytoplasm as the endosomal pH drops (Figure 2) [112]. In its native state, the HA2 trimer forms a stem of three helical hairpins each fastened by the N-terminal fusion peptide which is buried within the core of a coil-coil structure [113]. Transport of virion cargo to the late endosome exposes the proteins to pH of ~5.0 which activates the ion channel activity of the tetrameric IAV M2 protein. This activation induces a conformation change resulting in the opening of the ion channel allowing hydrogen ions to diffuse into the interior of the virion. This reduction of the endosomal pH causes an irreversible conformational change, resulting in refolding of the HA2 to expose the hydrophobic fusion peptide from its buried position allowing extension of the fusion peptide toward the target membrane [113, 114]. To maintain its active fusion state, the HA2 relies on the structural constraints of the HA1 subunit, which acts as a clamp to keep the HA2 in correct orientation [112, 115]. Further, the vRNP complex must be functionally separated from the structural M1 protein within the endosomal compartment. Acidification weakens the interaction of the M1 and vRNP complex. This stimulates the uncoating of IAV RNP and allows the release of vRNP into the host cell cytoplasm [116, 117]. Once the viral envelop and endosomal membranes fuse, a pore is formed which allows the viral contents to be released into the cytoplasm [111].

Early studies demonstrated that IAV envelope fusion was activated in acidic media at a pH of 5.0 [97, 118, 119]. Changes in the ability of the virus to undergo membrane fusion at slightly lower or higher pH can affect host tropism. Specific mutations within the HA1 (N142K) and HA2 (E47K, E374K) of IAV strains can confer a higher thermos-stability to these proteins and therefore lower the pH required for fusion as compared to those without these mutations [120-122]. For example, some of the 2009 H1N1pdm viruses have a lysine at the 47 amino acid position in the HA2 subunit of the stalk region of the HA instead of a glutamic acid [121]. This mutation was shown to correlate with a reduction in the pH of fusion and increased acid stability of the HA2 [121]. Further this change resulted in a higher thermal stability of the HA2 when exposed to high temperatures, which was seen to correlate with infectivity in ferrets. Because the ferret and human share similar lung physiology and similar sialic acid distribution [123], the increase in E47K infectivity in ferrets suggested a fitness advantage for the E47K change in humans [121]. Further, studies analyzing differences among the HA sequences in their intermolecular interactions found that a residue at position 374 (HA0 numbering) of the HA2 is critical for HA trimer stability and that a specific mutation, E374K improves the pH stability of those viruses [124].

For avian IAV, the pH stability can also influence the outcome of infectivity. For example, changes of +0.4 and -0.5 units in the pH of activation by Y23H and K58I mutations in the HA1 gene reduced weight loss, mortality, shedding, and transmission of H5N1 in ducks [125]. Further, studies in vivo in mice and ferrets found that an increased tolerance to low pH (increased pH

stability) of the HA enhanced H5N1 growth in the upper respiratory tract of ferrets and mice [126, 127]. Additionally, Galloway et al. reported that the pH of fusion varies among different HA subtypes, and notably, the pH of fusion for most HAs from human IAVs ranged from 5.5 - 5.6, whereas HAs from avian IAVs ranged from 5.1-5.4 [128].

TRANSCRIPTION

Once the vRNPs are released into the host cytoplasm, they are imported to the nucleus via an energy-dependent importin-alpha-importin-beta-dependent nuclear import pathway [129] (Figure 2). Briefly, importin protein importin-alpha recognizes the nuclear localization signals on IAV NP [130, 131] , PB2 [132, 133], or PA/PB1 [134, 135], which is then recognized and bound to importin-beta transport receptor [136]. This complex diffuses through the nuclear pore complex and undergoes active RAN GTPase (RAN-GTP)-induced dissociation with the help of cytoplasmic RAN G-proteins, releasing the vRNP into the nucleus where transcription and replication take place [137, 138].

Differences in how IAV strains use importin-alpha within the host cell have been shown to control host adaptation [139-141]. Specifically, mutations in PB2 (D701N) and NP (N319K) alter the binding of vRNPs to importin-alpha in mammalian and avian cells, which limits RNP translocation into the nucleus of cells of a particular species while enhancing translocation in another [139]. More recent studies have shown a differential dependence on a specific importin-alpha proteins, with avian IAVs dependent on importin-alpha3 and mammalian IAVs

dependent on importin-alpha7 [142]. Regardless, once in the nucleus, mRNA and complementary viral RNA (cRNA) are transcribed from the vRNA template

Viral transcription of the viral mRNAs is mediated by the heterotrimeric RdRp (PB1, PB2 and PA), NP and host-derived components (described below) [143, 144]. First the RdRp complex recognizes and binds to newly transcribed host cellular mRNAs containing a 5' cap in the nucleus [145, 146]. The PB2 binds to the 5' cap of the host pre-mRNAs followed by the endonuclease activity of the PA which cleaves 10-12 nucleotides from the 5' end. This is commonly referred to as "cap snatching" [147]. The 5'-capped RNA serves to prime transcription of the viral template to produce viral mRNAs mediated by PB1 [148-150]. PB1 also adds a polyadenylated (poly(A)) tail by the 'stuttering mechanism' [151] on a sequence of uridine residues near the 5' end of the viral genome [152]. Two of the smaller vRNAs, the M segment and NS segment in concert with the spliceosome are further processed to yield M1, M2, NS1, and NS2/NEP. These splicing events are critical for IAV infection and are regulated by host nuclear splicing machinery as well as NS1 IAV protein [153, 154]. Once completed, the viral mRNAs are transported to the cytoplasm where they hijack host cell translational machinery to make IAV proteins [155] (Figure 2).

TRANSLATION

Once exported into the cytoplasm, viral mRNAs undergo translation on free and membrane bound ribosomes. IAV infection drives a selective translation of viral mRNAs over cellular mRNAs [156, 157]. This selective translation of viral mRNAs over cellular mRNAs has been suggested to be mediated in two ways.

First, the “cap snatching” mechanism limits newly synthesized cellular mRNA cap structures, resulting in premature degradation before nuclear export [158]. Second, viral translation occurs by selective recognition of sequences in the 5′UTR of viral mRNAs [156]. The NS1 protein of IAV has been shown to bind the 5′UTR of viral mRNAs and plays a critical role in suppressing the production of host mRNAs, including anti-viral host genes, by inhibiting the 3′-end processing (post-transcriptional processing) of host mRNAs [159-162]. Eukaryotic translation initiation is mediated by eukaryotic initiation factors (eIFs) interacting with the ribosomes and the mRNA [163]. IAV NS1 was shown to bind and recruit two of those factors, eiF4G and eiF4F, to the 5’UTR of viral mRNA thus increasing viral specific translation [164].

Regulation of eIF phosphorylation can lead to increases or decreases in translational events within cells. Phosphorylation of the eIF2α prevents the exchange of GDP for GTP by eIF2B, thus preventing the 43S pre-initiation complex from forming and ultimately inhibiting protein synthesis [163, 165]. A correlation between enhanced phosphorylation of eIF4E and increased rates of viral protein synthesis has been reported in a lymphocyte cell line [166]. Within an infected cell, activated double-stranded-RNA-dependent protein kinase (PKR) blocks cellular and viral protein synthesis by phosphorylating the alpha subunit of the eIF2 translation initiation [167, 168]. The NS1 protein of IAV has been shown to regulate these phosphorylation events by binding to PKR [169]. Mutant IAVs unable to express NS1 displayed high pathogenicity in mice with fully active PKR [170-173]. The regulation of host and viral protein production by IAV plays an

important role in the viral life cycle as it limits host protein and enhances viral protein production.

After IAV translation occurs proteins PA, PB1, PB2, NS1 and NP, are synthesized in the cytoplasm and transported back to the nucleus to perform viral genome replication. This occurs via their nuclear localization signals and importin-alpha [131, 133, 174, 175].

REPLICATION

Viral RNA replication starts with the synthesis of the cRNA from vRNA (Figure 2) [20, 176]. This process is mediated by the heterotrimeric RdRp (PB1, PB2 and PA), NP and host-derived components [143, 144]. Replication of the vRNA from the cRNA or cRNA from vRNA does not require a primer. This is possible because the 5' and 3' ends of the viral genomes and anti-genomes exhibit partial inverse complementarity and are able to base pair with one another to form a double-stranded promoter structure or "panhandle" that is recognized and bound by the viral RdRp [177-179]. The vRNA is combined with PB1, PB2, and PA to form the vRNP complex and shuttled to the cytoplasm for assembly at the plasma membrane and release. The mechanism for shuttling through the nuclear pore will be discussed in the following section.

The N-terminus of the NP protein contains an RNA-binding domain that plays a role in controlling the "switching" of RNA polymerase activity from transcription to replication [180]. Based on in vitro antibody depletion experiments, the NP protein binds the viral RNA template and act as an anti-termination factor for replication [181]. Shapiro and Krug *et al.* further confirmed

the requirement of NP for IAV replication with experiments with temperature-sensitive NP mutants which fail to synthesize cRNA, but not mRNA [181].

The RdRp has been implicated as a determinant of viral tropism [182]. A single residue in the PB2 of avian IAV, amino acid 627, regulates polymerase activity in a species-specific fashion [183]. PB2 derived from human viral isolates almost exclusively possesses a lysine at position 627 (K627), whereas in avian viruses glutamic acid (E627) at this position predominates [184]. The presence of an E627 mutation at this position has been shown to drastically reduce replication efficiency and pathogenicity in mammalian systems [184, 185]. Recently, Mehle *et al.*, reported that the glutamic acid-to-lysine mutation allows avian IAV to escape, however, in human cells an amino acid at this position restricts replication [186]. Thus, identification and monitoring of emerging mutations that increase polymerase activity in species specific cell types are important for assessing pandemic potential of IAVs.

NUCLEAR EXPORT

In the nucleus, newly synthesized vRNA genomes, bound to NP, are joined with newly synthesized PB1, PB2, and PA to form vRNPs which travel to the cytoplasm through the CRM1 export pathway [187]. The vRNP complex does not interact directly with CRM1 to form an export complex but uses an adaptor nuclear export protein (NEP/NS2). THE NEP/NS2 complex recognizes and binds to the export signal [188, 189] on the vRNPs and is followed by binding of the viral matrix M1 protein and CRM1, thus linking the viral RNP with CRM1 [190-192]. Additionally, NS2 interacts with nucleoporins and serves as an

adaptor between vRNPs and the nuclear pore complex [187, 191]. The export pathway functions in a reverse manner to importin under the control of RAN cargo complex [130]. Dissociation of vRNPs from the exportin requires RAN-GDP which occurs only in the cytoplasm. Mutations within the nuclear export protein can also drive the adaptation of a highly pathogenic avian influenza (HPAI) virus such as H5N1 to mammalian cells enabling increased replication [193]. Other viral components such as HA, NA, and M2 are transported to the plasma membrane via the Golgi network and assemble with RNPs to form mature virus particles that are released from the cell via budding [20].

ASSEMBLY AND BUDDING

During the final stage of IAV assembly, all 8 vRNPs are incorporated into the virion as it buds from the apical plasma membrane of the cell [194]. Studies have identified packaging signals in the 5' and 3' non-coding regions of the viral segments to mediate assembly [195-198]. IAVs utilize lipid raft domains in the plasma membrane of infected cells as sites of virus assembly and budding [199-203]. Lipid rafts are regions of the plasma membrane that are variable in size and enriched with cholesterol [204]. For IAV, HA and NA associate with lipid raft domains; the transmembrane domain being a critical component of HA for strong affinity for these rafts [199-203, 205]. These raft-associated proteins can cause a merging of lipid raft domains which help concentrate proteins in a defined region, forming the viral 'budzone' [206]. The HA functions as an important piece of the budding machinery. However, budding of the virion can occur without the HA, thus making other IAV proteins important to the process as well [207]. M1 has

been postulated to be the crosslink between the cytoplasmic portion of the HA and NA [202]; however, the domains required for this interaction have not been identified. As mentioned before, M1 binds to the newly synthesized vRNPs and by linking to the cytoplasmic tails of HA and NA suggests M1 is an important link to assemble the necessary viral components as the site of budding. Once assembled, budding results from HA induced membrane curving followed by detachment of the virion by NA cleavage of the sialic acid residues connecting the virion to the cell surface [208-211].

IAV MORPHOLOGY

IAVs are highly pleomorphic, showing mostly spherical (80-120nm diameter), but other forms have been reported including long filamentous particles (up to 400 nm long and 80-120 nm in diameter) (Figure 5) [20, 212]. Different strains of IAV vary in their shapes with filamentous forms of IAV being reported in the literature for many years [104, 213, 214]. Using a reverse genetics approach, the filamentous phenotype has been mapped to amino acids within HA, NA, M1, and M2 [39-44]. Changes in influenza HA and NA have result in irregularly shaped virions possibly as a result of clustering of HA and NA on lipid rafts prior to viral budding causing membrane deformation; however, these mechanisms remain unclear [44, 215]. Recently, several studies have linked the ability to form filaments to sequence variations in the M1 protein [40, 216, 217]. M2 has also been shown to have a role viral morphology [39, 218-221]. Further, Rossman *et al*. found an amphipathic helix located within the M2 cytoplasmic tail that is able to bind cholesterol, which may be necessary for both

filament formation and stabilizing the newly formed filamentous virus [39]. Recent work utilizing a filamentous strain of influenza virus (H3N2 Udorn) demonstrated that a filamentous IAV could enter cells as efficiently as the spherical forms [92]. However, this occurs with slightly delayed kinetics suggesting yet another source of variation in IAVs that could affect viral entry and tropism.

HOST IMMUNE RESPONSE TO IAV INFECTION

CYTOKINE AND CHEMOKINE RESPONSES

Infection of epithelial cells with IAV leads to the production of inflammatory cytokines and chemokines that initiate an innate immune response by recruiting monocytes, macrophages, and other leukocytes to the site of infection [222-224]. Specifically, in response to IAV infection, respiratory epithelial cells produce antiviral interferons alpha and beta (IFNα, IFNβ) [225, 226], leukocyte chemoattractants such as CCL5, CCL2, CXCL10, interleukin 8 (IL8), and migration inhibitory factor 1-alpha (MIP1α/CCL3) [227-231], and pro-inflammatory cytokines such as interleukin 6 (IL6), tumor necrosis factor (TNF) and interleukin 1-beta (IL1β) [231, 232]. Most studies suggest a positive correlation between inflammatory cytokine response and disease severity in human infections [233, 234]. For example, elevation of IL6 in the blood of humans infected with IAV has been linked to a greater number of intensive care hospital admissions and severe pneumonia [234]. Secretion of these cytokines and chemokines further activate bystander (uninfected) and cells of the immune system. Links between the lung microenvironment and disease outcome remain elusive.

PATHOGEN RECOGNITION AND INNATE IMMUNE SIGNALING

Early host responses elicited by IAV within infected and bystander host epithelial cells are crucial to controlling the magnitude, duration and lethality caused by IAV infection [230, 231]. This initial innate immune response activated by IAV is triggered by pattern recognition receptors (PRRs) recognizing pathogen associated molecular patterns (PAMPs) within the infected cells (Figure 6, left panel) [235-237]. These receptors include Toll-like receptors (TLR), RIG-I-like receptors (RLR), NOD-like receptors (NLR) and C-type lectin receptors (CLRs). During IAV infection, toll-like receptors 3 and 8 (TLR3 and TLR7) within the internal endosome recognize the structural components of IAV viruses, including viral single-stranded RNA (ssRNA) and surface glycoproteins [238]. RIG-I-like receptors recognize viral RNA during viral replication whereas NOD-like receptors recognize both viral RNA and viral induced stress within the infected cell [238, 239]. Once activated, the PRR pathways further activate intracellular signaling cascades, such as nuclear factor-kappa beta (NFκB), interferon regulatory factor 3 and/or 7 (IRF3, IRF7) and mitogen-activate protein kinase (MAPK). Activation of these pathways leads to the induction of inflammatory cytokines and type I interferon (IFN) secretion from the infected host cells. RIG-I, which is known to be the main sensor of IAV infection, is crucial to IFN production as demonstrated in cells whose RIG-I has been suppressed resulted in an inability to produce IFN in response to IAV [236, 240]. Once secreted, IFNs can further stimulate antiviral signals through IFN-stimulated genes (ISGs) in infected and uninfected neighbor cells (Figure 6, right panel) [236, 237, 240-244].

ANTIVIRAL RESPONSES IN BYSTANDER CELLS

One strategy the host cell uses to prevent virus proliferation occurs when virus-host interactions trigger a potent IFN antiviral response. The secreted IFN will activate bystander cells in the induction of IFN-stimulated genes (ISGs) whose protein products will assist in fighting off IAV infection and proliferation in the lung (Figure 6, right panel). IFNs mediate their responses by signaling via specific receptors that bind to Janus kinases (JAKs) and activate signal transducers and activators of transcription (STATs). Activation of these pathways results in expression of a broad range of ISGs in the bystander cells, including PKR [245], MxA [246], RNaseL [247], and ISG15 [248].These genes serve to inhibit protein synthesis (PKR), induce RNA cleavage (RNaseL), or interfere with viral replication (MxA) [249, 250]. However, IAV have evolved multiple mechanisms to evade the ISGs, allowing the virus to replicate and transmit between hosts.

Strategies to evade and inhibit the IFN response include increased replication speed, inhibiting host protein synthesis, and decreasing the sensitivity to host-cell interferon stimulated effectors such as Mx1 [251]. The viral NS1 protein is widely regarded as the common factor by which all influenza A viruses antagonize host immune responses by competing with cellular proteins for RNA binding which in turn prevents PKR and OAS activities [252].

EMERGENCE OF NEW INFLUENZA VIRUSES

Newly emerging IAV arise through mutations in the antigenic sites of HA and NA. Small alterations in these sites are referred to as antigenic drift, whereas

larger alterations caused by reassortment are referred to as antigenic shift [253]. Once inside the host, IAVs are targeted for clearance by the antiviral, innate, and adaptive immune responses. Reassortment of IAV genome segments results when two different virus genotypes or species infect the same host, exchange segments and undergo immunological selective pressure generating potentially novel, more “fit” viral mutants which escape or evade host immunity [253-256]. IBVs do not undergo this immunological pressure and, hence, mutate at a lower rate [257]. A study by Parvin *et al.* in 1986 reported the mutation rate for the NS gene of IAV A/WSN/33 (H1N1) (WSN) to be 1.5×10^5 mutations per nucleotide per infectious cycle [258]. More recent work in MDCK cells have shown the mutation rate of the IAV NS gene is two to three times faster than the NS gene in IBV [259]. This variation and how quickly the viruses evolve is depicted using a phylogenetic tree for 14 NS gene sequences from IAV, IBV, and ICV (Figure 7).

Drift and shift may vastly increase the diversity of circulating IAV strains. This diversity in turn allows for the survival of variants that escape pre-existing immunity in the population that may lead to widespread epidemics and potentially pandemics. New epidemics of IAV on average occur in the human population every 3 years with a similar process for IBV every 5 years [253]. Reassortment between IAV and IBV has not been shown to occur [260-262] despite the ability of IBV to cause significant morbidity and mortality every 1 in 3 years [263, 264]. This lack of reassortment is somewhat surprising but some studies have suggested the incompatibility between IAV and IBV occurs at the protein (complex formation) or viral RNA level (encapsidation) [264-266].

At least sixteen HA subtypes and nine NA subtypes exist in animal species that humans have little or no prior immunity/exposure to, making them a potential source of antigenic shift [2, 253, 254]. When animal IAVs acquire mutations directly or by reassortment with human IAVs, the resulting antigenic shift can improve viral replication, fitness, and human-to-human transmission [2, 254, 267, 268]. For example, in 2009, reassortment led to the emergence of an H1N1pdm with the capacity for transmission in human populations. This was as a result of mixing of influenza viruses from humans, birds and pigs, and will be discussed in more detail in the following section [269, 270]. To date, three subtypes of HA (H1, H2, H3) and two subtypes of NA (N1, N2) have caused pandemics in humans [2, 255, 267, 271] (Table 2).

IAVs can be further described as low pathogenic (LP) or high pathogenic (HP) based on virulence in humans and/or poultry. Highly pathogenic influenza (HPAIV) viruses, H5N1 and H7N9, cause mortality and morbidity in millions of poultry when outbreaks occur [272-274]. HPAIV emerge from low pathogenic avian IAV (LPAIV) within domestic poultry populations. The emergence of HPAIV was a result of an insertion of basic amino acids at the HA cleavage site [275] that confers a selective advantage by altering the spacing in the cleavage site, making it more accessible by ubiquitous proteases [276]. Currently, the pandemic potential of HPAIV circulating in wild birds is being closely monitored in humans as ongoing phylogenetic analyses have revealed that antigenic drift continues to diversify the H5N1 virus [277-279].

LPAIV and HPAIV spillover into human populations, however, they have not yet shown the ability to transmit between humans. H5N1 first emerged in 1997 in Hong Kong where 18 human infections were identified and six of the patients died [280, 281]. Since 2003, 650 human infections with highly pathogenic H5N1 viruses have been reported to the World Health Organization (WHO) by 15 countries. About 60% of these people died from their illness [282]. Current concern with HPAIV is the potential for sustained inter-human transmission with the potential to cause significant morbidity and mortality.

EMERGENCE OF THE 2009 PANDEMIC H1N1

In late March 2009, an outbreak of a respiratory illness emerged in Mexico [283]. The causative agent was a novel H1N1 IAV that quickly spread across North America in April 2009 and across the world by May 2009 [284]. The 2009 pandemic arose through a reassortment of two preexisting swine influenza viruses (Figure 8), a Eurasian avian-like virus and a North American triple reassortant [284, 285]. Epithelial cells of the pig trachea produce both alpha-2,3-SA and alpha-2,6-SA [78, 284]. This is believed to be the reason why pigs can be infected with both avian and human IAV strains and serve as a ‘mixing vessel’ for the emergence of new viruses.

The 2009 H1N1pdm virus initiated the first influenza pandemic of the 21st century [285-287]. Most illnesses caused by the H1N1pdm were acute and self-limiting, with the highest attack rates reported among children, young adults and pregnant women. As compared to seasonal IAV, those infected with the H1N1pdm shared similar risk factors and common underlying conditions [288].

However, in contrast to seasonal IAV, most of the severe illnesses occurred in those younger than 65 years of age. Sources speculated that adults older than 60 years of age were spared because of prior exposure to antigenically related influenza viruses earlier in life, resulting in the development of protective antibodies [289, 290]. In the United States, of the patients who were hospitalized with H1N1pdm, 32-45% were under the age of 18 years, with approximately 9-31% requiring admission to an intensive care unit (ICU) [291] and 25-50% of patients were hospitalized or died with no previously reported coexisting medical conditions [292-296]. Together this illustrates the impact of viral genotype and host phenotype on disease progression. However, early in a new pandemic, it is challenging to predict the public health impact of a circulating genotype based on sequence alone. Improving our ability to predict the relationship of genotype and disease phenotype may provide better strategies for intervention and treatment.

H1N1 INFLUENZA ISOLATE SPECIFIC DIFFERENCES

ISOLATE SPECIFIC DIFFERENCES IN MICE

The immune response to IAV infection in general is highly linked to differences in disease outcome [91, 233, 297]. Our laboratory has developed a unique panel of closely-related, clinical H1N1pdm isolates enabling hypothesis-driven investigation into isolate-specific differences in host immune responses and viral determinants of the infection processes. Our panel of H1N1pdm clinical isolates were obtained from hospitalized patients (nasal swabs) from an on-going Severe Influenza Pneumonia Surveillance (SIPS) in the state of Kentucky [298].

Further details of the SIPS project can be found on the study website, http://www.kyflu.net.

Our laboratory isolated a panel of H1N1pdm strains from patients ranging in age from 31 to 58 years old with both males and females represented (Table 3) [298]. The length of hospital stay and clinical outcome varied among this population (Table 3). We hypothesized that differences in disease severity of hospitalized patients, despite associated comorbidities, may be due to genetic variations in the circulating viruses that affect the trajectory of pathogenesis. To test this hypothesis, we first screened these 9 isolates in the DBA2 mouse model. The following summarizes the major results from Camp et al 2013 [298]. Specifically, our data suggested that genotypic differences were present among these closely related genotypes.

Using a previously established DBA2 mouse model of IAV infection, we observed IAV isolate-specific differences in immune responses among the panel of H1N1pdm isolates [298]. We characterized each isolate for viral infection, immune response and lethality. Using a principal components analysis based on a panel of key cytokine/chemokine responses, immune responses clustered into four general groups which correlated with virulence from low (group1) to high (group 4). The first group included what we considered a typical non-lethal course of disease in mice, and was exemplified by infection with the seasonal strain H1N1and H1N1pdm viruses. A second group included those strains with moderate lethality in the mouse model, and was similar to the first group in course of disease, but had increased inflammatory cytokines (e.g., IL6, KC, and

GCSF) and chemokines (e.g., MIG). The third group showed the highest level of chemoattractant chemokines, (e.g., MCP1, MIP1α, and CXCL10) and the highest levels of inflammatory cytokines late in infection (e.g., IL6, TNF, IL1β), but were similar to Group 2 in terms of lethality. The fourth group of isolates represents the most lethal, and relative to all other isolates, these were characterized by reduced responses of all cytokines and chemokines analyzed. Most notably, these isolates failed to produce any IFNα/β or IL10 [298]. The host and viral factors responsible for these differences between isolates and the mechanisms of action involved remain unclear.

As mentioned above, pro-inflammatory cytokine and chemokines are critical for recruiting immune cells to the site of infection that are key to clearing the virus, as well as activating the adaptive immune response [299-301]. Of importance, infection of primary human epithelial cells with H1N1pdm have shown a diminished induction of innate immune responses as compared to seasonal H1N1 [90]. Notably, recent findings suggest genotype-specific differences among H1N1pdm viruses as shown by their ability to induce varying degrees of early host antiviral and inflammatory responses in human respiratory epithelial cells [91]. Together these findings propelled the objectives of my thesis.

OBJECTIVE OF DISSERTATION

HUMAN EPITHELIAL CELL CULTURE MODELS TO STUDY IAV

Animal models of influenza virus induced pathogenesis are essential for research efforts aimed at understanding the viral and host factors that contribute

to disease and transmission of influenza virus infection in mammals [63, 72, 302-305]. These models also allow discovery and preclinical testing of antiviral drugs and vaccines aimed at reducing morbidity and mortality in the human population. However, these models do not allow specific dissection of human-host influenza specific interactions and mechanisms. Culture systems of primary epithelial cells from human airways provide valuable *in vitro* models for characterizing cellular tropism and IAV induced cell-specific responses and infectivity and dissecting these mechanisms [66, 90].

Primary epithelial cell cultures offer numerous advantages, including greater control of experimental conditions and the ability to study epithelial cell function and specific responses in the absence of other cell types. When focusing on human disease, it is beneficial to use human cell lines to identify host-specific proteins associated with viral infection and replication to establish potential new antiviral targets. Information collected from the primary cell model can provide valuable information that would otherwise be difficult to obtain *in vivo*.

The use of polarized/differentiated, primary human cell culture models that contains both types of SA receptors represent a more comprehensive model for infection and may be important to the advancement of our understanding of virus-host interactions such as those that modulate the outcome of IAV infection and disease [59, 84, 86, 91, 306]. During the 2009 H1N1 pandemic, pre-existing immune status and the existence of underlying chronic conditions definitely contributed to patient outcome; however, it is not entirely clear why some 2009

H1N1pdm-infected patients developed severe disease but others did not. We hypothesized that disease severity of certain hospitalized patients, despite associated comorbidities, may be due, additionally, to subtle genotypic variations in the circulating viruses that effect cellular tropism and intracellular responses. To further test this hypothesis, we compared the responses to two H1N1pdm isolates in both undifferentiated and well-differentiated human bronchial epithelial cells.

HUMAN IMMUNE CELL CULTURE MODELS TO STUDY IAV

In agreement with studies in patient populations, H5N1increases inflammatory cytokine in primary human lung epithelial cells [84] and immune cells, specifically macrophages [307]. Additionally, excessive recruitment of pulmonary macrophages and neutrophils correlates with severe infection with pandemic 1918 H1N1 influenza virus in the lungs of mice [222]. Immunopathology at the site of influenza infection suggests a role for immune cells infiltrates in severe influenza infection [308, 309]. Production of pro-inflammatory cytokines by virus-infected monocyte/macrophages can potentially contribute to lung pathology by inducing the activation and migration of additional blood monocytes, as well as T and B cells to the site of infection. Additionally, pro-inflammatory cytokines such as IL1β, TNF and IFNα/β promote up-regulation of the MCP1, MCP3 and CXCL10 chemokines, resulting in amplification of the inflammatory/chemotactic signal and further recruitment of monocyte/macrophages and T lymphocytes to the site of infection [299]. Together, these data strongly suggest that innate cells and their associated

responses may effect influenza disease manifestation. To date there is significant gap in our knowledge of innate immune cells and their response to different strains of influenza virus and individual clinical isolates. Moreover, most of the studies published to date have focused on strains adapted to mouse and specific isolates of IAV. Hence my dissertation asks whether different phenotypic outcomes would arise from closely-related genotypes using primary cell culture models of human epithelial and macrophage cell culture models.

SPECIFIC AIMS

The increasing threat of epidemic and pandemic influenza underscores the need to better understand the immune response to influenza virus infections and to better understand the factors that contribute to different outcomes of disease. Epithelial cells and macrophages play central roles in the innate immunity and anti-viral defense against IAV. Severe disease outcomes are associated with hypercytokenemia and infiltration and response of macrophages in the lung [297, 310]. The main goal of this dissertation was to characterize IAV-host interactions and define the viral determinants involved in the early host immune response to infection differentiating two genetically similar 2009 H1N1pdm isolates from one another. This was examined with the following aims;

1) To compare the infection of well-differentiated primary human bronchial epithelial cells by two H1N1pdm and seasonal IAV isolates in terms of viral titers, gene expression profiles by microarray analysis, the integrity of the epithelial cell layer, and the dynamics of the host cytokine and chemokine responses.

2) To compare infection and dynamics of the host response to genetically similar H1N1pdm IAV isolates in human monocyte-derived macrophages (MDM).

3) To define the mechanism and map the isolate-specific immune phenotypes in MDM to specific viral molecular determinants.

Table 1. Description of influenza A virus proteins. Information extracted from (Lamb and Krug, 1996 and Palese and Shaw, 2007 Fields Virology). IFN, interferon; Nt, nucleotide.

Genome Segment	Protein Name	Length (Nt)	Amino Acids	Copies per virus	Function
1	PB2	2341	759	30-60	Internal, virus replication
2	PB1 PB1-F2	2341	757 87	30-60	Internal, virus replication Internal, induction of apoptosis
3	PA	2233	716	30-60	Internal, virus replication
4	HA	1778	566	500	Surface glycoprotein, viral attachment, antigenic determinant, and membrane fusion
5	NP	1565	498	1000	Nucleocapsid protein, genome packaging, RNA transcription, and vRNP nuclear import
6	NA	1413	454	100	Surface glycoprotein, antigenic determinant, viral release from host cells through sialidase activity
7	M1 M2	1027	252 97	3000 20-60	Membrane protein stability Membrance protein, assembly and proton channel
8	NS1 NS2 (NEP)	890	230 21	unknown 130-200	Internal protein, IFN antagonist Regulation of mRNA transcription and vRNP nuclear export

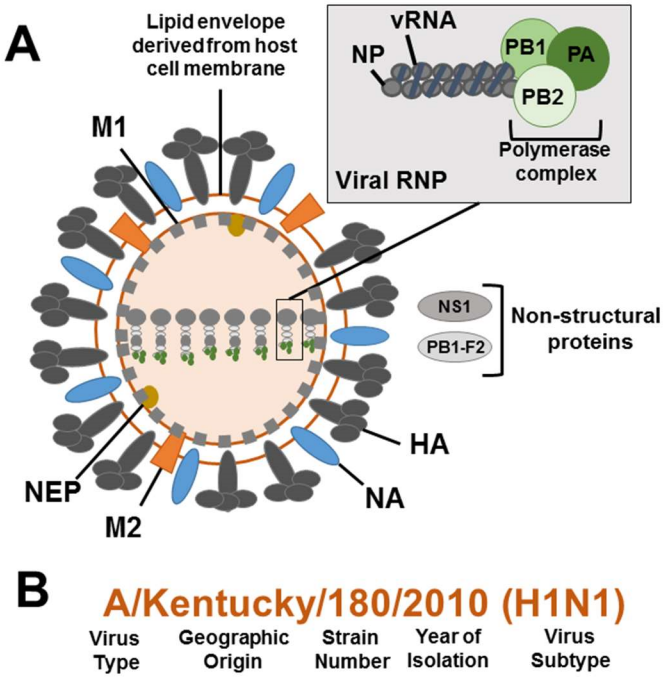

Figure 1. Schematic of Influenza A virion and nomenclauture. (A) Representation of influenza A virion and the associated proteins including both structural and non-structural proteins. (B) Description of how the nomenclatures of influenza viruses are represented in the literature and in this dissertation.

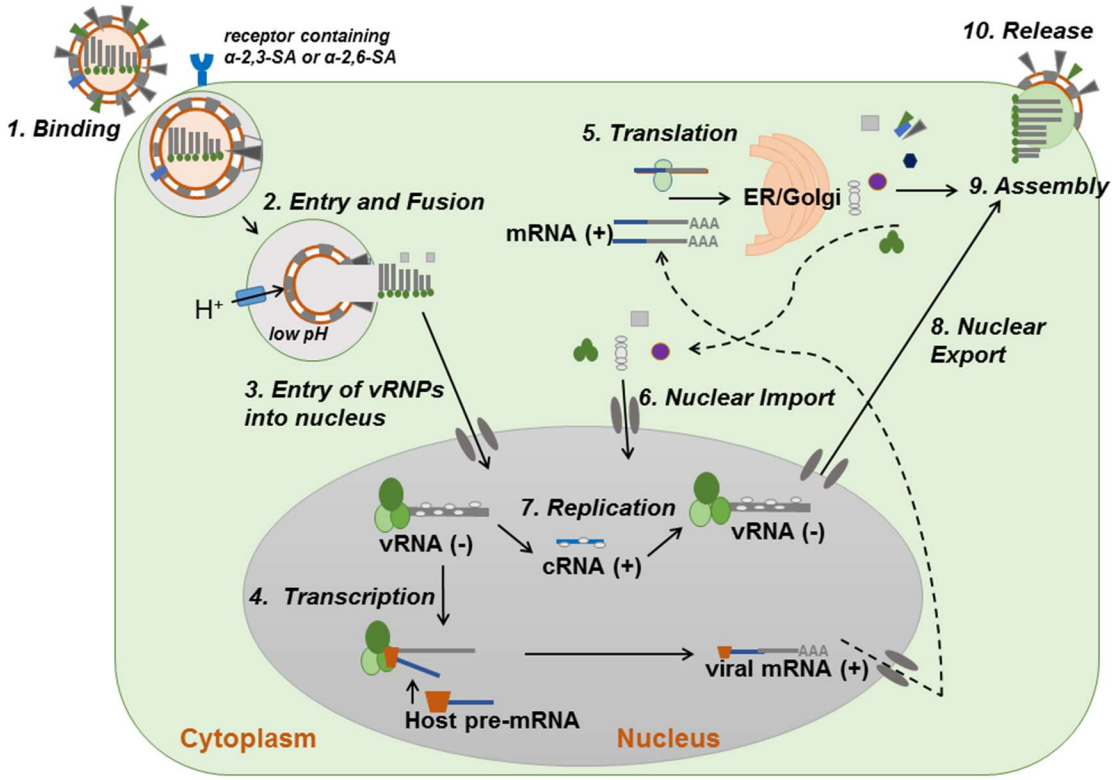

Figure 2. Life cycle of influenza A virus in cells. The virus binds to sialic acid residues on the cell surface and enters the cell by endocytosis. Influenza virsues enter through Clathrin-dependent and Clathrin-independent endocytosis and the vesicles formed then traffic through the endosomal pathways to the late endosome.The low pH in maturing or late endosomes triggers a conformational change of HA mediating fusion of viral envelope and endosomal membrane. The released genome in form of eight vRNPs translocates into the nucleus, where mRNA as well as vRNA synthesis take place. Viral proteins are then translated in the cytoplasm on ER-bound ribosomes and transported back into the nucleus to assist with viral replication. New viral proteins (PB1, PB2, PA, NP) assemble into vRNPs in the nucleus, and are exported by the help of M1 and NS2 and transferred to the budding site. The virus buds presumably by a concerted

interaction of the spike proteins and M1 and is finally released by M2-mediated membrane scission. SA, sialic acid.

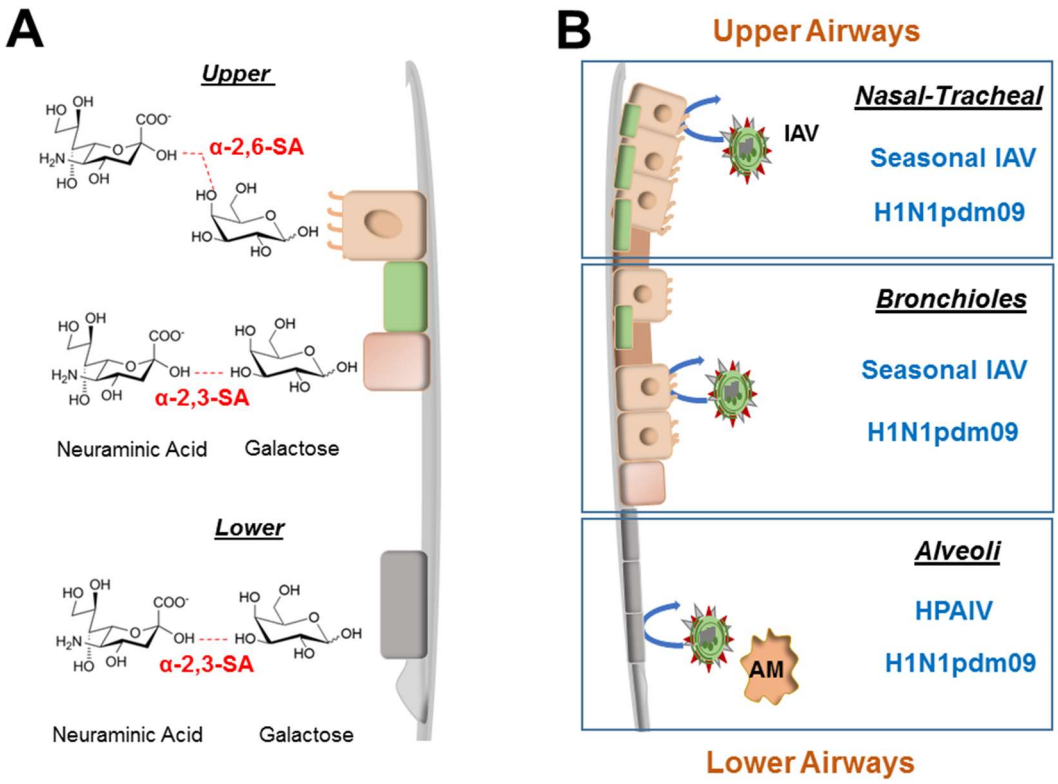

Figure 3. Schematic of the human respiratory tract and distribution of influenza A receptors. (A) Shows the distribution and chemical composition of sialic acid receptors located in the upper and/or lower respiratory tract. (B) The diversity of where Influenza A viruses infect in the respiratory tract is depicted here. Seasonal IAVs predominantly infect the upper airways whereas highly pathogenic avian influenza infects the lower airways. In 2009, the H1N1 triple reassortment emerged with properties of both upper and lower airway tropic viruses. SA, sialic acid; HPAIV, highly pathogenic avian influenza; pdm, pandemic; AM, alveolar macrophage

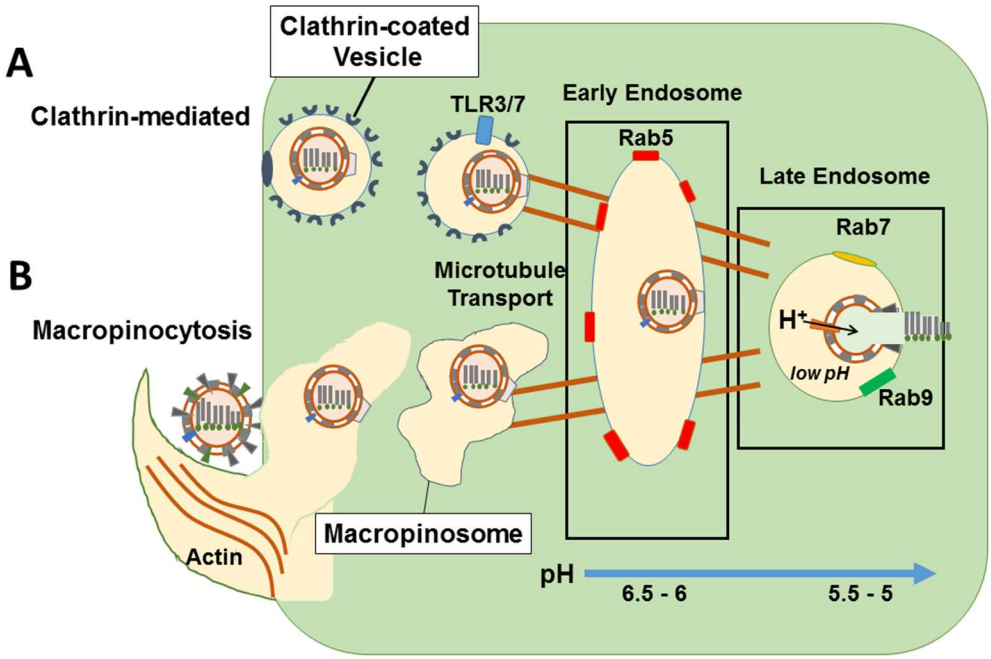

Figure 4. Schematic of two of the known entry pathways utilized by influenza A viruses. (A) Clathrin-mediated endocytosis begins by accumulation of clathrin adaptor proteins on the inside facing side of the plasma membrane, allowing clathrin to multimerize and form clathrin-coated pits. These pits are then pinched off from the plasma membrane by membrane scission proteins releasing the virus containing vesicle inside the cell within the clathrin-coated vesicle. (B) Macropinocytosis is characterized by actin-dependent reorganizations of the plasma membrane forming protrusions of the plasma membrane that bring the virus into the cell through an invagination of the plasma membrane. Once inside the host cell, both macropinosomes and clathrin-coated vesicles traffic from the early to late endosome via adaptor proteins Rab 5 and Rab 7. Once in the late endosome, a pH drop induces a conformational change in the viral envelope causing viral RNP to be released into the cytoplasm.

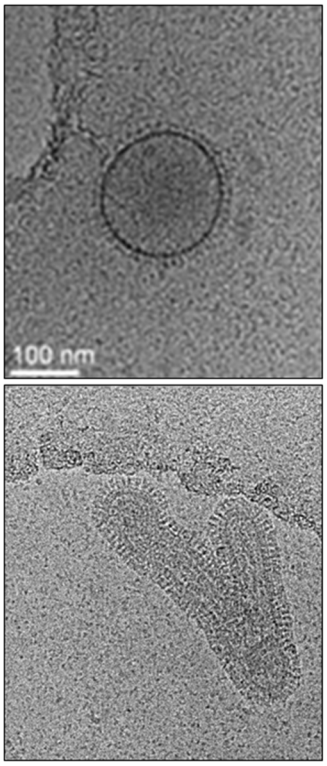

Figure 5. Cryo-EM micrographs influenza A virus structure. Influenza A viruses are pleiomorphic with both spherical (100-150nm) and filamentous viruses (250-400nm) existing in nature. SEM images were kindly provided by Dr. Jason Lanman and Amar Parvate, Purdue University Department of Biology. Scale bar: 100nm.

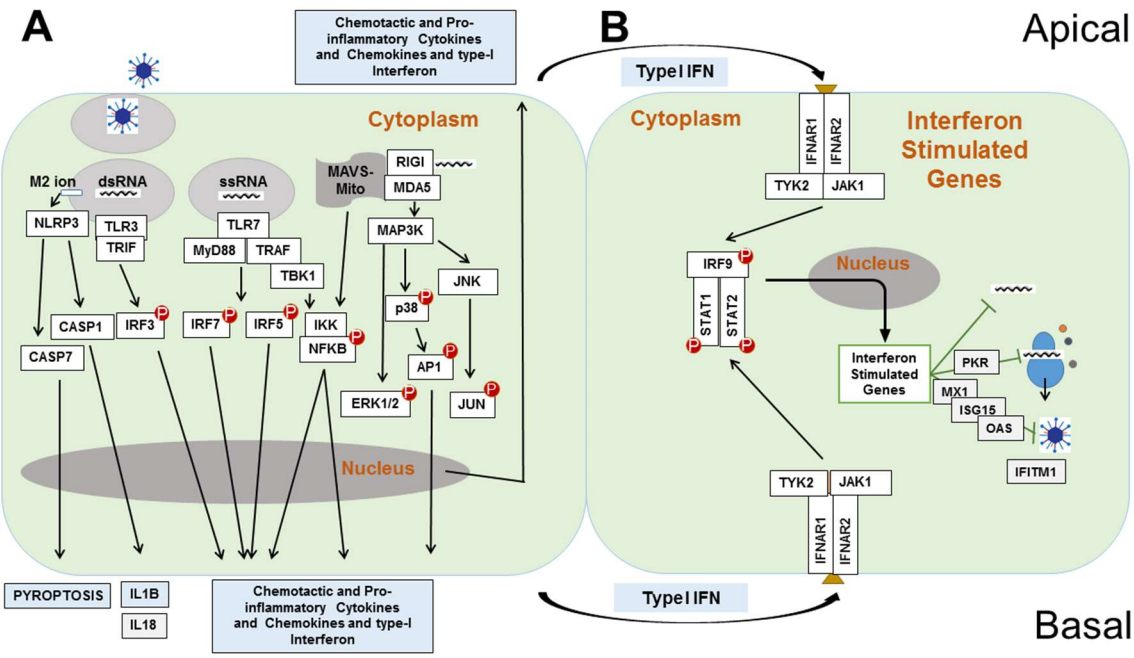

Figure 6. Current model of the activation of pattern-recognition receptors (PRRs) after IAV infection. (A) In infected cells, interaction of PRRs (TLR3, TLR7, RIGI, MDA5) with their specific pathogen-associated molecules (PAMPs) induces signaling thru NFkB, MAPK, IRF3 and 7 leading ultimately to secretion of cytokines, chemokines, and type I Interferon. (B) Type I interferon can further bind to IFNAR (interferon receptor) on bystander cell and induce signaling through STAT and IRF9 which activates interferon stimulated genes, which further block viral translation and replication. Mito, Mitochondria; IFN, Interferon.

Table 2. Description of influenza A subtypes resulting from antigenic shift which have historically caused pandemics.

Influenza A Virus Pandemics (Antigenic Shift)		
Year	Subtype	Severity of Pandemic
1889	H3N2	Moderate
1918	H1N1	Severe
1957	H2N2	Severe
1968	H3N2	Moderate
1977	H1N1	Mild
2009	H1N1	Moderate

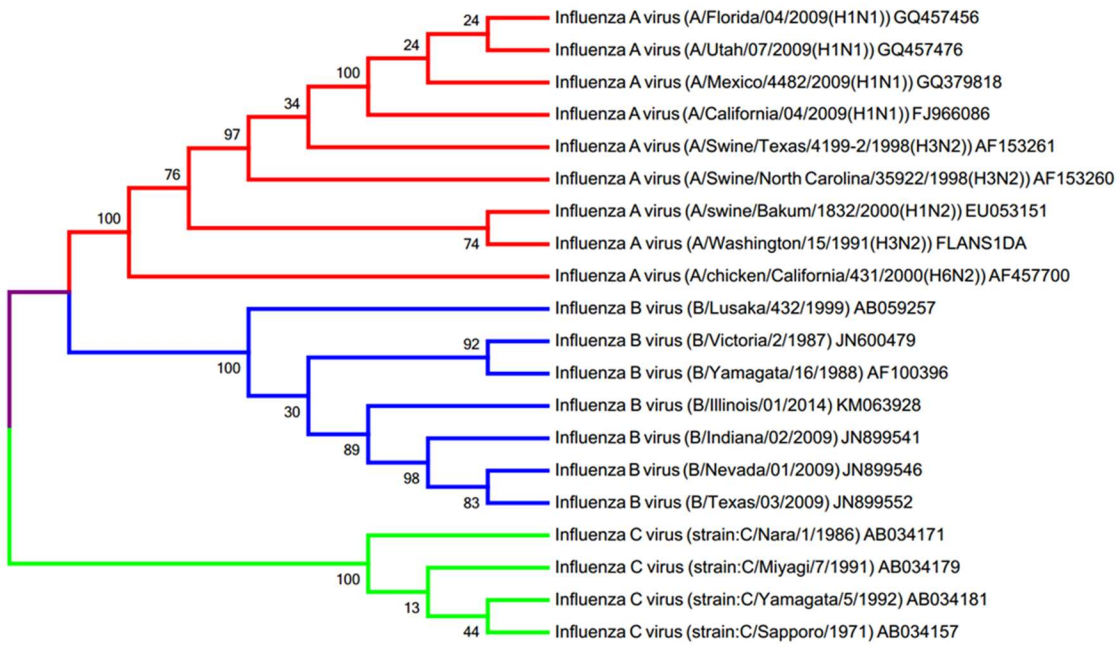

Figure 7. Phylogenetic tree demonstrating the variation in NS proteins of IAV, IBV, and ICV. The phylogenetic history was inferred by using the Maximum Likelihood method based on the Tamura-Nei model [1]. The tree with the highest log likelihood (-5152.9524) is shown. The percentage of trees in which the associated taxa clustered together is shown next to the branches. Initial tree(s) for the heuristic search were obtained automatically by applying Neighbor-Join and BioNJ algorithms to a matrix of pairwise distances estimated using the Maximum Composite Likelihood (MCL) approach, and then selecting the topology with superior log likelihood value. The tree is drawn to scale, with branch lengths measured in the number of substitutions per site. The analysis involved 20 nucleotide sequences. Codon positions included were 1st+2nd+3rd+Noncoding. All positions with less than 95% site coverage were eliminated. That is, fewer than 5% alignment gaps, missing data, and ambiguous

bases were allowed at any position. There were a total of 763 positions in the final dataset. Evolutionary analyses were conducted in MEGA5 [2].

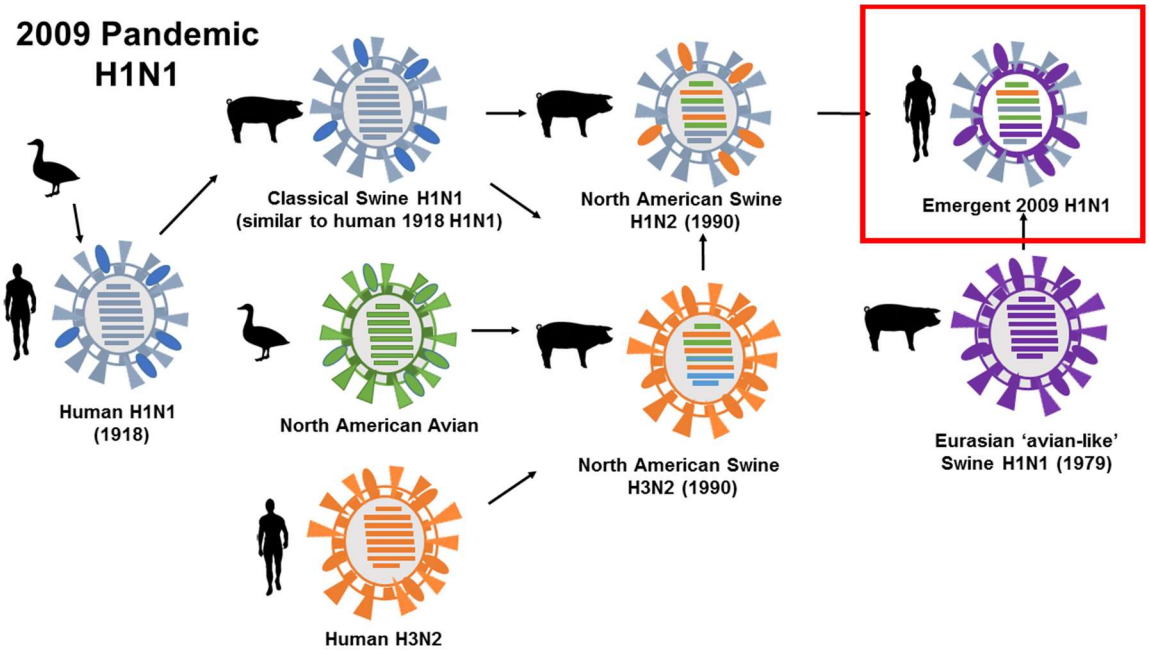

Figure 8. Depiction of emergence of 2009 pandemic (reassortment). (Adapted from Medina et al. Nature Reviews Microbiology 2011). The 2009 pandemic arose through a reassortment of two preexisting swine influenza viruses, a Eurasian avian-like virus and a North American triple reassortant. Two segments, NA and M, derived from the Eurasian avian-like swine lineage and six gene segments originated from the North American triple-reassortant swine lineage. Specifically the HA segment of the virus was genetically very similar to the 1918 H1N1 HA suggesting emergence from an avian source Epithelial cells of the pig trachea produce both alpha-2,3-SA and alpha-2,6-SA and could be the potential mechanism for the reassortment to occur in pigs. Pigs can be infected with both avian and human IAV strains and serve as a 'mixing vessel' for the emergence of new viruses such as the 2009 H1N1pdm virus.

Table 3. Panel of H1N1pdm clinical isolates obtained from hospitalized patients (nasal swabs) from an on-going Severe Influenza Pneumonia Surveillance (SIPS) program at the University of Louisville, Kentucky.

Patient ID (Case number)	Patient Age/Sex	Hospital Admission Date	Nasal Swab Sample Date	LOSΨ (Days)	Mortality
80	31/F	9/30/2009	9/30/2009	10	Died
96	51/M	10/24/2009	10/26/2009	4	Survived
99	35/F	10/28/2009	10/29/2009	3	Survived
104	58/M	10/30/2009	11/4/2009	2	Died
108	57/F	11/2/2009	11/3/2009	19	Survived
110	54/F	11/3/2009	11/4/2009	3	Survived
136	46/M	12/10/2009	12/11/2009	8	Survived
180	53/M	3/24/2010	4/1/2010	19	Died
190	55/F	4/10/2010	4/15/2010	12	Died

CHAPTER 2

EARLY HOST RESPONSES OF SEASONAL AND PANDEMIC INFLUENZA A VIRUSES IN PRIMARY WELL-DIFFERENTIATED HUMAN LUNG EPITHELIAL CELLS

OVERVIEW

Replication, cell tropism and the magnitude of the host's antiviral immune response each contribute to the resulting pathogenicity of influenza A viruses (IAV) in humans. In contrast to seasonal IAV in human cases, the 2009 H1N1 pandemic IAV (H1N1pdm) shows a greater tropism for infection of the lung similar to H5N1. We hypothesized that host responses during infection of well-differentiated, primary human bronchial epithelial cells (wdNHBE) may differ between seasonal (H1N1 A/BN/59/07) and H1N1pdm isolates from a fatal (A/KY/180/10) and nonfatal (A/KY/136/09) case. For each virus, the level of infectious virus and host response to infection (gene expression and apical/basal cytokine/chemokine profiles) were measured in wdNHBE at 8, 24, 36, 48 and 72 hours post-infection (hpi). At 24 and 36h post-infection, KY180 showed a significant, ten-fold higher titer as compared to the other two isolates. Apical cytokine/chemokine levels of IL6, IL8 and GRO were similar in wdNHBE cells infected by each of these viruses. At 24 and 36 hpi, NHBE cells had greater levels of pro-inflammatory cytokines including IFNα, CCL2, TNF, and CCL5,

when infected by pandemic viruses as compared with seasonal. Polarization of IL6 in wdNHBE cells was greatest at 36 hpi for all isolates. Differential polarized secretion was suggested for CCL5 across isolates. Despite differences in viral titer across isolates, no significant differences were observed in KY180 and KY136 gene expression intensity profiles. Microarray profiles of wdNHBE cells diverged at 36 hpi with 1647 genes commonly shared by wdNHBE cells infected by pandemic, but not seasonal isolates. Significant differences were observed in cytokine signaling, apoptosis, and cytoskeletal arrangement pathways. Our studies revealed differences in temporal dynamics and basal levels of cytokine/chemokine responses of wdNHBE cells infected with each isolate; however, wdNHBE cell gene intensity profiles were not significantly different between the two pandemic isolates suggesting post-transcriptional or later differences in viral-host interactions

INTRODUCTION

The 2009 pandemic H1N1 influenza virus (H1N1pdm) arose through reassortment of two preexisting swine influenza viruses, a Eurasian avian-like virus and a North American triple reassortant virus [311, 312]. Epidemiological data illustrated the speed of global spread of the 2009 pandemic virus; including significantly high infection attack rates in children and an 80% of H1N1pdm deaths in people younger than 65 years of age [313]. This was unlike seasonal IAV where morbidity and mortality are mainly seen in the elderly [314]. The illness associated with H1N1pdm infection was, however, very similar to seasonal influenza [315]. The risk factors associated with human cases of

H1N1pdm mirrored those of seasonal influenza [313], although in contrast to seasonal influenza, a greater proportion of severe and fatal cases had a pre-existing chronic illness [313, 314, 316]. The most common underlying chronic conditions among hospitalized patients were respiratory disease, asthma, cardiac disease, and diabetes [292, 313, 315]. Immunohistopathology of patients with lethal disease confirmed positive for H1N1pdm identified the major cellular targets of infection as being upper respiratory epithelial cells, type II pneumocytes, and occasionally macrophages, which is similar to the pattern previously observed in H5N1 cases [295].

Most seasonal IAV strains infect primarily the upper respiratory tract with limited lower respiratory tract involvement. The ability of H1N1pdm viruses to infect the lungs within lower respiratory track has been attributed to a broader specificity in the binding of the H1N1pdm surface HA with the alpha-2,3-SA (common on ciliated cells) and alpha-2,6-SA (common on non-ciliated secretory cells) [66, 74-76]. There are mixed conclusions in the field regarding what cell type is "readily" infected by seasonal influenza strains, with data supporting both ciliated and non-ciliated cell infections [61, 66]. Seasonal IAV and H1N1pdm viruses enter and replicate efficiently into non-ciliated cells which are present in the epithelial cell layer in both the large and small airways of the lower respiratory tract, while H5N1 enters and replicates more efficiently in ciliated cells within the small airways [74, 75, 83-86]. Hence, the spatial distribution and concentration of potential receptors associated within different areas of the respiratory tract and/or different cell types are integral in the study of IAV infection and disease [75, 88-

91]. Further, while the lung epithelium is a primary target for infection [46], it is a highly complex environment composed of a heterogeneous cell population, including secretory (Clara), goblet (secretory/mucus), ciliated, and basal cells that differ in frequency and distribution depending on location in the lung [317]. The use of polarized, primary cell culture models that contains both types of sialic acid receptors and represent a more comprehensive model for infection are important to the advancement of our understanding of virus-host interactions such as those that modulate the outcome of IAV infection and disease [59, 66, 84, 86, 306].

Early host responses elicited by IAV of host epithelial cells likely control the magnitude, duration and lethality of infection. Once infected by IAV, cells respond by eliciting antiviral response genes and pro-inflammatory/ chemotactic cytokines and chemokines [230, 231]. This initial innate immune response is triggered by pattern recognition receptors (PRRs) within the cell. PRR pathways further activate intracellular signaling cascades, such as nuclear factor-kappa beta (NFκB) and mitogen-activate protein kinase (MAPK). Activation of these pathways leads to the induction of inflammatory cytokines and type I interferon (IFN) secretion. This further stimulates the antiviral signals through IFN-stimulated genes (ISGs) [236, 237, 240, 241, 243, 244]. Pro-inflammatory cytokine and chemokine products are critical responses as they are important for recruiting immune cells to the site of infection that are key to clearing the virus, as well as activating the adaptive immune response [299, 301]. Of importance, infection of human epithelial cells with H1N1pdm virus have shown a

diminished induction of innate immune responses as compared to seasonal H1N1 [90]. Notably, recent findings suggest isolate-specific differences among H1N1pdm viruses as shown by their ability to induce varying degrees of early host antiviral and inflammatory responses in human respiratory epithelial cells [91].

To probe potential differences in early infectivity and host responses of cells infected with seasonal or pandemic IAVs, we utilized a polarized, model of primary, well-differentiated normal human bronchial epithelial (wdNHBE) cells. We hypothesized that early stages of infection in the airway epithelium may differ in terms of replication and host immune responses between a H1N1 seasonal isolate (A/BN/59/07) and two H1N1pdm strains shown to have fatal (A/KY180/10) and nonfatal (A/KY/136/09, A/BN/59/2007) outcomes in hospitalized patients (Table 4) [298]. The two H1N1pdm clinical isolates (KY180 and KY136) differ in their pathogenicity and cytokine/chemokine profiles in a DBA/2 mouse model [298]. In this study, we demonstrate a comparison of infection of wdNHBE cells with each IAV isolates show differences in virus titers and the dynamics of the host cytokine and chemokine responses. We show that infection with the lethal H1N1pdm isolate (KY180) alters the structure and cellular integrity of the epithelial layer, replicates more efficiently, and results in an increased, polarized pro-inflammatory cytokine and chemokine responses. Interestingly, the microarray profiles of the antiviral signaling pathways do not correlate with differences in the virus titer of host cytokine and chemokine responses. This

suggests that post-transcriptional events may mediate the isolate-specific nature of the host cytokine and chemokine responses.

METHODS

Viruses and cells. The 2009 H1N1pdm IAV strains used herein were A/KentucKY180/2010, (KY180), and A/KentucKY136/2009, (KY136), from nasal swabs taken from a fatal and non-fatal case, respectively [298]. The GenBank accession numbers for KY180 and KY136 are provided in Table S1. The seasonal H1N1 IAV vaccine strain A/Brisbane/59/2007 (BN59) was kindly provided by the Centers for Disease Control and Prevention, Virus Surveillance and Diagnosis Branch, Influenza Division. Viral seed stocks were prepared as previously described [298]. Virus titers were determined by $TCID_{50}$ (50% tissue culture infectious dose) using MDCK (Madin-Darby Canine Kidney Epithelial Cells) as described previously [298] and calculated using the method of Reed and Muench [318].

All cell culture reagents were purchased from Invitrogen unless otherwise noted. The human lung bronchial epithelial (Calu3), human adenocarcinomic alveolar basal epithelial (A549), and MDCK epithelial cells (ATCC) were cultured in Dulbecco's minimum essential medium supplemented with 5 mM L- glutamine, 1% pen-strep and 10% fetal bovine serum at 37°C under 5% CO_2. Undifferentiated (udNHBE) cells were purchased from Lonza and cultured according to the suppliers instructions in serum-free, hormone supplemented bronchial epithelial growth media.

Primary wdNHBE cells (EpiAirway PC-12, MatTek Corporation) were shipped in 12-well plates with agarose embedded in the basal layer and air apically after being maintained for 28 days under an air-liquid interface. Upon arrival, the transwell inserts were removed and placed into a 12-well plate with media in the basal compartment (AIR 100 complete growth media, MatTek). No media was added to the apical layer. Cells were incubated at 37°C, 5% CO_2 and the basal media was changed after 24 h. At this point the cells were ready for infection and this is described in the next section.

***In vitro* IAV infection.** Infection of continuous and primary cells lines were performed in triplicate for measurement of virus production, immune responses or microarray studies. Each experiment (except for microarray) was replicated three times. Calu3, A549, MDCK and udNHBE cells were infected with KY180, KY136, BN59 or mock-infected (using viral growth media as specified in prior section) at a multiplicity of infection (MOI) of 3 for 1 h at 37°C, 5% CO_2. IAV infection of Calu3, A549 or MDCK included 2 µg/ml of tosylsulfonyl phenylalanylchloromethyl ketone-treated trypsin (TPCK, Sigma) and 0.2% BSA in the media.

WdNHBE cells were washed twice with Dubelcco's phosphate buffered saline (DPBS) to remove mucus accumulation and infected at an MOI of 3 in triplicate in replicate experiments from a total of three donors. After 1 h, the apical layer was washed twice with DPBS to remove unbound virus. Basal medium was removed and replaced with complete medium. At each time point analyzed, the basal media was removed and apical layer washed twice with 0.5

ml DPBS supplemented with 0.2% BSA and stored at -80°C until use. Cells were collected in TRIzol and stored at -80°C until used for RNA and protein extraction.

Quantitative RT-PCR (qRT-PCR). Total RNA from each set of viral-infected cells was extracted at designated time points using TRIzol as described by Invitrogen. cDNA was synthesized from total RNA with random hexamer primers and Superscript III reverse transcriptase (Invitrogen). Gene specific primers were used to amplify the HA genomic RNA using SYBR green select (Invitrogen) and detected with a 7900HT Real-time PCR System (Applied Biosystems). The amount of HA copy number was determined by extrapolating the Ct of each replicate against the standard curve generated using 10-fold dilutions of HA plasmid with known copy number. The sequences of the forward primers for H1N1pdm were 5`-CACCAGTCCACGATTGCAATA-3` and for BN59 5`-GAGTAGAGGCTTTGGATCAGGA-3`. The reverse primer was the same for both H1N1pdm and seasonal (5`-ATGGGAGGCTGGTGTTTATAGC-3`).

Quantification of apical and basal levels of virus and immune responses in wdNHBE cells. Virus titers and cytokine/chemokine protein levels were measured in basal and apical supernatants in two experiments with two donors. Virus titer was measured by $TCID_{50}$ as discussed above. We measured levels of CCL2/MCP-1, CCL5/RANTES, IL6, CXCL8/IL8, G-CSF, GM-CSF, CXCL1/GRO, IFN-α, CCL4/MIP-1α, CXCL10/IP-10, IL10, and TNF using multiplexed arrays according to the manufacturer's protocol (Millipore) using a Luminex 100™ machine. Concentrations for each secreted cytokine and chemokine were determined using standard curves and Luminex xPONENT® software.

Microarray studies. Total RNA was extracted by TRIzol from three replicates of virus-infected or mock-infected wdNHBE cells from a single donor and further purified using RNeasy kit (Qiagen). The samples were run in triplicate on Affymetrix HG-U133 plus 2.0 chips (Affymetrix) and processed according to the manufacturer in the Microarray Core facility at the University of Louisville. The raw data have been deposited in a Gene Express Omnibus (GEO). The GEO accession number is GSE48466. Prior to statistical analyses, raw data were processed by Plier Workflow normalization method using Gene Console software (Affymetrix, version 1.3.1). After normalization, data were $\log_2$ transformed and differentially expressed genes (DEGs) were identified by one-way analysis of variance (ANOVA) using Partek Genomics Suite 6.5 software. Fold-change and p-values were calculated for each virus infection, as compared to the mock-infected. Principal component analysis was conducted as a quality control measure to ensure the three replicates per viral treatment grouped together with limited variation. The data set was further filtered to select statistically significant genes and corrected using a p-value of 0.05 with a 2-fold cut-off. Data filtering and pathway analyses were performed using Ingenuity Pathway Analysis (IPA, Ingenuity Systems) software.

Immunohistochemistry. Tissues were fixed in 10% buffered formalin, processed, and paraffin embedded. Four-micron thick sections from infected wdNHBE cells at 36 hpi were processed by immunohistochemistry (IHC). Antigen retrieval and staining of the paraffin-embedded sections of the wdNHBE cells were performed as others described [319]. Briefly, paraffin was removed;

sections were incubated with pronase and blocked with H_2O_2 in Tris-buffered saline and with avidin/biotin blocking kit (Vector Labs). The slides were incubated with primary antibody specific for NP protein (East Coast Bio), blocked with goat serum, and then incubated with VECTASTAIN ABC kit (Vector Labs). Development was then performed using either diaminobenzidine (Vector Labs), and secretory cells were counterstained with Alcian Blue (Sigma) and mounted with Permount (Fisher). Cell layers were measured using Zeiss software measurement tool using a 10X objective. Five pictures with 3-4 measurements per picture were taken. Five images per slide were used to quantitate cell layer thickness (3-4 segments/image).

Statistical analysis. The differences of $\log_{10}$-transformed viral titers among different viruses at different time points post-infection and the quantitative cytokine and chemokine mRNAs and proteins of influenza virus-infected cells were compared by using one-way ANOVA followed by a Bonferroni multiple-comparison test, unless otherwise stated. Differences were considered statistically significant at a *p*-value less than or equal to 0.05. The statistical analysis was performed using Graph-Pad Prism 5.04 and Partek Genomics Suite 6.5 software.

RESULTS

Kinetics of viral replication of pandemic and seasonal H1N1 isolates in continuous and primary cell lines. To select a cell type for microarray and cytokine studies, we used several cell types (primary and continuous) to screen for potential differences in the ability to infect and produce infectious virus among

the pandemic (KY180 and KY136) and seasonal (BN59) isolates. We chose Calu3, A549, udNHBE, and wdNHBE cells and an MOI of 3 for this study. We included primary cell lines (udNHBE and wdNHBE cells) to ascertain if a more complex cell culture model would reveal greater differences. Differences in entry were anticipated as the KY180 has a D222G signature in the HA [298]. The udNHBE was included to determine the general influence of the alpha-2,3-SA (common on ciliated cells) in the wdNHBE cells as compared to the alpha-2,6-SA (common on non-ciliated secretory cells) in the udNHBE cells. Supernatant was collected over 3 days to measure the kinetics of each virus with the $TCID_{50}$ assay.

All three isolates infected and produced infectious virus in the all cell types apically (Figure 9A-D). No virus was detected in basal supernatant of infected cells across all time points (data not shown). The wdNHBE as compared to the udNHBE cells conferred a distinct advantage showing a 2-3 fold higher level production of infection virus over time suggesting the importance of the alpha-2,6-SA (Fig 9A versus 9B). In the primary wdNHBE cells, the titer of all three isolates peaked at 24 hours post-infection (hpi) (Figure 9A). KY180 showed significantly higher levels of virus at 24 hpi than KY136 and BN59 apically (Figure 9A). In udNHBE cells, significant differences occurred between isolates over time (Figure 9B). In the A549 cells, viruses peaked at 36-48 hpi at the highest levels of any of the cells (Figure 9C). Pandemic isolates replicated more efficiently at 24 hpi as compared to the seasonal isolate (Figure 9C). In the Calu3 cells, no significant differences in replication occurred between isolates over the

time course of infection (Figure 9D). Given the greater differences between KY180 and the other viruses, the primary wdNHBE cell, a physiologically relevant model, was chosen for further analyses. The level of viral RNA as measured by the HA was assessed in NHBE to further explore the difference in viral titer. The viral RNA levels were similar among all three isolates at 24 hpi suggesting that another mechanism was responsible for the higher levels of virus such assembly of budding.

Infection of the wdNHBE cells was confirmed by IHC for each isolate as at 36 hpi (Figure 10 A-D). The 36h time point was chosen based on preliminary studies measuring the level of IFNβ which peaked at 36 hpi (data not shown) coupled with the differences in the viral titer data. Staining for IAV nucleoprotein (NP) showed a similar distribution of infected cells for all three isolates (Figure 10 A-D).

Cytokines and chemokines elicited in wdNHBE cells by H1N1pdm IAV isolates show different trajectories. Differences in replication among the three H1N1 isolates prompted us to ask whether differences occurred in the levels of cytokine and chemokine secreted from the infected wdNHBE cells. We analyzed the levels of 12 cytokines and chemokines over time in the apical and basal medium (Figure 11 and 12). At 24 and 36 hpi, both H1N1pdm isolates showed greater levels of pro-inflammatory markers, apically (CCL5, GM-CSF, CXCL10, MCP1, CCL4) and basally (CCL5, IL6, TNF), compared to BN59 (Figure 11 and 12). The concentration of apical IL6, IL8 and GRO secreted by cells were similar between all isolates (Figure 11). IFNα was secreted apically, and not basally, in

cells infected by pandemic or seasonal isolates. IL10 occurred in trace amounts apically and was absent basally in all three isolate infected cultures. Overall, the patterns were fairly similar for pandemic isolates in the apical wash. Significant differences were seen between isolates in the basal culture supernatants (Figure 13). The only notable differences between KY180 and KY136 were the greater levels of CCL2, IL8, IL6 and CCL5 in the basal media at 36 and 72 hpi (Figure 13).

Microarray analyses of NHBE cells infected with seasonal or pandemic isolates. To complement our cytokine and chemokine studies, we measured differences in gene transcription levels at 36 hpi by microarray. Overall, cells infected with KY180 or KY136 had roughly 2,000 genes that were significantly up- or down-regulated as compared to mock-infected, whereas the seasonal BN59 isolate had only 360 genes significantly up- or down-regulated (Table 5). A Venn diagram shows the agreement between the three lists of genes (Figure 14A). There were 355 significant DEGs ($p<0.05$) in wdNHBE cells common to all three isolates at the 2-fold cut-off (Figure 13A); of which, many of the genes were from the early innate immune response pathways (Table 6). For all three IAVs the largest category of up-regulated genes was the ISGs (e.g., RSAD2, IFIT2, IFI44L, IFIT3, OAS1, OASL, MX2, STAT1) (Tables 6). Other genes up-regulated by all three isolates included interferon-induced chemokines (e.g., CCL5, CXCL9, CXCL10, and CXCL11), type III-IFN (e.g., IL29, IL28A and IL1A), PRRs (e.g., DDX58, IFIH1, TLR3, MYD88, CASP1), and other regulatory factors (e.g., IDO1, SOCS, EIF2AK2). Surprisingly, when a 2-fold change cut-off with a significance

of $p<0.05$ was applied there were only three genes unique to BN59-infected cells, whereas KY180 and KY136 had 279 and 326 unique DEGs respectively.

We noted 1647 genes that were commonly expressed in KY180 or KY136-infected NHBE cells that were not significant in the BN59-infected cells (Figure 14). When comparing global gene expression levels, H1N1pdm-infected wdNHBE cells showed greater fold-changes in transcription as compared to seasonal IAV (Figure 14B). Cells infected with H1N1pdm isolates had very similar levels of global gene expression with KY136 showing slightly greater up-regulation at 36 hpi (Figure 14B). Genes common to both KY180 and KY136-infected cells but not BN59 included transcription factors (cMYC, CDK1, SP1, SOX9, and ATF3), keratinocyte factors (KRT24 and KRT6B), defensins (DEFB1), and protein folding proteins (HSPA6). Also significant were genes involved in activating signal transduction pathways through toll like (TICAM) and the chemokine receptors, CCR4 (Table 7) and apoptosis. The similarities of KY180 and KY136 to each other and their differences to BN59 are further revealed upon comparison of the raw numbers of genes within the top canonical pathways, IFN signaling and communication, that were up- and down-regulated were similar between KY136 and KY180-infected NHBE cells (Figure 15A). Both KY180 and KY136 differed with the pattern shown by BN59-infected NHBE cells (Figure 15A).

We further conducted pathway analyses using the Ingenuity Pathway Analysis (IPA) to identify the intracellular signaling pathways that were most significantly represented in seasonal and pandemic infected cells using Fisher's

Exact Test (Table 8). The top two ranking pathways for all three viruses were the same; IFN signaling and communication between innate and adaptive immune cells. The remaining three pathways and ranking differed in importance. The role of PRRs was shared but greatest for KY136. The importance of the complement system was suggested for only KY180, while antigen presentation was suggested for KY136 and BN59. Finally the aryl hydrocarbon pathway was significant for KY180 and KY136 but not BN59. Combined with the individual gene analysis, the pathway analysis underscores important similarities but resulting gene specific differences.

wdNHBE cell layer integrity changes overtime after infection. When evaluating the cells by IHC, we observed changes in epithelial layer integrity in infected epithelial layers compared to mock-infected wdNHBE cells (Figure 10). Cultures infected with KY180 appeared thinner than both mock-infected cells and cells infected with the other IAV isolates (Figure 10). To address this observation, we further analyzed paraffin-embedded sections by measuring the distance from the collagen layer to the top of the epithelial layer (Figure 16A). Significant differences were noted among all isolates compared to the mock-infected control. Cells infected with KY180 showed the smallest distance, followed by BN59 and KY136 as compared to mock (Figure 16A).

Having observed these differences, we turned to the microarray data to determine whether the observed changes in epithelial cell layers could be explained at the transcriptional level (Figure 16B). We evaluated expression levels of DEGs in bronchial epithelial cells after the air-liquid interface culture

process. These genes include those associated with cell adhesion, transport, and cilia formation and function, such as SPRR1A, KRT6B, KRT24, ASAM, FOXJ1, MUC5B, AKAP14, and PROM1 (and apoptosis genes CASP7 and BAK1). According to Ross *et al.* (2007) wdNHBE cells have decreased expression of the keratinocyte marker genes and an increased expression of genes involved in cell signaling, cilia formation and also cilia function [320]. We saw an increase in expression of keratinocyte genes and a decrease in expression of cilia genes in wdNHBE cells. Cells infected with KY180 showed a greater difference in gene expression levels over the mock compared to KY136 and BN59 (Figure 16B).

DISCUSSION

The contribution of the early host-virus interactions to the progression of disease remains a critical question. Using *in vitro* models that closely mimic physiological conditions within the lungs in evaluating respiratory infections is an important approach in elucidation of potential differences between strains with different virulence [321, 322]. For example, recent studies evaluating the pathogenesis of 2009 H1N1pdm in bronchial epithelial cells suggest that differentiation status of bronchial epithelial cells has a profound impact on the infection efficiency of different influenza strains and the host innate immune responses [75]. We sought to compare host responses in a wdNHBE cell culture model to determine whether lung epithelial cells infection differed between seasonal and pandemic influenza isolates.

Recently, Zeng *et al*. evaluated extracellular inflammatory molecules secreted by polarized bronchial epithelial cells (Calu-3) and pharyngeal cells (Detroit 562) infected with 2009 H1N1pdm compared to seasonal. They show the two isolates are considerably different in terms of inflammatory responses, such as type-I IFN, IL6, CXCL10, and TNF, as well as replication efficiency, with H1N1pdm being more efficient [90]. Furthermore, a study comparing different H1N1pdm isolates in udNHBE cells show critical differences in levels of cytokines and chemokines elicited from cells infected with closely-related influenza isolates [91]. They show distinct differences in viral infectivity as well as differences in IFNβ levels between 2009 H1N1pdm (CA/08, Mexico/4108, TX/15) and the seasonal H1N1 (Solomon/03) [91]. The differences seen in these models, prompted us to compare the phenotype induced by our genetically, closely-related H1N1pdm and seasonal influenza isolates in wdNHBE cells.

To select the optimal cell line for microarray and immune response studies to probe regulatory differences among pandemic and seasonal isolated, we screened several continuous and primary cell lines. We show that H1N1pdm isolate KY180, which was previously reported to be lethal in mice and humans [298], produced significantly more virus in NHBE cells than the other isolates from 24-72 hpi. The udNHBE cells were less permissive for production of virus presumably due to less differentiation and lack of the alpha-2,6-SA. Previous reports show productive replication of H1N1pdm in NHBE cells [323]. Differences in viral titers among strains of the same HA subtype (i.e., H1) in wdNHBE cells have not been reported previously. Interestingly, an examination

of the viral genomic HA RNA levels did not suggest that this was due to replication levels. Future studies to understand the reason for a higher virus titer will focus on the potential of differences in assembly and/or budding.

Because regulation of innate immunity by viruses is a key determinant of the subsequent host immune response and clinical outcome, we evaluated the cytokine and chemokine secreted apically and basally in wdNHBE cells. IAV infections lead to a variety of intracellular responses, inducing innate immune signaling cascades which serve as the first line of defense against the invading virus [324-326]. Cytokines and chemokines produced by these pathways play an important role in the production of airway inflammation and recruitment of immune cells to the site of infection. A key finding from our data was the greater levels of basolateral secretion of pro-inflammatory cytokines (IL6, CCL5, IL8 and CCL2) by wdNHBE infected with the lethal KY180 isolate as compared to KY136 and BN59. We are aware of only two studies of IAV infection in primary NHBE cells that have looked at secretion of cytokines and chemokines from both the apical and basal side of the epithelial culture [327, 328]. However, these studies were limited to the earliest time points and did not look at the later time points where we saw the greatest differences. We speculate that differences in basolateral signals such as CCL5 from epithelial cells may play a role in the recruitment, activation, and responses elicited by monocytes. Further, the magnitude of the CCL5 response may give rise to differences in outcome [328]. Recently, in mice, apoptosis of virus-infected macrophages was prevented by CCR5/CCL5 [329]. CCL5 has been demonstrated to send an anti-apoptotic

signal to the cell via the Akt and Erk1/2 pathways, which could support an increase in survival and scavenging of recruited and resident macrophages.

With replication and apical/basal chemokine/cytokine data suggesting differences among the isolates, we sought to evaluate the intracellular signals gene expression patterns triggered by the virus. These intracellular responses include the double-stranded vRNA recognition by PRRs [330], Nod-like receptors, TLR, and the MAPK pathway, which have all been reported to be important to control of cellular responses against invading pathogens [331]. Three different types of MAPKs, the ERKs, the JNKs, and ERKs, contribute to the generation of cytokines and chemokines, such as IL8, CCL5, and TNF [312]. We hypothesized that differences in up- or down- regulation of genes involved in these pathways would explain the phenotypic differences observed in replication and secretion of cytokines and chemokines in our wdNHBE infection model. Strikingly, we saw no significant differences in transcriptional profiles between KY180 and KY136 within these pathways; indicating a potential for differences in post-transcriptional regulation by KY180.

IAV have been shown to induce apoptosis *in vitro* and *in vivo* [332-336]. Inducers of apoptosis in epithelial cells include dsRNA signaling through PRRs, NS1, and NA. In our wdNHBE model we observed a change in the epithelial cell layer structure after infection. We observed a loss of monolayer depth and desquamated cells as seen in previous models of infection [336]. We sought to explain this change in phenotype using our microarray data. We found factors, previously shown to alter the epithelial phenotype of the cell, are differentially

regulated in KY180 compared to the other isolates including KRT genes and those involved in cilia formation (FOXJ1, AKAP14, and PROM1) (Figure 16B) [320]. Furthermore, we looked at apoptosis pathways to determine whether these pathways were different between infections. We found that KY180 and KY136 significantly up-regulated BAK1 and Caspase 7, an apoptosis inducer, and down-regulated the CDK1 gene, a cell division control protein (Figure 15 A-B). This suggests any differences in phenotype, such as replication and cytokine and chemokine secretion, between isolates may be related to cellular integrity and state of differentiation.

Limited research is available providing a comprehensive gene expression profile of DEG in response to IAV infection of wdNHBE cells. In a recent study conducted by Lee *et al*., on type I-like alveolar epithelial cells infected with H1N1pdm (A/Hong Kong/415742/2009) and seasonal H1N1 (A/Hong Kong/54/1998), 88 genes were found to be up or down-regulated in response to seasonal H1N1 infection while only 18 genes were affected in H1N1pdm infected cells [337]. IFN-induced genes, including IL28A, IL28B, IL29, IRF9, ISG15 and MX1, were significantly up-regulated in response to both H1N1pdm and seasonal H1N1 infections and to a similar degree. Additionally, Ioannidis *et al*. demonstrated that, in IAV infected primary differentiated lung epithelial cells, the most represented category of DEGs included the IFN-inducible genes, IFN-induced cytokines and chemokines, and PRRs [333]. Our data agree that both seasonal and pandemic isolates up-regulate IFN-induced genes; however, in our model, the degree of the response was greater in H1N1pdm infected cells

compared to seasonal. We saw similar trends overall in terms of an elevated type-I IFN and antiviral responses, and additionally, we show a difference in genes involved in cellular differentiation.

In summary, we demonstrate the value of the wdNHBE cell model in understanding the early events of viral infection, and unraveling clues to strain-specific, and pandemic versus seasonal virus-host interactions. Our studies provide preliminary evidence that strain specific differences between closely related pandemic viruses during infection of the lung epithelium may contribute to the trajectory of host responses and pathogenesis observed in mice and in humans [298]. By directly comparing pandemic and seasonal IAV isolates, we found unique differences in virus titer and cytokine and chemokine secretion between isolates. Intriguingly, there are only 22 amino acid mostly synonymous changes between KY180 and KY136 and of these only one of these so far in the HA (D222G) has been suggested to correlate with higher virulence in patients [338, 339]. Future studies will evaluate the role of the D222G and other amino acids in conferring the greater levels of virus, basal secretion of cytokines and apparent epithelial damage noted by KY180. Further, future studies that couple *in vitro* human primary cell culture models with immune cells will be an important step in developing a fuller understanding the outcomes of viral-host interactions.

Table 4. Seasonal and pandemic IAV isolates used in this study.

Virus	Subtype	Source	Phenotype
A/KY/180/2010	H1N1pdm	Fatal Case	Lethal
A/KY/136/2009	H1N1pdm	Non-fatal Case	Non-lethal
A/BN/59/2007	Seasonal H1N1	CDC	Non-lethal

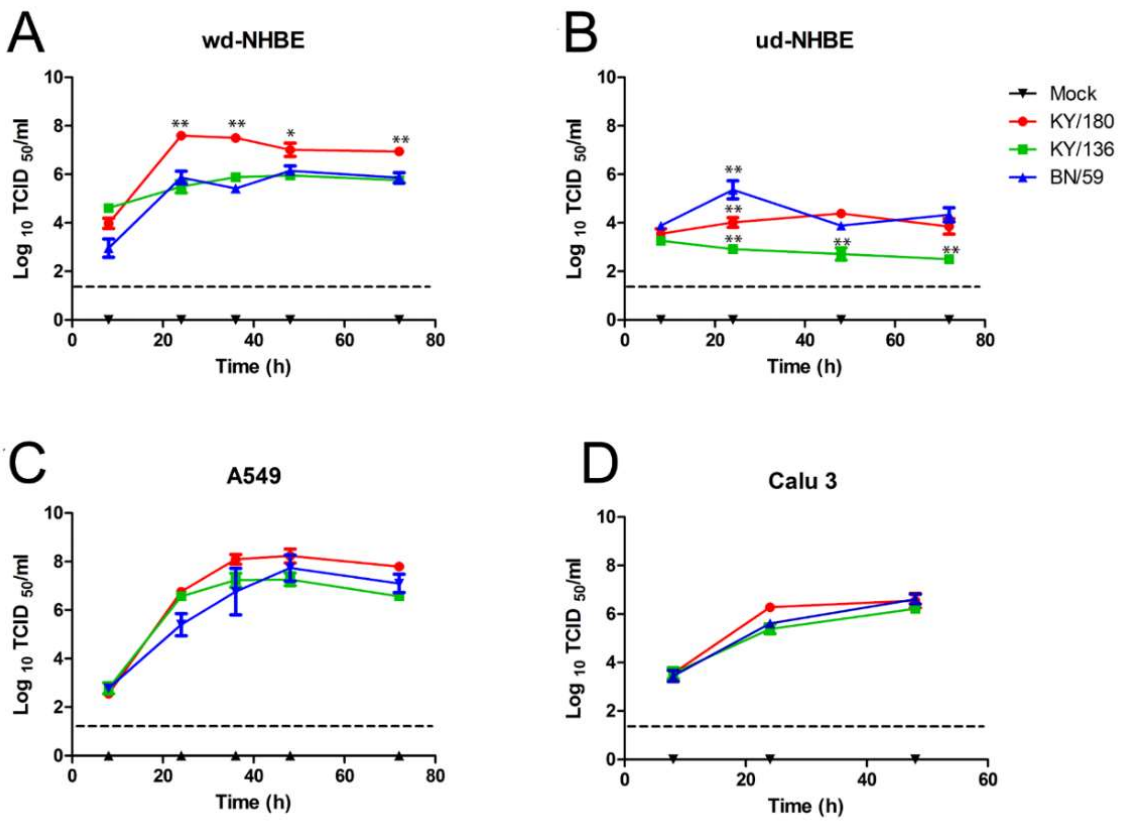

Figure 9. Virus titer detected in supernatant from cells infected seasonal and pandemic IAVs. (A) wdNHBE, (B) udNHBE, (C) A549, and (D) Calu3 cells were infected with 3 MOI of seasonal (BN59) or pandemic (KY180, KY136) viral isolates and apical wash from wdNHBE cells and supernatants from udNHBE, A549, and Calu3 cells were collected at 8, 24, 36, 48, and/or 72 hpi. The virus titer was determined using a $TCID_{50}$ assay. In (E), the amount of viral HA RNA in cells was quantified by qRT-PCR wdNHBE cells using the Ct method. Data are presented as the mean±SEM of the virus titer pooled from 3 replicates from three independent experiments with 3 donors (A-D) or 1 donor (E). Asterisks indicate significance of $p<0.05$(*), $p<0.01$(**), and $p<0.001$(***) respectively. The dotted line indicates the limit of detection of the $TCID_{50}$ assay.

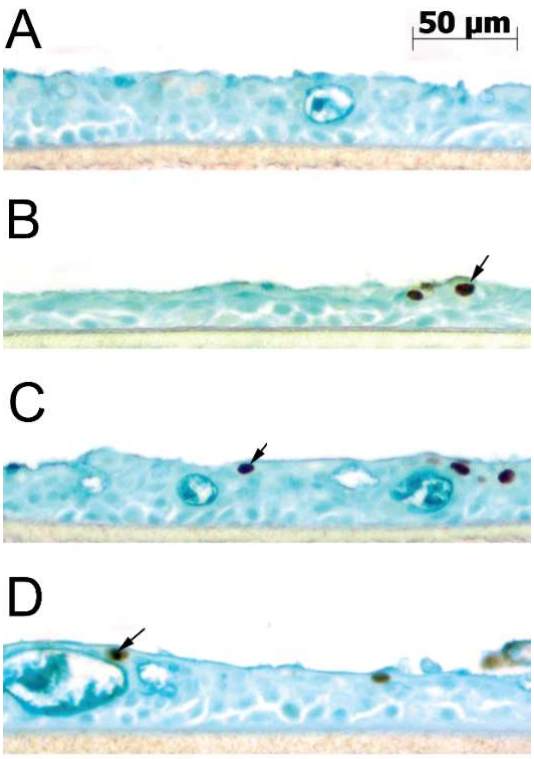

Figure 10. Immunohistochemical microscopy of wdNHBE cells after IAV infection. IHC microscopy of wdNHBE cells stained with Alcian blue and evaluated 36 h after infection with (A) MOCK, (B) KY180, (C) KY136, and (D) BN59 for localization of influenza nucleoprotein antigen (brown) in the epithelial cell nucleus.

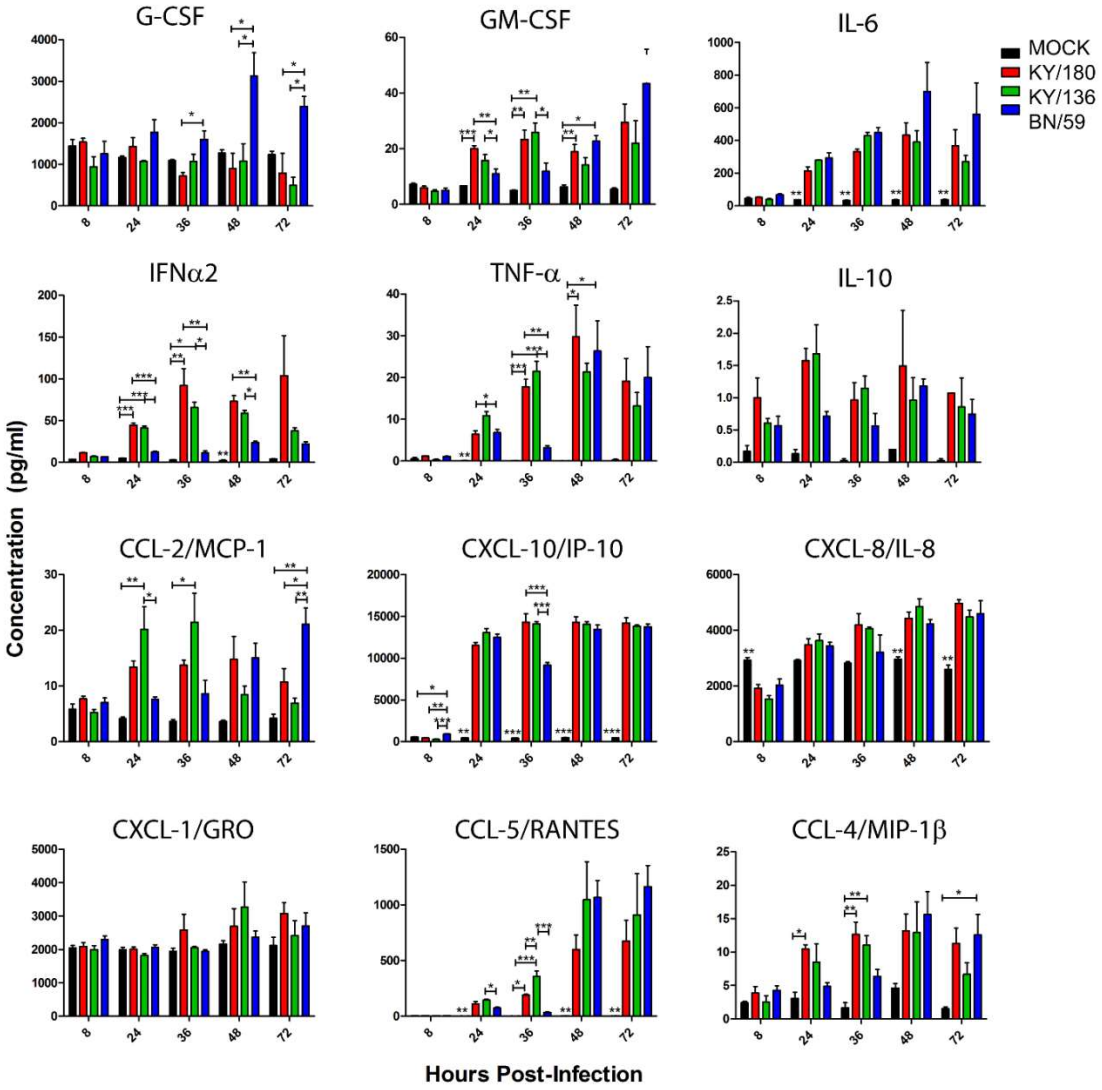

Figure 11. Apical cytokine and chemokine production by wdNHBE cells infected with seasonal and pandemic IAVs. After infection, the apical side of the culture insert was washed twice and harvested for Luminex multiplex analysis. The error bars indicate mean±SEM from 3 replicates per isolate per time point from one representative experiment. A total of two experiments were conducted with two donors. Letters indicate significant differences between isolates (a- different from KY180, b- different from KY136, c- different from BN59, and d- different from Mock).

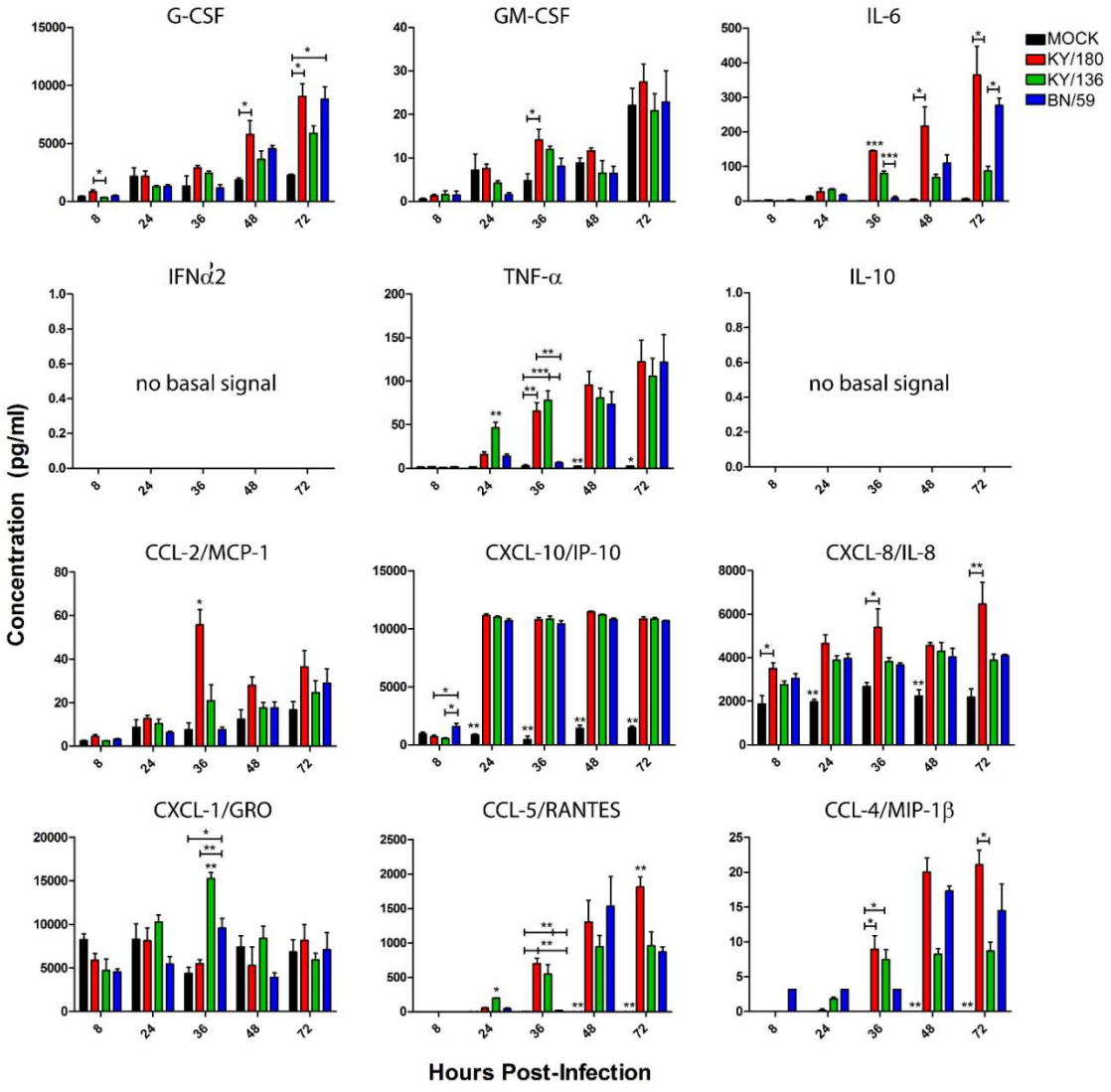

Figure 12. Basal cytokine and chemokine production by wdNHBE cells infected with seasonal and pandemic IAVs. After infection cell culture supernatants were harvested from the basal side of the culture insert and a multiplex analysis was performed using Luminex platform. A total of two experiments were conducted with two donors. The error bars indicate mean±SEM from 3 replicates per isolate per time point from one representative experiment. Letters indicate significant

differences between isolates (a- different from KY180, b- different from KY136, c- different from BN59, and d- different from Mock).

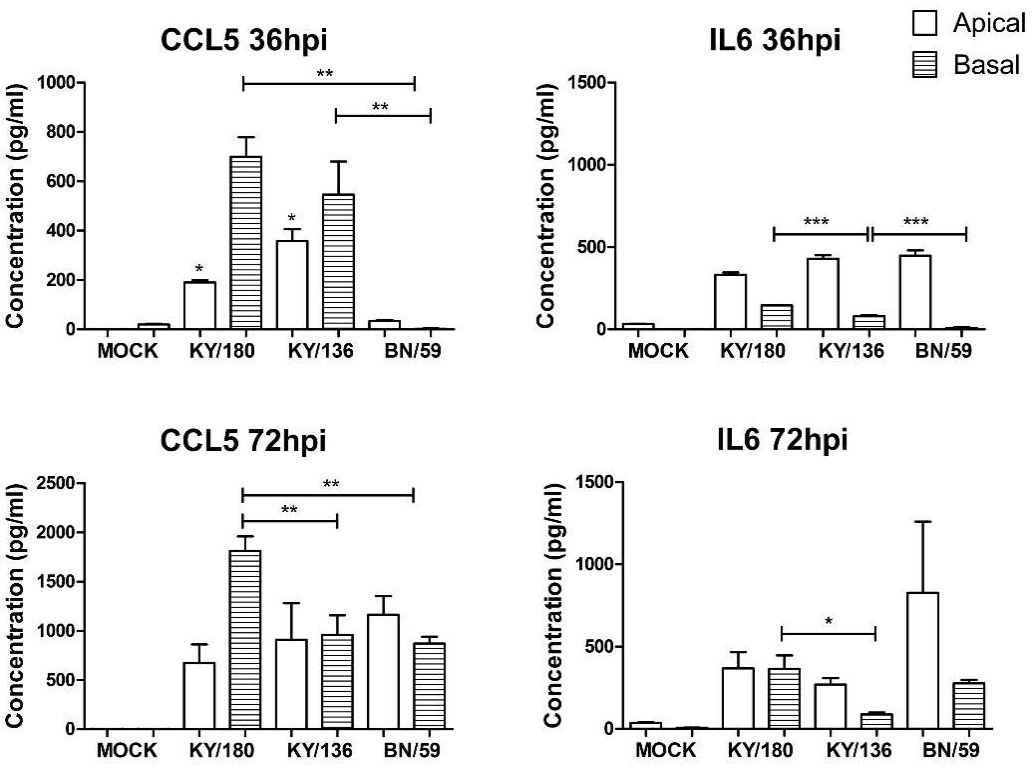

Figure 13. Apical and basal secretion of cytokines and chemokines in wdNHBE cultures infected with seasonal and pandemic IAV at 36hpi. Culture supernatants were harvested from the apical and basal side of the culture inserts and screened for presence of protein using Luminex platform. The error bars indicate mean±SEM from 3 replicates per isolate per time point from one representative experiment. The mean and SEM from 3 replicates per isolate per time point are shown. Asterisks indicate significance of $p<0.05$(*), $p<0.01$(**), and $p<0.001$(***).

Table 5. Differentially expressed genes in IAV–infected wdNHBE cells at 36 hpi.

Virus	No. Differentially Regulated Genes*
KY180	2281
KY136	2338
BN59	360

*No. significant genes $p<0.05$, 2-fold cut-off

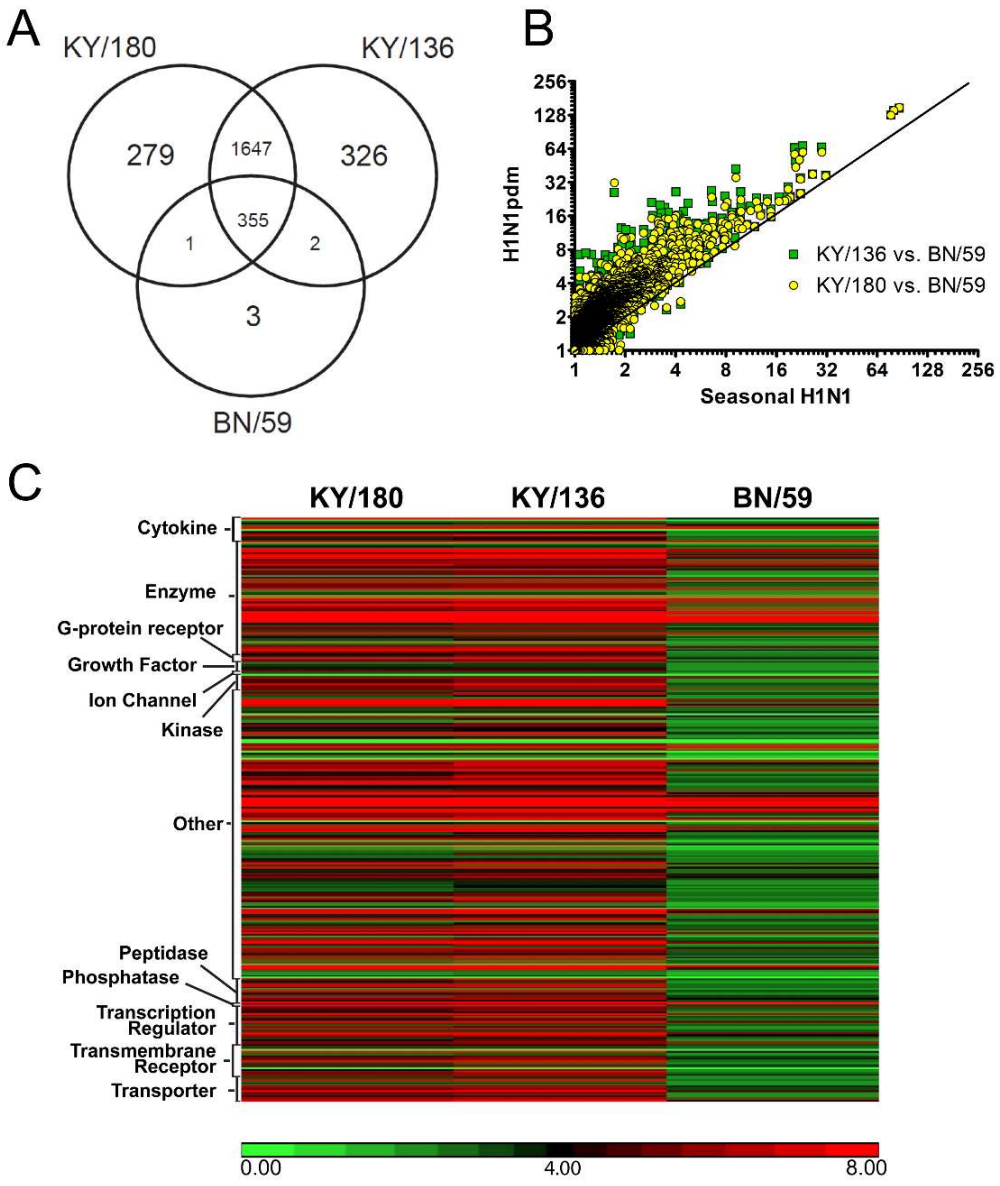

Figure 14. Summary of wdNHBE microarray analysis. Differentially expressed genes (DEGs) were identified by one-way ANOVA analysis by comparing mock and IAV-induced gene expression intensities in wdNHBE cells. DEGs were selected by filtering the genes whose expression changed by at least 2-fold relative to the level in the mock infected group with a $p<0.05$, as outlined in *Materials and Methods*. (A) The Venn diagram illustrates the agreement between the lists of DEGs detected by microarray. (B) Overall data are represented in

scatter plots of log-2 fold-change expression data of seasonal vs. pandemic infected cells at 36 hpi. The diagonal line indicates where the fold change values would be equivalent for the compared isolates. (C) Gene expression intensities were visualized by means of a heatmap of the 355 differentially expressed genes common to all three isolates. Clusters represent types of genes as defined by the Ingenuity pathway analysis output. The error bars indicate mean±SEM from 3 replicates per isolate per time point from a single donor. Asterisks indicate significance of $p<0.05$ (*), $p<0.01$ (**), and $p<0.001$ (***) respectively.

Table 6. Notable genes upregulated in wdNHBE cells infected with seasonal and pandemic IAV isolates at 36 hpi.

Gene Symbol	Affymetrix Probe ID	Fold Change KY180	Fold Change KY136	Fold Change BN59
RSAD2	213797_at	34.23	35.17	22.28
IFIT1	203153_at	25.48	25.28	22.24
IFIT2	226757_at	36.38	37.06	31.47
IFIT3	204747_at	27.81	29.10	18.81
SOCS1	210001_s_at	9.70	13.70	5.30
IFITM2	201315_x_at	8.77	9.13	6.46
IFI35	209417_s_at	16.30	17.24	8.67
IRF1	238725_at	4.18	5.09	3.09
IRF9	203882_at	3.07	3.35	2.64
IFI44L	204439_at	15.81	15.75	14.87
OAS1	205552_s_at	12.21	12.56	7.48
OASL	210797_s_at	57.01	65.33	20.55
MX1	202086_at	17.52	18.42	14.80
MX2	204994_at	22.35	23.55	18.55
JAK2	205842_s_at	4.94	5.65	2.28
STAT1	200887_s_at	4.07	4.16	4.00
STAT2	205170_at	3.14	3.29	2.37
PSMB8	209040_s_at	3.34	3.68	2.76
CCL5	1555759_a_at	15.06	19.06	3.45
CXCL9	203915_at	2.74	2.61	4.29
CXCL10	204533_at	127.36	128.62	77.29
CXCL11	210163_at	140.77	140.60	80.39
IL29	1552917_at	9.91	16.13	2.92
IL28A	1552915_at	12.53	20.10	3.23
IL1A	210118_s_at	4.32	3.98	2.00
DDX58	218943_s_at	21.42	23.25	12.17
IFIH1	219209_at	11.71	12.03	7.72
TLR3	206271_at	5.91	6.32	3.43
CASP1	211367_s_at	4.69	5.16	2.62
MYD88	209124_at	3.54	3.64	2.30
IDO1	210029_at	17.61	19.36	9.83
SOCS2	203373_at	5.73	6.08	2.05
EIF2AK2	204211_x_at	3.55	3.46	3.17

*Fold change values obtained by 1-way ANOVA analysis comparing gene expression intensities of seasonal and pandemic IAV-infected cells to mock. Analysis conducted using Ingenuity core analysis ($p<0.05$, 2-fold change cut-off).

Table 7. Fold change of significantly differentially expressed genes.

Gene Symbol	Affymetrix Probe ID	KY180	KY136	BN59
KRT24	220267_at	31.65	25.90	1.73
DEFB1	210397_at	8.10	8.41	1.82
KRT6B	213680_at	6.02	5.12	1.43
HSPA6	213418_at	5.82	7.17	1.52
CCR4	208376 _at	3.95	4.00	1.93
BAK1	203728_at	3.80	4.37	1.89
IFNB1	208173_at	3.58	6.90	1.69
TICAM1	213191_at	3.48	3.88	1.77
IL-6	205207_at	2.78	3.06	1.50
MYC	202431_s_at	2.73	2.72	1.38
CDK1	203213_at	-2.67	-3.00	-1.61
ATF3	202672_s_at	2.22	3.30	1.78
GSTA1	203924_at	-12.09	-12.03	-1.21
SOX9	202936_s_at	4.66	5.38	1.97
ICAM1	202638_s_at	2.28	2.27	1.67
SOCS2	200887_s_at	4.07	4.16	4.00

*Fold change values obtained by 1-way ANOVA analysis comparing gene expression intensities of IAV-infected cells to mock. Analysis conducted using Ingenuity ($p<0.05$, 2-fold change cut-off)

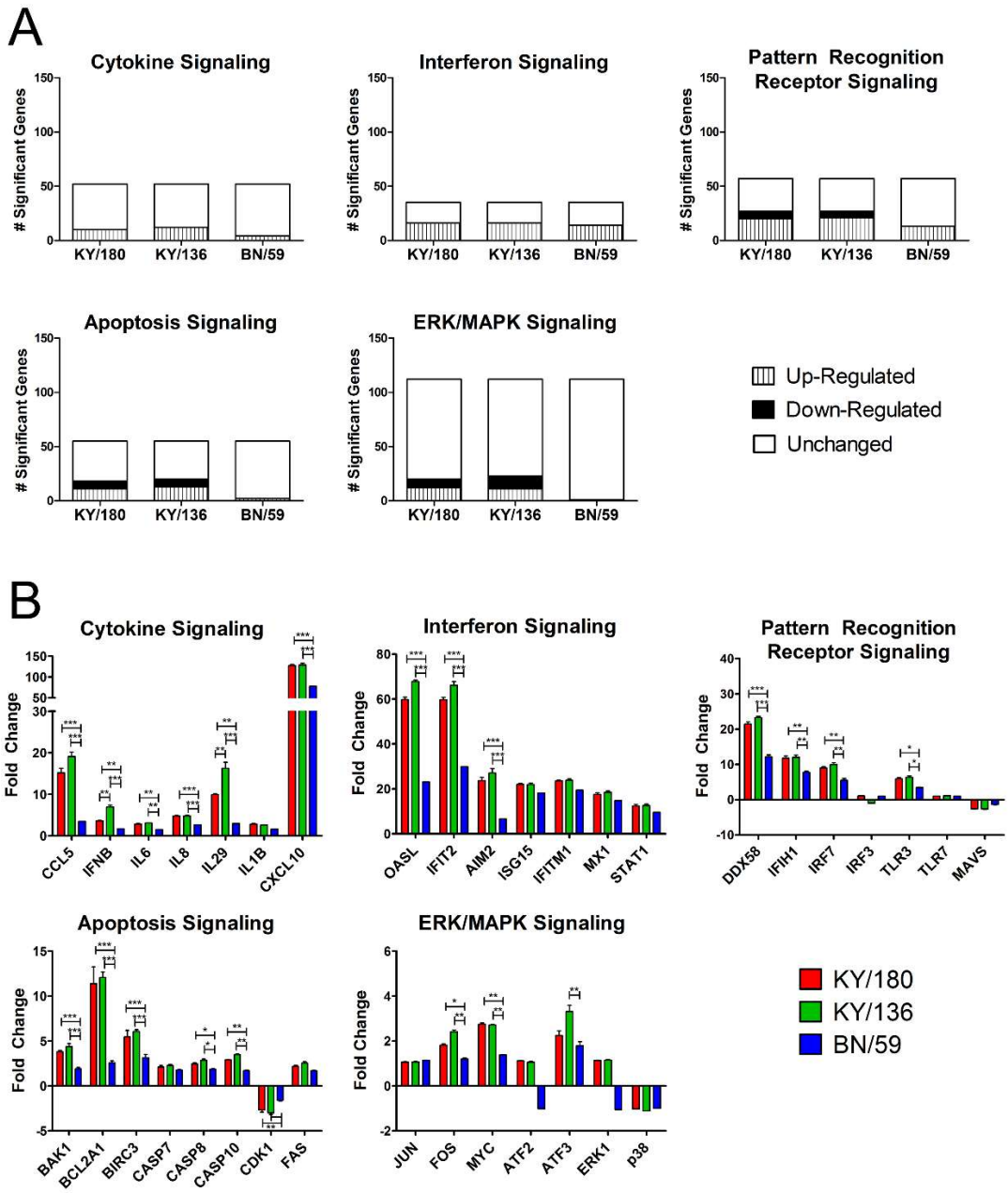

Figure 15. Pathways significantly represented by all isolates as compared to mock. (A) Graphs represent the number of genes differentially up- or down-regulated for each isolate compared to mock. Red represents the number of genes up-regulated, green represents the number of genes down-regulated, and white represents the number of genes that are not significantly different from

mock. (B) Graphs represent the fold change expression of significant DEGs within these pathways.

Table 8. Top five significant canonical pathways in IAV-infected wdNHBE cells at 36hpi relative to mock

RANK	KY180	KY136	BN59
1	IFN Signaling Pathway (6.47E-07, 0.471)	IFN Signaling Pathway (3.49E-07, 0.471)	IFN Signaling Pathway (3.36E-15, 0.412)
2	Communication between Immune Cells (3.07E-06, 0.471)	Communication between Immune Cells (4.70E-06, 0.258)	Communication between Immune Cells (6.51E-12, 0.172)
3	Complement System (2.37E-05, 0.424)	Role of PRRs in Recognition of Viruses (1.15E-05, 0.284)	Antigen Presentation Pathway (1.13E-10, 0.275)
4	Role of PRRs in Recognition of Viruses (2.75E-05, 0.284)	Aryl Hydrocarbon Receptor Signaling (7.14E-05, 0.234)	Activation of IRF of Cytosolic PRRs (1.14E-07, 0.175)
5	Aryl Hydrocarbon Receptor Signaling (7.65E-05, 0.241)	Antigen Presentation Pathway (1.04E-04, 0.325)	Role of PRRs in Recognition of Viruses (1.53E-07, 0.137)

* Rankings are listed based on statistical significance scored using Fischer's Exact Test (p-value<0.05). For each canonical pathway we report the p-value of Fisher's exact test to measure significance and the proportion of genes in the pathway that were actually significantly represented in the brackets.

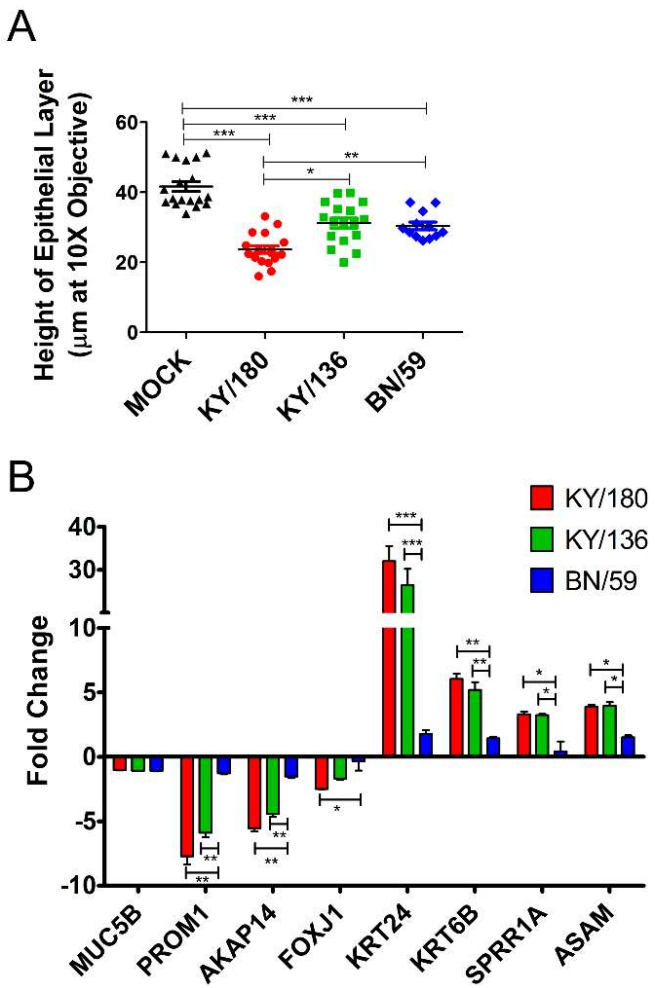

Figure 16: Changes in epithelial layer integrity in infected wdNHBE cells at 36h after infection. Cell layers were measured using Zeiss AxioVision version 4.8 software using a 10 X objective. Five pictures were taken with 3-4 measurements per picture. (A) Differences in epithelial layer thickness, as measured by mean height of the epithelial layer from the collagen are depicted. The error bars indicate SEM from 3 replicates per isolate per time point. Asterisks indicate significance of $p<0.05$ (*), $p<0.01$ (**), and $p<0.001$ (***) respectively. (B) Microarray gene expression of genes shown to be associated with differentiation of bronchial epithelial cells and apoptosis. Values are shown as fold-change over mock infected control at the 36h time point

CHAPTER 3

ESTABLISHING THE HUMAN MONOCYTE-DERIVED MACROPHAGE MODEL

INTRODUCTION

Severe cases of influenza A virus (IAV) infection are associated with pneumonia and bacterial co-infection, which predispose patients to a greater risk of severe outcomes including acute respiratory distress, sepsis, and death [340, 341]. The most common comorbidities associated with hospitalized patients include asthma, cardiac disease, and diabetes [311, 342]. In the recent 2009 pandemic influenza A H1N1, influenza-associated pneumonia was also a common complication among hospitalized patients within the United States in 2009, causing excess mortality in children and young adults [340, 343-346]. In these younger patients, however, comorbidity was less common. As seasonal IAV predominantly target the upper respiratory tract, the epidemiology of H1N1pdm suggested it had a broader tropism for the lower respiratory tract (Figure 17) [347, 348]. Subsequent research showed the H1N1pdm has tropism for the upper and lower respiratory tract [74, 349]. Histopathologic analysis of fatal cases of seasonal and pandemic influenza virus infection show a similar spectrum of pathologies [295, 350], however, strains vary in their ability to infect

and replicate in specific cell types (i.e., respiratory, alveolar, and lung endothelial cells) [66, 86, 91, 351-353]. Furthermore, different strains of IAV vary in their ability to infect and replicate productively in macrophages which also show differences in the magnitude of their pro-inflammatory responses [222, 307, 351, 354-357]. Given the apparent tropism of the H1N1pdm for the lung and the central importance macrophages play in innate immune responses [358], *in vitro* models that permit the study of IAV-macrophage interactions are critical.

Influenza-associated pneumonia is characterized by an early influx of neutrophils followed by the recruitment of large numbers of blood-derived monocytes within the first days of infection [309, 359]. Recruitment of neutrophils and monocytes to the infected lung relies heavily on early cytokines and chemokines (including CXCL10, IFNβ, CCL5 and IL6) produced by infected or bystander lung epithelial cells (Figure 17) [223, 232, 360]. An increase in the number of these cells and their respective inflammatory responses have been linked to severe lung immunopathology after infection [308, 309], suggesting an important link between recruited cells and the outcome of IAV infection. However, these cells have also been shown to play an important role in protection from infection. Animal studies of influenza infection (i.e., mice, ferrets, and pigs) by H1N1 and H3N2 viruses reported that alveolar macrophages are critical for protection. Clodronate liposome-mediated depletion of macrophages in these models resulted in greater virus replication in the lungs, systemic dissemination of the virus, and exacerbated disease severity [358, 361-364]. This highlights that macrophages, are necessary for protection but can also cause severe

immunopathology if dysregulated, thus the need for studies to understand how the viruses modulate macrophage responses are needed.

To date, studies evaluating IAV infection in human macrophages have employed tissue-resident alveolar macrophages (AM) and monocyte-derived macrophages (MDM) models; however the results of these studies vary as to whether IAVs productively replicate in human macrophages [222, 307, 351, 354-357]. Both models are relevant given that both are required for pathogen elimination and restoration of homeostasis following infection and tissue damage [365]. All macrophages originate from bone marrow hematopoietic stem cells and gain access to the respiratory tract via blood and lymph [366, 367]. MDM arrive in the lung after inflammation causes increased vascular permeability, permitting extravasation of plasma and blood cells [368]. These recruited cells can differentiate into different subsets (pro- and anti-inflammatory) of macrophages once they reach the site of infection [369].

Differentiation of macrophages to AM occurs through interactions within the lung microenvironment, although this is not completely understood. The presence of surfactant proteins A (SP-A) and D (SP-D) and the presence granulocyte-macrophage colony stimulating factor (GM-CSF) within the lung have suggested to influence differentiation [365, 370]. The activation status of the AM and their immune responses are critical to balance the epithelial response to protect the lung [371].

Studies to date on the macrophage phenotype induced by IAV infection have been limited mostly to *in vitro* models that pre-treat cells with growth factors

such as GM-CSF or M-CSF to drive differentiation and activation of macrophages [372-374]. Monocytes and MDM pretreated with GM-CSF result in a pro-inflammatory (previously known as M1) macrophage phenotype [375, 376], whereas M-CSF induces an anti-inflammatory (previously known as M2) macrophage phenotype *in vitro* [377, 378]. Up-regulation of NFκB is associated with the inhibition of M1-polarization *in vivo* [379], and up-regulation of IRF5 by GM-CSF pre-treatment in MDM is associated with activation of M1 markers [375]. Influenza viruses have been shown extensively to activate signal transduction pathways through pattern recognition receptor activation [325, 380, 381], suggesting a potential link to IAV infection and macrophage activation/polarization.

There is little known regarding the early events following MDM infiltration into the lung during infection. Herein we have developed a resting MDM model of seasonal and pandemic H1N1 viruses to uncover early IAV-MDM interactions. To characterize this model we first established the culture conditions as previously described for differentiating monocytes to macrophages over 7 days and confirmed this differentiation by evaluating surface marker and gene expression of CD14 and CD11b markers. We then confirmed the MDM cultures were not activated after the 7 day maturation. We evaluated the cells via light microscope to determine whether the macrophages were in an activated or resting state as previously described [382, 383]. This was further confirmed evaluating the presence of both anti- and pro-inflammatory activation surface markers on the surface of MDM by flow cytometry and RT-PCR. Lastly, to eliminate elements

that could prematurely affect the outcome of our experiments on IAV-MDM interactions, we optimized the infection culture conditions including infection media, multiplicity of infection, and the use of egg- or cell-derived IAV stock virus for infection.

METHODS

Isolation and differentiation of MDM. Peripheral blood mononuclear cells (PBMCs) were obtained from healthy donors and isolated using plasma-percoll gradients by the University of Louisville Nephrology Department. MDM were generated using a protocol developed by Dr. Suttles laboratory at the University of Louisville as previously described with slight modifications [384]. Briefly, PBMCs were washed twice in Dulbeccos PBS (DPBS, HyClone with Magnesium and Calcium, ThermoFisher) and resuspended with final concentration at $2x10^6$ cells/ml in R5 media, which contains RPMI 1640 (HyClone, ThermoFisher) supplemented with 5% heat inactivated human AB serum (Atlanta Biologics), 0.01M HEPES (Invitrogen Life Technologies), and 2ml Pen/Strep (Invitrogen Life Technologies). Monocytes were plated on 6 well low-attach plates (ThermoFisher) at a volume of 4 ml per well. Monocytes were allowed to mature for 5 days in a 37^o C incubator with 5% CO_2. After the maturation period, cells were removed from low-attach plates gently using a cell lifter (Costar, ThermoFisher), washed twice with DPBS supplemented with 0.2% human AB serum, and resuspended at $4x10^6$ cells/ml in R5 media. Cells were plated (4x10^6 cells/ml) and allowed to adhere for two days. Mature MDM were

selected by adherence after 2 days by washing with DPBS with 0.2% human AB serum. Cells were incubated in R5 media for 1 h prior to infection/treatment.

Influenza viruses. Viruses used for these experiments included H1N1 IAV isolates from human clinical patients during the 2009 pandemic A/KY180/2010 (KY180) and A/KY136/2009 (KY136) [298, 385]. For comparison, we also included a seasonal H1N1 IAV vaccine strain A/Brisbane/59/2007 (BN59) (kindly provided by the Centers for Disease Control and Prevention, Virus Surveillance and Diagnosis Branch, Influenza Division). Viral seed stocks were prepared as previously described [298] in egg and MDCK cells and stored at -80˚C. Viral titers of the stocks were characterized by median tissue culture-infective dose ($TCID_{50}$) assay in MDCK cells and calculated using the method of Reed and Muench [386].

***In vitro* infection of MDM**. For infection of adherent MDM, cells were washed 2 times with macrophage serum-free media (Invitrogen Life Technologies) to remove serum from the culture. The cells were infected at an MOI of 1.0 unless otherwise indicated diluted in viral growth media containing macrophage serum-free media supplemented with 0.1% BSA (Invitrogen Life Technologies), antibiotics, and Trypsin-TPCK (Sigma) for 1 h. After removing the inoculum, the cells were washed 3 times with DPBS. Viral growth media was then added to each well and cells were incubated at 37°C with 5% CO_2 for 1-36 h depending on the experiment.

Evaluation of MDM cells using light microscope. MDM cells were evaluated using a light microscope, Eclipse TS100 (Nikon) using the 4X and 40X

objectives. Cell pictures were taken using an attached Digital Sight Camera (Nikon). Using previously described methods for identifying resting and active macrophage phenotype by microscopy, we evaluated MDM after maturation and after IAV infection for their shape (spherical or elongated) and presence of protrustions (lamellipodia and filopodia) [382, 383].

RNA isolation and cDNA synthesis. At the designated time point, total cellular RNA was extracted from cells using the TRIzol reagent (Invitrogen Life Technologies) according to the manufacturer instructions. The quality and quantity of the extracted RNA was assessed using an Experion (BioRad), where RNA was accepted for downstream reaction with an integrity value greater than 7. We used 1 ug of extracted RNA, random hexamer primers, and Superscript III reverse transcriptase (Invitrogen Life Technologies) to generate complementary DNA (cDNA). HA gene sequences were amplified PCR using Taq Polymerase (Invitrogen) and products were visualized on a 1% agarose gel. The sequences of the forward primers for H1N1pdm isolates were 5′-CACCAGTCCACGATTGCAATA-3′ and for BN59 5′-GAGTAGAGGCTTTGGATCAGGA-3′. The reverse primer was the same for both H1N1pdm and seasonal (5′-ATGGGAGGCTGGTGTTTATAGC-3′).

Real-time PCR of cellular and viral genes. To characterize the surface and activation markers expressed in the two populations, monocytes and macrophages. Half of the monocytes were either collected in Trizol for RNA/DNA extraction for RT-PCR or collected using PBS/0.2% EDTA solution for flow cytometry. Monocytes were collected after cells were washed in DPBS and

before being placed in media with human serum. The other half were allowed to mature through the described protocol and at the 7th day, cells were collected for RT-PCR and flow cytometry. Total RNA was isolated, and the expression levels were determined by RT-PCR.

For RT-PCR reactions, 100 ng of cDNA, 10 μM of each gene specific primers, and Power SYBR® Green Real-Time PCR master mix (Invitrogen Life Technologies) were used. Primers were designed using PrimerBank software [387] or determined using previously published primer sets (Table 9) [376, 388-391]. The RT-PCR consisted of 1 cycle of 50°C for 5 min and 95°C for 2 min and 40 cycles of 95°C for 3 s, 60°C for 30 s using the 7900 Fast Real-Time System (Applied Biosystems) or VIIA7(Invitrogen Life Technologies). The threshold was automatically set and C_t (threshold cycle) determined. For all runs, samples were assayed in duplicate and non-template controls were included. Samples were normalized using β-actin as the reference endogenous control. The average threshold cycles of the replicates were used to compare the expression of the genes of interest to the endogenous control (β -actin). This was done using the)C_t method, where ΔC_t= (C_t (target gene) target-ΔC_t (β-actin). The greater the ΔC_t value, indicating a greater difference between the target gene and endogenous control Ct value, indicates a lower level of the target gene expression. A smaller ΔC_t value indicates a greater expression of the target gene.

Flow cytometry. For assessing extracellular and intracellular markers in monocytes and MDM, cells were detached on ice with 2.5 mM EDTA in PBS. For

extracellular staining only, cells were washed and incubated with conjugated antibodies (abCam) for 1 h and then fixed in 4% paraformaldehyde. Cells were washed and analyzed using a FACSCalibur (Becton-Dickinson) flow cytometer with 10,000 events collected. Data were analyzed using FlowJo® software, version 10 (Tree Star).

Cell viability assay. The CellTox™ Green Cytotoxicity Assay (Promega) was used to assess changes in membrane integrity that occur as a result of cell death during culture. This assay was performed according to the manufacturer's instructions. Briefly, MDM cells were cultures in a 96-well plate and infected at the indicated MOI for 24h. After 24h, the supernatant was removed, the cells were washed 3 times in DPBS, and a cyanine dye (Promega) was added to each well and allowed to incubate for 15 minutes. Viability (fluorescence) was assessed using a Synergy HT Multi-Mode Microplate Reader (Biotek). The cyanine dye used in this assay is excluded from viable cells but preferentially stains the DNA from dead cells. Therefore, the fluorescence signal produced by the binding interaction with dead cell DNA is proportional to cytotoxicity (meaning a greater fluorescence indicates greater cell death). A positive control (lysis buffer) was added to the cells to cause lysis 4h prior to reading, and represents cells that are dead.

Statistics. For the comparison of two sets of values, Student's t test (two-tailed, two-sample equal variance) was used. When comparing three or more sets of values, data were analyzed by one-way analysis of variance (ANOVA), followed

by posthoc analysis using Tukey's multiple-comparison test. A p-value of ≤0.05 was considered statistically significant.

RESULTS

CHARACTERIZATION OF THE RESTING MACROPHAGE AFTER 7 DAY MATURATION.

Monocytes, as described in the literature, are mostly classical monocytes making up 90% of the human monocyte population and are characterized as having high CD14 but no CD16 expression on their cell surface [392]. Macrophages on the other hand have been described as having CD11b surface expression, with low surface expression level of the monocyte marker CD14 [393]. In addition, previous studies have shown mRNA expression of the CHI3L1 gene to be exclusively present in macrophages and not monocytes [394]. To determine if our culture conditions favored the maturation from monocyte to macrophage, we evaluated PBMC's on day 0 to MDMs on day 7 by RT-PCR and flow cytometry. We found our MDM population to be CD11b +, CD14 –, CD16 –, and CHI3L1+ (Figure 18A,B) validating our protocol to generate MDM from monocytes.

After the 7 day maturation, we evaluated the cultured cells by light microscopy to determine if our cells agreed morphologically with previous studies using MDMs. Waldo et al., describe the morphology of MDM at different stages of differentiation from resting to activated. They found that under GM-CSF conditioning, the majority of MDM cells were elongated as compared to the resting MDMs which were spherical [383]. Additionally, Kannan *et al.* found that treating AMs with cultured media from bacterially infected alveolar epithelial cells

caused them to activate and the morphology of these activated AMs were shown to have lamellipodium and filopodium protrusions by confocal microscopy [382]. After selecting for adherence, we observed our 7 day matured MDM culture to be primarily made up of spherical cells and limited protrusions were noted on the MDM cells (Figure 19A) further confirming our resting model. To further confirm the inactive state of our MDM cultures, transcriptional analyses were performed showing expression levels of CD80, CD64, CD163, HO-1, CD200R, CD36 and CD206 to be consistent with low activation or a resting MDM population (Figure 19B) [376, 395].

OPTIMIZATION OF THE IAV-MDM INFECTION PROTOCOL

Media used for MDM infection. As mentioned in previous chapters, IAV requires host cell proteases for HA cleavage and entry into the host cell. For immortalized and non-epithelial cell lines, TPCK trypsin is added to the culture media to mimic that conditions the virus would see inside the human host. The concentration of trypsin to add to the culture media must be optimized to ensure there is enough to allow infection but also not too much to destroy the cells. For MDM, previous studies have used a concentration of 1ug/ml of TPCK trypsin in their media. We evaluated 0, 0.5, 1.0, and 1.5 ug/ml TPCK trypsin and evaluated toxicity by observing the cells using a light microscope at 8, 24, 48, and 72h after addition. We observed significant MDM cell detachment (characteristic of adverse effects of TPCK trypsin) when adding 1.5ug/ml starting at 24h after addition. We observed no difference in cells detaching for MDM treated with 0, 0.5, and 1.0 ug/ml across 8, 24, and 48h. However, by 72h we observed all three

induced detachment. Because this occurred at the 0 ug/ml TPCK treatment, we assumed the cells were dying as a result of serum starvation and not TPCK addition. With this information, we decided to evaluate the IAV-MDM interaction at the earlier time points when serum starvation did not seem to be a factor. Further, we used 1ug/ml of TPCK in our infection culture media as our observations showed no toxicity at 8, 24, and 48h after addition. Previous studies looking at IAV-MDM interactions used the 1ug/ml TPCK trypsin concentration [222, 353, 391] and since we did not see a difference between 0.5 and 1ug/ml we decided to move forward using 1ug/ml so we could best compare our results to others.

Influenza virus stock comparison. Influenza stock viruses are produced primarily through passage in the allantoic sac of embryonic chicken eggs or through passage in a susceptible mammalian cell line [396]. To summarize, the egg-derived virus is produced by serial passage of IAV in the allontoic fluid of eggs where the virus replicates to high titers in the chorioallantoic membrane cells. The amplified virus is then collected in the allontoic fluid and the titer confirmed by $TCID_{50}$ assay. Cell-derived virus is produced by serial passage of IAV in confluent, susceptible mammalian cells in cell culture infection media containing bovine-serum albumin, HEPES buffer, and TPCK trypsin. Once substantial cytopathic effect occurs in these cells, the supernatant is collected, spun down and the titer confirmed by $TCID_{50}$ assay.

Here we compared influenza isolates derived in eggs to those derived in cell cultures to determine if there was a difference in activation and their ability to

infect MDM. Using 1ug/ml of TPCK and an MOI of 1.0 we first looked at the cellular morphology 24h post-infection. We saw significant changes in morphology in cultures infected with egg-derived viruses compared to cell-derived viruses (Figure 20A). We then evaluated the amount of virus present in the supernatant after 24h by $TCID_{50}$ assay as an indication of virus infection and replication in those cells. We found the egg-derived virus stocks replicated very poorly in MDM with the two H1N1pdm isolate titers below the limit of detection (Figure 20B).

We then asked if this discrepancy could be a result of sequence variations selected for after passage in the different systems. Previous studies have shown serial passage of human IAVs (H3N2 and H1N1) in eggs create viruses that acquire mutations in their HA gene after isolation compared to sequences of those isolated in mammalian cells [397-402]. Further, human H3N2 viruses isolated in cell culture were reported to bind with a high affinity to alpha-2,6-SA, while viruses isolated in eggs often had increased specificity for alpha-2,3-SA [403, 404]. According to sequencing analysis, done by Ryan McAllister in our laboratory, the egg-derived and MDCK-derived H1N1pdm and seasonal viruses shared the same sequence and does not explain the discrepancy in cell changes and differences in the viral isolate's abilities to infect MDM. Therefore suggesting a component of the allontoic fluid induces changes in the MDM that decrease permissibility to infection. Hence we moved forward to study IAV-MDM interactions using MDCK-derived viruses.

Multiplicity of infection. Studies on IAV-macrophage interactions have used a wide range of MOIs [222, 307, 351, 405]. One study specifically by Hoeve *et al*. showed a significant difference in HA expression in MDM at different MOIs of H3N2 [355]. We sought to determine the optimal amount of virus to add that permits infection of MDM but that minimizes harm to the cells. To do this we performed infections with two H1N1pdm and one seasonal H1N1 isolate in MDM at 0, 1, 3, and 5 MOI. We monitored both the cell viability by Cytotoxicity Assay and viral titer by $TCID_{50}$ assay 24h post-infection. For KY180, there was no significant difference in cellular cytotoxicity (Figure 21A). By $TCID_{50}$ assay, the viral titers produced from infected MDM were not dose dependent and this was shown for both H1N1pdm and seasonal H1N1 isolates (Figure 21B). Thus, our question became which MOI to choose.

The major limitation of our laboratory is that our MDCK-derived virus stock titers are low. The current titers of our stocks are roughly $5x10^6$ pfu/ml, meaning to obtain an MOI of 1.0 on a culture of 200,000 cells requires 40 µl of virus stock per well. This virus is diluted up to 100 µl in macrophage serum-free infection media for the 1h duration of the infection. However, if we use an MOI of 5.0, it would require us to use 5 times the volume of the stock virus (200 µl). This volume is greater than the 100 µl of media generally used for infection which could affect the overall infection protocol. Additionally, the MDCK-derived viruses may contain cytokines produced from the infected cultures. Diluting these factors out during infection likely minimizes their effects on the MDM; however, if we add 5 times the amount of stock virus, it could potentially alter the MDM activation

state and prematurely affect the outcome of our experiment. Thus not allowing us to determine whether the effects were viral or culture induced (Figure 21). Because we saw no significant difference in titers, we decided to move forward with an MOI that would allow us to utilize the standard 100 µl infection conditions.

Confirmation of infection of MDM with IAV by PCR. To determine whether the 'resting' MDM culture model supported infection of H1N1pdm and seasonal isolates, we infected MDM for 8, 12 and 24h and confirmed the presence of intracellular viral RNA by PCR amplification of HA. All three isolates were shown to infect MDM as demonstrated in figure 3-5. By 24 hpi, MDM showed comparable amounts of intracellular HA for all isolates (Figure 22). The ability of our viruses to enter into MDM provided us the confidence to move forward to compare IAV-MDM interactions using the resting MDM model with our H1N1pdm and seasonal isolates.

DISCUSSION

To better understand the early events that take place after IAV-infection, we have developed a "resting" MDM model of IAV infection. This model represents a non-activated macrophage that is recruited to the site of infection with no previous exposures to the lung microenvironment. While developing and optimizing the conditions this model, careful consideration was taken to obtain a resting MDM model that is permissive to IAV infection while minimizing confounding factors that could affect our experimental outcome. Taking into account the conditions utilized by previous studies, we confirmed that our model

was indeed “resting”, that these cells were permissive to IAV infection and that the viral infection culture conditions were minimally harmful to the cells.

Previously published studies suggest that influenza viruses differ in their ability to infect and replicate in macrophages [353, 357]. In contrast [405], and in support of the work of others [353, 354, 356], we demonstrated that seasonal and pandemic (H1N1) viruses are not restricted in their ability to be internalized by macrophages. Further, results on the innate immune responses generated in infected macrophages differed when comparing low pathogenic IAV (LPIAV) to high pathogenic IAV (HPIAV). Specifically, some show greater induction of pro-inflammatory and anti-viral responses in MDM after HPIAV infection [307, 406] whereas others found an impaired induction after HPIAV infection [405]. These inconsistencies may be a result of the culture methods used as pre-treating the human macrophages with GM-CSF has been shown polarize these cells into “activated” phenotypes and represent macrophages in the later stages of infection. By minimizing the confounding factors before infection, we have established an MDM model that will allow us to uncover the composition and magnitude of early influenza-specific responses after infection. This allows us to focus on what the virus does to the cell (early events) instead of what the cell potentially does to the virus (late events).

The susceptibility and early functional responses that take place after IAV-infection in human immune cells remains ill defined. Specifically, there are limited reports on infectivity and the phenotype of human blood-derived macrophages infected with different IAVs and the induction of PRRs has not been assessed.

Our prior studies in mice suggested that the composition of the innate responses in macrophages may differ between closely-related clinical isolates of H1N1pdm [298]. The next chapter will focus our analysis of isolate specific differences within the resting MDM model to determine how the IAV-MDM interactions differ between isolates of the same strain.

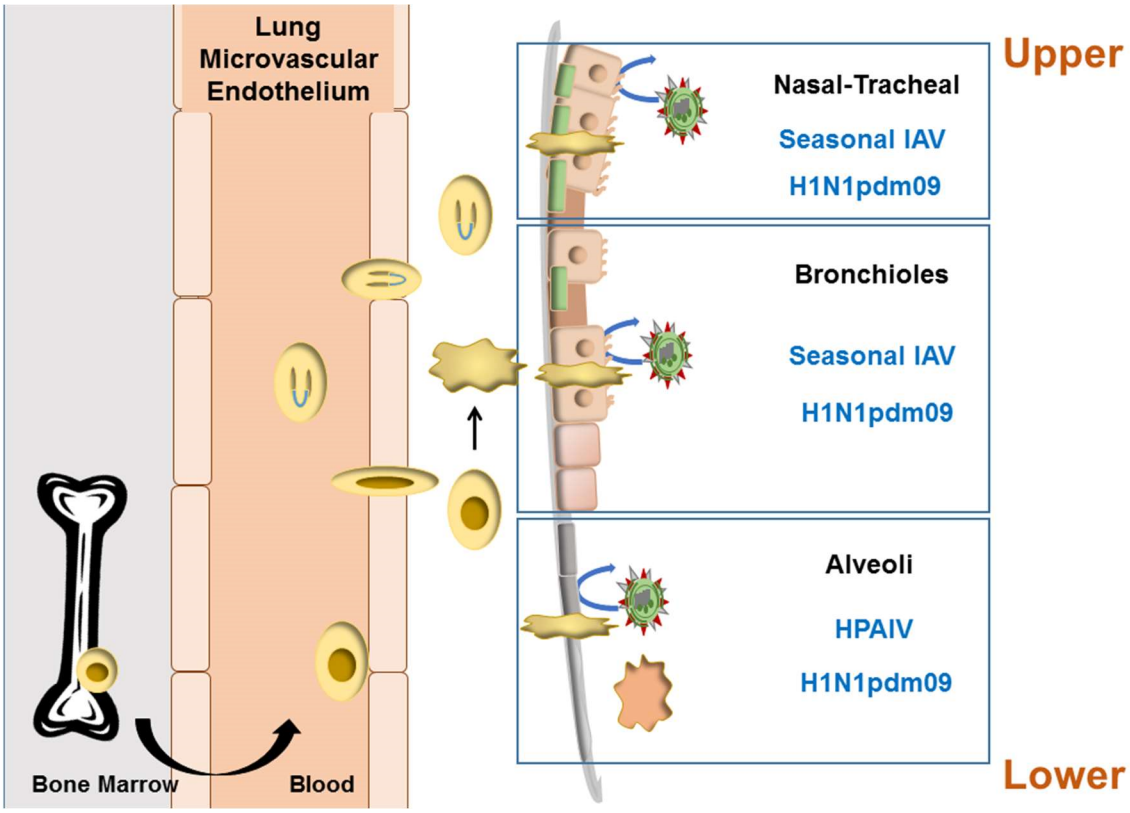

Figure 17. Schematic of recruitment of macrophages to site of infection. Monocytes originate from progenitors in the bone marrow and traffic via the bloodstream to peripheral tissues. During both homeostasis and inflammation, circulating monocytes leave the bloodstream and migrate into tissues where, following conditioning by local growth factors and cytokines, they differentiate into macrophage or dendritic cell populations. Recruitment of monocytes is essential for effective control and clearance of viral infections. An increase in the number of these cells and their respective inflammatory responses have been linked to severe lung immunopathology after IAV infection with influenza-associated pneumonia characterized by an early influx of neutrophils and a large number of blood-derived monocytes within the first days of infection. Seasonal IAV predominantly targets the upper respiratory tract and severe HPAIV H5N1

targets the lower. The epidemiology of H1N1pdm suggested it had a broader tropism for both the upper and lower respiratory tracts indicating a range of pathologies are possible depending on which lung compartment becomes flooded with recruited cells.

Table 9. Primers utilized for RT-PCR and cDNA synthesis.

Primer	M1 or M2	Ref	Forward	Reverse
TNF	M1	4	AACCTCCTCTCTGCCATC	ATGTTCGTCCTCCTCACA
IL6	M1	6	ACTCACCTCTTCAGAACGAATTG	CCATCTTTGGAAGGTTCAGGTTG
CXCL11 (IP11)	M1	4	CCTGGGGTAAAAGCAGTGAA	TGGGATTTAGGCATCGTTGT
CXCL10 (IP10)	M1	6	GTGGCATTCAAGGAGTACCTC	TGATGGCCTTCGATTCTGGATT
CCL5	M1	6	CCAGCAGTCGTCTTTGTCAC	CTCTGGGTTGGCACACACTT
TGFB	M2	2	AAGGACCTCGGCTGGAAGTG	CCCGGGTTATGCTGGTTGTA
IL1B	M1	4	GGGCCTCAAGGAAAAGAATC	TTCTGCTTGAGAGGTGCTGA
IL10	M2	6	GACTTTAAGGGTTACCTGGGTTG	TCACATGCGCCTTGATGTCTG
IL12p35	M1	4	GATGGCCCTGTGCCTTAGTA	TCAAGGGAGGATTTTTGTGG
IDO1	M2	4	GCGCTGTTGGAAATAGCTTC	CAGGACGTCAAAGCACTGAA
PPARy	M2	4	TTCAGAAATGCCTTGCAGTG	CCAACAGCTTCTCCTTCTCG
IFNB	M1	6	GCTTGGATTCCTACAAAGAAGCA	ATAGATGGTCAATGCGGCGTC
IFNA	M1	6	TCATGGTGTATATCAGCCTCGT	AGTTGGTACAATGGAGTGGTTTT
IFNY	M1	6	TCGGTAACTGACTTGAATGTCCA	TCGCTTCCCTGTTTTAGCTGC
RIGI		6	CTGGACCCTACCTACATCCTG	GGCATCCAAAAAGCCACGG
MDA5		6	GCCCGCTACATGAACCCTG	CAGCAATCCGGTTTCTGTCTT
TLR3		6	TTGCCTTGTATCTACTTTTGGGG	TCAACACTGTTATGTTTGTGGGT
TLR7		6	CACATACCAGACATCTCCCCA	CCCAGTGGAATAGGTACAGTT
MyD88		6	GGCTGCTCTCAACATGCGA	CTGTGTCCGCACGTTCAAGA
TRIF (TICAM1)		6	CCTGGAATCATCATCGGAACAG	TGAGTGGTCTATGGCGTCCT
NFKB		6	GAAGCACGAATGACAGAGGC	GCTTGGCGGATTAGCTCTTTT
IRF3		6	AGAGGCTCGTGATGGTCAAG	AGGTCCACAGTATTCTCCAGG

IRF7		6	CCCACGCTATACCATCRACCT	GATGTCGTCATAGAGGCTGTTG
CASP1		6	TTTCCGCAAGGTTCGATTTTCA	GGCATCTGCGCTCTACCATC
CD11b	Mϕ, Mo	5	GCCGGTGAAATCTGCTGTCT	GCGGTCCCATATGACAGTCT
CD36	Mϕ, Mo	4	AGATGCAGCCTCATTTCCAC	GCCTTGGATGGAAGAACAAA
CD80	Mϕ, M1	3	CTGCCTGACCTACTGCTTTG	GGCGTACACTTTCCCTTCTC
CD64	Mϕ, Mo	6	AGCTGTGAAACAAAGTTGCTC	GGTCTTGCTGCCCATGTAGA
CD200R	M2	6	TGGTTGTTGAAAGTCAATGGCT	CTCAGATGCCTTCACCTTGTTT
CD14	Mϕ, Mo	3	AAAGCACTTCCAGAGCCTGT	ATCGTCCAGCTCACAAGGTT
CD163	Mo	3	ACATAGATCATGCATCTGTCATTG	ATTCTCCTTGGAATCTCACTTCTA
CD16	Mϕ	3	CACCATCACTCAAGGTTTGG	AGTCCTGTGTCCACCTGCAAA
CHI3TL1	Mϕ, M1	4	GATAGCCTCCAACACCCAGA	AATTCGGCCTTCATTTCCTT
HO-1	Mϕ, M2	3	ACTTTCAGAAGGGCCAGGT	TTGTTGCGCTCAATCTCCT
CCR7	M1	3	GTGGTGGCTCTCCTTGTCAT	TGTGGTGTTGTCTCCGATGT
CCL22	M2	3	ATTACGTCCGTTACCGTCTG	TAGGCTCTTCATTGGCTCAG
MRC1 (CD206)	Mϕ, M2	3	GGCGGTGACCTCACAAGTAT	ACGAAGCCATTTGGTAAACG
Beta Actin		6	ATTGCCGACAGGATGCAGAA	GCTGATCCACATCTGCTGGAA
Influenza NP mRNA (for PCR)		1	CCAGATCGTTCGAGTCGT	CGATCGTGCCTTCCTTTG
Influenza NP vRNA (for PCR)		1	GGCCGTCATGGTGGCGAAT	CTCAGAATGAGTGCTGACCGTGCC
Influenza NP cRNA (for PCR)		1	GCTAGCTTCAGCTAGGCATC	CGATCGTGCCTTCCTTTG

Influenza NP mRNA (for cDNA)		1	CCAGATCGTTCGAGTCGTTTTTTTTTTTTTTTTCTTCAACTGTC
Influenza NP vRNA (for cDNA)		1	GGCCGTCATGGTGGCGAATAAATGGACGAAGGACAAGGGTTGC
Influenza NP cRNA (for cDNA)		1	GCTAGCTTCAGCTAGGCATCAGTAGAAACAAGGGTATTTTTCTTC

M1, pro-inflammatory macrophage marker; M2, anti-inflammatory macrophage marker; Mo, monocyte marker; Mϕ macrophage marker.

Source of primer (Ref): [1] Cline TD, et al. 2013. *Journal of virology* 87:1411-1419. [2] Soulitzis N, 2006. *International journal of oncology,* 29:305-314. [3] Ambarus, C.A., et al., 2012. *J Immunol Methods*, 375(1-2): p. 196-206; [4]Jaguin, M., et al., 2013. *Cell Immunol*, 281(1): p. 51-61; [5] Moeenrezakhanlou A, et al., 2008. *Journal of leukocyte biology* 84:519-528. [6] Spandidos A, et al. 2010. *Nucleic acids research* 38:D792-799.

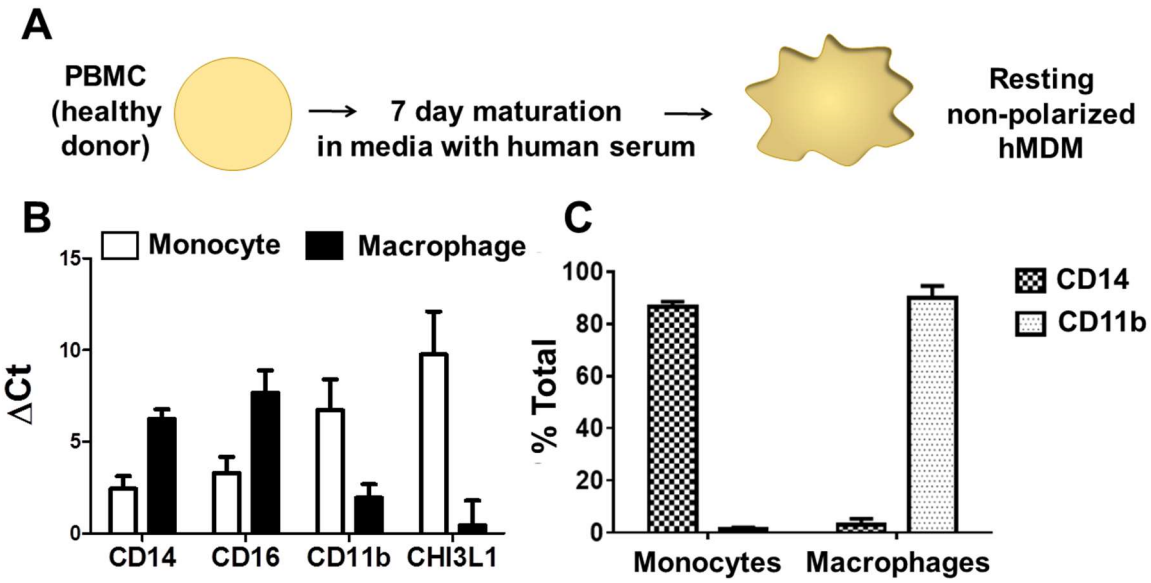

Figure 18. Schematic of approach used to culture resting MDM and characterization of the 'resting' human monocyte-derived macrophage model by RT-PCR and flow cytometry. (A) Peripheral blood mononuclear cells (PBMCs) were obtained from healthy donors and isolated using plasma-percoll gradients by the University of Louisville Nephrology Department. MDM were generated as previously described with slight modifications. PBMCs were washed twice in DPBS and resuspended in culture media containing human serum and plated on 6 well low-attach plates. Monocytes were allowed to mature for 5 days and further removed from low-attach plates gently using a cell lifter, washed twice with DPBS supplemented with human serum, and resuspended and plated on an adherent cell culture plate for 2 days. MDM were selected by adherence after 2 days by washing with DPBS with human serum. RT-PCR and flow cytometry were employed to characterize the known monocyte and macrophage surface markers expressed in the two populations, monocytes and macrophages. Half of

the monocytes were either collected in Trizol for RNA/DNA extraction for RT-PCR or collected using PBS/0.2% EDTA solution for flow cytometry. Monocytes were collected after cells were washed in DPBS and before being placed in media with human serum. The other half were allowed to mature through the described protocol and at the 7^{th} day, cells were collected for RT-PCR and flow cytometry. (B) Total RNA was isolated, and the expression levels were determined by RT-PCR. The data shown represent three replicates of 1 representative donor of 2. RNA levels were normalized to β-actin and presented as ΔCt as described in the materials and methods. (C) The percentage of CD14 and CD11b MDM cells was determined by flow cytometry. Cells were collected in PBS/0.2%EDTA, fixed with 4% paraformaldehyde and stained with anti-CD11b (FITC-labeled) or anti-CD14 (APC-labeled) antibodies and evaluated on flow cytometer. Gates were established with unstained cells where less than 1% were FITC or APC positive. Analysis was conducted using FlowJo® software.

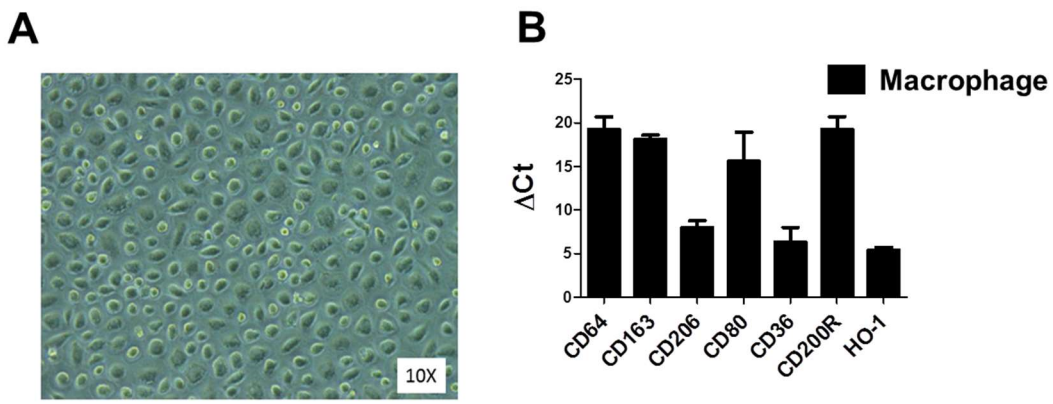

Figure 19. Characterization of 'resting' human monocyte-derived macrophages model by microscopy and RT-PCR. Human MDM were cultured as described in the Methods section from peripheral blood mononuclear cells (PBMCs). (A) After the 7 day maturation process, adherent macrophages were selected for and the morphology was assessed using light microscope using the 10X objective. (B) Further RT-PCR was employed to characterize the activation markers expressed in the adherent macrophages. The cells were collected in Trizol and total RNA was isolated, and the expression levels were determined by RT-PCR. The data shown represent three replicates of 1 representative donor of 2. Expression levels were normalized to β-actin and presented as ΔCt as described in the materials and methods.

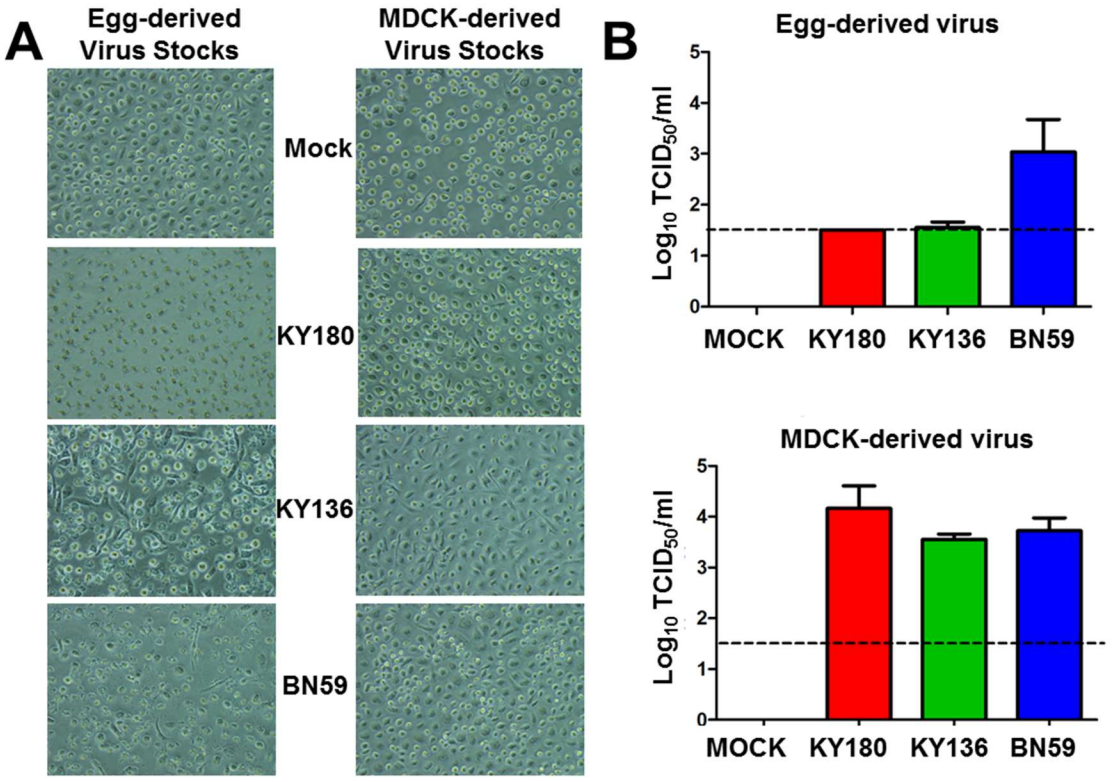

Figure 20. Evaluation cell morphology and permissibility of MDM infection to egg-derived and cell-derived viral stocks. MDM cells were infected with an MOI of 1 of seasonal (BN59) or pandemic (KY180, KY136) isolates. The figure is representative of results from 2 donors. (A) Cell morphology was assessed using light microscope using the 10X objective. (B) $TCID_{50}$ assay was performed on supernatants from infected MDM cultures pictured in (A) at 24h post-infection. Data are presented as the mean$\pm$SD from 3 replicates from one donor. Asterisks indicate significance of $p<0.05$(*), $p<0.01$(**), and $p<0.001$(***) respectively. The dotted line indicates the limit of detection of the $TCID_{50}$ assay.

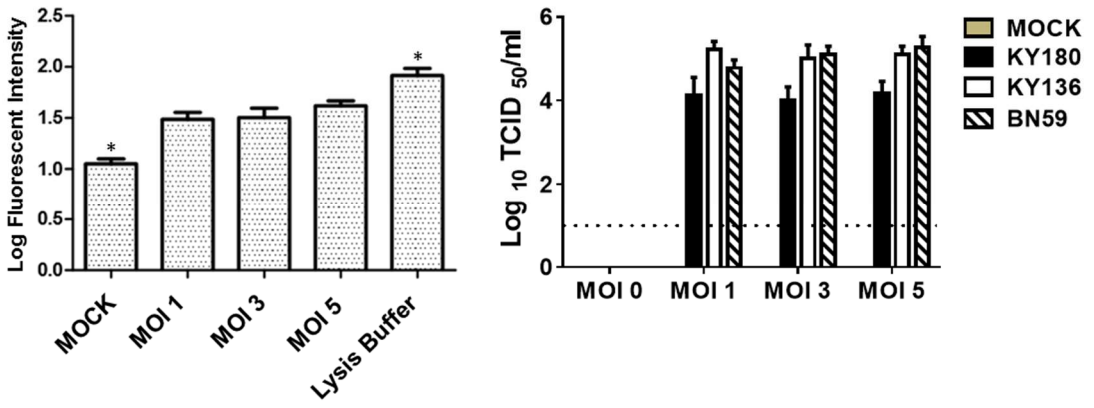

Figure 21. Cell Viability at different MOIs 24h post-infection. (A) For cell viability assay, the CellTox Cytotoxicity assay (Promega) was performed according to manufacturer's instructions. Positive control wells received lysis buffer approximately 4 hours before cytotoxicity assay was performed. At 24h post-infection with KY180 (MDCK-derived virus) cyanine dye (Promega) was added to each well and allowed to incubate for 15 minutes. Fluorescence was then measured on a multi-well fluorescence plate reader (BioTek). Raw fluorescent intensity values were converted to base 10 logarithm values for analysis. (B) $TCID_{50}$ assay was performed on supernatants from MDM infected with 1 MOI of seasonal (BN59) or pandemic (KY180, KY136) MDCK-derived viral isolates at 24h post-infection. Data are presented as the mean$\pm$SD from 3 replicates from one donor. Asterisks indicate significance of $p<0.05$(*), $p<0.01$(**), and $p<0.001$(***) respectively. The dotted line indicates the limit of detection of the $TCID_{50}$ assay.

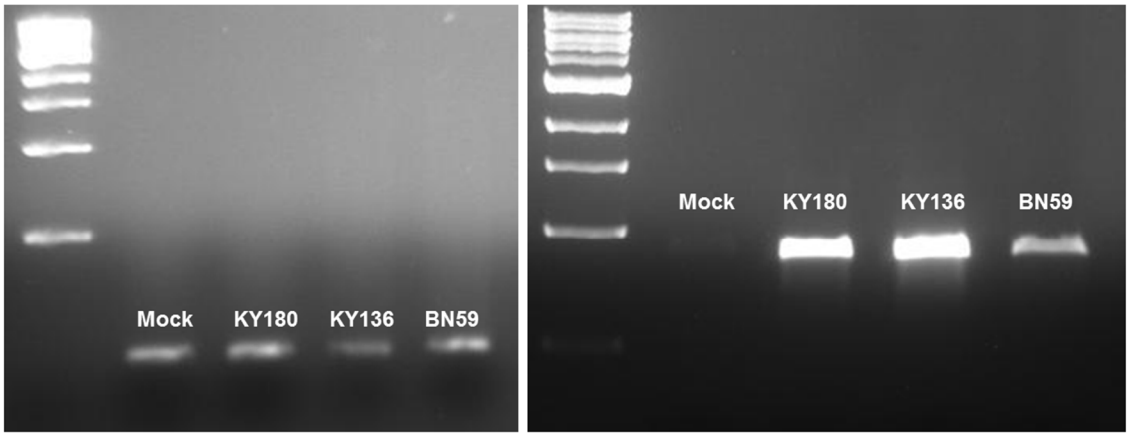

Figure 22. Infection of MDM by H1N1pdm isolates. Cells were infected with and MOI of 1.0 and cell lysates were collected at 24h post-infection and vRNA levels were determined by PCR using HA gene specific primers. The data shown is representative 2 donors tested at 24h post-infection. Primers to amplify 18sRNA were used as a control.

CHAPTER 4

ENTRY-DEPENDENT INNATE SIGNALING OF INFLUENZA H1N1 VIRUSES IN HUMAN MACROPHAGES

OVERVIEW

Responses to IAV infection are mediated by multiple immune and non-immune cell populations. Specifically, macrophages play a central role in the early innate immune responses and are found in abundance in lungs of patients with fatal pneumonia. These macrophages include resident alveolar and also infiltrating peripheral blood monocyte-derived macrophages. The precise contribution of these individual cell populations to H1N1pdm induced inflammation remains to be defined. Using an *in vitro* model of primary human monocyte-derived macrophages (MDM), our laboratory sought to define isolate specific differences between 2009 pandemic H1N1 (H1N1pdm) isolates shown to have a fatal (A/KY/180/10) and nonfatal (A/KY/136/09) outcome in hospitalized patients but share greater than 99% sequence homology. Our previous *in vitro* studies of human well-differentiated epithelial cells infected with these isolates identified a differential polarized secretion for CCL5 with greater basal levels in cells infected with KY180. Given the role of CCL5 in monocyte recruitment, we postulated that differences in virus-host interactions between these two closely-related isolates may occur in recruited macrophages. To address our hypothesis,

the kinetics of infection (plaque assay and gene expression) and innate immune responses (gene expression) were assessed in “resting” MDM at 8, 24 and 36 hours post-infection (hpi). We infected MDM with H1N1pdm (A/KY/180/10, A/KY/136/09, A/NL/602/09) or seasonal H1N1 (A/BN/59/07) viruses at an MOI=1. All isolates infected macrophages showing increased titers over time. Pro- and anti-inflammatory mRNA levels differed markedly between the lethal (KY180) isolate compared to the nonlethal (KY136) and seasonal (BN59) H1N1 isolates. At 8 HPI, KY136 and BN59-infected MDM showed significantly greater levels of IFNy, CCL5, CXCL11, CXCL10, TNF, and IDO as well as pattern-recognition receptors RIGI, TLR3, TLR7, IRF3, and IRF7 compared to KY180. IL10, TGFβ and PPARy (all anti-inflammatory) were not elevated by any virus. By 24hpi, all 3 IAVs showed similar profiles, although the magnitude of the response was lower in cells infected by KY/180. This apparent delay in pro-inflammatory response and intracellular signaling by KY180 was found to be dependent on the mode of viral entry, as determined using inhibitors to macropinocytosis, and were mapped to the D222G mutation within the HA1 gene of KY180. We further revealed a greater number of KY180 viruses to have a filamentous shape suggesting the differences in route of entry may be dependent on the viral shape. This study reveals a novel mechanism for differences between the host responses to different circulating IAV isolates of the same strain.

INTRODUCTION

In response to viral infection, the release of cytokines and chemokines from the host shows both beneficial activation of innate and adaptive immunity,

and harmful effects, including high fever, shock symptoms, and cell damage. [232, 407-409]. The composition, timing, and magnitude of the host response to the virus infection is critical to the outcome of infection. The complex nature of pathogen-host interactions are reflected in the diverse range of patient outcomes such as those observed each year from seasonal influenza A virus (IAV) infection [345, 410-412]. Specifically, during the 2009 pandemic, severe clinical cases showed a slower decline in nasopharyngeal viral loads and had higher plasma levels of pro-inflammatory cytokines and chemokines [413]. Thus suggesting that timing and regulation of the host response is critical to the outcome of infection.

MDM can be categorized into two subsets including a healing/growth promoting anti-inflammatory macrophages (previously known as M2 or alternatively activated), to a killing pro-inflammatory macrophage (previously known as M1 or classically activated) [414]. Specific markers associated with these two phenotypes are summarized in figure 23 [370, 376, 378, 388, 395, 415-417]. A balance between the pro- and anti- inflammatory conditions in the lung is critical for lung homeostasis and limiting immunopathology associated with infection (Figure 24) [418]. Hypercytokenemia, a hallmark of HPAIV, is characterized by an unusually high pro-inflammatory and low anti-inflammatory response in MDM [307]. Further, studies have found AM are less responsive to MDM in pro-inflammatory cytokine induction, suggesting the source of hypercytokenemia during H5N1 infection are the MDMs [353]. Thus highlighting the importance of understanding the IAV-MDM interaction and how this may relate to disease.

Studies evaluating IAV infection in MDM also show variation between IAVs with some studies reporting productive replication in MDM [222, 307, 351, 353-357, 405] while others show IAV does not replicate productively [353, 357]. Further, results on the innate immune responses generated in infected macrophages differed when comparing low pathogenic IAV (LPAIV) to high pathogenic IAV (HPAIV). Specifically, some show greater induction of pro-inflammatory and anti-viral responses in MDM after HPAIV infection [307, 406] whereas others found an impaired induction after HPAIV infection [405]. One possible explanation that may distinguish IAVs within the human macrophage models may occur through interactions with pattern recognition receptors (PRRs). PRRs that recognize IAV RNA include cytoplasmic RLRs (RIGI and MDA5), and endosome-associated TLRs (TLR3, 7) [325, 381]. These recognition receptors are important in activating downstream transcription factors resulting in activation of gene expression and synthesis of cytokines, chemokines, cell adhesion molecules, and immune receptors [325, 381]. Specifically, these early host responses to infection represent an important link to the adaptive immune response.

IAVs are highly pleomorphic, showing mostly spherical (80-120nm diameter), but other forms have been reported including long filamentous particles (up to 400 nm long and 80-120 nm in diameter) [20, 212] (Figure 5). Different strains of IAV vary in their shapes with filamentous forms of IAV being noted in the literature for many years [104, 213, 214]. The filamentous phenotype has been mapped to HA, NA, M1, and M2 [39-44]. Specifically, studies using a

reverse genetics approach identified specific viral genes and amino acids within those genes that influence filament formation. They were able to link the ability to form filaments to sequence variations in the M1 protein and M2 protein [39, 40, 216-221]. Recent work utilizing a filamentous strain of influenza virus (H3N2 Udorn) showed that the virus entered cells as efficiently as the spherical forms; however, this occurred with slightly delayed kinetics suggesting another source of variation that could affect viral tropism [92]. Thus this delayed entry may be due to differences in the virus shape and therefore, differences in viral entry pathways elicited. IAVs have been shown to enter epithelial cells via both clathrin-mediated endocytosis and macropinocytosis [92-96]. No current evidence exists that toll-like receptors exist within macropinosomes suggesting a potential correlation with mode of viral entry and exposure to the full range of recognition receptors [110]. Thus differences in mode of viral entry into susceptible macrophages may provide a mechanism for differences in activation of inflammatory responses in MDM models.

Herein we report a delayed expression of activation markers in MDM, specifically CD80, CD64, CD200R, and CCR7, by our more lethal H1N1pdm isolate KY180. Further, we found a delay in pro-inflammatory responses and intracellular signaling by KY180 which was not found to be due to differences in apoptosis, requiring a replicating virus to induce a response, the ability of the viruses to regulate the intracellular signaling and protein synthesis, or the pH of viral fusion and entry. To further determine the mechanism for this delay, we evaluated the shape of KY180 and KY136 by electron microscopy. We revealed

a greater number of KY180 viruses to have a filamentous shape suggesting the route of entry may be different between the two viruses. Using specific inhibitors of clathrin-mediated endocytosis and macropinocytosis, we found KY180 to have a greater sensitivity to macropinocytosis inhibitors suggesting this to be the main route of KY180 entry into MDM. Using reverse genetics and interchanging KY180 HA gene onto the NL602 virus (another 2009pdm H1N1 virus) background, we were able to map the entry phenotype as well as the gene expression of innate signaling genes to the HA gene of KY180. Further, we found the D222G mutation within the HA1 gene to be strongly associated with the KY180 phenotype. This study reveals a novel mechanism for differences between the host responses to different circulating IAV isolates of the same strain.

METHODS

Isolation and differentiation of MDM. Peripheral blood mononuclear cells (PBMCs) were obtained from healthy donors and isolated using plasma-percoll gradients by the University of Louisville Nephrology Department. protocol developed by Dr. Suttles laboratory at the University of Louisville as previously described with slight modifications [384]. Briefly, PBMCs were washed twice in Dulbeccos PBS (DPBS, HyClone with Magnesium and Calcium, ThermoFisher) and resuspended with final concentration at $2x10^6$ cells/ml in R5 media, which contains RPMI 1640 (HyClone, ThermoFisher) supplemented with 5% heat inactivated human AB serum (Atlanta Biologics), 0.01M HEPES (Invitrogen Life Technologies), and 2ml Pen/Strep (Invitrogen Life Technologies). Monocytes were plated on 6 well low-attach plates (ThermoFisher) at a volume of 4 ml per

well. Monocytes were allowed to mature for 5 days in a 37° C incubator with 5% CO_2. After the maturation period, cells were removed from low-attach plates gently using a cell lifter (Costar, ThermoFisher), washed twice with DPBS supplemented with 0.2% human AB serum, and resuspended at $4x10^6$ cells/ml in R5 media. Cells were plated (4x10^6 cells/ml) and allowed to adhere for two days. Mature MDM were selected by adherence after 2 days by washing with DPBS with 0.2% human AB serum. Cells were incubated in R5 media for 1 h prior to infection/treatment.

Influenza viruses. Viruses used for these experiments included H1N1 IAV isolates from human clinical patients during the 2009 pandemic A/KY180/2010 (KY180) and A/KY136/2009 (KY136) [298, 385]. For comparison, we also included a seasonal H1N1 IAV vaccine strain A/Brisbane/59/2007 (BN59) (kindly provided by the Centers for Disease Control and Prevention, Virus Surveillance and Diagnosis Branch, Influenza Division). Viral seed stocks were prepared as previously described [298] in MDCK cells and stored at -80˚C. Viral titers of the stocks were characterized by median tissue culture-infective dose ($TCID_{50}$) assay in MDCK cells and calculated using the method of Reed and Muench [386].

***In vitro* infection of MDM.** For infection of adherent MDM, cells were washed 2 times with macrophage serum-free media (Invitrogen Life Technologies) to remove serum from the culture. The cells were infected at an MOI of 1.0 unless otherwise indicated diluted in viral growth media containing macrophage serum-free media supplemented with 0.1% BSA (Invitrogen Life Technologies), antibiotics, and 1μg/ml Trypsin-TPCK (Sigma) for1 h. After removing the

inoculum, the cells were washed 3 times with DPBS. Viral growth media was then added to each well and cells were incubated at 37°C with 5% CO2 for 1-36 h depending on the experiment.

Plaque assay was used to determine viral titers on supernatant from MDM after infection. Briefly, MDCK cells were plated in six-well format, viral dilutions were added to cell monolayer with 2.5% Avicel, and plates were allowed to incubate for 3 days. Cells were fixed in 0.4% paraformaldehyde and visualized using crystal violet. Plaques were counted and the number of plaque forming units (pfu) per milliter (pfu/ml) was determined.

RNA isolation and cDNA synthesis. At the designated timepoint, total cellular RNA was extracted from cells using the Trizol reagent (Invitrogen Life Technologies) according to the manufacturer instructions. The quality and quantity of the extracted RNA was assessed using an Experion (BioRad), where RNA was accepted for downstream reaction with an integrity value greater than 7. For evaluation of cytokine and intracellular signaling genes, we used 1 ug of extracted RNA, random hexamer primers, and Superscript III reverse transcriptase (Invitrogen Life Technologies) to generate complementary DNA (cDNA) for downstream real time-PCR (RT-PCR) reactions.

For detection of viral RNA (vRNA), messenger RNA (mRNA), and complimentary RNA (cRNA) we used 1 μg of RNA along with primers specific for amplifying influenza A nucleoprotein vRNA, mRNA, and cRNA to generate cDNA. Gene specific primers (10 μM) ([391], primers summarized in Table 9)

were combined with RNA and SuperScript III reverse transcriptase for this reaction (Invitrogen Life Technologies).

Real-time PCR of cellular and viral genes. To characterize the surface and activation markers expressed in the two populations, monocytes and macrophages. Half of the monocytes were either collected in Trizol for RNA/DNA extraction for RT-PCR or collected using PBS/0.2% EDTA solution for flow cytometry. Monocytes were collected after cells were washed in DPBS and before being placed in media with human serum. The other half were allowed to mature through the described protocol and at the 7th day, cells were collected for RT-PCR and flow cytometry. Total RNA was isolated, and the expression levels were determined by RT-PCR.

For RT-PCR reactions, 100 ng of cDNA, 10 μM of each gene specific primers, and Power SYBR® Green Real-Time PCR master mix (Invitrogen Life Technologies) were used. Primers were designed using PrimerBank software [387] or determined using previously published primer sets (Table 9) [376, 388-391]. The RT-PCR consisted of 1 cycle of 50°C for 5 min and 95°C for 2 min and 40 cycles of 95°C for 3 s, 60°C for 30 s using the 7900 Fast Real-Time System (Applied Biosystems) or VIIA7(Invitrogen Life Technologies). The threshold was automatically set and C_t (threshold cycle) determined. For all runs, samples were assayed in duplicate and non-template controls were included. Samples were normalized using β-actin as the reference endogenous control. The average threshold cycles of the replicates were used to compare the infected and uninfected controls using delta-delta $(\Delta\Delta)C_t$ method, using the following formula:

$\Delta\Delta C_t$= (ΔC_t (infected) target-ΔC_t (infected) reference)- (ΔC_t target (uninfected)-ΔC_t (uninfected) reference). The fold change was determined using the following formula: $2^{-\Delta\Delta Ct}$.

Flow cytometry. For assessing extracellular and intracellular markers in monocytes and MDM, cells were detached on ice with 2.5 mM EDTA in PBS. For extracellular staining only, cells were washed and incubated with conjugated antibodies (abCam) for 1 h and then fixed in 4% paraformaldehyde. For intracellular staining, cells were collected, washed and fixed in 4% paraformaldehyde for 15 minutes, followed by permeabilization with 10X permeabilization buffer (2% saponin, 4% Goat Serum in DPBS) for 20 minutes. 1×10^5 cells were incubated with either influenza nucleoprotein fluorescein isothiocyanate conjugated antibody (NP-FITC, AbCam #ab20921) or intracellular cytokine primary antibodies (BD Biosciences) diluted in 1X permeabilization buffer for 1h. Cells were washed and analyzed using a FACSCalibur (Becton-Dickinson) flow cytometer with 10,000 events collected. Data were analyzed using FlowJo® software, version 10 (Tree Star).

Immunofluorescence. MDM were cultured on hydrogen chloride treated glass coverslips (Bioscience Tools) in a 24-well plate (Corning). Cells were infected at an MOI of 1.0 for 1h and washed 3 times with DPBS to remove unbound virus. Viral growth media was replaced and incubated for 24h. Cells were fixed with 4% paraformaldehyde in DPBS and permeabilized using 0.2% saponin. After blocking with 5% FBS/2%BSA in phosphate buffered saline, cells were stained with the primary antibodies as indicated (diluted in DPBS containing 5% FBS)

followed by incubation with AlexaFluor-conjugated secondary antibodies (diluted in DPBS containing 5% FBS). Slides were embedded using Pro-Long anti-fade (Molecular Probes), mounted and analyzed using a Zeiss LSM710 Meta confocal laser-scanning microscope.

Kynurenine Assay (Indirect assay for IDO1 enzymatic activity). This assay was done on culture supernatants from two donor sets. 100µL of supernatant was collected from infected MDM, as described above. The supernatants were mixed with 30% trichloroacetic acid (Sigma) and vortexed. Mixture was centrifuged for 5 minutes (9000 xg) and supernatant was then mixed in a 1:1 ratio with Ehrlich reagent (Sigma) in a 96 well plate format. The optical density was measured immediately at 492nm on a plate reader. This is an indirect method for measuring kynurenines. The reaction of the aromatic amino group of kynurenine with p-dimethylaminobenzaldehyde (in the Ehrlich reagent) results in an imine product that can be measured at 492nm. This protocol was provided by Jessica Zourelias from the University of New York in Buffalo.

Protein Isolation. Mock- or influenza virus-infected MDM cells were collected in Trizol reagent (Invitrogen Life Technologies) and protein isolated according to the manufacturer. Briefly, protein was dialyzed using 10,000 molecular weight cut-off SnakeSkin® dialysis tubing (ThermoFisher) in 0.1% SDS overnight. Dialyzed protein was centrifuged at 10,000xg for 10 min and protein pellets were resuspended in 8M Urea/1%SDS and heated to 50^{o}C. Amount of protein in each sample was quantitated using Bradford Assay (Thermo Scientific).

Western blot. For Western blot analysis, 15 μg of protein from whole-cell lysate was heat denatured in cracking buffer (60 mM Tris (pH 6.8), 6M Urea, 1% SDS, 1% 2-ME, 1% bromophenol blue). Cell lysates were separated by electrophoresis on 12% SDS-PAGE gel and transferred to nitrocellulose membranes. The membranes were blocked in Tris-buffered saline plus 1% Tween 20 (TBST) containing 5% (weight-to-volume ratio) non-fat milk for 1h and immunoblotted with mouse primary antibodies to NFkB, Iκκ, phosphor-NFκB, IRF3, phospho-IRF3, IRF7, phosphor-IRF7, RIGI, MDA5, or rabbit primary antibody GAPDH overnight at 4°C. Bound antibodies were visualized by incubation with HRP-coupled goat anti-rabbit or anti-mouse IgG antibodies (Abcam) and bands were detected using Novex® ECL Chemiluminescent reagent (Invitrogen Life Technologies) and developed using X-ray film in a dark room.

Culture of macrophages for TNF production. Macrophages ($1x10^5$ cells per well of 24-well plate) were infected or mock-infected as previously described by exposure at an MOI of 1.0 for 1h in macrophage infection media. After 1h cells were washed with DPBS and fresh infection media replaced. At 4h after infection, LPS from *Escherichia coli* 0127:B8 (source) was added to culture media at 10ng/ml. At 6h after infection, Brefeldin A (eBioscience) was added to LPS treated and untreated wells at a 1:1000 dilution. At 8h after infection, the cells were detached on ice with 2.5 mM EDTA in PBS, washed and fixed in 4% paraformaldehyde for 15 minutes, followed by permeabilization with 10X permeabilization buffer (2% saponin, 4% Goat Serum in DPBS) for 20 minutes. 1×10^5 cells were incubated with influenza nucleoprotein fluorescein

isothiocyanate conjugated antibody (NP-FITC, AbCam #ab20921) and BD Pharmingen™ TNF allophycocyanin conjugated antibody (clone MAb11, BD Biosciences) diluted in 1X permeabilization buffer for 1h. Cells were analyzed as stated above.

Ultra-violet irradiation of IAV before infection. For UV-inactivation, 500 µl of virus seed stock was placed in a 4-cm^2 well and irradiated for 1h at 4°C on a UV Transilluminator (Spectroline). Viral inactivation was demonstrated by plaque assay on MDCK cells as described above. On the day of infection, MDM were inoculated with live virus at an MOI of 1.0 or with the same amount of UV-inactivated virus for 1h. After inoculation, cells were washed 3 times with DPBS, viral growth media (as above) was added to each well, and cells were incubated at 37°C with 5% CO2 for the duration of the experiment.

Threshold pH of IAV by syncytia assay. Syncytia assay to assess the threshold pH for viral fusion for KY180 and KY136 was performed by Jeremy Camp at the University Of Louisville Department Of Microbiology. The approach is outlined Figure 33. Briefly, MDCK cells were incubated with virus for 1h, washed and then incubated for 24h. MDCK cells were then submerged in buffered solutions at varying pH for a 3 minute pulse followed by another 24h incubation. Cells were then washed, stained with Geimsa, and evaluated under light microscope for syncytia formation. Depicted here is an example of MDCK cells that have syncytia formation (KY136 with pH 5.3 buffer treatment) and no syncytia (KY136 with pH 5.4 buffer treatment). Using a light microscope, the

threshold pH was determined by the presence or absence of syncytia at a specific pH.

Pharmacological inhibitors. 5-(N-Ethyl-N-isopropyl) Amiloride (EIPA), Chlorpromazine (CPZ), and Ammonium Chloride (NH_4Cl) were obtained from Sigma-Aldrich and Dynole 2-24 (DYN) from abCam. All inhibitors (except NH_4Cl) were dissolved in dimethyl sulfoxide (DMSO) and further diluted in serum-free macrophage media (Invitrogen Life Technologies). NH_4Cl was dissolved in serum-free macrophage media. To exclude any cytotoxic effects of the inhibitors and DMSO, control cells were included which were incubated in the same dilution of the inhibitors.

Treatment of macrophages with pharmacological entry pathway inhibitors. MDM were incubated with specific concentrations of pharmacological inhibitors before viral exposure (1h of pre-incubation at 37 °C). Following incubation, MDM were infected with IAV diluted to an MOI of 1.0 in viral growth media containing the inhibitors. Inhibitor levels were maintained during viral exposure. Cells were then washed to remove unbound virus 3 times with DPBS and viral growth media with inhibitors was replaced. Twenty four hours later, viral entry was assessed by measuring intracellular IAV-NP protein levels by flow cytometry.

Flow Cytometry. The percentage of infected MDM cells was determined by assessing intracellular NP expression following infection with IAVs in the presence or absence of inhibitors. Mock infected cells treated with equal concentration of inhibitor served as controls. At the 24h time point, the cells were removed from the culture plate using PBS/0.2% EDTA, fixed with 4%

paraformaldehyde, permeabilized with 2% saponin 4% serum, and stained with anti-NP (FITC-labeled) antibody and evaluated by flow cytometry. Gates were established with unstained and mock infected controls where less than 1% NP positive. Percent inhibition was determined by comparing the percentage of IAV positive cells in inhibitor untreated versus treated cultures. Counts on y-axis of the histograms were normalized to mode. Analysis was conducted using FlowJo® software.

Cryo-electron microscopy of influenza A viruses. 3.5 ul of purified and concentrated KY136 and KY180 was loaded onto glow discharged Holey Carbon grids and plunge frozen on a Cryoplunge™ 3 machine. Grids were loaded on to a Titan Krios (FEI) or a CM200 (FEG Phillips) and images were obtained for both strains to compare the morphology. 100 to 125 virus particles were imaged for both strains to document the morphology. Measurements of virus morphology were done using ImageJ. Cryo-EM imaging was conducted at Purdue University in collaboration with Dr. Jason Lanman and Amar Parvate.

Reverse genetics to create recombinant NL602 viruses with KY180 HA gene and NL602 virus with specific mutations in the HA gene. This approach is outlined in Figure 25. Briefly, 8 plasmid rescue systems based on pDZ for NL602 and pDZ for KY180 were used to transfect 293T cells co-cultured with MDCK cells. Subsequent passaging of supernatant was performed until a cytopathic effect was seen in the culture. Supernatant was collected, spun down and viral stocks made. Stock titers were determined by $TCID_{50}$ assay. Cells were also collected and RNA extracted for sequencing to confirm recombination occurred.

(B) To introduce specific mutations into the NL602 HA pDZ plasmids, primers were designed to amplify plasmids containing the mutation, and then treated using a kinase-ligase-DpnI enzyme kit (New England Biolabs) to prepare the mutant plasmids for transformation. Transfection, viral stock preparation, and sequencing were done as described above. The reverse genetics virus recovery and preparation of viral stocks was performed by Jeremy Camp, University of Louisville Department of Microbiology. Plasmids were kindly provided by Dr. Adolfo Garcia-Sastre Mount Sinai School of Medicine New York.

Statistics. For the comparison of two sets of values, Student's t test (two-tailed, two-sample equal variance) was used. When comparing three or more sets of values, data were analyzed by one-way analysis of variance (ANOVA), followed by posthoc analysis using Tukey's multiple-comparison test. A p-value of ≤0.05 was considered statistically significant.

RESULTS

H1N1pdm and seasonal H1N1 isolates exhibit a low infectivity of MDM but an increase in virus production over time. To determine whether the 'resting' MDM culture model supported infection and replication of pandemic H1N1, we infected MDM with seasonal and pandemic H1N1 influenza viral isolates and evaluated viral nucleoprotein levels using both flow cytometry and confocal microscopy. Surprisingly, there was no significant difference in infectivity between different isolates (Figure 26 A,B). Infection of MDM was examined by immunofluorescent staining and confocal microscopy of NP. Positive staining for the NP in influenza virus infected macrophages was shown at 24hpi (Figure

26A). Additionally, the number of NP positive cells by flow cytometry was similar with ~20% of cells becoming infected with virus (Figure 26B)

Considering that all three, KY180, KY136, and BN59 infected resting MDM, we next asked whether they permitted replication and release of infectious virions. To achieve this we measured the amount of virus produced by plaque assay on culture supernatant from infected cells at 8, 24, and 36 hpi. Although inefficient, all three isolates showed increased and similar titers overtime by plaque assay (~10^3) (Figure 27A). To further confirm replication was occurring in infected MDM, we evaluated the time course of viral RNA synthesis over time by RT-PCR using tagged primers specific for NP mRNA (Figure 27B), vRNA (Figure 27C), and cRNA (Figure 27D). Overtime, accumulation of all three species of RNA were consistently detected in MDM. Our observation that viral RNA increases overtime, while viral titers remain somewhat low prompted us to conclude that the viral isolates studied here infect MDM productively but inefficiently.

H1N1pdm and seasonal H1N1 isolates showed differential activation marker profiles after infection. Because all three isolates infected the resting MDM model, we sought to determine whether the cells became activated after infection by all three isolates. We infected MDM for 8h and performed RT-PCR analysis of macrophage activation markers including CD80, CD64, CD200R, and CCR7. Transcriptional analysis showed mRNA expression levels of all our markers were lower for KY180 compared to KY136 and BN59. This suggests a delayed activation of MDM infected by KY180 (Figure 28). These results warrant

further investigation into the interactions between these isolates and the MDM cells.

Differential expression kinetics of immune response genes in MDM among H1N1pdm and seasonal H1N1 isolates. Considering that macrophages are a major source of cytokine production during infection [358], we compared the gene expression profile of pro-inflammatory, anti-inflammatory, and interferon genes in IAV-infected MDM by quantitative real-time PCR at 8 and 24 hpi. The comparison of $\Delta\Delta C_t$ values of infected cultures to mock infected cultures show a delayed expression of immune response genes by KY180 (Figure 29). Specifically, KY180 induced much less TNF, IL6, CCL5, CXCL10, IFNβ, IFNγ, and IDO1 mRNA expression than KY136 and BN59 at 8h post-infection. By 24 hpi, all 3 IAVs showed similar innate immune response profiles, although the magnitude of the response was lower in cells infected by KY180 (Figure 29). Consequently all isolates showed no expression of anti-inflammatory markers such as IL10 and TGFβ and PPARγ at 8 or 24 hpi. Next we sought to determine whether KY180 had a reduced IDO (Indoleamine 2, 3-dioxygenase) protein level and IDO enzymatic activity compared to the other isolates as suggested by RT-PCR mRNA expression results. We compared intracellular protein levels of IDO1 by flow cytometry and found no difference in the percentage of IDO1 positive cells in the infected and uninfected cells populations (data not shown).

Delayed expression of PRRs in MDM infected with KY180. Previous studies have shown differential induction of cytokines by H5N1 viruses in human macrophages, which can be regulated by IRF3 and p38 MAPK [419]. Because

IFN-β as well as other pro-inflammatory genes (TNF, CCL5, etc) showed differential kinetics of expression between KY180 and KY136 and BN59 in MDM at 8hpi (Figure 29) we sought to determine which upstream genes within the Toll-like receptor, RIG-I-like receptor, and the NOD-like receptor (NLR) pathways were contributing to this outcome.

We compared the gene expression of TLR, RLR, and NLR genes in IAV-infected MDM by quantitative real-time PCR at 8 and 24 hpi. When comparing the $\Delta\Delta C_t$ values of infected cultures to mock infected cultures, we again observed a delayed expression of a number of genes by KY180 (Figure 30A). At 8 hpi, a delayed response within the RLR pathway, specifically RIGI and MDA5, and the TLR pathway, specifically TLR7 were noted in KY180 but not KY136 (Figure 30A). The significant differences in gene expression levels of TLR3, TLR7, IRF3 and IRF7 at 8 and 24hpi suggest MDM may detect these two viruses differently (Figure 30A).To further confirm these findings, we compared the protein levels of selected innate immune response genes at 8hpi by western blot analysis after infection. These studies suggest KY136 has greater toll-like receptors protein levels than KY180 agreeing with the RT-PCR findings (Figure 30B). Interestingly, the levels of NFκB and IRF3 did not differ between viruses (Figure 30B). This suggests activation of TLRs are important to the delayed response by KY180 infected MDMs.

Differential expression of immune response genes by H1N1pdm viruses cannot be attributed to how the viruses regulate the immune response within the cell. Because of the observed delay and significantly different mRNA

expression levels of immune response genes, specifically TNF, between the two viruses, we sought to compare the regulation and protein production of TNF. Elevated mRNA and protein TNF levels have been shown for more pathogenic avian influenza viruses in human macrophages [357]. TNF has pleiotropic functions by promoting apoptosis [420] , the inflammatory response [421, 422], and providing host resistance to pathogens [423]. IAV proteins have been shown to interact with cellular machinery and disrupt protein synthesis and inflammatory gene pathways affecting mRNA and protein levels within the infected cell [424, 425]. We hypothesized the delayed TNF response in KY180 infected macrophages was due to viral manipulation of cellular machinery.

To test this we employed a previously published method looking at TNF protein production in the presence of a secondary bacterial signal, LPS. Early studies have shown that most phagocytic mononuclear cells support viral replication and responded with a high TNF mRNA accumulation accompanied by low TNF protein production. Only when small amounts of LPS were co-cultured with virus was the TNF protein production detected [426, 427]. Thus, we co-cultured IAV-infected MDM with LPS to see if there was a difference in activation or suppression of the TNF response by the two viruses. Between two donors, no difference was observed in the activation and suppression of the TNF response between KY180, KY136, and NL602 (Figure 31). Specifically, the percent of IAV positive cells, TNF positive cells, and the percent of both IAV and TNF positive cells did not differ between viruses (Figure 31). This suggests the delayed response by KY180 is not a result of viral protein manipulation of the host cellular

machinery but by a different mechanism. The following series of studies aim to identify the mechanism(s) underlying the delayed MDM immune response to KY180 compared to KY136.

H1N1pdm and seasonal H1N1 require a replicating virus to activate immune response gene expression. To investigate whether the responses from infected MDM were dependent on a replicating virus, we performed a time-course infection experiment in MDM from 2 additional donors using both live (Figure 32A) and UV-inactivated IAVs (Figure 32B). We examined the mRNA expression of cytokine and interferon genes and show UV-irradiated viruses did not induce cytokine or chemokine gene expression at 24hpi (Figure 32B). This suggests that the induction of cytokines and chemokines after infection requires an intact genome and a replicating virus.

As discussed previously, KY180 and KY136 replicated at a comparable level (Figure 27 A-B). Thus the differential kinetics of MDM up-regulation of cytokine expression cannot be explained based on replication. To further understand the mechanism we looked at whether the delayed response was due to differences in IAV-induced anti-viral response (apoptosis) or simply a differences in the isolate's ability to overcome entry/replication limitations within MDMs.

MDM are equally susceptible to IAV-induced apoptosis. Previous reports relate cytokine dysregulation to the variable onset of apoptosis by different influenza strains [428, 429]. We hypothesized that the delayed signaling response in KY180-infected MDM may be due to differential onset of apoptosis.

By flow cytometric quantification of Annexin V positive cells, we found the percentage of apoptotic cells increased in IAV-infected compared to mock-infected MDM (Figure 32C). Consequently, the percentage of apoptotic cells was similar between isolates and did not explain differences in innate signaling responses of MDM to infection of two isolates.

Low pH is required for entry of both H1N1pdm into the MDM. In order for IAV to enter a cell, the bound virus must undergo endocytosis. Viral components are released into the cell once the IAV hemagglutinin protein encounters a low-pH to undergo a conformational change and facilitate membrane fusion. Our first question was whether entry of both H1N1pdm viral isolates into MDM requires a low pH. To accomplish this, we treated MDM cells with ammonium chloride (NH_4Cl) and measured viral entry by staining for intracellular nucleoprotein at 24hpi and evaluated by flow cytometry. Inhibition of endosomal acidification by NH_4Cl completely blocked the ability of both H1N1pdm viruses to enter MDM (Figure 33A).

H1N1pdm isolates showed similar thresholds of pH for membrane fusion. As expected, both viruses require a drop in pH to enter MDM. We next sought to determine if the threshold pH of fusion differed between the two viruses. Previous studies have found that the presence of the E47K mutation in the HA2 gene of H1N1 viruses reduces the threshold pH for membrane fusion from 5.4 to 5.0 [121]. Through sequencing analysis, one of the 22 mutations that distinguish KY180 from KY136 is this E47K mutation in the HA2 gene [298]. We hypothesized that the threshold pH of fusion for KY180 within the MDM

endosomes occurs at a lower pH than KY136. To address this hypothesis, we performed a syncytia formation assay to determine the threshold pH of fusion for the two viral isolates. Despite the apparent mutation differences in the HA2, the pH of fusion for the two isolates was identical (Figure 33B). This suggests the differences in innate signaling may be a result of the two viruses entering the MDM by different pathways.

H1N1pdm (KY180) has greater sensitivity to macropinocytosis inhibitors compared to H1N1pdm (KY136) suggesting differences in intracellular trafficking. Clathrin-mediated endocytosis is considered the primary route of endocytic entry of influenza virus into cells [95, 96]. To determine whether the delayed kinetics of cytokine expression observed was a result of an alternate route of entry taken by KY180, we inhibited clathrin-mediated endocytosis using pharmacological inhibitors and assessed the resulting viral infectivity by staining for intracellular nucleoprotein at 24hpi and evaluated by flow cytometry. As with previous reports, we observed that blocking clathrin-mediated endocytosis by the inhibitor chlorpromazine (CPZ) moderately inhibited both KY180, KY136 and an additional H1N1pdm isolate NL602 from infecting human cells (Figure 34 A,C).

The blockade of dynamin formation by the inhibitor Dynole (DYN), showed that KY136 to be slightly more sensitive to the dynamin inhibitor; however, cytotoxicity was observed when MDM were treated with 10uM or greater concentrations, limiting the sensitivity of our assay to detect any significant difference between the isolates. Previous reports have utilized anywhere from 10μM-80μM of dynamin inhibitors to dissect the entry of influenza viruses in

HeLa and MDCK cells [107, 430]; however, based on technical limitations of MDM, we were unable to distinguish whether there were differences in susceptibility to dynamin inhibitors. No differences were observed at 1 and 5μM concentrations. Next we asked whether the delayed kinetics of cytokine expression observed was a result of an alternate route of entry taken by KY180.

Macropinocytosis has recently been identified as an alternate entry pathway for influenza viruses [106, 107]. To evaluate whether the two isolates relied on alternative pathways of entry into human macrophages, we inhibited macropinocytosis using pharmacological inhibitors and assessed the resulting viral infectivity 24h post-infection by staining for intracellular NP and evaluating by flow cytometry. Interestingly, inhibition of macropinocytosis by EIPA significantly reduced KY180 infectivity but not KY136 or NL602 (Figure 34 B,C). This suggests KY180 favors macropinocytosis for entry into MDM and further explain the differences in innate signaling in MDM. This further confirms macropinocytosis as an alternate entry pathway for influenza virus and a potential mechanism for differences in intracellular responses in MDM.

The delayed immune phenotype induced in KY180-infected MDM is dependent on mode of entry, specifically macropinocytosis. To confirm whether the immune gene expression phenotype was altered in the presence of the inhibitors, we compared the gene expression of pro-inflammatory and PRR genes in IAV-infected, treated or non-treated MDM by real-time PCR at the 24h time point. When comparing the ΔΔCt values of infected cultures to mock infected cultures with or without inhibitors, we see a hindered expression of

immune response genes by KY180 in the presence of EIPA (Figure 35). This hindrance was not as apparent in KY136-infected MDM treated with EIPA, specifically TNF, NFκB, and the TLRs. This collectively confirms our conclusion that the delayed immune phenotype induced in KY180-infected MDM is dependent on mode of entry via macropinocytosis.

IAV morphology differs between KY180 and KY136. According to recent studies, IAV can take on different shapes, which can influence the route of entry taken by the virus [104]. To determine if KY180 and KY136 viruses have different morphologies, cryo-EM was employed, in collaboration with Purdue University. Purified and concentrated viruses were cryo-frozen onto grids and images obtained using a Titan Krios (FEI) imager. Roughly 100 to 125 virus particles were imaged for both strains to document the morphology and measurements of virus morphology were performed. Only a handful of images were chosen to highlight the morphological variation (Figure 36 A-H). For KY136, all the particles were of round morphology with diameter varying from 80-350 nm. Only 1 particle was seen which had elongated morphology (Figure 36 A-D). For KY180, 80 (~61%) particles were round (80-120 nm diameter), 40 (~31%) particles were oblong (100-300 nm) and 10 (<1%) were filamentous (100 nm diameter and >300 nm long) (Figure 36 E-H). These images emphasize the different morphologies between the two isolates suggesting a potential source of the variation in inhibitor susceptibility.

IAV sensitivity to macropinocytosis inhibitors in MDM was mapped to the HA gene. To further delineate the exact mechanism driving differences in

sensitivity to macropinocytosis, we used reverse genetics to identify the viral determinants responsible for the increased sensitivity of KY180 to macropinocytosis inhibitors. We used reverse genetics to swap the HA gene segment KY180 into the background of another early pandemic isolate NL602 and evaluated the susceptibility to EIPA inhibitor. As expected, swapping the HA segment of KY180 into the NL602 background made the NL602 virus more susceptible to the macropinocytosis inhibitor, acting more like KY180 (Figure 37). This demonstrated that a specific mutation within the HA gene of KY180 drives the viruses phenotype in MDM. Specifically, two genes within KY180-HA map to the sensitivity phenotype, D222G which have previously been reported to correlate with increased pathogenicity.

Interestingly, there are only 22 amino acid (mostly synonymous) changes between KY180 and KY136 and of these only one of these so far in the HA (D222G) has been suggested to correlate with higher virulence in patients [338, 339, 431]. This specific mutation in the HA1 shows dual receptor specificity for both alpha-2,3- and alpha-2,6-SA, with a particular increase in binding to macrophages and type II pneumocytes in the alveoli and to cells in both the tracheal and bronchial submucosal glands [79].

To determine if the D222G mutation and 5 other mutations found in the HA gene (Table 10) were responsible for the KY180 phenotype, we generated NL602 viruses containing these mutations in the HA gene using site-directed mutagenesis (Figure 38). We subjected these viruses to the same experimental conditions as before, where we infected MDM for 24h in the presence or absence

of macropinocytosis inhibitor, EIPA. We then assessed whether any of these mutant viruses became KY180-like in their sensitivity to EIPA. Interestingly, we found two specific mutations that mapped to the EIPA sensitivity, D222G and S183P in KY180 HA1 (Table 11). The phenotype resulting from these two mutations suggests receptor and binding affinity may be a potential mechanism (Figure 38, Table 10).

IAV sensitivity to macropinocytosis inhibitors in MDM are dependent on genes previously associated with IAV pathogenicity. To confirm the immune gene expression phenotype of KY180 in the presence of EIPA was similar to the NL602 HA D222G mutant virus, we performed RT-PCR of inflammatory and PRR genes after infection. Gene expression was compared in mutant (D222G and S83P) and wild type (KY180 and NL602) infected MDM, treated or non-treated MDM by real-time PCR at 24h post infection. When comparing the ΔΔCt values of infected cultures to mock infected cultures with or without inhibitors, we see a slightly hindered expression of immune response genes, RIGI, TLR3, IRF7 and cytokines CCL5 and TNF, by NL602 HA D222G mutant virus in the presence of EIPA as was seen with KY180 (Figure 39). This hindrance was not as apparent in KY180 infected cultures and hindrance of expression was also seen for the NL602 wild-type virus suggesting an earlier time point may be necessary to see the true effect.

The phenotype of KY180-infected MDM was confirmed by a greater inhibition of viral infection and PRR and cytokine expression in MDM infected with the D222G HA mutant viruses compared to wild type. This study further

supports that this mutation is responsible for the KY180 phenotype and suggests a mechanism for its action.

DISCUSSION

To better understand the early events that take place after IAV-infection, we employed a “resting” human monocyte-derived macrophages (MDM). This model represents a non-activated macrophage with no previous exposures. Utilizing this model allowed us to uncover the composition and magnitude of early influenza-specific responses after infection. Previously published studies suggest that influenza viruses differ in their ability to infect and replicate in macrophages [353, 357]. In contrast [405], and in support of the work of others [353, 354, 356], we demonstrated that seasonal and pandemic (H1N1) viruses are not restricted in their ability to be internalized by macrophages.

Further, our analyses revealed that the seasonal and pandemic (H1N1) viruses replicated in MDM and differed temporally in their induction of the innate immune responses. Analysis of the replication revealed comparable speeds of replication, yet the amount of virus produced was relatively low. Within a couple of hours after infection, viral RNA expression was taking place at high levels, and no major differences were noted between the viral isolates. This data suggests the MDM cells had no inherent resistance to both pandemic and seasonal viruses, yet they did not serve as powerful viral factories.

Previous studies have shown that human influenza viruses infect macrophages inducing the release of TNF, IL6, IL10, IL1β, IFN α/β, and

chemokines such as CCL5, MIP-1β, CCL2, and CXCL10 [307, 351, 353, 357]. The mRNA expression kinetics of cytokines from MDM in response to infection with H1N1 viruses in our experiments (Figure 29) were similar to those documented previously. However, we found our more lethal H1N1pdm isolate to induce a delayed transcription of cytokine and PRR genes (Figure 29 and 30). These novel findings may provide clues as to why this virus behaved differently in mice [298] and humans compared to other closely related IAV isolates. Similar to what was seen in the MDM model, H1N1pdm isolates have been shown previously to have a delayed rate of infection compared to seasonal influenza virus in differentiated bronchial epithelial cells [91]. However, the mechanism for this delay is still undefined.

Using the resting MDM model, our laboratory was able to identify specific molecular determinants associated with different outcomes of IAV infection. IAV virus morphology was visualized using cryo-electron microscopy allowing us to image the virus particles in their native state. Of the total virus particles imaged for the KY180 strain, we observed about 1% particles to be filamentous and about 31% particles to have elongated morphology. However, 99% of all the virus particles of the KY136 strain had round morphology. While the percentage of filamentous as well as elongated particles for the KY180 strain is lower than that reported for the Udorn strain [40] the KY136 strain was predominantly found to have round particles. This suggests the two viruses may interact and enter differently in susceptible cells. Filamentous virus formation has been linked to mutations in the M1 and M2 gene of IAV. The only mutation in the M1 gene

between KY180 and KY136 is a S30G mutation suggesting another unknown mechanism may create the different morphologies of KY180. Regardless, to confirm that the filamentous virus is responsible for delayed immune signaling, future studies will employ a reverse genetics site-directed mutagenesis of the M1 gene in NL602 to create a filamentous virus, as previously reported [40]. This filamentous virus will be confirmed by cryo-EM and compared to the non-filamentous virus by measuring temporal expression of PRR and cytokine genes after MDM infection.

Our studies indicate the phenotype of KY180 is dependent on the pathway of entry and can be mapped to specific mutations in the HA gene (D222G and S183P). These mutations are located within the receptor binding site of the HA gene and have been shown to alter binding affinity [432, 433]. The Asp222 in IAV HA is predominantly found in human-adapted H1N1 viruses and has been shown to create optimal contact with the galactose sugar in glycans terminated by alpha-2-6-SA [434]. Consequently, a change from aspartic acid (D) to a glycine (G) has been shown to alter the electrostatic potential of the receptor binding domain resulting in a higher affinity for alpha-2,3-SA by increasing the flexibility of 220-loop within the HA [435]. With this in mind, we can hypothesize that differences in receptor-IAV binding affinity between KY180 and KY136 might explain phenotypic differences seen in the MDM model.

A possible explanation for our results is that these mutations promote binding to alternative receptors on the macrophage surface, potentially altering the timing of entry depending on their affinity. Many cell surface lipids and

proteins contain sialic acids making them potential targets for IAV binding. Mannose and galactose-type lectins found on the surface of macrophages have been shown previously to assist IAV infection murine macrophages; however entry through these receptors did not permit replication [436]. However, this study was not conducted using primary human macrophages. The presence and distribution of these lectins and their role in IAV binding and entry in MDM may shed light onto the differences between isolates.

Alternatively, other studies have found IAV capable of binding to multiple host receptor tyrosine kinases (RTKs) on the surface of A549 cells, further activating intracellular PI3K and ERK1/2 pathways which enhance IAV uptake [437]. Expression and activation of these receptors has been shown to alter the uptake of IAV, specifically selecting for clathrin-mediated endocytosis of IAV [438, 439] and others selecting for macropinocytosis of IAV [440]. To further support the role of RTKs in viral entry, Brindley *et al.* have shown filamentous Ebola-Zaire virus uptake in human tumor cells is promoted by the receptor tyrosine kinase Axl [441]. This further suggests entry of our viruses, both spherical and filamentous, may rely on different RTK for binding and signaling. It is possible that the distribution of RTKs on the surface of resting MDM may favor induction of clathrin-mediated endocytosis over macropinocytosis. Future studies will be conducted to determine whether our viruses rely on the same receptors for entry into MDM and also what the receptor distribution profile is on the resting MDM that may isolate specific entry.

Our work is the first to determine that the mechanism for viral entry is critical to activation of innate signaling and that this distinguishes influenza viral isolates showing different pathogenicity in mice and humans.

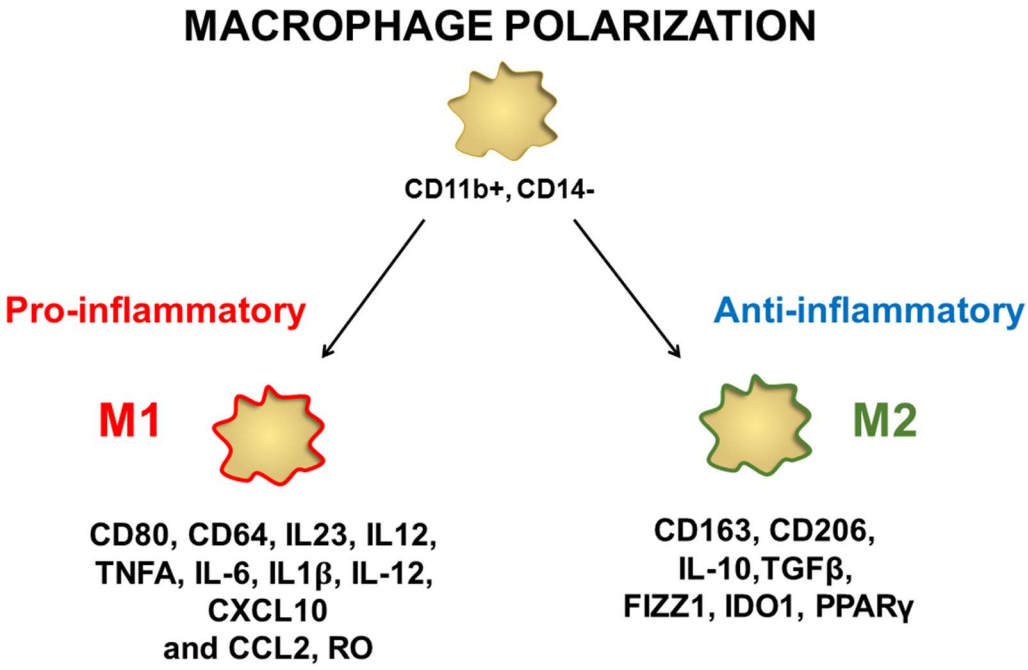

Figure 23. Subsets of macrophages and their associated markers. Macrophages derived from monocyte precursors undergo specific differentiation depending on the local tissue environment. Two distinct states of polarized activation have been identified: M1 pro-inflammatory and M2 anti-inflammatory macrophage phenotype. Pro- and anti-inflammatory phenotypes of macrophages have distinct chemokine and surface marker signatures as designated above.

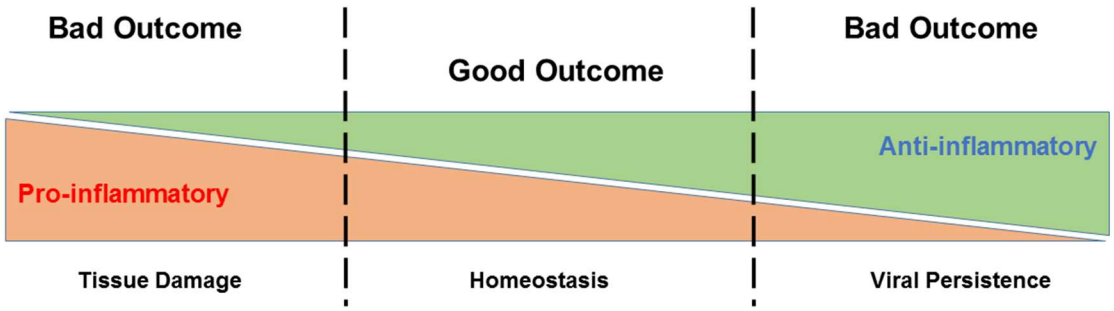

Figure 24. Balance of pro-inflammatory and anti-inflammatory response to IAV. In response to IAV there is a critical balance between pro- and anti-inflammatory immune response. Uncontrolled pro-inflammatory immune responses can result in damage to host tissues, whereas anti-inflammatory immune responses initiated prematurely can result in the survival of the pathogen which is deleterious to the host. It is thought that in a natural healthy immune response, there is a homeostatic balance between these two responses, resulting in the elimination of IAV and reducing the risk of creating extensive tissue damage. (Picture adapted from Rouse, B. T., & Sehrawat, S. (2010). Immunity and Immunopathology to viruses: what decides the outcome? Nature Reviews. Immunology, 10(7), 514–526).

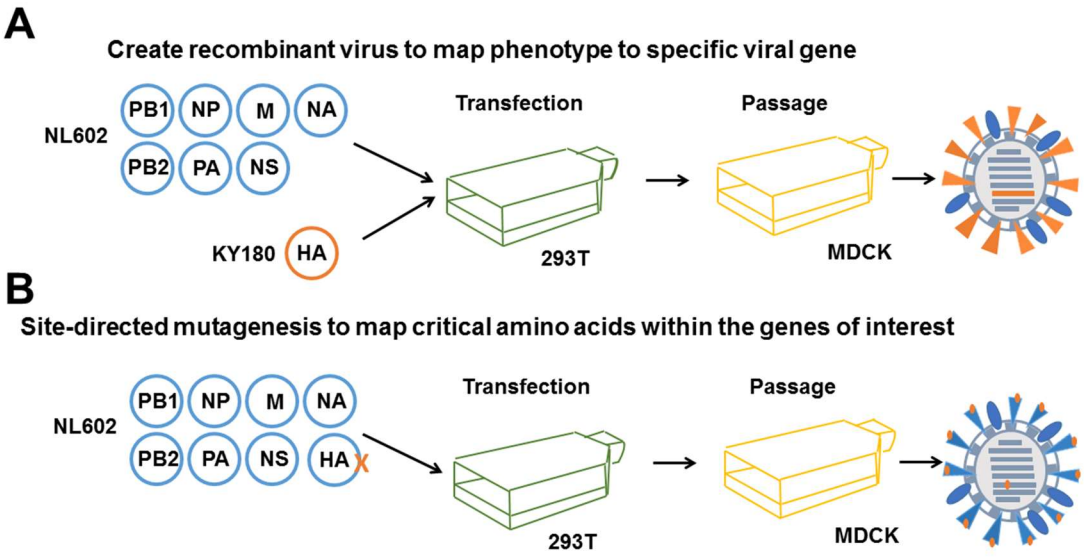

Figure 25. Approach used to recover reverse genetics recombinant NL602 viruses with KY180 HA gene and NL602 virus with specific mutations in the HA gene. (A) Plasmids for IAV proteins were transfected into 293T cells co-cultured with MDCK cells. Subsequent passaging of supernatant was performed until a cytopathic effect was seen in the culture. Supernatant was collected, spun down and viral stocks made. Stock titers were determined by $TCID_{50}$ assay. Cells were also collected and RNA extracted for sequencing to confirm recombination occurred. (B) To introduce specific mutations into the NL602 HA pDZ plasmids, primers were designed to amplify plasmids containing the mutation, then treated using a kinase-ligase-DpnI enzyme kit to prepare the mutant plasmids for transformation. Transfection, viral stock preparation, and sequencing were done as described above. The reverse genetics system and preparation of viral stocks was performed by Jeremy Camp, University of Louisville Department of Microbiology.

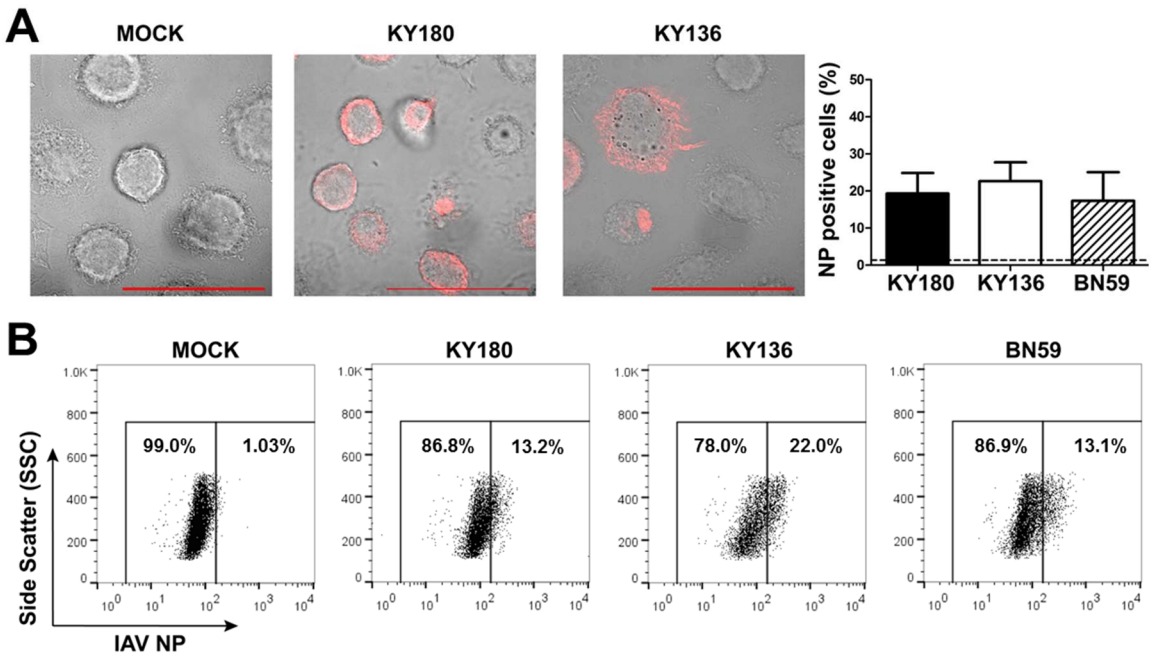

Figure 26. Pandemic and seasonal influenza viruses infect primary human monocyte-derived macrophages. In three independent experiments, human monocyte-derived macrophages were infected with influenza A viruses KY180 (H1N1pdm), KY136 (H1N1pdm) and BN59 (H1N1) at an MOI of 1. (A) MDM cells were fixed, permeabilized, and stained with anti-influenza nucleoprotein (NP)-FITC antibody conjugate and analyzed by flow cytometry 24h post-infection. Error bars show mean +/- standard deviation of percent NP-positive cells corresponding to the amount of infected cells. The lower limit of detection is indicated by the dotted line. (B) Immunofluorescence staining of MDM 24 h post-inoculation with KY180, KY136, and uninfected control (Mock). Influenza virus matrix protein was stained red (Alexa flour 633), while actin filaments were stained purple (Phalloidin). Image magnifications are at 100X. The slides were viewed by confocal microscopy as described in Materials and Methods.

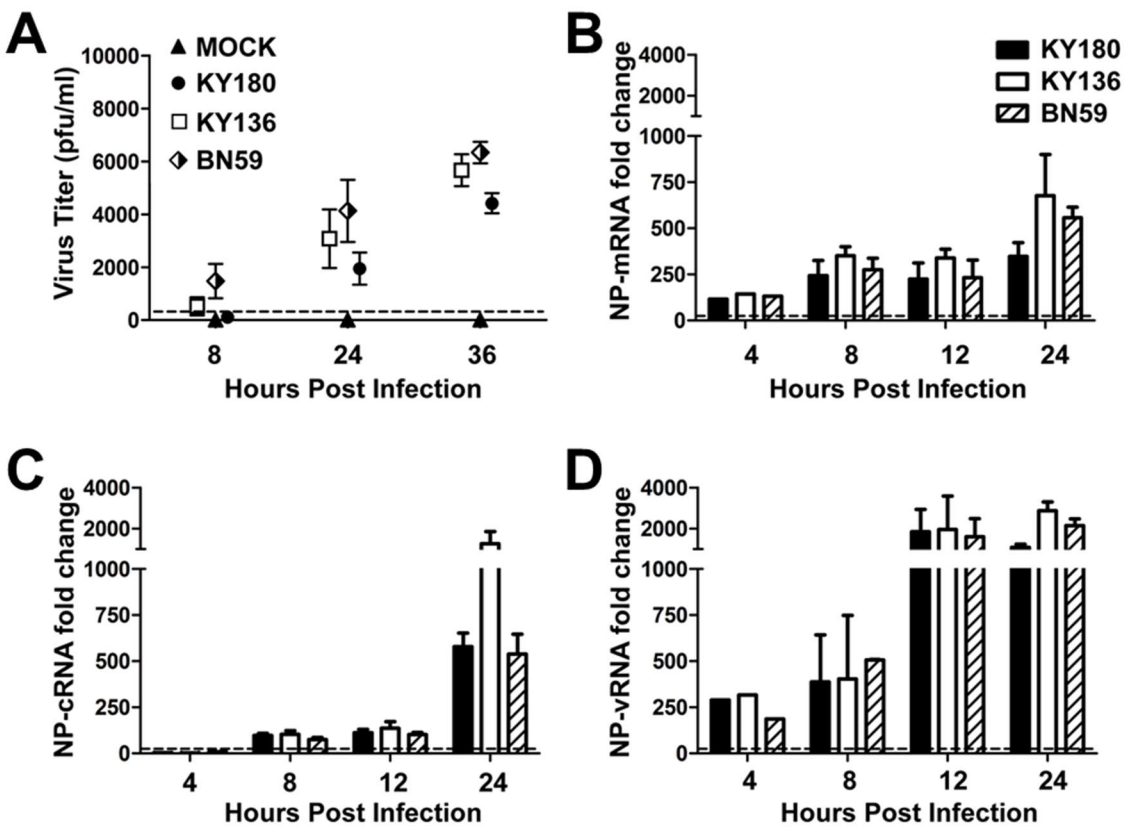

Figure 27. Replication of seasonal and pandemic IAV in MDM cells. (A) Replication of pandemic and seasonal influenza A (H1N1) viruses in MDM was analyzed by plaque assay performed on supernatants from three independent donors. Cells were infected with and MOI of 1.0 and supernatant was collected at 8, 24, and 36h post-infection. Data represent the mean ± SD of virus titer. Further, at the indicated time points, total RNA was isolated, and the levels of viral NP (B) mRNA, (C) cRNA, and (D) vRNA were determined by RT-PCR using gene specific primers. The data shown is three replicates of 1 representative donor of 2 (4h post-infection 1 replicate). RNA levels were normalized to β-actin and fold change determined by the ΔΔCt method as described in the materials

and methods. Results are expressed as mean ± SD. *, $p < 0.05$; **, $p < 0.01$; *** $p<0.001$. The lower limit of detection is indicated by the dotted line.

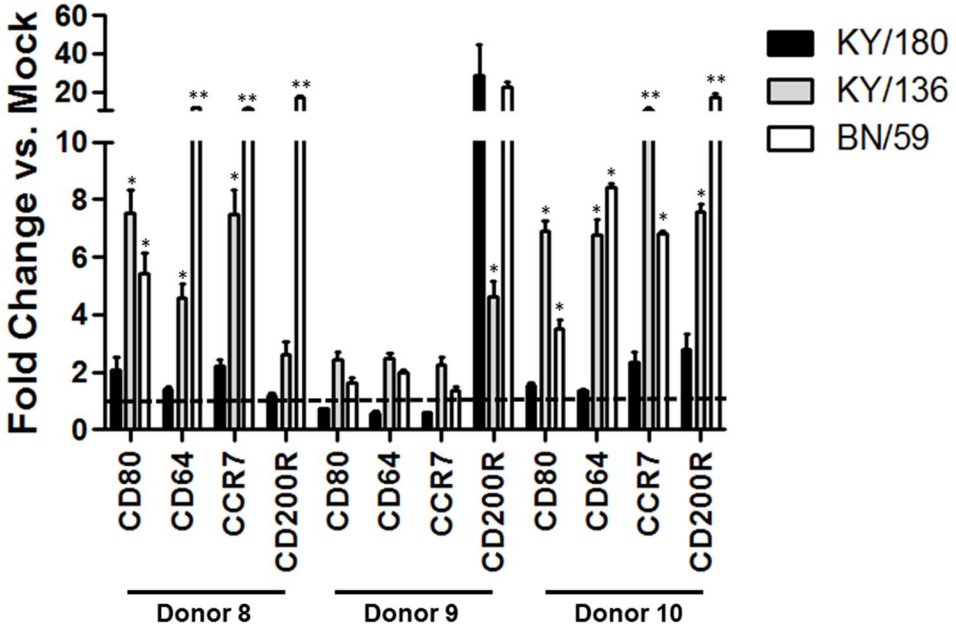

Figure 28. Differential expression of macrophage activation genes in MDM after infection by KY180, KY136, and BN59. MDM were infected with influenza viruses KY180 (H1N1pdm), KY136 (H1N1pdm) and BN59 (H1N1) at an MOI of 1. Cell lysates were collected at 24h post infection and mRNA expression of macrophage activation genes were measured by real-time PCR. Results are depicted from 3 donors (2 replicates of each treatment for each donor) and are expressed as mean ± SD fold change as compared to mock (uninfected) control. Fold change of 1, indicative of equal expression between infected and mock infected controls is indicated by the dotted line. Asterisks represent significance as related to KY180 expression. Significance as determined by ANOVA *, $p < 0.05$; **, $p < 0.01$; *** $p<0.001$.

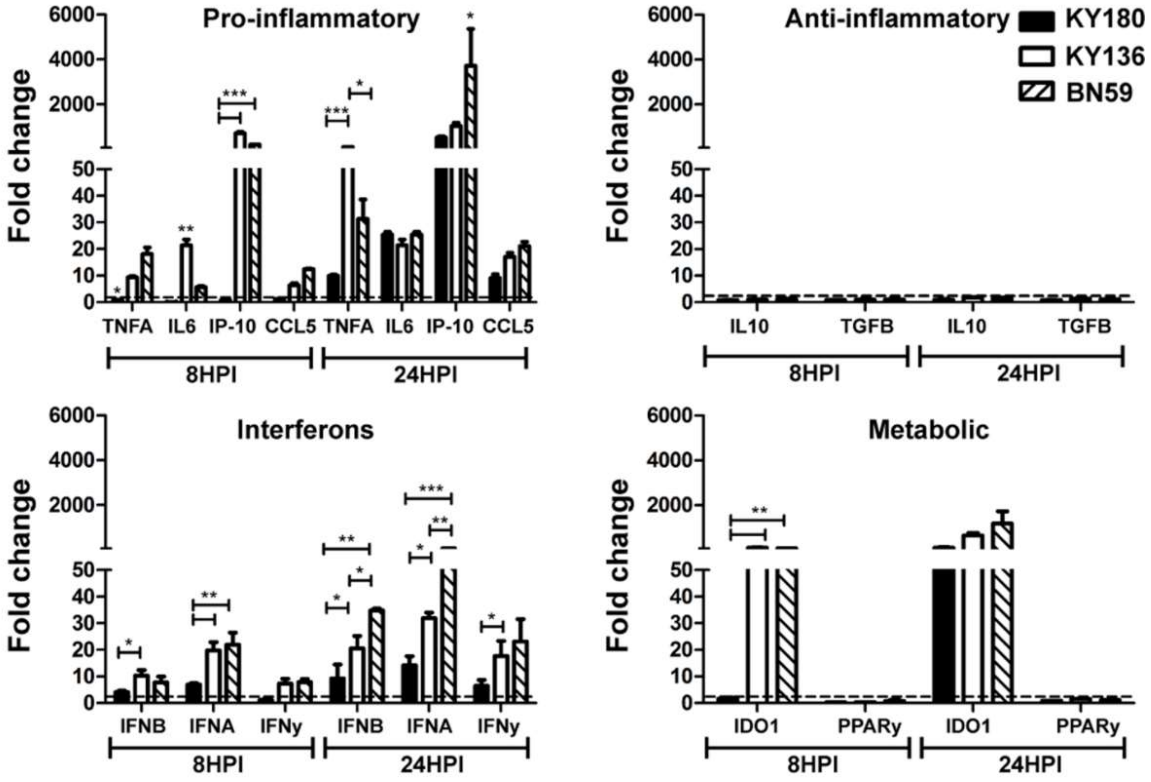

Figure 29. Influenza virus-mediated expression of cytokines and chemokines in MDM. MDM cells were infected with influenza viruses KY180 (H1N1pdm), KY136 (H1N1pdm) and BN59 (H1N1) at an MOI of 1. Cell lysates were collected at 8 and 24 h post-infection, and mRNA expression of pro-inflammatory, anti-inflammatory, interferon, and metabolic genes were measured by real-time PCR. Results are from one representative donor (3 done in total) and are expressed as mean ± SD fold change as compared to mock (uninfected) control. Fold change of 1, indicative of equal expression between infected and mock infected controls is indicated by the dotted line. IP-10 is also referred to as CXCL10 in the text. Significance as determined by ANOVA *, $p < 0.05$; **, $p < 0.01$; *** $p<0.001$.

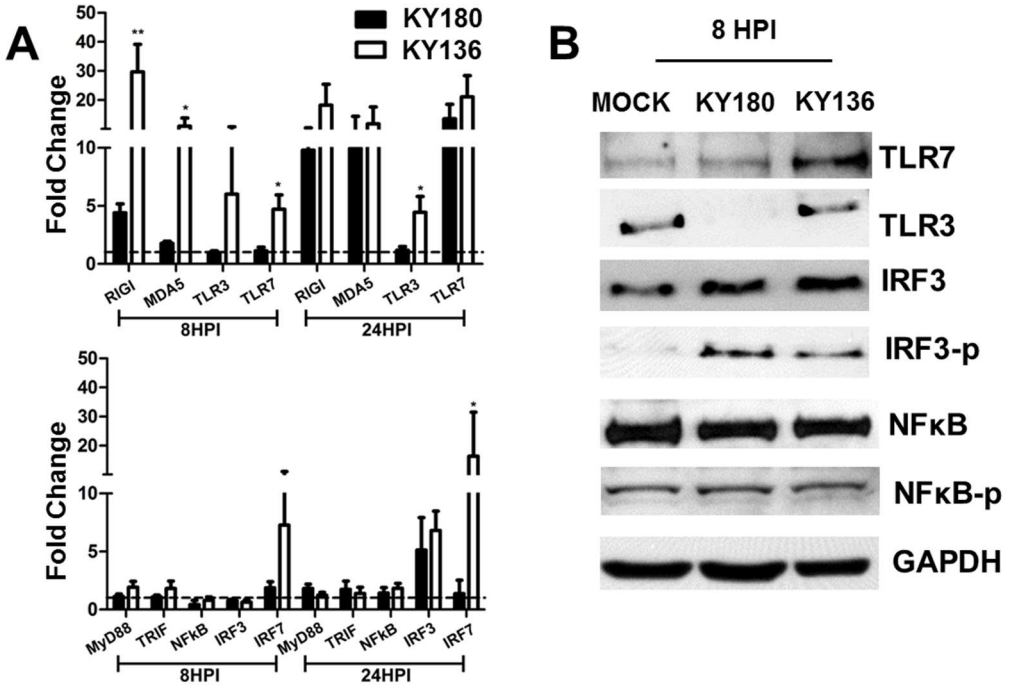

Figure 30. Influenza virus-mediated expression of pattern recognition receptor genes. MDM were infected with influenza viruses KY180 (H1N1pdm), KY136 (H1N1pdm) and BN59 (H1N1) at an MOI of 1. (A) Cell lysates were collected at 8 and 24h post-infection, and mRNA expression was measured by real-time PCR on two donors. Results expressed as mean ± SD fold change as compared to mock (uninfected) control. Fold change of 1, indicative of equal expression between infected and mock infected controls is indicated by the dotted line *, $p < 0.05$; **, $p < 0.01$; *** $p<0.001$.(B) MDM from two donors were infected as previously indicated and cell lysates were collected at 8 h post-infection. Protein levels were confirmed by western blot.

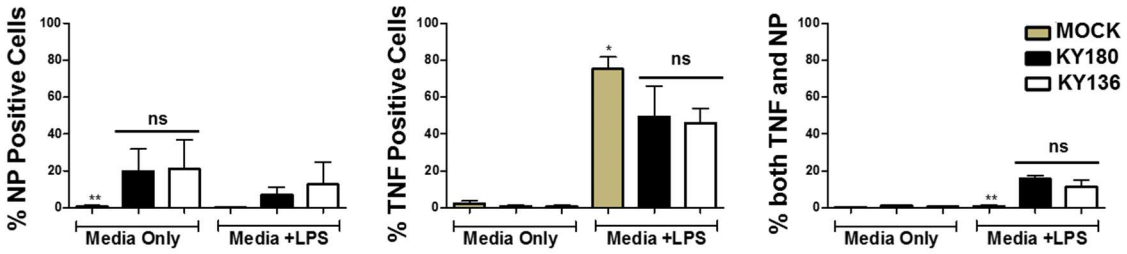

Figure 31. TNF protein production in the presence or absence of secondary signal, LPS in IAV-infected cells. The percentage of infected MDM cells was determined by assessing intracellular NP and TNF expression following 8h infection with 1 MOI of KY180, KY136 or NL602 in the presence or absence of a LPS. Mock infected cells treated with equal concentration of LPS served as controls. Cells were treated with LPS (10ng/ml) or equal parts infection media at 4h after infection followed by Brefeldin A treatment (1:1000) at 6h after infection. At the 8h time point, the cells were collected, fixed with 4% paraformaldehyde, permeabilized with 2% saponin 4% serum, and stained with anti-NP (FITC-labeled) and anti-TNF (APC-labeled) antibodies evaluated by flow cytometry. Gates (% gated macrophages) were established with unstained and mock infected controls where less than 1% NP positive and TNF positive cells. % positive cells were determined using FlowJo® software. Significance was determined by ANOVA *, $p < 0.05$; **, $p < 0.01$; *** $p<0.001$.

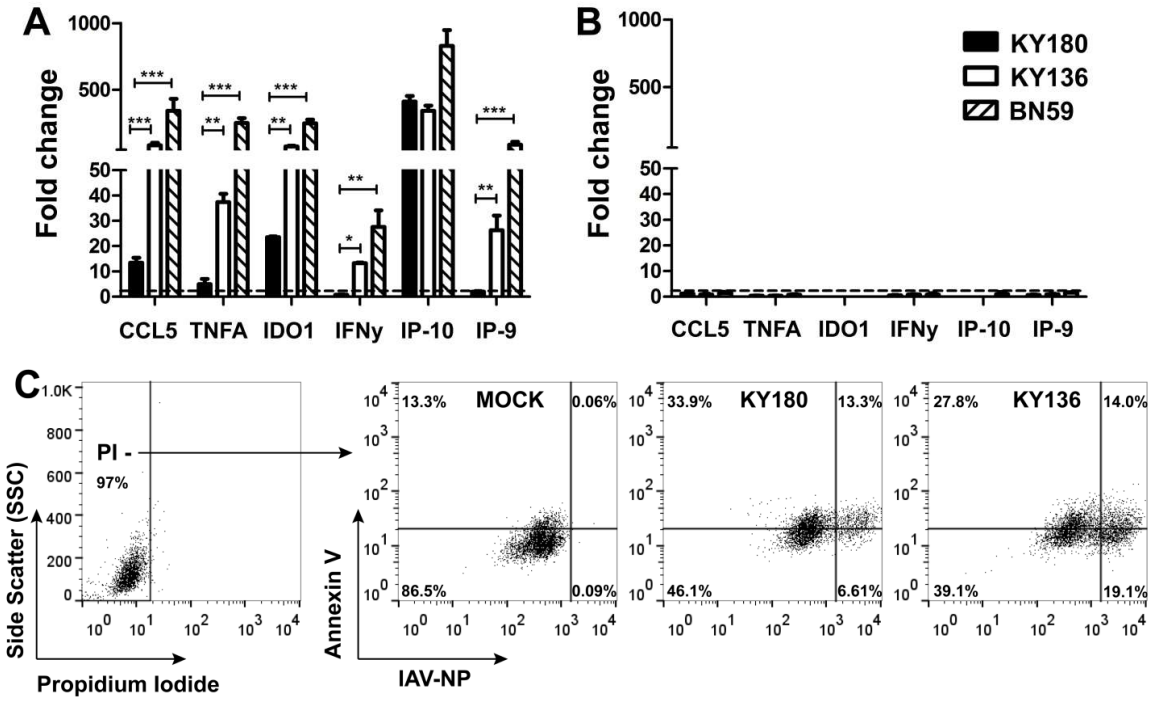

Figure 32. Innate immune response gene expression (with UV) and apoptosis. MDM were inoculated with live virus at an MOI of 1.0 or with the same amount of UV-inactivated virus for 1 h. Cell lysates were collected at 24 h post-infection from MDM infected with live (A) or UV-inactive (B) virus and mRNA expression of selected pro-inflammatory and anti-inflammatory genes were measured by real-time PCR. Results expressed as mean ± SD. *, $p < 0.05$; **, $p < 0.01$; *** $p<0.001$. IP-9 and IP-10 are referred to as CXCL11 and CXCL10 in the text. (C) The percentage of apoptotic MDM cells was determined by flow cytometry. Cell were infected with 1 MOI of KY180 or KY136. At the 24h time point, the cells were collected, stained with propidium iodide (PI) and AnnexinV, then fixed with 4% paraformaldehyde, permeabilized with 2%saponin 4% serum, and stained with anti-NP (FITC-labeled) antibody and evaluated on flow cytometer. Gates were established with unstained and mock infected controls where less than 1%

NP positive. As shown above, PI negative populations were assessed for Annexin and NP staining. Percentages represent those within the PI negative population for each treatment. Analysis was conducted using FlowJo® software.

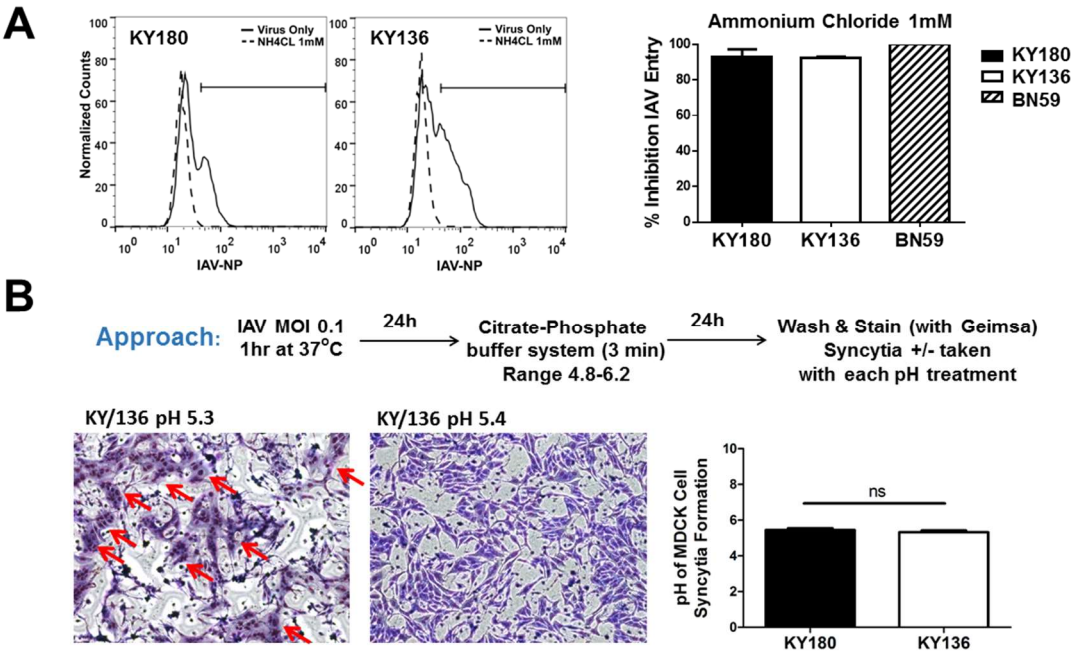

Figure 33. Requirement for low pH for entry and determination of the threshold pH of fusion for KY180 and KY136 by syncytia assay in MDCK cells. (A) The percentage of infected MDM cells was determined by assessing intracellular NP expression following 24h infection with 1 MOI of KY180, KY136 or NL602 in the presence or absence of NH_4Cl (dissolved in serum-free macrophage media). Mock infected cells treated with equal concentration of inhibitor served as controls. At the 24h time point, the cells were collected, fixed with 4% paraformaldehyde, permeabilized with 2% saponin 4% serum, and stained with anti-NP (FITC-labeled) antibody and evaluated by flow cytometry. Gates were established with unstained and mock infected controls where less than 1% NP positive. Percent inhibition was determined by comparing the percentage of IAV positive cells in inhibitor untreated versus treated cultures. Counts on y-axis of the histograms were normalized to mode. Analysis was conducted using FlowJo® software. NH_4Cl (ammonium chloride, prevents endosomal

acidification). (B) Syncytia assay to assess the threshold pH for viral fusion for KY180 and KY136 was performed by Jeremy Camp at the University of Louisville Department Of Microbiology. The approach is outlined in the figure. Briefly, MDCK cells were incubated with virus for 1h, washed and then incubated for 24h. MDCK cells were then submerged in buffered solutions at varying pH for a 3 minute pulse followed by another 24h incubation. Cells were then washed, stained with Geimsa, and evaluated under light microscope for syncytia formation. Depicted here is an example of MDCK cells that have syncytia formation (KY136 with pH 5.3 buffer treatment) and no syncytia (KY136 with pH 5.4 buffer treatment). Using a light microscope, the threshold pH was determined by the presence or absence of syncytia at a specific pH.

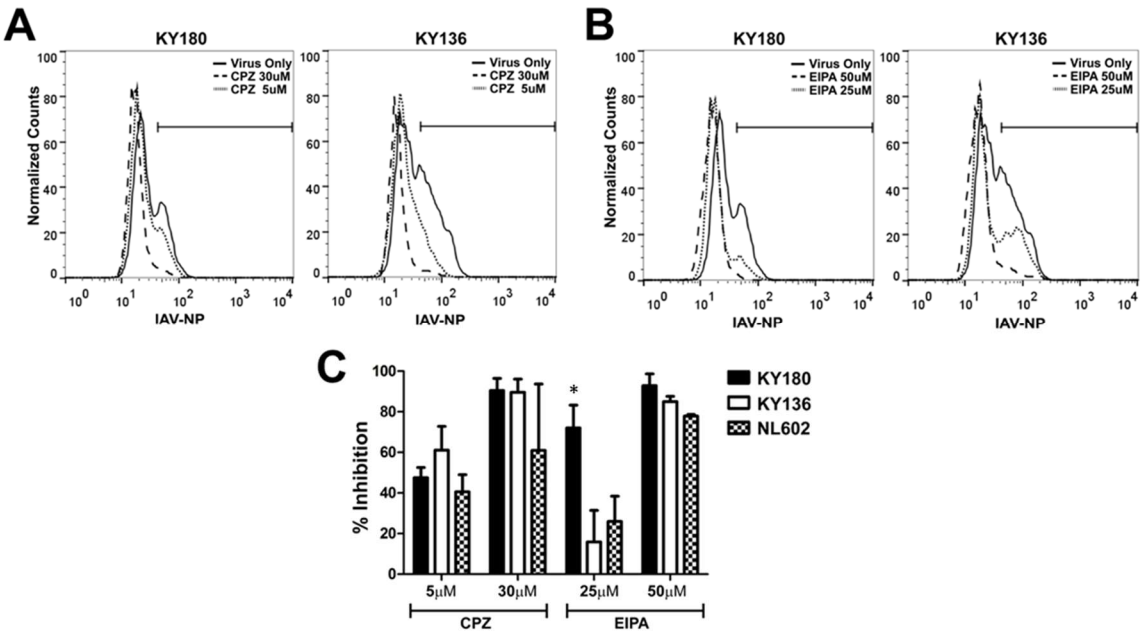

Figure 34. Effects of macropinocytosis and clathrin-mediated endocytosis inhibitors on viral entry into MDM. The percentage of infected MDM cells was determined by assessing intracellular NP expression following 24h infection with 1 MOI of KY180, KY136 or NL602 in the presence or absence of the indicated inhibitors. Mock infected cells treated with equal concentration of inhibitor served as controls. At the 24h time point, the cells were collected, fixed with 4% paraformaldehyde, permeabilized with 2% saponin 4% serum, and stained with anti-NP (FITC-labeled) antibody and evaluated by flow cytometry. Gates were established with unstained and mock infected controls where less than 1% NP positive. Percent inhibition was determined by comparing the percentage of IAV positive cells in inhibitor untreated versus treated cultures. Counts on y-axis of the histograms were normalized to mode. Analysis was conducted using FlowJo® software. EIPA, 5-(N-Ethyl-N-isopropyl) amiloride (macropinocytosis inhibitor); CPZ, Chlorpromazine (clathrin-mediated endocytosis inhibitor).

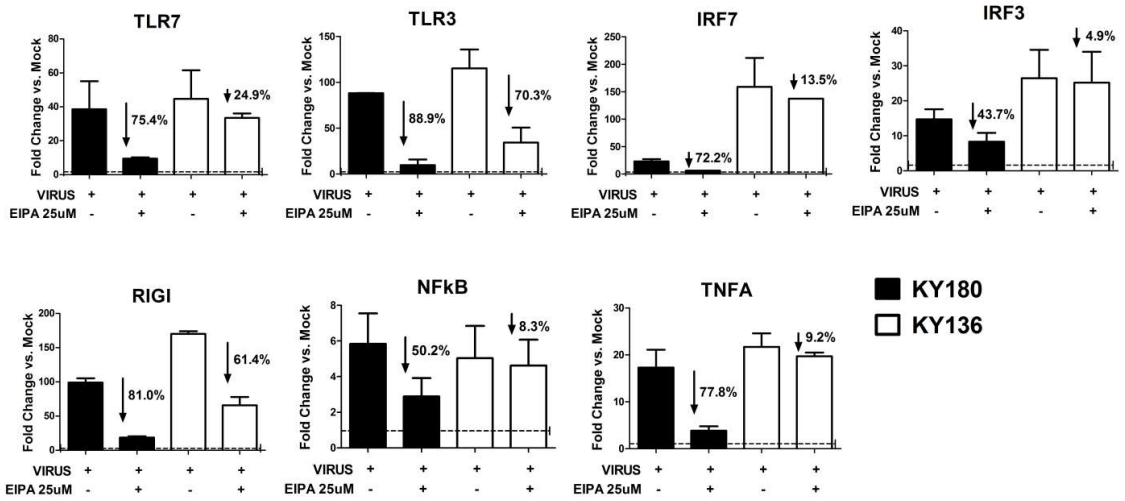

Figure 35. Expression of immune response genes in the presence or absence of inhibitor. MDM were infected with influenza viruses KY180 (H1N1pdm) or KY136 (H1N1pdm) at an MOI of 1 in the presence or absence of EIPA at 25uM concentration. mRNA expression of pro-inflammatory and viral recognition genes were measured by real-time PCR. Results shown are representative of 1 of 2 donors tested with 2 replicates per donors and are expressed as mean ± SD. *, $p < 0.05$; **, $p < 0.01$; *** $p<0.001$. Percentages listed are percent inhibition of fold expression with inhibitor treatment compared to virus alone. EIPA, 5-(N-Ethyl-N-isopropyl) amiloride (macropinocytosis inhibitor).

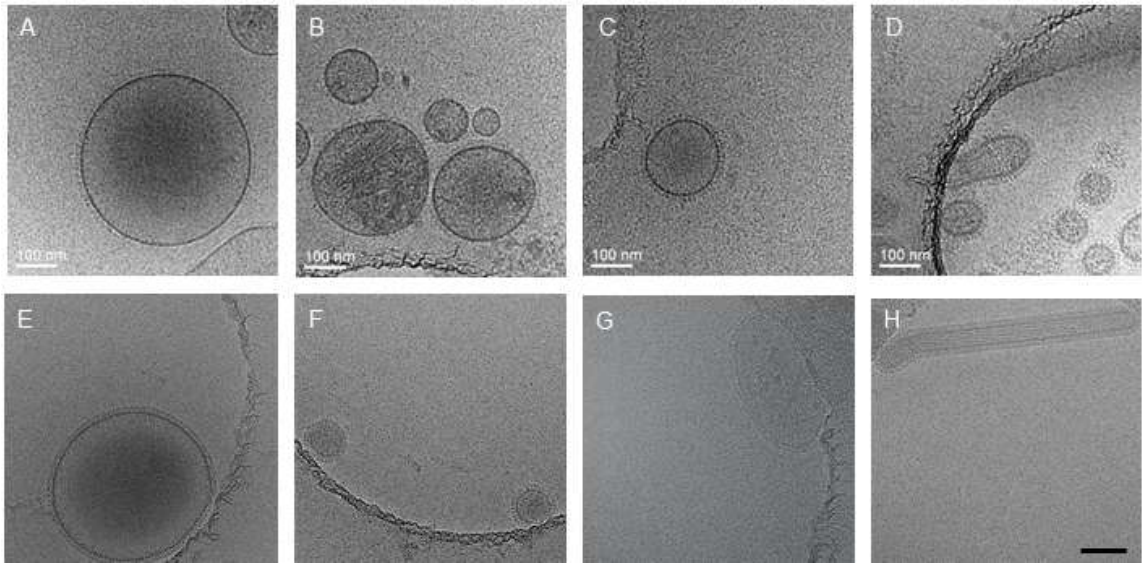

Figure 36. Cryo-EM pictures of KY180 and KY136. Representative cryo-EM images of KY136 exhibiting mainly round morphology (A to D). Diameter of particles ranges from 80-300 nm. Representative images of KY180 showing mostly round (E, F, G) and occasionally filamentous morphology (J). Diameter of the round particles ranged from 100 – 350 nm. Scale bar 100 nm (E to H). 3.5 ul of purified and concentrated KY136 and KY180 was loaded onto glow discharged Holey Carbon grids and plunge frozen on a Cryoplunge™ 3 machine. Grids were loaded on to a Titan Krios (FEI) or a CM200 (FEG Phillips) and images were obtained for both strains to compare the morphology. 100 to 125 virus particles were imaged for both strains to document the morphology. Measurements of virus morphology were done using ImageJ. Cryo-EM imaging was conducted at Purdue University in collaboration with Dr. Jason Lanman and Amar Parvate.

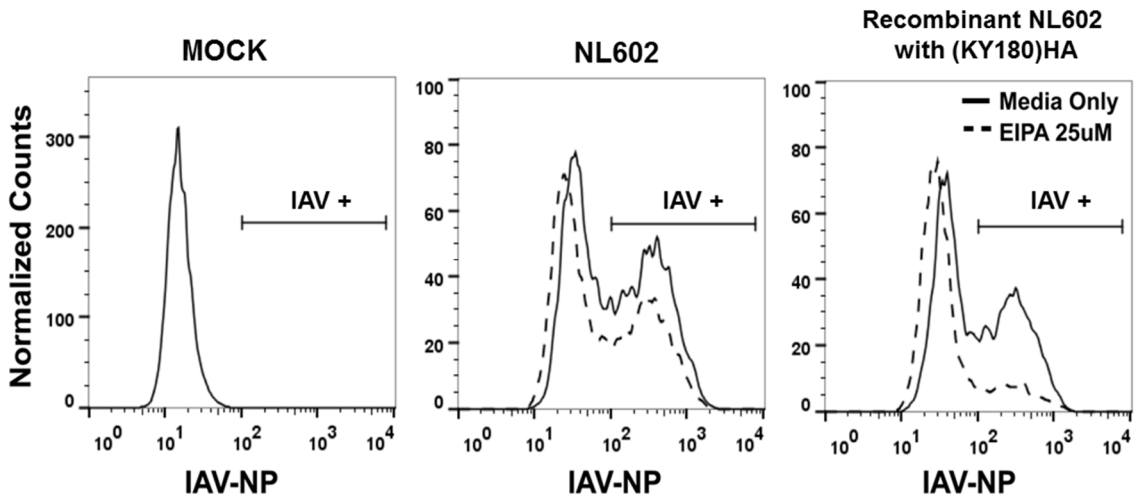

Figure 37. Sensitivity to macropinocytosis inhibitors can be mapped to the HA protein of KY180. The percentage of infected MDM cells was determined by assessing intracellular NP expression following 24h infection with 1 MOI of influenza viruses KY180 (H1N1pdm), NL602 (H1N1pdm), or the NL602 virus with a KY180 HA swapped in by reverse genetics. Infection was performed in the presence or absence of the EIPA at 25uM concentration. Mock infected cells, treated with equal concentration of inhibitor, served as controls. At the 24h time point, the cells were collected, fixed with 4% paraformaldehyde, permeabilized with 0.2% saponin 4% serum, and stained with anti-NP (FITC-labeled) antibody and evaluated on flow cytometer. Gates were established with unstained and mock infected controls where less than 1% NP positive. Counts on y-axis were normalized to mode. Analysis was conducted using FlowJo Software. EIPA, 5-(N-Ethyl-N-isopropyl) amiloride (macropinocytosis inhibitor).

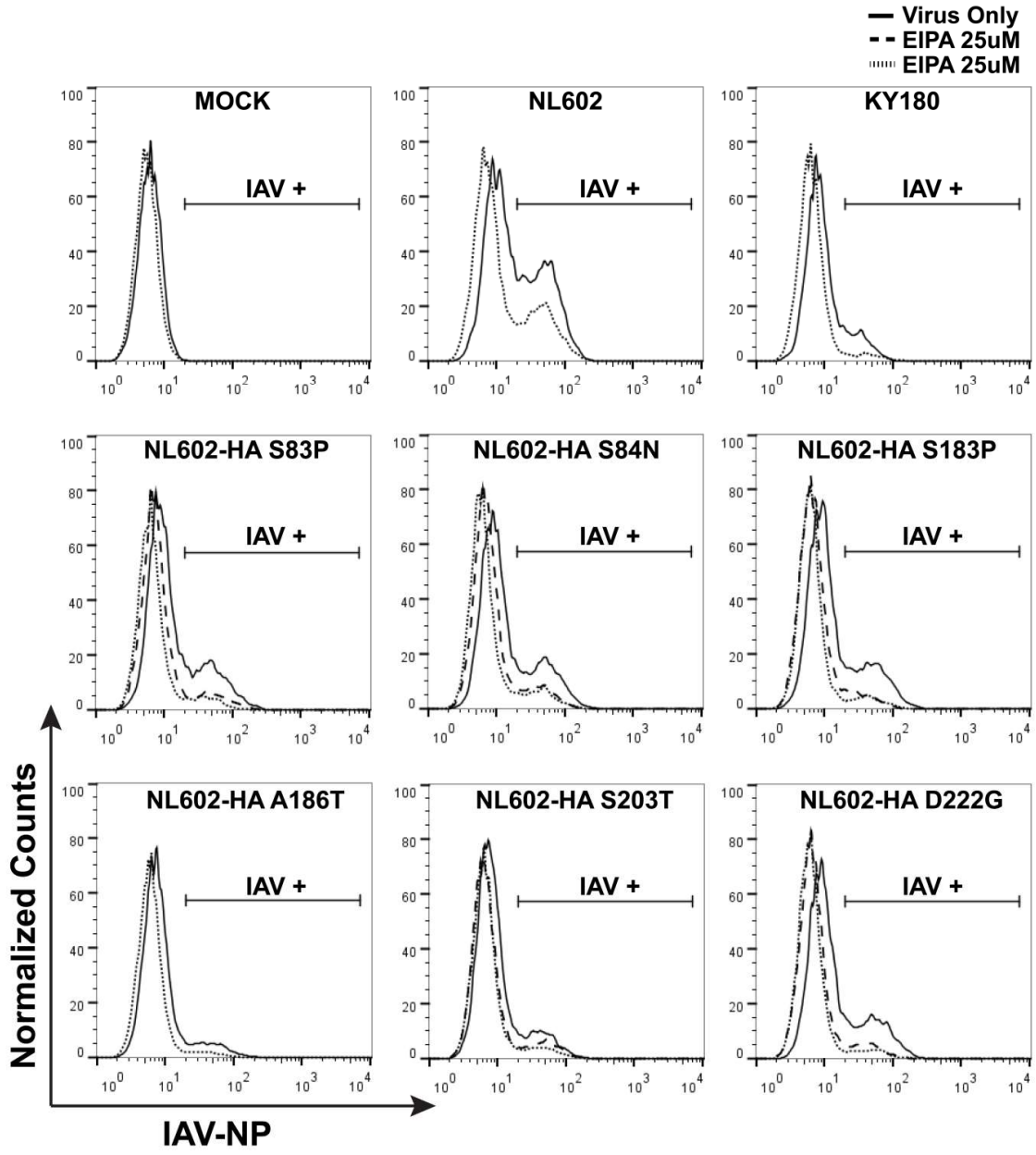

Figure 38. Sensitivity to macropinocytosis inhibitors can be mapped to specific mutations within the HA1 protein in KY180. MDM were infected with influenza viruses KY180 (H1N1pdm), NL602 (H1N1pdm), or viruses produced by reverse genetics and induction of point mutations in the HA1 gene of NL602 virus including NL602-S83P, S84N, S183P, A186T, S203T, D222G. Infection was

performed at an MOI of 1 in the presence or absence of EIPA at a 25uM concentration. Mock infected cells, treated with equal concentration of inhibitor, served as controls. At the 24h time point, the cells were collected, fixed with 4% paraformaldehyde, permeabilized with 0.2% saponin 4% serum, and stained with anti-NP (FITC-labeled) antibody and evaluated on flow cytometer. Gates were established with unstained and mock infected controls where less than 1% NP positive. % Inhibition (as indicated) was determined by comparing the % IAV positive cells in inhibitor untreated versus treated cultures. Counts on y-axis were normalized to mode. Analysis was conducted using FlowJo Software. EIPA, 5-(N-Ethyl-N-isopropyl) amiloride (macropinocytosis inhibitor). Percent inhibition is presented in Table 11.

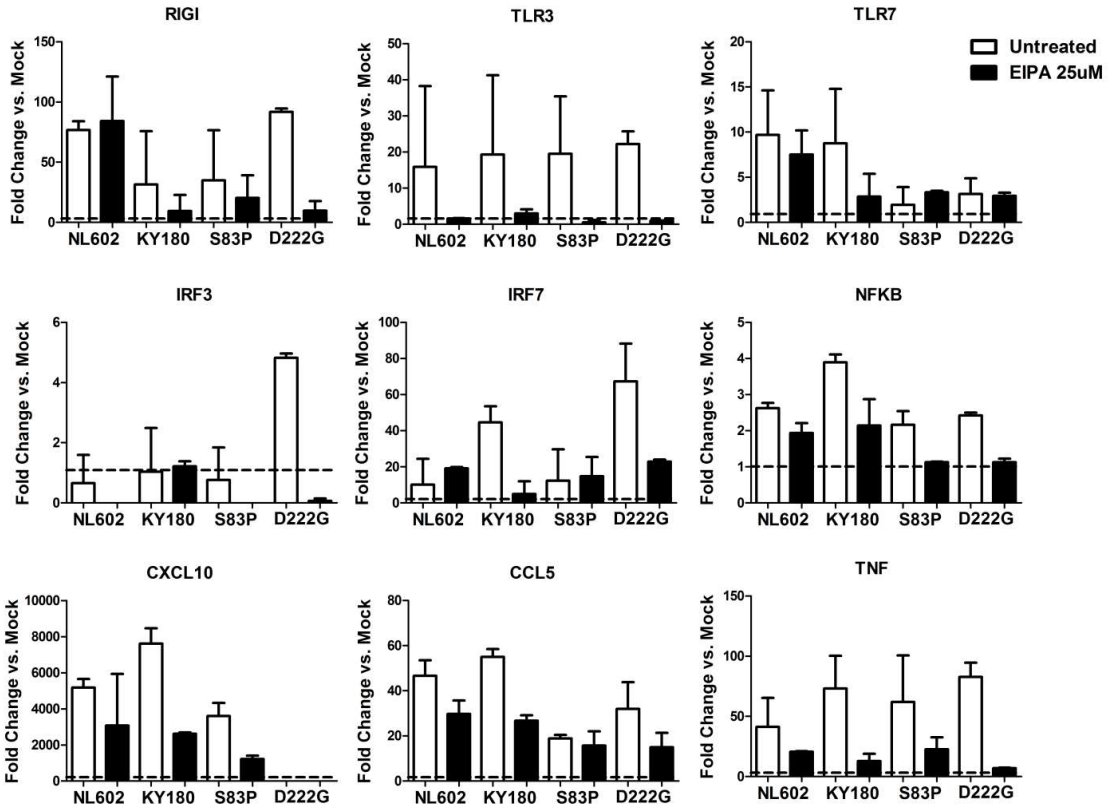

Figure 39. Gene expression of innate signaling and pro-inflammatory genes with recombinant viruses in the presence of absence of inhibitors. MDM were infected with influenza viruses KY180 (H1N1pdm), NL602 (H1N1pdm), or viruses produced by reverse genetics and induction of point mutations in the HA gene NL602-D222G, and NL602-S83P. Infection was performed at an MOI of 1 in the presence or absence of EIPA at a 25uM concentration. mRNA expression of pro-inflammatory and viral recognition genes were measured by SYBR green real-time PCR. Results shown represent the average across 2 donors tested with 1 to 2 replicates per donors and are expressed as mean ± SD. *, $p < 0.05$; **, $p < 0.01$; *** $p<0.001$. EIPA, 5-(N-Ethyl-N-isopropyl) amiloride (macropinocytosis inhibitor).

Table 10. Description of mutations within the HA gene of KY180.

Nucleotide location of HA mutation	Amino Acid Change	Literature Reference
83	S → P	Common in 2009 pdm H1N1 viruses circulating in Shanghai [442]; not associated with severe disease.
84	S → N	Common in 2009 pdm H1N1 viruses circulating in Brazil [443]; not associated with severe disease.
183	S → P	Associated with receptor binding and increased disease severity in humans [431, 444, 445]
186	A → T	Associated with improved replication in cell culture and egg [446]
203	S → T	Common in 2009 pdm H1N1 viruses circulating in UK [447]; not associated with severe disease.
222	D → G	Associated with receptor binding and increased disease severity in humans [338, 339, 431]

Table 11. Percent inhibition of viral entry in the presence of macropinocytosis inhibitor EIPA (data from figure 38).

Virus	% Inhibition
MOCK	0
NL602	32
KY180	70
NL602-HA S83P	59
NL602-HA S84N	52
NL602-HA S183P	68
NL602-HA A186T	57
NL602-HA S203T	34
NL602-HA D222G	70

CHAPTER 5

CONCLUSIONS AND FUTURE DIRECTION

CONCLUSIONS

Influenza A viruses (IAV) cause a spectrum of respiratory diseases that fall into three general pathologies (Figure 40, left panel). Seasonal IAV are predominantly associated with self-limiting, upper respiratory infections (URI) across the globe. In the elderly or as a result of comorbidity, however, seasonal IAV infections can progress to lower respiratory infections (LRI) resulting in pneumonia and secondary bacterial co-infections. Complications from LRI can lead to serious complications such as shock/sepsis and organ failure, resulting in an average annual attack rate of influenza-associated death of 2.4 deaths per 100,000 in the USA [448]. On the opposite side of the spectrum are highly pathogenic avian influenza viruses (HPAIV) infections that occur in geographically localized cases of few individuals that only target the lower respiratory system but show greater fatality (50%) (Figure 40, right panel). These viruses of avian-origin are not adapted to humans, do not transmit person to person and infected patients present with hypercytokinemia [186, 233, 449]. There has been great concern among the public health and scientific community that the HPAIV may “jump” to humans and result in a global pandemic of high

consequence [450]. Regardless of the origin of the infection, HPAIV or seasonal, pulmonary infection leads to very similar pathology within the lung (Figure 40, center panel).

IAV subtypes and even genotypes within subtypes can show differences in tropism (host, cell type), magnitude of infection, immune response and progression of illness. While we know a great deal about influenza viruses and their disease, we are not able to predict accurately the pandemic potential and impact of new emerging strains. My thesis focused on the development and use of two in vitro physiologically-relevant human cell culture models of IAV, well-differentiated normal human bronchial epithelial cells and monocyte-derived macrophages. These models have given new insight into early host responses of seasonal H1N1 and the pandemic (H1N1) 2009 (referred to as H1N1pdm herein). Continued advancement of the in vitro human cell culture models is important as they will allow rapid insight into characteristics of new strains as well as those circulating annually.

My dissertation focused on the H1N1pdm, however, because of certain clinical observations and outcomes that suggested the pandemic viruses differed from seasonal H1N1, we included a recent strain of seasonal H1N1 in my studies. We viewed this as critical since the models we were using differed in some aspects from others and including strains employed by others provided benchmarks to better interpret our data. As discussed in earlier chapters, the H1N1pdm strains at the start of the 2009 pandemic caused alarm given the attack rate in young children and healthy adults. The sequence of the H1N1pdm

revealed it arose as a reassortment from at least three viruses circulating in bird, pig and human. At the beginning of any outbreak, it is immensely difficult to predict a trajectory of infection and mortality. However given the rapid spread, age distribution and the lack of a vaccine with protective efficacy, the H1N1pdm was predicted by some to be as potentially as dangerous as the HPAIV for its impact on public health. One of the major aspects of H1N1pdm that caused concern was the finding of upper and lower respiratory infection. Subsequent studies in ferret supported the observation that the H1N1pdm had the ability to infect the upper and lower respiratory tract [284, 349, 451, 452]. Secondly, the HA and NA had an avian and some genotypes retained avian signatures in important function domains. Together, the clinical reports and animal studies suggested that during the pandemic, different genotypes may have circulated with different pathogenic phenotypes. To address this question, we proposed the hypothesis that different clinical isolates with distinct clinical outcomes may exhibit diverging early host responses in human cell culture models. The major conclusions from my collaborations within the lab and my experiments in these models are summarized in the following.

H1N1pdm show pro-inflammatory signaling in human bronchial epithelial that is not necessarily correlated with viral load. H1N1 viruses are reported to cause differential pathogenicity that correlates with viral load [413, 453-456]. In my studies with the well-differentiate normal human bronchial epithelial (wdNHBE) primary cell culture model, we used two clinical isolates from hospitalized patients, A/KY180/2010 and A/KY136/2009 from lethal and nonlethal

cases respectively [385]. The pathogenicity of these two isolates was mirrored in the DBA2 mouse model [298]. Overall, over a 48 hour time period, the host responses in wdNHBE cells to the H1N1pdm isolates showed similar transcriptional profiles by microarray analysis (Figure 14). The overall similarity in the gene expression pathways were surprising given the different outcomes in the mouse model [298]. However, when comparing the temporal dynamics of secreted cytokines and chemokines from wdNHBE cells in response to the H1N1pdm isolates we saw an increased, polarized pro-inflammatory response by KY180 compared to KY136 (Figure 12 and 13).

When comparing seasonal versus H1N1pdm in wdNHBE, all three isolates showed similar up- and down-regulation of genes within the intracellular signaling pathways, including IFN signaling and communication between innate and adaptive immune cells (Table 8). However, when comparing global gene expression levels, H1N1pdm-infected wdNHBE cells showed greater fold-changes in transcription as compared to seasonal IAV (Figure 14, Table 7). These differences, were also reflected in cytokine and chemokine secretion, at 24 and 36 hpi, both H1N1pdm isolates showed greater levels of pro-inflammatory markers, apically (CCL5, GM-CSF, CXCL10, CCL2, CCL4) and basally (CCL5, IL6, TNF), compared to BN59.

My studies of a panel of secreted cytokines and chemokines suggested one potential clue. I noted significant differences in the polarization of immune signals secreted from the wdNHBE cells from the lethal and nonlethal strains. Differences were noted over the time course, however, in the polarity of apical

and basal signals of 5 immune proteins, CCL5, IL6, IL8, CCL2, and MIP1β. All of these showed polarity toward the basal side in wdNHBE cultures infected with KY180, the more pathogenic isolate. This observation suggested the hypothesis that infected wdNHBE may differ in their potential to recruit immune cells or perhaps in their interactions with those immune cells (Figure 41). Hence we discussed development of a co-culture model of human wdNHBE and macrophage cells to address IAV-host interactions within the cell that may give rise to different outcomes in immune cell recruitment. However given the state of the field in macrophage studies discussed in chapter 3, we decide to first address and define an optimal in vitro macrophage system for such future efforts. And hence my first efforts were in exploring the resting MDM as a model of early macrophage infection.

CHARACTERIZATION OF MDM FOR THE STUDY OF INFLUENZA INFECTION

I adapted a resting MDM model for the study of seasonal and pandemic H1N1 viruses to uncover early IAV-MDM interactions. To characterize this model I first established the culture conditions as previously described for differentiating monocytes to macrophages over 7 days and confirmed this differentiation by evaluating surface marker and gene expression of CD14 and CD11b markers. I then confirmed the MDM cultures were not activated after the 7 day maturation. I evaluated the cells via light microscope to determine whether the macrophages were in an activated or resting state as previously described [382, 383]. This was further confirmed evaluating the presence of both anti- and pro-inflammatory activation surface markers on the surface of MDM by flow cytometry and RT-

PCR. Lastly, to eliminate elements that could prematurely affect the outcome of our experiments on IAV-MDM interactions, I optimized the infection culture conditions including infection media, multiplicity of infection, and the use of egg- or cell-derived IAV stock virus for infection. Taking into account the conditions utilized by previous studies, I confirmed that our culture MDMs were truly "resting" and were permissive to viral infection. By establishing this model, I was able to ask our first question; would KY180 and KY136 infect macrophages similarly? And more broadly, what is the role of peripheral blood monocyte-derived macrophages (MDM) recruited to the site of IAV infection in the subsequent phenotype of the macrophage?

In "recruited" MDM cells, we reported the rate of infection and replication by a lethal and nonlethal isolate of H1N1pdm were similar but showed differences in the temporal pattern of innate immune response profiles. After a series of experiments, our studies indicate the phenotype (delayed innate immune response) in KY180-infected MDM is dependent on the pathway of viral entry and can be mapped to specific mutations in the HA1 gene (D222G and S183P). These mutations are located within the receptor binding site of the HA gene and have been shown to alter binding affinity [432, 433]. Thus, differences in receptor-IAV binding affinity between KY180 and KY136 might explain phenotypic differences seen in this model.

PRIMARY MODEL LIMITATIONS

The main advantage of *in vitro* models of IAV infection based on one cell type is the ability to gain information about a particular cell type's reaction to an infectious virus. Primary cells represent a strong model for studying these reactions as we can make direct comparisons between isolates of the same strain in cell types that mimic what the virus actually encounters in its host. However, limitations within these models do exist, no matter how physiologically relevant they are. For example, MDM and dendritic cells which are cultured on plastic dishes and selected for adherence have been shown previously to have different characteristics from non-adherent cells. Specifically adherent monocytes are shown to have higher phagocytic activity compared to non-adherent cells [457] as well as having greater viability and a greater ability to induce T-cell proliferation [458]. The activity of primary human cells, once extracted and grown in culture, may differ from those circulating in the blood and tissues. Hence, my studies focused on determining the viral factors that differentiate two genetically similar isolates with different clinical outcomes. The experiments do not hold necessarily direct relevance to human disease.

The monoculture *in vitro* environment of "resting" MDM that we created represented a simplistic model containing few cytokines in isolation and may not adequately represent the complex cytokine milieu that is present before human disease. Because of this, we proposed co-culturing human MDM with epithelial cells shown to produce cytokines, chemokines, mucus, and other factors which are present in the natural lung. While caution must be taken to approach this as completely representative; the co-culture allows for the evaluation of the critical

processes that drive immune responses to IAV such as bystander IFN and apoptotic responses. With the limitations of each system in mind, caution was taken not to make too bold of hypotheses around the cell types themselves. However, based on our *in vitro* results in the wdNHBE and MDM cultures, we developed hypotheses specific to how the viruses affect the bystander responses and how the microenvironment is affected.

CO-CULTURE HYPOTHESES

We hypothesize that the delayed activation of MDM infected by KY180 may lead to a delayed clearance of virus and a dysregulated microenvironment in the infected lung. We speculate this will ultimately affect downstream host immune responses to the virus. The long term goal of our laboratory is to look at the interactions between epithelial cells and macrophages but the data presented thus far has looked at the responses of wdNHBE and MDM to pandemic and seasonal isolates in separate systems.

Thus, we hypothesized that upon contact with infected epithelial cells, the immune cells (MDM) would differ in their influence on the lung microenvironment. With the delayed response phenotype in MDM, we generated a broad hypothesis we term “the Goldilocks” hypothesis after the Goldilocks and the three bears fairy tale. Previous reports have demonstrated H5N1 induces a very high (“too hot”) cytokine response in macrophages after infection. Further, in MDM we show KY180 induces a delayed, weak (“too cold”) cytokine response. Finally, KY136 induces a response that is “just right” in MDM that may lead to just enough of a response to activate the immune system and resolve the IAV infection properly

(Figure 42 and 43). Thus we hypothesize that this phenomenon will become apparent when macrophages are co-cultured with infected epithelial cells.

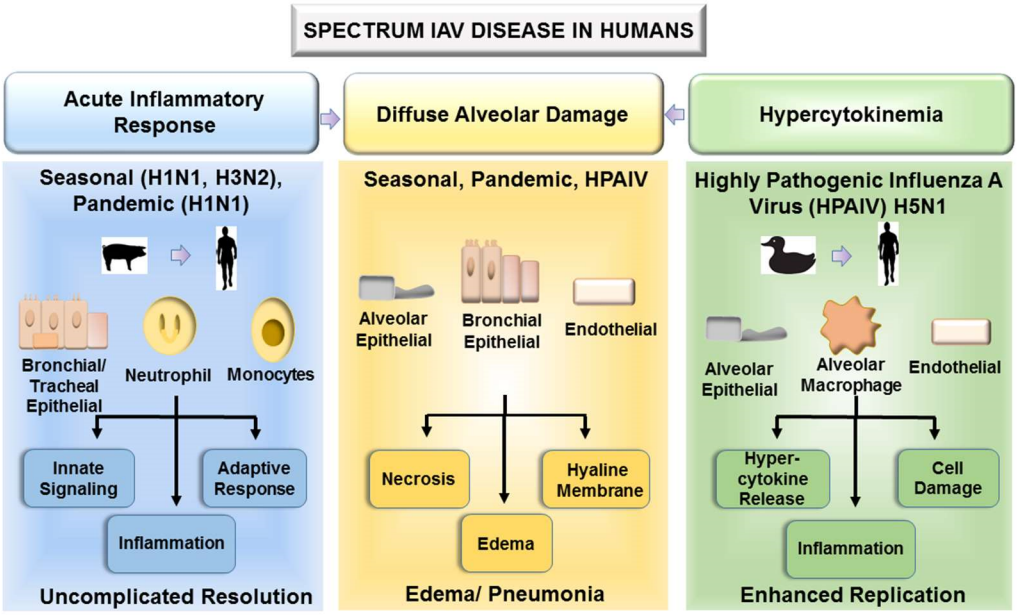

Figure 40. Schematic of Influenza Virus in Humans. Influenza A virus causes a spectrum of diseases from acute inflammatory response to hypercytokenemia that can both lead to diffuse alveolar damage. These diseases are mainly caused by seasonal (which circulate in pigs and spill over into humans; characterized as having a high incidence and low mortality) and highly pathogenic avian influenza viruses (emerge through contact with wildlife or infected poultry; low incidence and high mortality). The roadmap to disease is dependent upon the cells the virus infects and the responses they induced by those infected cells. In our lab we hypothesized that closely related isolates of the same strain may differ in the magnitude of host responses which may lead to differences in disease progression.

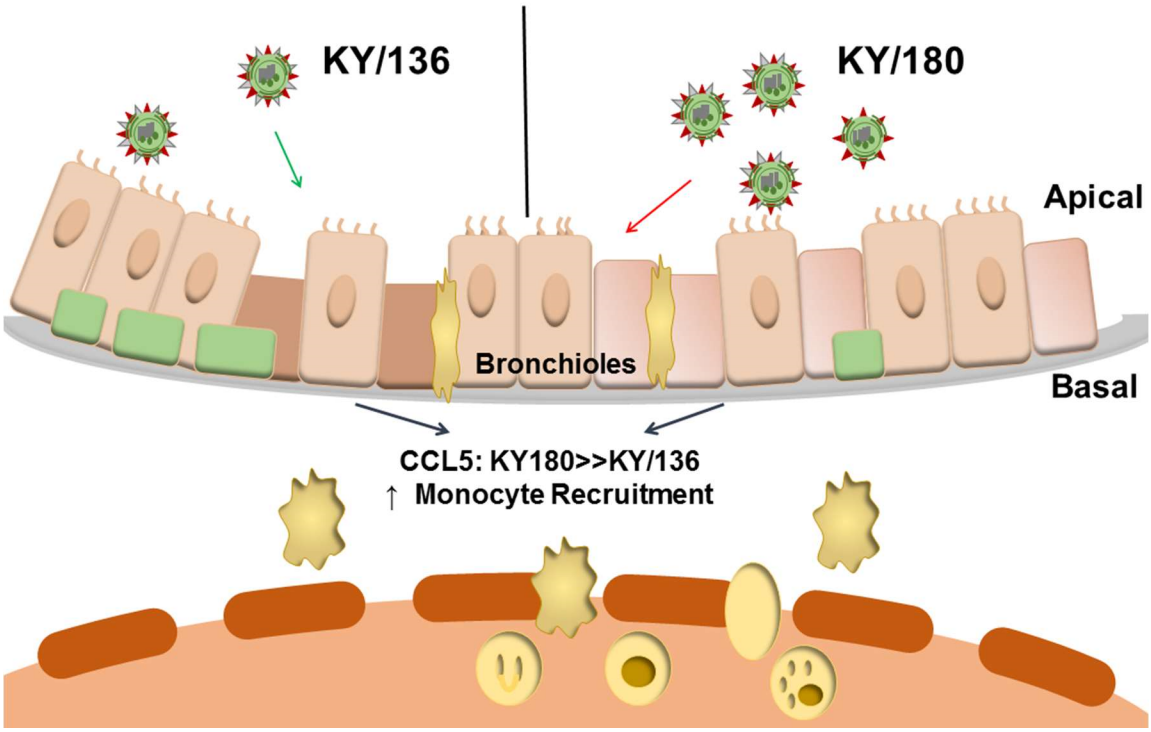

Figure 41. Results and hypothesis generated from wdNHBE studies. A key finding from wdNHBE studies was the greater levels of basolateral secretion of pro-inflammatory cytokines (IL6, CCL5, IL8 and CCL2) by cells infected with the lethal KY180 isolate compared to KY136 and BN59. We hypothesized that differences in basolateral signals such as CCL5 from epithelial cells may play a role in the recruitment, and responses elicited by monocytes/macrophages.

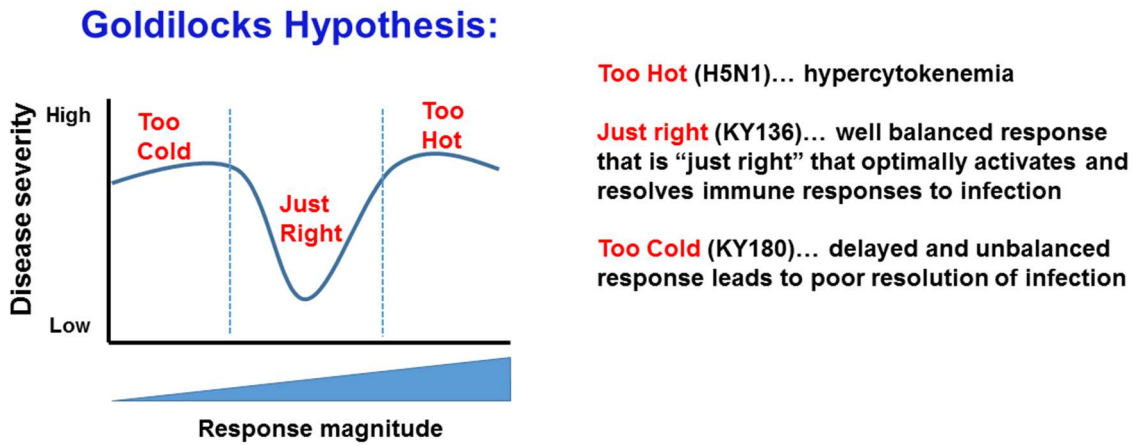

Figure 42. Hypothesis generated from MDM studies. We hypothesized that upon contact with infected epithelial cells, the difference in magnitude of the immune cell responses to KY180 and KY136 may alter viral clearance and anti-viral response. With the delayed response phenotype by KY180 in MDM, we generated a broad hypothesis we term "the Goldilocks" hypothesis after the Goldilocks and the three bears fairy tale. Previous reports have demonstrated H5N1 induces a very high ("too hot") cytokine response in macrophages whereas we showed KY180 induces a delayed, weak ("too cold") cytokine response. Thus we hypothesize that the KY136 response is "just right" in MDM that leads to a well-balanced response (Figure 24) that optimally activates and resolves the immune response to IAV infection.

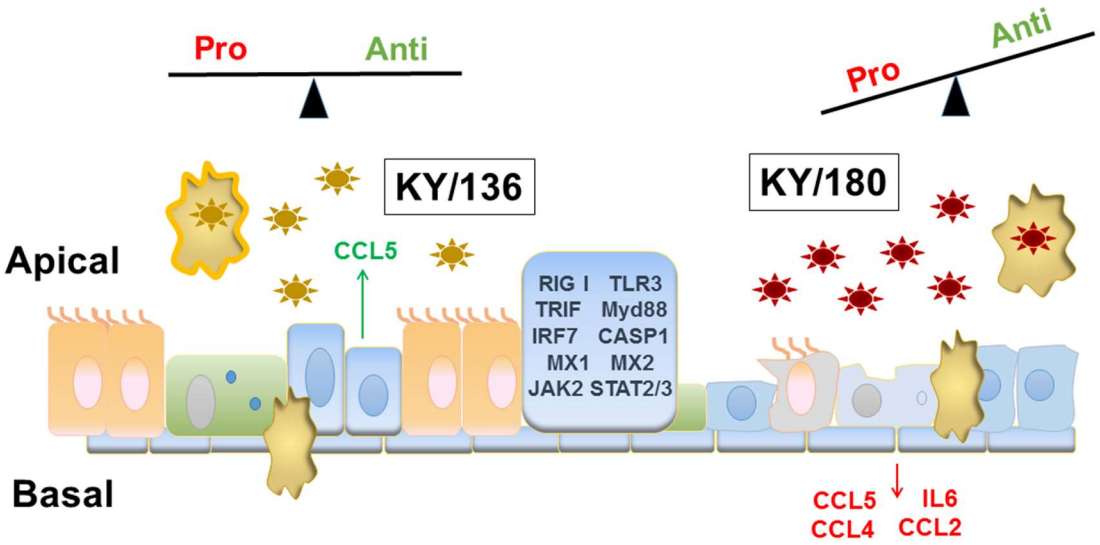

Figure 43. Proposed model of the interaction between macrophages and epithelial cells based on data presented in this dissertation. This model depicts the hypothesized difference in interaction between epithelial cells and recruited macrophages when infected with our pdmH1N1 isolates. We hypothesize that the delayed activation of MDM infected by KY180 may lead to a delayed clearance of virus and a dysregulated microenvironment within the infected lung.

PRELIMINARY STUDIES AND FUTURE DIRECTIONS

INTERACTIONS BETWEEN MACROPHAGES AND EPITHELIAL CELLS BY CO-CULTURE

For co-culture experiments, we employed an immortalized human bronchial epithelial cells 16HBE14o- (16HBE), which were kindly provided by Dr. Gruenert from the University of California, San Francisco, CA and the primary wdNHBE cell culture system as previously described. For 16HBE cells, culture plates, flasks and transwells were coated with a fibronectin coating solution containing bovine serum albumin, type-I collagen and human fibronectin. The cells were cultured in Minimum essential medium (Invitrogen) containing fetal bovine serum, l-glutamine, and penicillin/streptomycin. The primary wdNHBE and MDM were cultured as described in the previous chapters. The protocol for co-culture was modified from the only other study found that looked at responses after co-culture of epithelial cells and macrophages [459].

The timeline for the co-culture is depicted in Figure 44. Briefly, 16HBE and wdNHBE cells were differentiated in culture for 28 days. Meanwhile, PBMCs were collected and processed to create the MDM cells. On the day before co-culture, cells were infected as previously described in chapter 2 (wdNHBE) and chapter 3 (MDM). On the day of co-culture, basal media was kept in the culture plates, and MDM were gently collected (using a cell lifter) and placed on with wdNHBE cells in a very small volume of media. The cells were then kept at the air-liquid interface for the throughout the rest of the infection time course. At the 24h time point, basal media was collected and the apical side was washed 2

times with DPBS+0.2% BSA. The pooled washes were collected, spun down and the supernatant saved. The spun down pellet was combined with the remaining cells from the apical side of the transwell collected in Trizol. Four experiments were conducted in total, two with 16HBE cells, two with primary wdNHBE cells and each one with a separate PBMC donor.

Within the lung, specific cytokines and chemokines have important functions early after IAV infection, including anti-IAV responses and resolution of inflammation. During experimental IAV infection in humans, early nasal cytokine and chemokine responses have been shown to include type-I Interferons and also pro-inflammatory cytokines such as TNF and IL6 [297, 460]. For example, infections with highly pathogenic IAVs can sometimes result in the excessive and dangerous production of pro-inflammatory cytokines and IFN known as a ‘cytokine storm’, and may contribute to morbidity and mortality during the associated infection [461]. Infection of MDM with more pathogenic isolates, such as H5N1, have been shown to amplify those responses [307]. Because TNF and IFN have been shown to exert powerful anti-viral effects [462], we sought to determine whether infection by our different isolates in a co-cultured setting would amplify these pro-inflammatory signals and how the responses to those viruses compared to one another. Additionally, anti-inflammatory mechanisms following acute IAV infection may be a result of phagocytic APCs attempting to clear apoptotic epithelial cells, also known as ‘efferocytosis’. This mechanism of apoptotic cells being consumed by macrophages is associated with TGFβ and IL10 secretion, which are linked to reducing pro-inflammatory cytokines and

inflammation resolution after influenza infection [463, 464]. We sought to determine whether infection by our different isolates would amplify the anti-inflammatory signals how this related to the pro-inflammatory TNF and IFN responses.

Preliminary studies were done to compare the pro- and anti-inflammatory responses using 16HBE and MDM cells. After co-culture and infection, cells were collected in Trizol and total RNA was isolated and converted to cDNA, and the expression levels were determined by real time-PCR as described in the previous chapters. The ratio of pro- to anti-inflammatory cytokines in co-cultured 16NHBE with MDM cells was determined by comparing the fold change over mock of the pro-inflammatory gene expression (TNF and IFNβ) to the anti-inflammatory gene expression (IL10 and TGFβ). The ratios revealed a greater anti-inflammatory gene expression by KY136 compared to KY180 (Figure 45). The ratio for KY180 was 3.02 whereas for KY136 was 1.02 suggesting that KY136 has a more balanced response 24 h after co-culture compared to KY180. This preliminary data supports our hypothesis that KY136 may be better at resolving the infection in a co-culture setting. This experiment lacked the necessary controls, including infected macrophages and infected NHBE cells only.

With these preliminary results, we moved forward with the more costly and technically challenging protocol to conduct the co-culture experiment with the necessary controls using primary human wdNHBE cells. The co-culture experiments have been done and the results of the ELISA and viral titers are still

pending. Briefly, cell culture supernatants were collected 24h after co-culture and the levels of TNF and IL10 will be compared by enzyme-linked immunosorbent assay (ELISA) using Ready-set-go ELISA kits (eBiosciences) as recommended by the manufacturer. Ratios of pro-inflammatory (TNF) to anti-inflammatory (IL10) will be determined by comparing concentrations of TNF to IL10 in supernatants for each condition.

Our expected results for the primary cell co-culture experiment:

1. KY136- greater clearance; lower ratio of TNF:IL10 (indicating an anti-inflammatory, infection resolution state); lower virus compared to NHBE and macrophage alone
2. KY180- delayed clearance of virus resulting in greater amplification of virus; greater ratio of TNF:IL10 (indicating a pro-inflammatory state, delayed viral resolution); higher virus compared to NHBE and MDM alone

To broaden this model to become more translational, preliminary studies as described below have been conducted in our laboratory using a “diseased” epithelial cell culture model. During the 2009 pandemic, the most common underlying chronic conditions among hospitalized patients were respiratory disease, asthma, cardiac disease, and diabetes with a greater proportion of fatal cases occurring in those with these pre-existing conditions [288]. Future studies will employ this co-culture model to explore the interactions between infected wdNHBE (with pre-existing condition) and “recruited” MDM. We will evaluate how differences in epithelial condition may alter the MDM response to IAV and how this may relate to disease outcome.

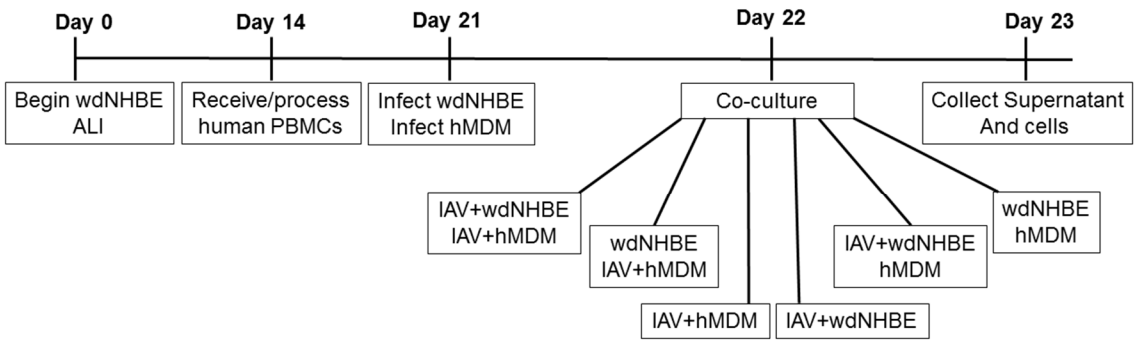

Figure 44. Timeline of co-culture experiment including description of all treatment and control groups. To evaluate the interactions between epithelial cells and macrophages we followed this experimental timeline.

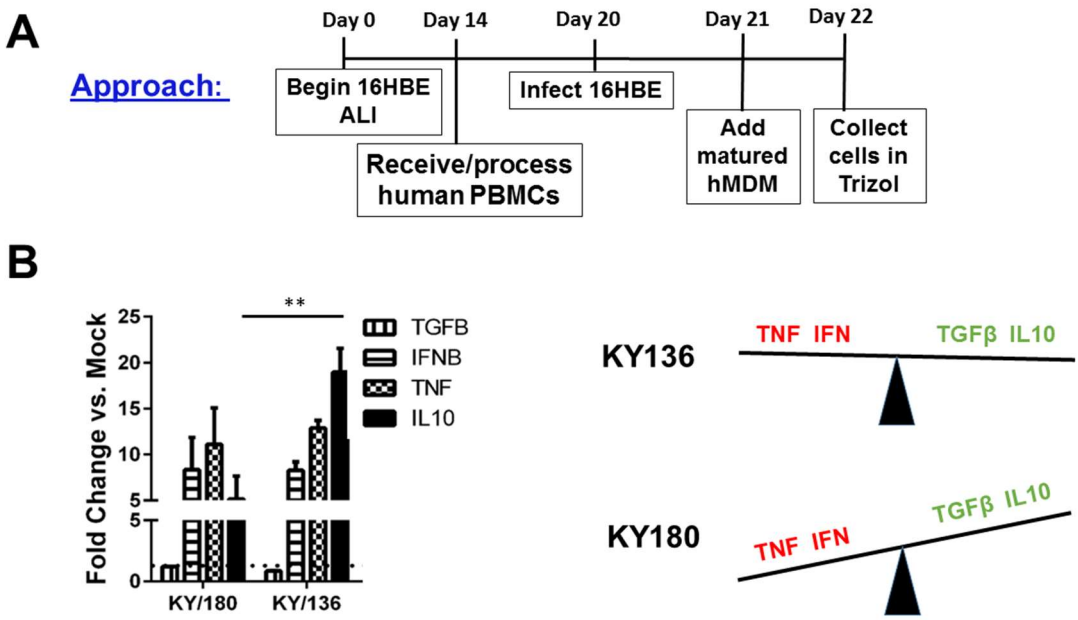

Figure 45. Preliminary results from co-culture of infected 16HBE cells with MDM. (A) 16HBE cells were cultured for 21 days to create differentiated cells on transwell inserts. 16HBE cells were infected at an MOI of 3.0 with KY180, KY136 or mock. 24h after infection, MDM were gently removed from their culture dish and placed on the apical side of the infected or un-infected 16HBE cells. At 24h and 48h time points, the cells were collected in Trizol. (B) RNA was extracted and expression of two anti-inflammatory (TGFB and IL10) and two pro-inflammatory (IFNB and TNF) cytokines were evaluated by RT-PCR. Results reflect 2 replicates from one representative donor (1 done in total) and are expressed as mean ± SD fold change as compared to mock (uninfected) control. Fold change of 1, indicative of equal expression between infected and mock infected controls is indicated by the dotted line. Significance as determined by ANOVA *, $p < 0.05$; **, $p < 0.01$; *** $p<0.001$.

ENVIRONMENTAL EXPOSURE AND SUSCEPTIBILITY TO IAV INFECTION

For years, investigators have wrestled with the concept that environmentally-driven events during embryogenesis and early childhood could set the stage for the development of asthma and other obstructive airways disease. Epidemiological data strongly support this notion and highlights associations between smoking, respiratory infections, and impaired wound healing [465, 466]. However, the factors responsible for these events and the mechanisms of action involved are unclear and few studies have been published that examine this question for respiratory infections. Thus a pilot study was conceived in collaboration with Dr. Roman. Dr. Roman has studied mechanisms by which nicotine effects airway development and the development of obstructive airways disease in mice [467]. Specifically, we hypothesized that nicotine may promote influenza infection by: (i) up-regulation of the receptors used for entry, (ii) increasing the levels of endogenous host trypsin-like serine proteases and thereby enhancing the proteolytic cleavage of viral HA and entry, (iii) modulating the innate immune defense molecules that inhibit replication, and/or (iv) modulating the antiviral mediators that limit viral replication and budding/shedding of virus particles [468, 469]. These pilot studies will provide guidance to future studies about the effects of chronic nicotine exposure and Influenza A infection as they relate to chronic airways dysfunction. We hypothesized that cigarette smoke (nicotine) suppresses anti-viral responses allowing for increased replication and increased susceptibility to infection.

Nicotine enhances influenza A infection in primary small airway epithelial cells. To ask whether nicotine enhanced influenza virus infection, we used primary human small airway epithelial cells (SAEC). Cells were purchased from Lonza and differentiated according to the manufacturer's instructions. Cells were differentiated (wd) using the transwell system as previously described for 16HBE and wdNHBE. For infection studies, wdSAEC cells were pretreated with Nicotine (Sigma) for 4 hr at the following concentrations (0, 10, and 50 ug/ml). The untreated and nicotine-treated cells were mock infected or infected with H1N1 (BN59), H1N1pdm (KY136 and KY180) at an MOI of 3.0. At 24h post-infection apical washes were obtained to determine viral titers as described in Chapter 2 by $TCID_{50}$ assay. The addition of nicotine to SAEC is seen to create a cell type that is more permissive to infection by KY180 as compared to KY136 and BN59 (Figure 46). These results suggest that the mechanisms by which nicotine may enhance KY180 infection may be virus specific.

Future work may focus on how nicotine may affect host cell-dependent factors that control influenza virus attachment, uptake or PRR activation. Nicotine from cigarette smoke can suppress RIGI activation [468]. As discussed in Chapter 1, RIGI is an important PRR that activates downstream anti-viral responses such as type-I interferons. Without these signals, infected cells may not know they are infected and the virus could replicate uncontrollably.

Based on our preliminary data, I show that KY180 replicated more efficiently in nicotine-treated cells suggesting it may escape the antiviral responses of the host. Based on our studies using entry inhibitors, we found that

KY180 enters through macropinocytosis whereas KY136 enters primarily through clathrin-mediated endocytosis. If viruses trafficking in macropinosomes escape TLR PRR recognition, then the suppression of RIGI by nicotine would lead to a complete evasion of recognition by KY180 in SAECs leading to increased viral replication. Future studies may utilize inhibitors to determine the mechanism of entry of these viruses in both nicotine treated and untreated cells as well as the expression of the PRRs within those cell types (before and after infection). We suspect differences in the mode of entry and PRR activation would explain the differences in infection in nicotine treated cells.

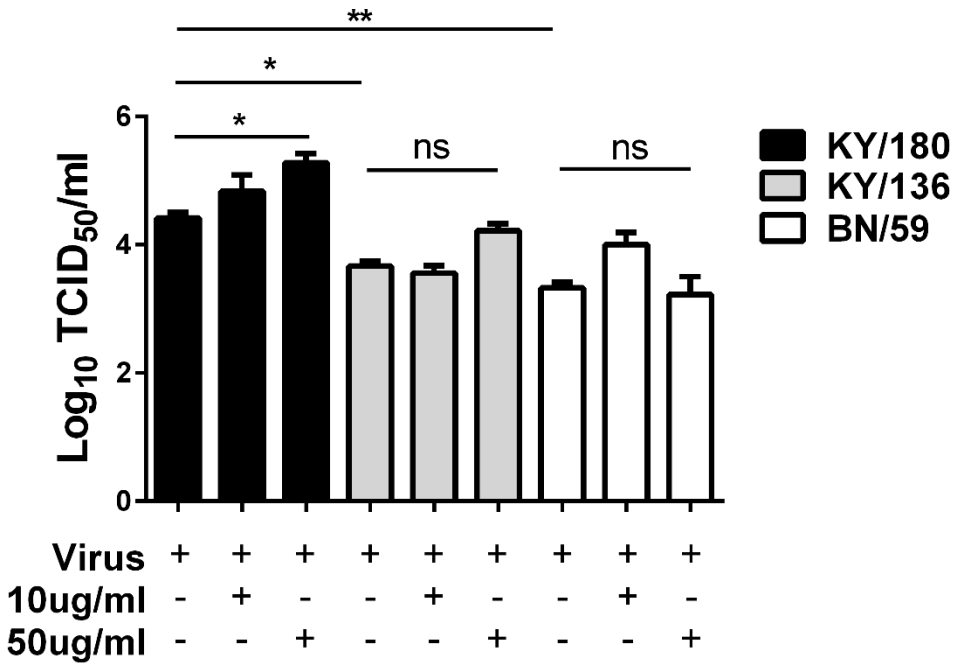

Figure 46. Human airway nicotine (environmental) exposure and susceptibility to IAV infection. Well-differentiated primary human small airway epithelial cells (SAEC) were pretreated with Nicotine (Sigma) for 4hr at the following concentrations (0, 10, and 50 ug/ml). The untreated and nicotine-treated cells were mock infected or infected with H1N1 (BN59), H1N1pdm (KY136 and KY180) at an MOI of 3.0. At 24h post-infection apical washes were obtained to determine viral titers by TCID50 assay.

REFERENCES

1. Alexander, D.J., *Ecological aspects of influenza A viruses in animals and their relationship to human influenza: a review.* J R Soc Med, 1982. **75**(10): p. 799-811.
2. Webster, R.G., *The importance of animal influenza for human disease.* Vaccine, 2002. **20 Suppl 2**: p. S16-20.
3. Webster, R.G., et al., *Evolution and ecology of influenza A viruses.* Microbiol Rev, 1992. **56**(1): p. 152-79.
4. Osterhaus, A.D., et al., *Influenza B virus in seals.* Science, 2000. **288**(5468): p. 1051-3.
5. Alford, R.H., et al., *Human influenza resulting from aerosol inhalation.* Proc Soc Exp Biol Med, 1966. **122**(3): p. 800-4.
6. Li, S. and S. Leader, *Economic burden and absenteeism from influenza-like illness in healthy households with children (5-17 years) in the US.* Respir Med, 2007. **101**(6): p. 1244-50.
7. WHO Pandemic Influenza A(H1N1) Vaccine Deployment Initiative. and World Health Organization., *Report of the WHO Pandemic Influenza A(H1N1) Vaccine Deployment Initiative*. 2012, Geneva: World Health Organization. iv , 44 pages.
8. Chaves, S.S., et al., *The Burden of Influenza Hospitalizations in Infants From 2003 to 2012, United States.* Pediatric Infectious Disease Journal, 2014. **33**(9): p. 912-919.
9. Cruzeta, A.P., I.J. Schneider, and J. Traebert, *Impact of seasonality and annual immunization of elderly people upon influenza-related hospitalization rates.* Int J Infect Dis, 2013. **17**(12): p. e1194-7.
10. Molinari, N.A., et al., *The annual impact of seasonal influenza in the US: measuring disease burden and costs.* Vaccine, 2007. **25**(27): p. 5086-96.
11. Dushoff, J., et al., *Mortality due to influenza in the United States--an annualized regression approach using multiple-cause mortality data.* Am J Epidemiol, 2006. **163**(2): p. 181-7.
12. Louria, D.B., et al., *Studies on influenza in the pandemic of 1957-1958. II. Pulmonary complications of influenza.* J Clin Invest, 1959. **38**(1 Part 2): p. 213-65.
13. Murata, Y., E.E. Walsh, and A.R. Falsey, *Pulmonary complications of interpandemic influenza A in hospitalized adults.* J Infect Dis, 2007. **195**(7): p. 1029-37.
14. Jackson, M.L., et al., *Influenza vaccination and risk of community-acquired pneumonia in immunocompetent elderly people: a population-based, nested case-control study.* Lancet, 2008. **372**(9636): p. 398-405.

15. McBean, A.M. and P.L. Hebert, *New estimates of influenza-related pneumonia and influenza hospitalizations among the elderly.* Int J Infect Dis, 2004. **8**(4): p. 227-35.
16. Sethi, S., *Bacterial pneumonia. Managing a deadly complication of influenza in older adults with comorbid disease.* Geriatrics, 2002. **57**(3): p. 56-61.
17. Bhat, N., et al., *Influenza-associated deaths among children in the United States, 2003-2004.* N Engl J Med, 2005. **353**(24): p. 2559-67.
18. Centers for Disease, C. and Prevention, *Bacterial coinfections in lung tissue specimens from fatal cases of 2009 pandemic influenza A (H1N1) - United States, May-August 2009.* MMWR Morb Mortal Wkly Rep, 2009. **58**(38): p. 1071-4.
19. Suzuki, Y. and M. Nei, *Origin and evolution of influenza virus hemagglutinin genes.* Mol Biol Evol, 2002. **19**(4): p. 501-9.
20. P, P. and S. ML, *Orthomyxivirdae: the viruses and their replication*. 5th ed. Fields Virology, ed. B.N. Fields, D.M. Knipe, and P.M. Howley. 2007, Philadelphia: Wolters Kluwer Health/Lippincott Williams & Wilkins.
21. Wright PF, N.G., Kawaoka Y, *Orthomyxoviruses*, ed. F. Virology. 2007: Williams & Wilkins; Philadelphia Lippincott.
22. Smith W, A.C., Laidlaw PP. , *A virus isolated from influenza patients.* Lancet, 1933. **2**: p. 66-68.
23. Rota, P.A., et al., *Cocirculation of two distinct evolutionary lineages of influenza type B virus since 1983.* Virology, 1990. **175**(1): p. 59-68.
24. Bao, Y., et al., *The influenza virus resource at the National Center for Biotechnology Information.* J Virol, 2008. **82**(2): p. 596-601.
25. Chen, J.M., et al., *Exploration of the emergence of the Victoria lineage of influenza B virus.* Arch Virol, 2007. **152**(2): p. 415-22.
26. Shen, J., et al., *Diversifying selective pressure on influenza B virus hemagglutinin.* Journal of Medical Virology, 2009. **81**(1): p. 114-24.
27. Katz, G., et al., *Morphology of influenza B/Lee/40 determined by cryo-electron microscopy.* PLoS One, 2014. **9**(2): p. e88288.
28. Lamb, R.A.a.R.M.K., *Orthomyxoviridae: the viruses and their repliction*. Fields Virology. 2001: Lippincott, Williams, and Wilkins
29. Brassard, D.L., G.P. Leser, and R.A. Lamb, *Influenza B virus NB glycoprotein is a component of the virion.* Virology, 1996. **220**(2): p. 350-60.
30. Hatta, M., H. Goto, and Y. Kawaoka, *Influenza B virus requires BM2 protein for replication.* J Virol, 2004. **78**(11): p. 5576-83.
31. Hatta, M. and Y. Kawaoka, *The NB protein of influenza B virus is not necessary for virus replication in vitro.* J Virol, 2003. **77**(10): p. 6050-4.
32. WHO, *A revision of the system of nomenclature for influenza viruses: a WHO memorandum.* Bull World Health Organ, 1980. **58**(4): p. 585-91.
33. Dowdle, W.R., et al., *A simple double immunodiffusion test for typing influenza viruses.* Bull World Health Organ, 1974. **51**(3): p. 213-5.
34. Ambrose, C.S. and M.J. Levin, *The rationale for quadrivalent influenza vaccines.* Hum Vaccin Immunother, 2012. **8**(1): p. 81-8.

35. Furukawa, T., et al., *Role of the CM2 protein in the influenza C virus replication cycle.* J Virol, 2011. **85**(3): p. 1322-9.
36. Greenbaum, E., A. Morag, and Z. Zakay-Rones, *Isolation of influenza C virus during an outbreak of influenza A and B viruses.* J Clin Microbiol, 1998. **36**(5): p. 1441-2.
37. Herrler, G., et al., *The glycoprotein of influenza C virus is the haemagglutinin, esterase and fusion factor.* J Gen Virol, 1988. **69 (Pt 4)**: p. 839-46.
38. Bouvier, N.M. and P. Palese, *The biology of influenza viruses.* Vaccine, 2008. **26 Suppl 4**: p. D49-53.
39. Rossman, J.S., et al., *Influenza virus m2 ion channel protein is necessary for filamentous virion formation.* J Virol, 2010. **84**(10): p. 5078-88.
40. Bourmakina, S.V. and A. Garcia-Sastre, *Reverse genetics studies on the filamentous morphology of influenza A virus.* J Gen Virol, 2003. **84**(Pt 3): p. 517-27.
41. Campbell, P.J., et al., *The M segment of the 2009 pandemic influenza virus confers increased neuraminidase activity, filamentous morphology, and efficient contact transmissibility to A/Puerto Rico/8/1934-based reassortant viruses.* J Virol, 2014. **88**(7): p. 3802-14.
42. Hughey, P.G., et al., *Effects of antibody to the influenza A virus M2 protein on M2 surface expression and virus assembly.* Virology, 1995. **212**(2): p. 411-21.
43. Smirnov Yu, A., M.A. Kuznetsova, and N.V. Kaverin, *The genetic aspects of influenza virus filamentous particle formation.* Arch Virol, 1991. **118**(3-4): p. 279-84.
44. Jin, H., et al., *Influenza virus hemagglutinin and neuraminidase cytoplasmic tails control particle shape.* EMBO J, 1997. **16**(6): p. 1236-47.
45. Medina, R.A. and A. Garcia-Sastre, *Influenza A viruses: new research developments.* Nat Rev Microbiol, 2011. **9**(8): p. 590-603.
46. Ebisawa, I.T., et al., *Immunocytologic study of nasal epithelial cells in influenza.* Am Rev Respir Dis, 1969. **99**(4): p. 507-15.
47. Marsh, M. and A. Helenius, *Virus entry: open sesame.* Cell, 2006. **124**(4): p. 729-40.
48. Kawaoka, Y. and R.G. Webster, *Sequence requirements for cleavage activation of influenza virus hemagglutinin expressed in mammalian cells.* Proc Natl Acad Sci U S A, 1988. **85**(2): p. 324-8.
49. Epand, R.F., et al., *The ectodomain of HA2 of influenza virus promotes rapid pH dependent membrane fusion.* J Mol Biol, 1999. **286**(2): p. 489-503.
50. Bullough, P.A., et al., *Crystals of a fragment of influenza haemagglutinin in the low pH induced conformation.* J Mol Biol, 1994. **236**(4): p. 1262-5.
51. Suarez, D.L., et al., *Recombination resulting in virulence shift in avian influenza outbreak, Chile.* Emerg Infect Dis, 2004. **10**(4): p. 693-9.
52. Rogers, G.N., et al., *Single amino acid substitutions in influenza haemagglutinin change receptor binding specificity.* Nature, 1983. **304**(5921): p. 76-8.

53. Wood, G.W., et al., *Deduced amino acid sequences at the haemagglutinin cleavage site of avian influenza A viruses of H5 and H7 subtypes.* Arch Virol, 1993. **130**(1-2): p. 209-17.
54. Senne, D.A., et al., *Survey of the hemagglutinin (HA) cleavage site sequence of H5 and H7 avian influenza viruses: amino acid sequence at the HA cleavage site as a marker of pathogenicity potential.* Avian Dis, 1996. **40**(2): p. 425-37.
55. Chen, J., et al., *Structure of the hemagglutinin precursor cleavage site, a determinant of influenza pathogenicity and the origin of the labile conformation.* Cell, 1998. **95**(3): p. 409-17.
56. Klenk, H.D. and W. Garten, *Host cell proteases controlling virus pathogenicity.* Trends Microbiol, 1994. **2**(2): p. 39-43.
57. Bottcher, E., et al., *Proteolytic activation of influenza viruses by serine proteases TMPRSS2 and HAT from human airway epithelium.* J Virol, 2006. **80**(19): p. 9896-8.
58. Swayne, D.E., *Avian influenza*. 1st ed. 2008, Ames, Iowa: Blackwell Pub. xvi, 605 p., 4 p. of plates.
59. Ibricevic, A., et al., *Influenza virus receptor specificity and cell tropism in mouse and human airway epithelial cells.* J Virol, 2006. **80**(15): p. 7469-80.
60. Garcia-Sastre, A., *Influenza virus receptor specificity: disease and transmission.* Am J Pathol, 2010. **176**(4): p. 1584-5.
61. van Riel, D., et al., *Human and avian influenza viruses target different cells in the lower respiratory tract of humans and other mammals.* Am J Pathol, 2007. **171**(4): p. 1215-23.
62. Imai, M. and Y. Kawaoka, *The role of receptor binding specificity in interspecies transmission of influenza viruses.* Curr Opin Virol, 2012. **2**(2): p. 160-7.
63. Imai, M., et al., *Experimental adaptation of an influenza H5 HA confers respiratory droplet transmission to a reassortant H5 HA/H1N1 virus in ferrets.* Nature, 2012. **486**(7403): p. 420-8.
64. Skehel, J.J. and D.C. Wiley, *Receptor binding and membrane fusion in virus entry: the influenza hemagglutinin.* Annu Rev Biochem, 2000. **69**: p. 531-69.
65. Gottschalk, A., *On the mechanism underlying initiation of influenza virus infection.* Ergeb Mikrobiol Immunitatsforsch Exp Ther, 1959. **32**: p. 1-22.
66. Matrosovich, M.N., et al., *Human and avian influenza viruses target different cell types in cultures of human airway epithelium.* Proc Natl Acad Sci U S A, 2004. **101**(13): p. 4620-4.
67. Yamada, S., et al., *Haemagglutinin mutations responsible for the binding of H5N1 influenza A viruses to human-type receptors.* Nature, 2006. **444**(7117): p. 378-82.
68. Stevens, J., et al., *Structure and receptor specificity of the hemagglutinin from an H5N1 influenza virus.* Science, 2006. **312**(5772): p. 404-10.
69. Connor, R.J., et al., *Receptor specificity in human, avian, and equine H2 and H3 influenza virus isolates.* Virology, 1994. **205**(1): p. 17-23.

70. Shinya, K., et al., *Avian flu: influenza virus receptors in the human airway.* Nature, 2006. **440**(7083): p. 435-6.
71. Shinya, K. and Y. Kawaoka, *[Influenza virus receptors in the human airway].* Uirusu, 2006. **56**(1): p. 85-9.
72. Herfst, S., et al., *Airborne transmission of influenza A/H5N1 virus between ferrets.* Science, 2012. **336**(6088): p. 1534-41.
73. Maines, T.R., et al., *Lack of transmission of H5N1 avian-human reassortant influenza viruses in a ferret model.* Proc Natl Acad Sci U S A, 2006. **103**(32): p. 12121-6.
74. Childs, R.A., et al., *Receptor-binding specificity of pandemic influenza A (H1N1) 2009 virus determined by carbohydrate microarray.* Nat Biotechnol, 2009. **27**(9): p. 797-9.
75. Chan, M.C., et al., *Tropism and innate host responses of the 2009 pandemic H1N1 influenza virus in ex vivo and in vitro cultures of human conjunctiva and respiratory tract.* Am J Pathol, 2010. **176**(4): p. 1828-40.
76. Jayaraman, A., et al., *Decoding the distribution of glycan receptors for human-adapted influenza A viruses in ferret respiratory tract.* PLoS One, 2012. **7**(2): p. e27517.
77. Liu, Y., et al., *Altered receptor specificity and cell tropism of D222G hemagglutinin mutants isolated from fatal cases of pandemic A(H1N1) 2009 influenza virus.* J Virol, 2010. **84**(22): p. 12069-74.
78. Matrosovich, M., et al., *Early alterations of the receptor-binding properties of H1, H2, and H3 avian influenza virus hemagglutinins after their introduction into mammals.* J Virol, 2000. **74**(18): p. 8502-12.
79. Chutinimitkul, S., et al., *Virulence-associated substitution D222G in the hemagglutinin of 2009 pandemic influenza A(H1N1) virus affects receptor binding.* J Virol, 2010. **84**(22): p. 11802-13.
80. van Riel, D., et al., *Seasonal and pandemic human influenza viruses attach better to human upper respiratory tract epithelium than avian influenza viruses.* Am J Pathol, 2010. **176**(4): p. 1614-8.
81. Jeffery, P.K. and D. Li, *Airway mucosa: secretory cells, mucus and mucin genes.* European Respiratory Journal, 1997. **10**(7): p. 1655-62.
82. Baum, L.G. and J.C. Paulson, *Sialyloligosaccharides of the respiratory epithelium in the selection of human influenza virus receptor specificity.* Acta Histochem Suppl, 1990. **40**: p. 35-8.
83. Crystal, R.G., et al., *Airway epithelial cells: current concepts and challenges.* Proc Am Thorac Soc, 2008. **5**(7): p. 772-7.
84. Chan, M.C., et al., *Proinflammatory cytokine responses induced by influenza A (H5N1) viruses in primary human alveolar and bronchial epithelial cells.* Respir Res, 2005. **6**: p. 135.
85. van den Brand, J.M., et al., *Comparison of temporal and spatial dynamics of seasonal H3N2, pandemic H1N1 and highly pathogenic avian influenza H5N1 virus infections in ferrets.* PLoS One, 2012. **7**(8): p. e42343.
86. Chan, M.C., et al., *Influenza H5N1 virus infection of polarized human alveolar epithelial cells and lung microvascular endothelial cells.* Respir Res, 2009. **10**: p. 102.

87. Zeng, H., et al., *Tropism and infectivity of influenza virus, including highly pathogenic avian H5N1 virus, in ferret tracheal differentiated primary epithelial cell cultures.* J Virol, 2013. **87**(5): p. 2597-607.
88. Song, B.M., et al., *Induction of inflammatory cytokines and toll-like receptors in human normal respiratory epithelial cells infected with seasonal H1N1, 2009 pandemic H1N1, seasonal H3N2, and highly pathogenic H5N1 influenza virus.* Viral Immunol, 2011. **24**(3): p. 179-87.
89. Yang, X.X., et al., *Gene expression profiles comparison between 2009 pandemic and seasonal H1N1 influenza viruses in A549 cells.* Biomed Environ Sci, 2010. **23**(4): p. 259-66.
90. Zeng, H., et al., *The 2009 pandemic H1N1 and triple-reassortant swine H1N1 influenza viruses replicate efficiently but elicit an attenuated inflammatory response in polarized human bronchial epithelial cells.* J Virol, 2011. **85**(2): p. 686-96.
91. Patel, J.R., et al., *Infection of lung epithelial cells with pandemic 2009 A(H1N1) influenza viruses reveals isolate-specific differences in infectivity and host cellular responses.* Viral Immunol, 2011. **24**(2): p. 89-99.
92. Sieczkarski, S.B. and G.R. Whittaker, *Characterization of the host cell entry of filamentous influenza virus.* Arch Virol, 2005. **150**(9): p. 1783-96.
93. Sieczkarski, S.B. and G.R. Whittaker, *Influenza virus can enter and infect cells in the absence of clathrin-mediated endocytosis.* J Virol, 2002. **76**(20): p. 10455-64.
94. Nunes-Correia, I., et al., *Caveolae as an additional route for influenza virus endocytosis in MDCK cells.* Cell Mol Biol Lett, 2004. **9**(1): p. 47-60.
95. Matlin, K.S., et al., *Infectious entry pathway of influenza virus in a canine kidney cell line.* J Cell Biol, 1981. **91**(3 Pt 1): p. 601-13.
96. Patterson, S., J.S. Oxford, and R.R. Dourmashkin, *Studies on the mechanism of influenza virus entry into cells.* J Gen Virol, 1979. **43**(1): p. 223-9.
97. Yoshimura, A., et al., *Infectious cell entry mechanism of influenza virus.* J Virol, 1982. **43**(1): p. 284-93.
98. Chen, C. and X. Zhuang, *Epsin 1 is a cargo-specific adaptor for the clathrin-mediated endocytosis of the influenza virus.* Proc Natl Acad Sci U S A, 2008. **105**(33): p. 11790-5.
99. McClure, S.J. and P.J. Robinson, *Dynamin, endocytosis and intracellular signalling (review).* Mol Membr Biol, 1996. **13**(4): p. 189-215.
100. Brett, T.J. and L.M. Traub, *Molecular structures of coat and coat-associated proteins: function follows form.* Curr Opin Cell Biol, 2006. **18**(4): p. 395-406.
101. McMahon, H.T. and E. Boucrot, *Molecular mechanism and physiological functions of clathrin-mediated endocytosis.* Nat Rev Mol Cell Biol, 2011. **12**(8): p. 517-33.
102. Kirchhausen, T., D. Owen, and S.C. Harrison, *Molecular structure, function, and dynamics of clathrin-mediated membrane traffic.* Cold Spring Harb Perspect Biol, 2014. **6**(5): p. a016725.

103. Cocucci, E., R. Gaudin, and T. Kirchhausen, *Dynamin recruitment and membrane scission at the neck of a clathrin-coated pit.* Mol Biol Cell, 2014. **25**(22): p. 3595-609.
104. Rossman, J.S., G.P. Leser, and R.A. Lamb, *Filamentous influenza virus enters cells via macropinocytosis.* J Virol, 2012. **86**(20): p. 10950-60.
105. Kerr, M.C. and R.D. Teasdale, *Defining macropinocytosis.* Traffic, 2009. **10**(4): p. 364-71.
106. Mercer, J. and A. Helenius, *Virus entry by macropinocytosis.* Nat Cell Biol, 2009. **11**(5): p. 510-20.
107. de Vries, E., et al., *Dissection of the influenza A virus endocytic routes reveals macropinocytosis as an alternative entry pathway.* PLoS Pathog, 2011. **7**(3): p. e1001329.
108. Lakadamyali, M., M.J. Rust, and X. Zhuang, *Endocytosis of influenza viruses.* Microbes Infect, 2004. **6**(10): p. 929-36.
109. Rust, M.J., et al., *Assembly of endocytic machinery around individual influenza viruses during viral entry.* Nat Struct Mol Biol, 2004. **11**(6): p. 567-73.
110. Mercer, J. and U.F. Greber, *Virus interactions with endocytic pathways in macrophages and dendritic cells.* Trends Microbiol, 2013. **21**(8): p. 380-8.
111. White, J.M., et al., *Structures and mechanisms of viral membrane fusion proteins: multiple variations on a common theme.* Crit Rev Biochem Mol Biol, 2008. **43**(3): p. 189-219.
112. Bullough, P.A., et al., *Structure of influenza haemagglutinin at the pH of membrane fusion.* Nature, 1994. **371**(6492): p. 37-43.
113. Carr, C.M. and P.S. Kim, *A spring-loaded mechanism for the conformational change of influenza hemagglutinin.* Cell, 1993. **73**(4): p. 823-32.
114. Cross, K.J., et al., *Composition and functions of the influenza fusion peptide.* Protein Pept Lett, 2009. **16**(7): p. 766-78.
115. Ohuchi, M., et al., *Tight binding of influenza virus hemagglutinin to its receptor interferes with fusion pore dilation.* J Virol, 2002. **76**(24): p. 12405-13.
116. Isin, B., P. Doruker, and I. Bahar, *Functional motions of influenza virus hemagglutinin: a structure-based analytical approach.* Biophysical journal, 2002. **82**(2): p. 569-81.
117. Schnell, J.R. and J.J. Chou, *Structure and mechanism of the M2 proton channel of influenza A virus.* Nature, 2008. **451**(7178): p. 591-5.
118. Yoshimura, A. and S. Ohnishi, *Uncoating of influenza virus in endosomes.* J Virol, 1984. **51**(2): p. 497-504.
119. Stegmann, T., et al., *Fusion of influenza virus in an intracellular acidic compartment measured by fluorescence dequenching.* Biochim Biophys Acta, 1987. **904**(1): p. 165-70.
120. Daniels, R.S., et al., *Fusion mutants of the influenza virus hemagglutinin glycoprotein.* Cell, 1985. **40**(2): p. 431-9.

121. Cotter, C.R., H. Jin, and Z. Chen, *A single amino acid in the stalk region of the H1N1pdm influenza virus HA protein affects viral fusion, stability and infectivity.* PLoS Pathog, 2014. **10**(1): p. e1003831.
122. Rudneva, I.A., et al., *Pleiotropic effects of hemagglutinin amino acid substitutions of H5 influenza escape mutants.* Virology, 2013. **447**(1-2): p. 233-9.
123. Belser, J.A., J.M. Katz, and T.M. Tumpey, *The ferret as a model organism to study influenza A virus infection.* Dis Model Mech, 2011. **4**(5): p. 575-9.
124. Yang, H., et al., *Structural stability of influenza A(H1N1)pdm09 virus hemagglutinins.* J Virol, 2014. **88**(9): p. 4828-38.
125. Reed, M.L., et al., *The pH of activation of the hemagglutinin protein regulates H5N1 influenza virus pathogenicity and transmissibility in ducks.* J Virol, 2010. **84**(3): p. 1527-35.
126. Zaraket, H., et al., *Increased acid stability of the hemagglutinin protein enhances H5N1 influenza virus growth in the upper respiratory tract but is insufficient for transmission in ferrets.* J Virol, 2013. **87**(17): p. 9911-22.
127. Zaraket, H., O.A. Bridges, and C.J. Russell, *The pH of activation of the hemagglutinin protein regulates H5N1 influenza virus replication and pathogenesis in mice.* J Virol, 2013. **87**(9): p. 4826-34.
128. Galloway, S.E., et al., *Influenza HA subtypes demonstrate divergent phenotypes for cleavage activation and pH of fusion: implications for host range and adaptation.* PLoS Pathog, 2013. **9**(2): p. e1003151.
129. Kemler, I., G. Whittaker, and A. Helenius, *Nuclear import of microinjected influenza virus ribonucleoproteins.* Virology, 1994. **202**(2): p. 1028-33.
130. Neumann, G., M.R. Castrucci, and Y. Kawaoka, *Nuclear import and export of influenza virus nucleoprotein.* J Virol, 1997. **71**(12): p. 9690-700.
131. Wang, P., P. Palese, and R.E. O'Neill, *The NPI-1/NPI-3 (karyopherin alpha) binding site on the influenza a virus nucleoprotein NP is a nonconventional nuclear localization signal.* J Virol, 1997. **71**(3): p. 1850-6.
132. Tarendeau, F., et al., *Structure and nuclear import function of the C-terminal domain of influenza virus polymerase PB2 subunit.* Nat Struct Mol Biol, 2007. **14**(3): p. 229-33.
133. Mukaigawa, J. and D.P. Nayak, *Two signals mediate nuclear localization of influenza virus (A/WSN/33) polymerase basic protein 2.* J Virol, 1991. **65**(1): p. 245-53.
134. Nieto, A., et al., *Complex structure of the nuclear translocation signal of influenza virus polymerase PA subunit.* J Gen Virol, 1994. **75 (Pt 1)**: p. 29-36.
135. Nath, S.T. and D.P. Nayak, *Function of two discrete regions is required for nuclear localization of polymerase basic protein 1 of A/WSN/33 influenza virus (H1 N1).* Mol Cell Biol, 1990. **10**(8): p. 4139-45.
136. Wu, W.W., Y.H. Sun, and N. Pante, *Nuclear import of influenza A viral ribonucleoprotein complexes is mediated by two nuclear localization sequences on viral nucleoprotein.* Virol J, 2007. **4**: p. 49.

137. Chou, Y.Y., et al., *Colocalization of different influenza viral RNA segments in the cytoplasm before viral budding as shown by single-molecule sensitivity FISH analysis.* PLoS Pathog, 2013. **9**(5): p. e1003358.
138. O'Neill, R.E., et al., *Nuclear import of influenza virus RNA can be mediated by viral nucleoprotein and transport factors required for protein import.* J Biol Chem, 1995. **270**(39): p. 22701-4.
139. Gabriel, G., A. Herwig, and H.D. Klenk, *Interaction of polymerase subunit PB2 and NP with importin alpha1 is a determinant of host range of influenza A virus.* PLoS Pathog, 2008. **4**(2): p. e11.
140. Hudjetz, B. and G. Gabriel, *Human-like PB2 627K influenza virus polymerase activity is regulated by importin-alpha1 and -alpha7.* PLoS Pathog, 2012. **8**(1): p. e1002488.
141. Resa-Infante, P. and G. Gabriel, *The nuclear import machinery is a determinant of influenza virus host adaptation.* Bioessays, 2013. **35**(1): p. 23-7.
142. Gabriel, G., et al., *Differential use of importin-alpha isoforms governs cell tropism and host adaptation of influenza virus.* Nat Commun, 2011. **2**: p. 156.
143. Shapiro, G.I. and R.M. Krug, *Influenza virus RNA replication in vitro: synthesis of viral template RNAs and virion RNAs in the absence of an added primer.* Journal of virology, 1988. **62**(7): p. 2285-90.
144. Boivin, S., et al., *Influenza A virus polymerase: structural insights into replication and host adaptation mechanisms.* J Biol Chem, 2010. **285**(37): p. 28411-7.
145. Cianci, C., L. Tiley, and M. Krystal, *Differential activation of the influenza virus polymerase via template RNA binding.* J Virol, 1995. **69**(7): p. 3995-9.
146. Lee, M.T., et al., *Activation of influenza virus RNA polymerase by the 5' and 3' terminal duplex of genomic RNA.* Nucleic Acids Res, 2003. **31**(6): p. 1624-32.
147. Dias, A., et al., *The cap-snatching endonuclease of influenza virus polymerase resides in the PA subunit.* Nature, 2009. **458**(7240): p. 914-8.
148. Resa-Infante, P., et al., *Structural and functional characterization of an influenza virus RNA polymerase-genomic RNA complex.* J Virol, 2010. **84**(20): p. 10477-87.
149. Rao, P., W. Yuan, and R.M. Krug, *Crucial role of CA cleavage sites in the cap-snatching mechanism for initiating viral mRNA synthesis.* EMBO J, 2003. **22**(5): p. 1188-98.
150. Plotch, S.J., et al., *A unique cap(m7GpppXm)-dependent influenza virion endonuclease cleaves capped RNAs to generate the primers that initiate viral RNA transcription.* Cell, 1981. **23**(3): p. 847-58.
151. Zheng, H., et al., *Influenza A virus RNA polymerase has the ability to stutter at the polyadenylation site of a viral RNA template during RNA replication.* J Virol, 1999. **73**(6): p. 5240-3.

152. Luo, G.X., et al., *The polyadenylation signal of influenza virus RNA involves a stretch of uridines followed by the RNA duplex of the panhandle structure.* J Virol, 1991. **65**(6): p. 2861-7.
153. Fortes, P., A. Beloso, and J. Ortin, *Influenza virus NS1 protein inhibits pre-mRNA splicing and blocks mRNA nucleocytoplasmic transport.* EMBO J, 1994. **13**(3): p. 704-12.
154. Momose, F., et al., *Cellular splicing factor RAF-2p48/NPI-5/BAT1/UAP56 interacts with the influenza virus nucleoprotein and enhances viral RNA synthesis.* J Virol, 2001. **75**(4): p. 1899-908.
155. Garfinkel, M.S. and M.G. Katze, *Translational control by influenza virus. Selective and cap-dependent translation of viral mRNAs in infected cells.* The Journal of biological chemistry, 1992. **267**(13): p. 9383-90.
156. Garfinkel, M.S. and M.G. Katze, *Translational control by influenza virus. Selective translation is mediated by sequences within the viral mRNA 5'-untranslated region.* J Biol Chem, 1993. **268**(30): p. 22223-6.
157. Garfinkel, M.S. and M.G. Katze, *How does influenza virus regulate gene expression at the level of mRNA translation? Let us count the ways.* Gene Expr, 1993. **3**(2): p. 109-18.
158. Chen, Z. and R.M. Krug, *Selective nuclear export of viral mRNAs in influenza-virus-infected cells.* Trends Microbiol, 2000. **8**(8): p. 376-83.
159. Chen, Z., Y. Li, and R.M. Krug, *Influenza A virus NS1 protein targets poly(A)-binding protein II of the cellular 3'-end processing machinery.* EMBO J, 1999. **18**(8): p. 2273-83.
160. Enami, K., et al., *Influenza virus NS1 protein stimulates translation of the M1 protein.* J Virol, 1994. **68**(3): p. 1432-7.
161. de la Luna, S., et al., *Influenza virus NS1 protein enhances the rate of translation initiation of viral mRNAs.* J Virol, 1995. **69**(4): p. 2427-33.
162. Park, Y.W. and M.G. Katze, *Translational control by influenza virus. Identification of cis-acting sequences and trans-acting factors which may regulate selective viral mRNA translation.* J Biol Chem, 1995. **270**(47): p. 28433-9.
163. Asano, K., et al., *A multifactor complex of eIF1, eIF2, eIF3, eIF5, and tRNA(i)Met promotes initiation complex assembly and couples GTP hydrolysis to AUG recognition.* Cold Spring Harbor symposia on quantitative biology, 2001. **66**: p. 403-15.
164. Aragon, T., et al., *Eukaryotic translation initiation factor 4GI is a cellular target for NS1 protein, a translational activator of influenza virus.* Mol Cell Biol, 2000. **20**(17): p. 6259-68.
165. Webb, B.L. and C.G. Proud, *Eukaryotic initiation factor 2B (eIF2B).* The international journal of biochemistry & cell biology, 1997. **29**(10): p. 1127-31.
166. Rychlik, W., et al., *Increased rate of phosphorylation-dephosphorylation of the translational initiation factor eIF-4E correlates with the induction of protein and glycoprotein biosynthesis in activated B lymphocytes.* The Journal of biological chemistry, 1990. **265**(32): p. 19467-71.

167. Zurcher, T., R.M. Marion, and J. Ortin, *Protein synthesis shut-off induced by influenza virus infection is independent of PKR activity.* J Virol, 2000. **74**(18): p. 8781-4.
168. Katze, M.G., et al., *Translational control by influenza virus: suppression of the kinase that phosphorylates the alpha subunit of initiation factor eIF-2 and selective translation of influenza viral mRNAs.* Mol Cell Biol, 1986. **6**(5): p. 1741-50.
169. Tan, S.L. and M.G. Katze, *Biochemical and genetic evidence for complex formation between the influenza A virus NS1 protein and the interferon-induced PKR protein kinase.* J Interferon Cytokine Res, 1998. **18**(9): p. 757-66.
170. Bergmann, M., et al., *Influenza virus NS1 protein counteracts PKR-mediated inhibition of replication.* J Virol, 2000. **74**(13): p. 6203-6.
171. Kochs, G., et al., *Properties of H7N7 influenza A virus strain SC35M lacking interferon antagonist NS1 in mice and chickens.* J Gen Virol, 2007. **88**(Pt 5): p. 1403-9.
172. Min, J.Y., et al., *A site on the influenza A virus NS1 protein mediates both inhibition of PKR activation and temporal regulation of viral RNA synthesis.* Virology, 2007. **363**(1): p. 236-43.
173. Hatada, E., S. Saito, and R. Fukuda, *Mutant influenza viruses with a defective NS1 protein cannot block the activation of PKR in infected cells.* J Virol, 1999. **73**(3): p. 2425-33.
174. Resa-Infante, P., et al., *The host-dependent interaction of alpha-importins with influenza PB2 polymerase subunit is required for virus RNA replication.* PLoS One, 2008. **3**(12): p. e3904.
175. Fodor, E. and M. Smith, *The PA subunit is required for efficient nuclear accumulation of the PB1 subunit of the influenza A virus RNA polymerase complex.* J Virol, 2004. **78**(17): p. 9144-53.
176. Neumann, G., et al., *Orthomyxovirus replication, transcription, and polyadenylation.* Curr Top Microbiol Immunol, 2004. **283**: p. 121-43.
177. Azzeh, M., R. Flick, and G. Hobom, *Functional analysis of the influenza A virus cRNA promoter and construction of an ambisense transcription system.* Virology, 2001. **289**(2): p. 400-10.
178. Deng, T., F.T. Vreede, and G.G. Brownlee, *Different de novo initiation strategies are used by influenza virus RNA polymerase on its cRNA and viral RNA promoters during viral RNA replication.* J Virol, 2006. **80**(5): p. 2337-48.
179. Flick, R., et al., *Promoter elements in the influenza vRNA terminal structure.* RNA, 1996. **2**(10): p. 1046-57.
180. Newcomb, L.L., et al., *Interaction of the influenza a virus nucleocapsid protein with the viral RNA polymerase potentiates unprimed viral RNA replication.* J Virol, 2009. **83**(1): p. 29-36.
181. Shapiro, G.I. and R.M. Krug, *Influenza virus RNA replication in vitro: synthesis of viral template RNAs and virion RNAs in the absence of an added primer.* J Virol, 1988. **62**(7): p. 2285-90.

182. Neumann, G. and Y. Kawaoka, *Host range restriction and pathogenicity in the context of influenza pandemic.* Emerg Infect Dis, 2006. **12**(6): p. 881-6.
183. Subbarao, E.K., W. London, and B.R. Murphy, *A single amino acid in the PB2 gene of influenza A virus is a determinant of host range.* J Virol, 1993. **67**(4): p. 1761-4.
184. Chen, G.W., et al., *Genomic signatures of human versus avian influenza A viruses.* Emerg Infect Dis, 2006. **12**(9): p. 1353-60.
185. Li, J., et al., *Single mutation at the amino acid position 627 of PB2 that leads to increased virulence of an H5N1 avian influenza virus during adaptation in mice can be compensated by multiple mutations at other sites of PB2.* Virus Res, 2009. **144**(1-2): p. 123-9.
186. Mehle, A. and J.A. Doudna, *An inhibitory activity in human cells restricts the function of an avian-like influenza virus polymerase.* Cell Host Microbe, 2008. **4**(2): p. 111-22.
187. Neumann, G., M.T. Hughes, and Y. Kawaoka, *Influenza A virus NS2 protein mediates vRNP nuclear export through NES-independent interaction with hCRM1.* EMBO J, 2000. **19**(24): p. 6751-8.
188. O'Neill, R.E., J. Talon, and P. Palese, *The influenza virus NEP (NS2 protein) mediates the nuclear export of viral ribonucleoproteins.* EMBO J, 1998. **17**(1): p. 288-96.
189. Watanabe, K., et al., *Inhibition of nuclear export of ribonucleoprotein complexes of influenza virus by leptomycin B.* Virus Res, 2001. **77**(1): p. 31-42.
190. Ma, K., A.M. Roy, and G.R. Whittaker, *Nuclear export of influenza virus ribonucleoproteins: identification of an export intermediate at the nuclear periphery.* Virology, 2001. **282**(2): p. 215-20.
191. Elton, D., et al., *Interaction of the influenza virus nucleoprotein with the cellular CRM1-mediated nuclear export pathway.* J Virol, 2001. **75**(1): p. 408-19.
192. Martin, K. and A. Helenius, *Nuclear transport of influenza virus ribonucleoproteins: the viral matrix protein (M1) promotes export and inhibits import.* Cell, 1991. **67**(1): p. 117-30.
193. Manz, B., et al., *Adaptive mutations in NEP compensate for defective H5N1 RNA replication in cultured human cells.* Nat Commun, 2012. **3**: p. 802.
194. Cheung, T.K. and L.L. Poon, *Biology of influenza a virus.* Ann N Y Acad Sci, 2007. **1102**: p. 1-25.
195. Fujii, Y., et al., *Selective incorporation of influenza virus RNA segments into virions.* Proc Natl Acad Sci U S A, 2003. **100**(4): p. 2002-7.
196. Watanabe, T., et al., *Exploitation of nucleic acid packaging signals to generate a novel influenza virus-based vector stably expressing two foreign genes.* J Virol, 2003. **77**(19): p. 10575-83.
197. Liang, Y., Y. Hong, and T.G. Parslow, *cis-Acting packaging signals in the influenza virus PB1, PB2, and PA genomic RNA segments.* J Virol, 2005. **79**(16): p. 10348-55.

198. Fujii, K., et al., *Importance of both the coding and the segment-specific noncoding regions of the influenza A virus NS segment for its efficient incorporation into virions.* J Virol, 2005. **79**(6): p. 3766-74.
199. Chen, B.J., et al., *Influenza virus hemagglutinin and neuraminidase, but not the matrix protein, are required for assembly and budding of plasmid-derived virus-like particles.* J Virol, 2007. **81**(13): p. 7111-23.
200. Chen, B.J., M. Takeda, and R.A. Lamb, *Influenza virus hemagglutinin (H3 subtype) requires palmitoylation of its cytoplasmic tail for assembly: M1 proteins of two subtypes differ in their ability to support assembly.* J Virol, 2005. **79**(21): p. 13673-84.
201. Leser, G.P. and R.A. Lamb, *Influenza virus assembly and budding in raft-derived microdomains: a quantitative analysis of the surface distribution of HA, NA and M2 proteins.* Virology, 2005. **342**(2): p. 215-27.
202. Zhang, J., A. Pekosz, and R.A. Lamb, *Influenza virus assembly and lipid raft microdomains: a role for the cytoplasmic tails of the spike glycoproteins.* J Virol, 2000. **74**(10): p. 4634-44.
203. Takeda, M., et al., *Influenza virus hemagglutinin concentrates in lipid raft microdomains for efficient viral fusion.* Proc Natl Acad Sci U S A, 2003. **100**(25): p. 14610-7.
204. Brown, D.A. and J.K. Rose, *Sorting of GPI-anchored proteins to glycolipid-enriched membrane subdomains during transport to the apical cell surface.* Cell, 1992. **68**(3): p. 533-44.
205. Tsurudome, M., et al., *Lipid interactions of the hemagglutinin HA2 NH2-terminal segment during influenza virus-induced membrane fusion.* J Biol Chem, 1992. **267**(28): p. 20225-32.
206. Schmitt, A.P. and R.A. Lamb, *Influenza virus assembly and budding at the viral budozone.* Adv Virus Res, 2005. **64**: p. 383-416.
207. Pattnaik, A.K., D.J. Brown, and D.P. Nayak, *Formation of influenza virus particles lacking hemagglutinin on the viral envelope.* J Virol, 1986. **60**(3): p. 994-1001.
208. Rossman, J.S. and R.A. Lamb, *Influenza virus assembly and budding.* Virology, 2011. **411**(2): p. 229-36.
209. Nayak, D.P., E.K. Hui, and S. Barman, *Assembly and budding of influenza virus.* Virus research, 2004. **106**(2): p. 147-65.
210. Bukrinskaya, A.G., A.I. Staroff, and A. Issayeffa Kh, *Influenza virus assembly and its defects.* Bio Systems, 1981. **13**(3): p. 157-161.
211. Palese, P. and J.L. Schulman, *Mapping of the influenza virus genome: identification of the hemagglutinin and the neuraminidase genes.* Proc Natl Acad Sci U S A, 1976. **73**(6): p. 2142-6.
212. RA Lamb, R.K., *Orthomyxoviridae: the viruses and their replication.* 4th ed. Fields Virology, ed. B.N. Fields, et al. 2001, Philadelphia: Lippincott Williams & Wilkins. xix, 3087 p.
213. Chu, C.M., I.M. Dawson, and W.J. Elford, *Filamentous forms associated with newly isolated influenza virus.* Lancet, 1949. **1**(6554): p. 602.
214. Calder, L.J., et al., *Structural organization of a filamentous influenza A virus.* Proc Natl Acad Sci U S A, 2010. **107**(23): p. 10685-90.

215. Mitnaul, L.J., et al., *The cytoplasmic tail of influenza A virus neuraminidase (NA) affects NA incorporation into virions, virion morphology, and virulence in mice but is not essential for virus replication.* J Virol, 1996. **70**(2): p. 873-9.
216. Burleigh, L.M., et al., *Influenza a viruses with mutations in the m1 helix six domain display a wide variety of morphological phenotypes.* J Virol, 2005. **79**(2): p. 1262-70.
217. Elleman, C.J. and W.S. Barclay, *The M1 matrix protein controls the filamentous phenotype of influenza A virus.* Virology, 2004. **321**(1): p. 144-53.
218. Chen, B.J., et al., *The influenza virus M2 protein cytoplasmic tail interacts with the M1 protein and influences virus assembly at the site of virus budding.* J Virol, 2008. **82**(20): p. 10059-70.
219. Iwatsuki-Horimoto, K., et al., *The cytoplasmic tail of the influenza A virus M2 protein plays a role in viral assembly.* J Virol, 2006. **80**(11): p. 5233-40.
220. McCown, M.F. and A. Pekosz, *The influenza A virus M2 cytoplasmic tail is required for infectious virus production and efficient genome packaging.* J Virol, 2005. **79**(6): p. 3595-605.
221. McCown, M.F. and A. Pekosz, *Distinct domains of the influenza a virus M2 protein cytoplasmic tail mediate binding to the M1 protein and facilitate infectious virus production.* J Virol, 2006. **80**(16): p. 8178-89.
222. Perrone, L.A., et al., *H5N1 and 1918 pandemic influenza virus infection results in early and excessive infiltration of macrophages and neutrophils in the lungs of mice.* PLoS Pathog, 2008. **4**(8): p. e1000115.
223. Herold, S., et al., *Alveolar epithelial cells direct monocyte transepithelial migration upon influenza virus infection: impact of chemokines and adhesion molecules.* J Immunol, 2006. **177**(3): p. 1817-24.
224. Sladkova, T. and F. Kostolansky, *The role of cytokines in the immune response to influenza A virus infection.* Acta Virol, 2006. **50**(3): p. 151-62.
225. Garcia-Sastre, A. and C.A. Biron, *Type 1 interferons and the virus-host relationship: a lesson in detente.* Science, 2006. **312**(5775): p. 879-82.
226. Durbin, J.E., et al., *Type I IFN modulates innate and specific antiviral immunity.* J Immunol, 2000. **164**(8): p. 4220-8.
227. Matsukura, S., et al., *Expression of RANTES by normal airway epithelial cells after influenza virus A infection.* Am J Respir Cell Mol Biol, 1998. **18**(2): p. 255-64.
228. Arndt, U., et al., *Release of macrophage migration inhibitory factor and CXCL8/interleukin-8 from lung epithelial cells rendered necrotic by influenza A virus infection.* J Virol, 2002. **76**(18): p. 9298-306.
229. Choi, A.M. and D.B. Jacoby, *Influenza virus A infection induces interleukin-8 gene expression in human airway epithelial cells.* FEBS Lett, 1992. **309**(3): p. 327-9.
230. Adachi, M., et al., *Expression of cytokines on human bronchial epithelial cells induced by influenza virus A.* Int Arch Allergy Immunol, 1997. **113**(1-3): p. 307-11.

231. Matsukura, S., et al., *Expression of IL-6, IL-8, and RANTES on human bronchial epithelial cells, NCI-H292, induced by influenza virus A.* J Allergy Clin Immunol, 1996. **98**(6 Pt 1): p. 1080-7.
232. Message, S.D. and S.L. Johnston, *Host defense function of the airway epithelium in health and disease: clinical background.* J Leukoc Biol, 2004. **75**(1): p. 5-17.
233. de Jong, M.D., et al., *Fatal outcome of human influenza A (H5N1) is associated with high viral load and hypercytokinemia.* Nat Med, 2006. **12**(10): p. 1203-7.
234. Lee, N., et al., *Cytokine response patterns in severe pandemic 2009 H1N1 and seasonal influenza among hospitalized adults.* PLoS One, 2011. **6**(10): p. e26050.
235. Guillot, L., et al., *Involvement of toll-like receptor 3 in the immune response of lung epithelial cells to double-stranded RNA and influenza A virus.* J Biol Chem, 2005. **280**(7): p. 5571-80.
236. Kato, H., et al., *Differential roles of MDA5 and RIG-I helicases in the recognition of RNA viruses.* Nature, 2006. **441**(7089): p. 101-5.
237. Lund, J.M., et al., *Recognition of single-stranded RNA viruses by Toll-like receptor 7.* Proc Natl Acad Sci U S A, 2004. **101**(15): p. 5598-603.
238. Akira, S., S. Uematsu, and O. Takeuchi, *Pathogen recognition and innate immunity.* Cell, 2006. **124**(4): p. 783-801.
239. Jensen, S. and A.R. Thomsen, *Sensing of RNA viruses: a review of innate immune receptors involved in recognizing RNA virus invasion.* J Virol, 2012. **86**(6): p. 2900-10.
240. Loo, Y.M., et al., *Distinct RIG-I and MDA5 signaling by RNA viruses in innate immunity.* J Virol, 2008. **82**(1): p. 335-45.
241. Kawai, T., et al., *IPS-1, an adaptor triggering RIG-I- and Mda5-mediated type I interferon induction.* Nat Immunol, 2005. **6**(10): p. 981-8.
242. Kumar, H., et al., *Essential role of IPS-1 in innate immune responses against RNA viruses.* J Exp Med, 2006. **203**(7): p. 1795-803.
243. Schoggins, J.W., et al., *A diverse range of gene products are effectors of the type I interferon antiviral response.* Nature, 2011. **472**(7344): p. 481-5.
244. Takeuchi, O. and S. Akira, *Recognition of viruses by innate immunity.* Immunol Rev, 2007. **220**: p. 214-24.
245. Pindel, A. and A. Sadler, *The role of protein kinase R in the interferon response.* J Interferon Cytokine Res, 2011. **31**(1): p. 59-70.
246. Haller, O., et al., *Host gene influences sensitivity to interferon action selectively for influenza virus.* Nature, 1980. **283**(5748): p. 660-2.
247. Chakrabarti, A., B.K. Jha, and R.H. Silverman, *New insights into the role of RNase L in innate immunity.* J Interferon Cytokine Res, 2011. **31**(1): p. 49-57.
248. Lenschow, D.J., et al., *IFN-stimulated gene 15 functions as a critical antiviral molecule against influenza, herpes, and Sindbis viruses.* Proc Natl Acad Sci U S A, 2007. **104**(4): p. 1371-6.

249. Der, S.D., et al., *Identification of genes differentially regulated by interferon alpha, beta, or gamma using oligonucleotide arrays.* Proc Natl Acad Sci U S A, 1998. **95**(26): p. 15623-8.
250. Min, J.Y. and R.M. Krug, *The primary function of RNA binding by the influenza A virus NS1 protein in infected cells: Inhibiting the 2'-5' oligo (A) synthetase/RNase L pathway.* Proc Natl Acad Sci U S A, 2006. **103**(18): p. 7100-5.
251. Dittmann, J., et al., *Influenza A virus strains differ in sensitivity to the antiviral action of Mx-GTPase.* J Virol, 2008. **82**(7): p. 3624-31.
252. Gack, M.U., et al., *Influenza A virus NS1 targets the ubiquitin ligase TRIM25 to evade recognition by the host viral RNA sensor RIG-I.* Cell Host Microbe, 2009. **5**(5): p. 439-49.
253. Ferguson, N.M., A.P. Galvani, and R.M. Bush, *Ecological and immunological determinants of influenza evolution.* Nature, 2003. **422**(6930): p. 428-33.
254. Hay, A.J., et al., *The evolution of human influenza viruses.* Philos Trans R Soc Lond B Biol Sci, 2001. **356**(1416): p. 1861-70.
255. Nelson, M.I., et al., *Multiple reassortment events in the evolutionary history of H1N1 influenza A virus since 1918.* PLoS Pathog, 2008. **4**(2): p. e1000012.
256. Fitch, W.M., et al., *Positive Darwinian evolution in human influenza A viruses.* Proc Natl Acad Sci U S A, 1991. **88**(10): p. 4270-4.
257. Air, G.M., et al., *Evolutionary changes in influenza B are not primarily governed by antibody selection.* Proc Natl Acad Sci U S A, 1990. **87**(10): p. 3884-8.
258. Parvin, J.D., et al., *Measurement of the mutation rates of animal viruses: influenza A virus and poliovirus type 1.* J Virol, 1986. **59**(2): p. 377-83.
259. Nobusawa, E. and K. Sato, *Comparison of the mutation rates of human influenza A and B viruses.* J Virol, 2006. **80**(7): p. 3675-8.
260. Ghenkina, D.B. and Y.Z. Ghendon, *Recombination and complementation between orthomyxoviruses under conditions of abortive infection.* Acta Virol, 1979. **23**(2): p. 97-106.
261. Gotlieb, T. and G.K. Hirst, *The experimental production of combination forms of virus. III. The formation of doubly antigenic particles from influenza A and B virus and a study of the ability of individual particles of X virus to yield two separate strains.* J Exp Med, 1954. **99**(4): p. 307-20.
262. Baker, S.F., et al., *Influenza A and B virus intertypic reassortment through compatible viral packaging signals.* J Virol, 2014. **88**(18): p. 10778-91.
263. Lin, Y.P., et al., *Recent changes among human influenza viruses.* Virus Res, 2004. **103**(1-2): p. 47-52.
264. Xu, X., et al., *Reassortment and evolution of current human influenza A and B viruses.* Virus Res, 2004. **103**(1-2): p. 55-60.
265. Mikheeva, A. and Y.Z. Ghendon, *Intrinsic interference between influenza A and B viruses.* Arch Virol, 1982. **73**(3-4): p. 287-94.

266. Kaverin, N.V., et al., *Studies on heterotypic interference between influenza A and B viruses: a differential inhibition of the synthesis of viral proteins and RNAs.* J Gen Virol, 1983. **64 (Pt 10)**: p. 2139-46.
267. Hsieh, Y.C., et al., *Influenza pandemics: past, present and future.* J Formos Med Assoc, 2006. **105**(1): p. 1-6.
268. Li, C. and H. Chen, *Enhancement of influenza virus transmission by gene reassortment.* Curr Top Microbiol Immunol, 2014. **385**: p. 185-204.
269. Garten, R.J., et al., *Antigenic and genetic characteristics of swine-origin 2009 A(H1N1) influenza viruses circulating in humans.* Science, 2009. **325**(5937): p. 197-201.
270. Smith, G.J., et al., *Origins and evolutionary genomics of the 2009 swine-origin H1N1 influenza A epidemic.* Nature, 2009. **459**(7250): p. 1122-5.
271. Yoon, S.W., R.J. Webby, and R.G. Webster, *Evolution and ecology of influenza a viruses.* Curr Top Microbiol Immunol, 2014. **385**: p. 359-75.
272. Banks, J., et al., *Phylogenetic analysis of H7 haemagglutinin subtype influenza A viruses.* Arch Virol, 2000. **145**(5): p. 1047-58.
273. Alexander, D.J. and I.H. Brown, *History of highly pathogenic avian influenza.* Rev Sci Tech, 2009. **28**(1): p. 19-38.
274. Monne, I., et al., *Emergence of a highly pathogenic avian influenza virus from a low-pathogenic progenitor.* J Virol, 2014. **88**(8): p. 4375-88.
275. Suarez, D.L., et al., *Recombination resulting in virulence shift in avian influenza outbreak, Chile.* Emerging Infectious Diseases, 2004. **10**(4): p. 693-9.
276. Kawaoka, Y., C.W. Naeve, and R.G. Webster, *Is virulence of H5N2 influenza viruses in chickens associated with loss of carbohydrate from the hemagglutinin?* Virology, 1984. **139**(2): p. 303-16.
277. Abdelwhab, E.M., et al., *Diversifying evolution of highly pathogenic H5N1 avian influenza virus in Egypt from 2006 to 2011.* Virus Genes, 2012. **45**(1): p. 14-23.
278. Neumann, G., M.A. Green, and C.A. Macken, *Evolution of highly pathogenic avian H5N1 influenza viruses and the emergence of dominant variants.* J Gen Virol, 2010. **91**(Pt 8): p. 1984-95.
279. Sims, L.D., et al., *Origin and evolution of highly pathogenic H5N1 avian influenza in Asia.* Vet Rec, 2005. **157**(6): p. 159-64.
280. Claas, E.C., et al., *Human influenza virus A/HongKong/156/97 (H5N1) infection.* Vaccine, 1998. **16**(9-10): p. 977-8.
281. Yuen, K.Y., et al., *Clinical features and rapid viral diagnosis of human disease associated with avian influenza A H5N1 virus.* Lancet, 1998. **351**(9101): p. 467-71.
282. World Health Organization Global Influenza Program Surveillance, N. *Cumulative Number of Confirmed Human Cases of Avian Influenza*. 2013.

.
283. Centers for Disease, C., *Update: Novel Influenza A (H1N1) Virus Infection--Mexico, March--May, 2009.* MMWR Morb Mortal Wkly Rep, 2009. **58**(21): p. 585-589.

284. Itoh, Y., et al., *In vitro and in vivo characterization of new swine-origin H1N1 influenza viruses.* Nature, 2009. **460**(7258): p. 1021-5.
285. Sebastian, M.R., R. Lodha, and S.K. Kabra, *Swine origin influenza (swine flu).* Indian J Pediatr, 2009. **76**(8): p. 833-41.
286. Perez-Padilla, R., et al., *Pneumonia and respiratory failure from swine-origin influenza A (H1N1) in Mexico.* N Engl J Med, 2009. **361**(7): p. 680-9.
287. Novel Swine-Origin Influenza, A.V.I.T., et al., *Emergence of a novel swine-origin influenza A (H1N1) virus in humans.* N Engl J Med, 2009. **360**(25): p. 2605-15.
288. Van Kerkhove, M.D., et al., *Risk factors for severe outcomes following 2009 influenza A (H1N1) infection: a global pooled analysis.* Plos Medicine, 2011. **8**(7): p. e1001053.
289. Hancock, K., et al., *Cross-reactive antibody responses to the 2009 pandemic H1N1 influenza virus.* N Engl J Med, 2009. **361**(20): p. 1945-52.
290. Li, Z.N., et al., *IgM, IgG, and IgA antibody responses to influenza A(H1N1)pdm09 hemagglutinin in infected persons during the first wave of the 2009 pandemic in the United States.* Clin Vaccine Immunol, 2014. **21**(8): p. 1054-60.
291. Nickel, K.B., et al., *Age as an independent risk factor for intensive care unit admission or death due to 2009 pandemic influenza A (H1N1) virus infection.* Public Health Reports, 2011. **126**(3): p. 349-53.
292. Louie, J.K., et al., *Factors associated with death or hospitalization due to pandemic 2009 influenza A(H1N1) infection in California.* JAMA, 2009. **302**(17): p. 1896-902.
293. Donaldson, L.J., et al., *Mortality from pandemic A/H1N1 2009 influenza in England: public health surveillance study.* BMJ, 2009. **339**: p. b5213.
294. Van Kerkhove, M.D., et al., *Risk factors for severe outcomes following 2009 influenza A (H1N1) infection: a global pooled analysis.* PLoS Med, 2011. **8**(7): p. e1001053.
295. Shieh, W.J., et al., *2009 pandemic influenza A (H1N1): pathology and pathogenesis of 100 fatal cases in the United States.* Am J Pathol, 2010. **177**(1): p. 166-75.
296. Koegelenberg, C.F., et al., *High mortality from respiratory failure secondary to swine-origin influenza A (H1N1) in South Africa.* QJM : monthly journal of the Association of Physicians, 2010. **103**(5): p. 319-25.
297. Hayden, F.G., et al., *Local and systemic cytokine responses during experimental human influenza A virus infection. Relation to symptom formation and host defense.* J Clin Invest, 1998. **101**(3): p. 643-9.
298. Camp, J.V., et al., *Phenotypic differences in virulence and immune response in closely related clinical isolates of influenza A 2009 H1N1 pandemic viruses in mice.* PLoS One, 2013. **8**(2): p. e56602.
299. Julkunen, I., et al., *Inflammatory responses in influenza A virus infection.* Vaccine, 2000. **19 Suppl 1**: p. S32-7.
300. Yu, X., et al., *Intensive cytokine induction in pandemic H1N1 influenza virus infection accompanied by robust production of IL-10 and IL-6.* PLoS One, 2011. **6**(12): p. e28680.

301. Wu, S., J.P. Metcalf, and W. Wu, *Innate immune response to influenza virus.* Curr Opin Infect Dis, 2011. **24**(3): p. 235-40.
302. Lu, X., et al., *A mouse model for the evaluation of pathogenesis and immunity to influenza A (H5N1) viruses isolated from humans.* J Virol, 1999. **73**(7): p. 5903-11.
303. Novak, M., et al., *Murine model for evaluation of protective immunity to influenza virus.* Vaccine, 1993. **11**(1): p. 55-60.
304. Govorkova, E.A., et al., *Lethality to ferrets of H5N1 influenza viruses isolated from humans and poultry in 2004.* J Virol, 2005. **79**(4): p. 2191-8.
305. Wu, A., et al., *Ferret thoracic anatomy by 2-deoxy-2-(18F)fluoro-D-glucose (18F-FDG) positron emission tomography/computed tomography (18F-FDG PET/CT) imaging.* ILAR J, 2012. **53**(1): p. E9-21.
306. Nicholls, J.M., et al., *Tropism of avian influenza A (H5N1) in the upper and lower respiratory tract.* Nat Med, 2007. **13**(2): p. 147-9.
307. Cheung, C.Y., et al., *Induction of proinflammatory cytokines in human macrophages by influenza A (H5N1) viruses: a mechanism for the unusual severity of human disease?* Lancet, 2002. **360**(9348): p. 1831-7.
308. Kuiken, T., et al., *Comparative pathology of select agent influenza a virus infections.* Vet Pathol, 2010. **47**(5): p. 893-914.
309. Taubenberger, J.K. and D.M. Morens, *The pathology of influenza virus infections.* Annu Rev Pathol, 2008. **3**: p. 499-522.
310. Peiris, J.S., et al., *Re-emergence of fatal human influenza A subtype H5N1 disease.* Lancet, 2004. **363**(9409): p. 617-9.
311. Peiris, J.S., L.L. Poon, and Y. Guan, *Emergence of a novel swine-origin influenza A virus (S-OIV) H1N1 virus in humans.* J Clin Virol, 2009. **45**(3): p. 169-73.
312. Wang, Q., et al., *NF-kappaBeta inhibition is ineffective in blocking cytokine-induced IL-8 production but P38 and STAT1 inhibitors are effective.* Inflamm Res, 2012. **61**(9): p. 977-85.
313. Writing Committee of the, W.H.O.C.o.C.A.o.P.I., et al., *Clinical aspects of pandemic 2009 influenza A (H1N1) virus infection.* N Engl J Med, 2010. **362**(18): p. 1708-19.
314. Dawood, F.S., et al., *Estimated global mortality associated with the first 12 months of 2009 pandemic influenza A H1N1 virus circulation: a modelling study.* Lancet Infect Dis, 2012. **12**(9): p. 687-95.
315. Fowlkes, A.L., et al., *Epidemiology of 2009 pandemic influenza A (H1N1) deaths in the United States, April-July 2009.* Clin Infect Dis, 2011. **52 Suppl 1**: p. S60-8.
316. Carcione, D., et al., *Comparison of pandemic (H1N1) 2009 and seasonal influenza, Western Australia, 2009.* Emerg Infect Dis, 2010. **16**(9): p. 1388-95.
317. Jeffery, P.K. and D. Li, *Airway mucosa: secretory cells, mucus and mucin genes.* Eur Respir J, 1997. **10**(7): p. 1655-62.
318. Reed LJ, M.H., *A Simple Method of Estimating Fifty Percent Endpoints.* American journal of epidemiology, 1938. **27**: p. 493-497.

319. Chan, R.W., et al., *Influenza H5N1 and H1N1 virus replication and innate immune responses in bronchial epithelial cells are influenced by the state of differentiation.* PLoS One, 2010. **5**(1): p. e8713.
320. Ross, A.J., et al., *Transcriptional profiling of mucociliary differentiation in human airway epithelial cells.* Am J Respir Cell Mol Biol, 2007. **37**(2): p. 169-85.
321. Proudfoot, A.G., et al., *Human models of acute lung injury.* Dis Model Mech, 2011. **4**(2): p. 145-53.
322. Stewart, C.E., et al., *Evaluation of differentiated human bronchial epithelial cell culture systems for asthma research.* J Allergy (Cairo), 2012. **2012**: p. 943982.
323. Frank, J.A., et al., *Physiological and biochemical markers of alveolar epithelial barrier dysfunction in perfused human lungs.* Am J Physiol Lung Cell Mol Physiol, 2007. **293**(1): p. L52-9.
324. Thomas, P.G., et al., *The intracellular sensor NLRP3 mediates key innate and healing responses to influenza A virus via the regulation of caspase-1.* Immunity, 2009. **30**(4): p. 566-75.
325. Diebold, S.S., et al., *Innate antiviral responses by means of TLR7-mediated recognition of single-stranded RNA.* Science, 2004. **303**(5663): p. 1529-31.
326. Koyama, S., et al., *Differential role of TLR- and RLR-signaling in the immune responses to influenza A virus infection and vaccination.* J Immunol, 2007. **179**(7): p. 4711-20.
327. Ioannidis, I., et al., *Plasticity and virus specificity of the airway epithelial cell immune response during respiratory virus infection.* J Virol, 2012. **86**(10): p. 5422-36.
328. Oshansky, C.M., et al., *Avian influenza viruses infect primary human bronchial epithelial cells unconstrained by sialic acid alpha2,3 residues.* PLoS One, 2011. **6**(6): p. e21183.
329. Tyner, J.W., et al., *CCL5-CCR5 interaction provides antiapoptotic signals for macrophage survival during viral infection.* Nat Med, 2005. **11**(11): p. 1180-7.
330. Seth, R.B., L. Sun, and Z.J. Chen, *Antiviral innate immunity pathways.* Cell Res, 2006. **16**(2): p. 141-7.
331. Pearson, G., et al., *Mitogen-activated protein (MAP) kinase pathways: regulation and physiological functions.* Endocr Rev, 2001. **22**(2): p. 153-83.
332. Hinshaw, V.S., et al., *Apoptosis: a mechanism of cell killing by influenza A and B viruses.* J Virol, 1994. **68**(6): p. 3667-73.
333. Mori, I., et al., *In vivo induction of apoptosis by influenza virus.* J Gen Virol, 1995. **76 (Pt 11)**: p. 2869-73.
334. Nichols, J.E., J.A. Niles, and N.J. Roberts, Jr., *Human lymphocyte apoptosis after exposure to influenza A virus.* J Virol, 2001. **75**(13): p. 5921-9.

335. Price, G.E., H. Smith, and C. Sweet, *Differential induction of cytotoxicity and apoptosis by influenza virus strains of differing virulence.* J Gen Virol, 1997. **78 (Pt 11)**: p. 2821-9.
336. Takizawa, T., et al., *Induction of programmed cell death (apoptosis) by influenza virus infection in tissue culture cells.* J Gen Virol, 1993. **74 (Pt 11)**: p. 2347-55.
337. Lee, S.M., et al., *Systems-level comparison of host responses induced by pandemic and seasonal influenza A H1N1 viruses in primary human type I-like alveolar epithelial cells in vitro.* Respir Res, 2010. **11**: p. 147.
338. Berdal, J.E., et al., *Excessive innate immune response and mutant D222G/N in severe A (H1N1) pandemic influenza.* J Infect, 2011. **63**(4): p. 308-16.
339. Chan, P.K., et al., *Clinical and virological course of infection with haemagglutinin D222G mutant strain of 2009 pandemic influenza A (H1N1) virus.* J Clin Virol, 2011. **50**(4): p. 320-4.
340. Jain, S., et al., *Influenza-associated pneumonia among hospitalized patients with 2009 pandemic influenza A (H1N1) virus--United States, 2009.* Clin Infect Dis, 2012. **54**(9): p. 1221-9.
341. Brundage, J.F., *Interactions between influenza and bacterial respiratory pathogens: implications for pandemic preparedness.* Lancet Infect Dis, 2006. **6**(5): p. 303-12.
342. Vaillant, L., et al., *Epidemiology of fatal cases associated with pandemic H1N1 influenza 2009.* Euro Surveill, 2009. **14**(33).
343. (WHO), W.H.O., *Human infection with new influenza A (H1N1) virus: clinical observations from Mexico and other affected countries, May 2009.* , in *Wkly Epdiemiol Rec*. 2009. p. 173-179.
344. Cao, B., et al., *Clinical features of the initial cases of 2009 pandemic influenza A (H1N1) virus infection in China.* N Engl J Med, 2009. **361**(26): p. 2507-17.
345. Shiley, K.T., et al., *Differences in the epidemiological characteristics and clinical outcomes of pandemic (H1N1) 2009 influenza, compared with seasonal influenza.* Infect Control Hosp Epidemiol, 2010. **31**(7): p. 676-82.
346. Viboud, C., et al., *Preliminary Estimates of Mortality and Years of Life Lost Associated with the 2009 A/H1N1 Pandemic in the US and Comparison with Past Influenza Seasons.* PLoS Curr, 2010. **2**: p. RRN1153.
347. Lee, C.S. and J.H. Lee, *Dynamics of clinical symptoms in patients with pandemic influenza A (H1N1).* Clin Microbiol Infect, 2010. **16**(4): p. 389-90.
348. Yeh, E., et al., *Preferential lower respiratory tract infection in swine-origin 2009 A(H1N1) influenza.* Clin Infect Dis, 2010. **50**(3): p. 391-4.
349. Maines, T.R., et al., *Transmission and pathogenesis of swine-origin 2009 A(H1N1) influenza viruses in ferrets and mice.* Science, 2009. **325**(5939): p. 484-7.
350. Gill, J.R., et al., *Pulmonary pathologic findings of fatal 2009 pandemic influenza A/H1N1 viral infections.* Arch Pathol Lab Med, 2010. **134**(2): p. 235-43.

351. Osterlund, P., et al., *Pandemic H1N1 2009 influenza A virus induces weak cytokine responses in human macrophages and dendritic cells and is highly sensitive to the antiviral actions of interferons.* J Virol, 2010. **84**(3): p. 1414-22.
352. Weinheimer, V.K., et al., *Influenza A viruses target type II pneumocytes in the human lung.* J Infect Dis, 2012. **206**(11): p. 1685-94.
353. Yu, W.C., et al., *Viral replication and innate host responses in primary human alveolar epithelial cells and alveolar macrophages infected with influenza H5N1 and H1N1 viruses.* J Virol, 2011. **85**(14): p. 6844-55.
354. Geiler, J., et al., *Comparison of pro-inflammatory cytokine expression and cellular signal transduction in human macrophages infected with different influenza A viruses.* Med Microbiol Immunol, 2011. **200**(1): p. 53-60.
355. Hoeve, M.A., et al., *Influenza virus A infection of human monocyte and macrophage subpopulations reveals increased susceptibility associated with cell differentiation.* PLoS One, 2012. **7**(1): p. e29443.
356. Sakabe, S., et al., *Cytokine production by primary human macrophages infected with highly pathogenic H5N1 or pandemic H1N1 2009 influenza viruses.* J Gen Virol, 2011. **92**(Pt 6): p. 1428-34.
357. van Riel, D., et al., *Highly pathogenic avian influenza virus H5N1 infects alveolar macrophages without virus production or excessive TNF-alpha induction.* PLoS Pathog, 2011. **7**(6): p. e1002099.
358. Tate, M.D., et al., *Critical role of airway macrophages in modulating disease severity during influenza virus infection of mice.* J Virol, 2010. **84**(15): p. 7569-80.
359. Kuiken, T. and J.K. Taubenberger, *Pathology of human influenza revisited.* Vaccine, 2008. **26 Suppl 4**: p. D59-66.
360. See, H. and P. Wark, *Innate immune response to viral infection of the lungs.* Paediatr Respir Rev, 2008. **9**(4): p. 243-50.
361. Kim, H.M., et al., *The severe pathogenicity of alveolar macrophage-depleted ferrets infected with 2009 pandemic H1N1 influenza virus.* Virology, 2013. **444**(1-2): p. 394-403.
362. Kim, H.M., et al., *Alveolar macrophages are indispensable for controlling influenza viruses in lungs of pigs.* J Virol, 2008. **82**(9): p. 4265-74.
363. Ghoneim, H.E., P.G. Thomas, and J.A. McCullers, *Depletion of alveolar macrophages during influenza infection facilitates bacterial superinfections.* J Immunol, 2013. **191**(3): p. 1250-9.
364. Tumpey, T.M., et al., *Pathogenicity of influenza viruses with genes from the 1918 pandemic virus: functional roles of alveolar macrophages and neutrophils in limiting virus replication and mortality in mice.* J Virol, 2005. **79**(23): p. 14933-44.
365. Lambrecht, B.N., *Alveolar macrophage in the driver's seat.* Immunity, 2006. **24**(4): p. 366-8.
366. Fogg, D.K., et al., *A clonogenic bone marrow progenitor specific for macrophages and dendritic cells.* Science, 2006. **311**(5757): p. 83-7.
367. Hettinger, J., et al., *Origin of monocytes and macrophages in a committed progenitor.* Nat Immunol, 2013. **14**(8): p. 821-30.

368. Sprague, A.H. and R.A. Khalil, *Inflammatory cytokines in vascular dysfunction and vascular disease.* Biochem Pharmacol, 2009. **78**(6): p. 539-52.
369. Strauss-Ayali, D., S.M. Conrad, and D.M. Mosser, *Monocyte subpopulations and their differentiation patterns during infection.* J Leukoc Biol, 2007. **82**(2): p. 244-52.
370. Gordon, S. and F.O. Martinez, *Alternative activation of macrophages: mechanism and functions.* Immunity, 2010. **32**(5): p. 593-604.
371. Holt, P.G., *Down-regulation of immune responses in the lower respiratory tract: the role of alveolar macrophages.* Clin Exp Immunol, 1986. **63**(2): p. 261-70.
372. Berclaz, P.Y., et al., *GM-CSF, via PU.1, regulates alveolar macrophage Fcgamma R-mediated phagocytosis and the IL-18/IFN-gamma -mediated molecular connection between innate and adaptive immunity in the lung.* Blood, 2002. **100**(12): p. 4193-200.
373. Berclaz, P.Y., et al., *GM-CSF regulates a PU.1-dependent transcriptional program determining the pulmonary response to LPS.* Am J Respir Cell Mol Biol, 2007. **36**(1): p. 114-21.
374. Baleeiro, C.E., et al., *GM-CSF and the impaired pulmonary innate immune response following hyperoxic stress.* Am J Physiol Lung Cell Mol Physiol, 2006. **291**(6): p. L1246-55.
375. Krausgruber, T., et al., *IRF5 promotes inflammatory macrophage polarization and TH1-TH17 responses.* Nat Immunol, 2011. **12**(3): p. 231-8.
376. Jaguin, M., et al., *Polarization profiles of human M-CSF-generated macrophages and comparison of M1-markers in classically activated macrophages from GM-CSF and M-CSF origin.* Cell Immunol, 2013. **281**(1): p. 51-61.
377. Fleetwood, A.J., et al., *Granulocyte-macrophage colony-stimulating factor (CSF) and macrophage CSF-dependent macrophage phenotypes display differences in cytokine profiles and transcription factor activities: implications for CSF blockade in inflammation.* J Immunol, 2007. **178**(8): p. 5245-52.
378. Martinez, F.O., et al., *Macrophage activation and polarization.* Front Biosci, 2008. **13**: p. 453-61.
379. Porta, C., et al., *Tolerance and M2 (alternative) macrophage polarization are related processes orchestrated by p50 nuclear factor kappaB.* Proc Natl Acad Sci U S A, 2009. **106**(35): p. 14978-83.
380. Schoenemeyer, A., et al., *The interferon regulatory factor, IRF5, is a central mediator of toll-like receptor 7 signaling.* J Biol Chem, 2005. **280**(17): p. 17005-12.
381. Le Goffic, R., et al., *Cutting Edge: Influenza A virus activates TLR3-dependent inflammatory and RIG-I-dependent antiviral responses in human lung epithelial cells.* J Immunol, 2007. **178**(6): p. 3368-72.

382. Kannan, S., et al., *Alveolar epithelial type II cells activate alveolar macrophages and mitigate P. Aeruginosa infection.* PLoS One, 2009. **4**(3): p. e4891.
383. Waldo, S.W., et al., *Heterogeneity of human macrophages in culture and in atherosclerotic plaques.* Am J Pathol, 2008. **172**(4): p. 1112-26.
384. Schlesinger, L.S. and M.A. Horwitz, *Phagocytosis of Mycobacterium leprae by human monocyte-derived macrophages is mediated by complement receptors CR1 (CD35), CR3 (CD11b/CD18), and CR4 (CD11c/CD18) and IFN-gamma activation inhibits complement receptor function and phagocytosis of this bacterium.* J Immunol, 1991. **147**(6): p. 1983-94.
385. Gerlach, R.L., et al., *Early host responses of seasonal and pandemic influenza A viruses in primary well-differentiated human lung epithelial cells.* PLoS One, 2013. **8**(11): p. e78912.
386. Reed LJ, M.H., *A simple method of estimating fifty percent endpoints.* American Journal of Hygiene, 1938. **27**: p. 493–497.
387. Spandidos, A., et al., *PrimerBank: a resource of human and mouse PCR primer pairs for gene expression detection and quantification.* Nucleic Acids Res, 2010. **38**(Database issue): p. D792-9.
388. Ambarus, C.A., et al., *Systematic validation of specific phenotypic markers for in vitro polarized human macrophages.* J Immunol Methods, 2012. **375**(1-2): p. 196-206.
389. Moeenrezakhanlou, A., et al., *Myeloid cell differentiation in response to calcitriol for expression CD11b and CD14 is regulated by myeloid zinc finger-1 protein downstream of phosphatidylinositol 3-kinase.* J Leukoc Biol, 2008. **84**(2): p. 519-28.
390. Soulitzis, N., et al., *Expression analysis of peptide growth factors VEGF, FGF2, TGFB1, EGF and IGF1 in prostate cancer and benign prostatic hyperplasia.* Int J Oncol, 2006. **29**(2): p. 305-14.
391. Cline, T.D., et al., *The hemagglutinin protein of highly pathogenic H5N1 influenza viruses overcomes an early block in the replication cycle to promote productive replication in macrophages.* J Virol, 2013. **87**(3): p. 1411-9.
392. Geissmann, F., S. Jung, and D.R. Littman, *Blood monocytes consist of two principal subsets with distinct migratory properties.* Immunity, 2003. **19**(1): p. 71-82.
393. Schwende, H., et al., *Differences in the state of differentiation of THP-1 cells induced by phorbol ester and 1,25-dihydroxyvitamin D3.* J Leukoc Biol, 1996. **59**(4): p. 555-61.
394. Rehli, M., et al., *Transcriptional regulation of CHI3L1, a marker gene for late stages of macrophage differentiation.* J Biol Chem, 2003. **278**(45): p. 44058-67.
395. Porcheray, F., et al., *Macrophage activation switching: an asset for the resolution of inflammation.* Clin Exp Immunol, 2005. **142**(3): p. 481-9.

396. Balish, A.L., J.M. Katz, and A.I. Klimov, *Influenza: propagation, quantification, and storage.* Curr Protoc Microbiol, 2013. **Chapter 15**: p. Unit 15G 1.
397. Stevens, J., et al., *Receptor specificity of influenza A H3N2 viruses isolated in mammalian cells and embryonated chicken eggs.* J Virol, 2010. **84**(16): p. 8287-99.
398. Rocha, E.P., et al., *Comparison of 10 influenza A (H1N1 and H3N2) haemagglutinin sequences obtained directly from clinical specimens to those of MDCK cell- and egg-grown viruses.* J Gen Virol, 1993. **74 (Pt 11)**: p. 2513-8.
399. Mochalova, L., et al., *Receptor-binding properties of modern human influenza viruses primarily isolated in Vero and MDCK cells and chicken embryonated eggs.* Virology, 2003. **313**(2): p. 473-80.
400. Lu, B., et al., *Single amino acid substitutions in the hemagglutinin of influenza A/Singapore/21/04 (H3N2) increase virus growth in embryonated chicken eggs.* Vaccine, 2006. **24**(44-46): p. 6691-3.
401. Ito, T., et al., *Differences in sialic acid-galactose linkages in the chicken egg amnion and allantois influence human influenza virus receptor specificity and variant selection.* J Virol, 1997. **71**(4): p. 3357-62.
402. Xu, L., et al., *A single-amino-acid substitution in the HA protein changes the replication and pathogenicity of the 2009 pandemic A (H1N1) influenza viruses in vitro and in vivo.* Virol J, 2010. **7**: p. 325.
403. Gambaryan, A.S., et al., *Specification of receptor-binding phenotypes of influenza virus isolates from different hosts using synthetic sialylglycopolymers: non-egg-adapted human H1 and H3 influenza A and influenza B viruses share a common high binding affinity for 6'-sialyl(N-acetyllactosamine).* Virology, 1997. **232**(2): p. 345-50.
404. Gambaryan, A.S., J.S. Robertson, and M.N. Matrosovich, *Effects of egg-adaptation on the receptor-binding properties of human influenza A and B viruses.* Virology, 1999. **258**(2): p. 232-9.
405. Friesenhagen, J., et al., *Highly pathogenic avian influenza viruses inhibit effective immune responses of human blood-derived macrophages.* J Leukoc Biol, 2012. **92**(1): p. 11-20.
406. Lee, S.M., et al., *Systems-level comparison of host-responses elicited by avian H5N1 and seasonal H1N1 influenza viruses in primary human macrophages.* PLoS One, 2009. **4**(12): p. e8072.
407. Gern, J.E., et al., *Relationship of upper and lower airway cytokines to outcome of experimental rhinovirus infection.* Am J Respir Crit Care Med, 2000. **162**(6): p. 2226-31.
408. McNamara, P.S., et al., *Pro- and anti-inflammatory responses in respiratory syncytial virus bronchiolitis.* Eur Respir J, 2004. **23**(1): p. 106-12.
409. McNamara, P.S., et al., *Production of chemokines in the lungs of infants with severe respiratory syncytial virus bronchiolitis.* J Infect Dis, 2005. **191**(8): p. 1225-32.

410. Belongia, E.A., et al., *Clinical characteristics and 30-day outcomes for influenza A 2009 (H1N1), 2008-2009 (H1N1), and 2007-2008 (H3N2) infections.* JAMA, 2010. **304**(10): p. 1091-8.
411. Irving, S.A., et al., *Comparison of clinical features and outcomes of medically attended influenza A and influenza B in a defined population over four seasons: 2004-2005 through 2007-2008.* Influenza Other Respir Viruses, 2012. **6**(1): p. 37-43.
412. Nitsch-Osuch, A., et al., *Clinical features and outcomes of influenza A and B infections in children.* Adv Exp Med Biol, 2013. **788**: p. 89-96.
413. To, K.K., et al., *Delayed clearance of viral load and marked cytokine activation in severe cases of pandemic H1N1 2009 influenza virus infection.* Clin Infect Dis, 2010. **50**(6): p. 850-9.
414. Lawrence, T. and G. Natoli, *Transcriptional regulation of macrophage polarization: enabling diversity with identity.* Nat Rev Immunol, 2011. **11**(11): p. 750-61.
415. Benoit, M., B. Desnues, and J.L. Mege, *Macrophage polarization in bacterial infections.* J Immunol, 2008. **181**(6): p. 3733-9.
416. Mosser, D.M. and J.P. Edwards, *Exploring the full spectrum of macrophage activation.* Nat Rev Immunol, 2008. **8**(12): p. 958-69.
417. Zhang, X. and D.M. Mosser, *Macrophage activation by endogenous danger signals.* J Pathol, 2008. **214**(2): p. 161-78.
418. Park, W.Y., et al., *Cytokine balance in the lungs of patients with acute respiratory distress syndrome.* Am J Respir Crit Care Med, 2001. **164**(10 Pt 1): p. 1896-903.
419. Hui, K.P., et al., *Induction of proinflammatory cytokines in primary human macrophages by influenza A virus (H5N1) is selectively regulated by IFN regulatory factor 3 and p38 MAPK.* J Immunol, 2009. **182**(2): p. 1088-98.
420. Herold, S., et al., *Lung epithelial apoptosis in influenza virus pneumonia: the role of macrophage-expressed TNF-related apoptosis-inducing ligand.* J Exp Med, 2008. **205**(13): p. 3065-77.
421. Ermolaeva, M.A., et al., *Function of TRADD in tumor necrosis factor receptor 1 signaling and in TRIF-dependent inflammatory responses.* Nat Immunol, 2008. **9**(9): p. 1037-46.
422. Peschon, J.J., et al., *TNF receptor-deficient mice reveal divergent roles for p55 and p75 in several models of inflammation.* J Immunol, 1998. **160**(2): p. 943-52.
423. DeBerge, M.P., K.H. Ely, and R.I. Enelow, *Soluble, but not transmembrane, TNF-alpha is required during influenza infection to limit the magnitude of immune responses and the extent of immunopathology.* J Immunol, 2014. **192**(12): p. 5839-51.
424. Fernandez-Sesma, A., et al., *Influenza virus evades innate and adaptive immunity via the NS1 protein.* J Virol, 2006. **80**(13): p. 6295-304.
425. Garaigorta, U. and J. Ortin, *Mutation analysis of a recombinant NS replicon shows that influenza virus NS1 protein blocks the splicing and nucleo-cytoplasmic transport of its own viral mRNA.* Nucleic Acids Res, 2007. **35**(14): p. 4573-82.

426. Nain, M., et al., *Tumor necrosis factor-alpha production of influenza A virus-infected macrophages and potentiating effect of lipopolysaccharides.* J Immunol, 1990. **145**(6): p. 1921-8.
427. Gong, J.H., et al., *Influenza A virus infection of macrophages. Enhanced tumor necrosis factor-alpha (TNF-alpha) gene expression and lipopolysaccharide-triggered TNF-alpha release.* J Immunol, 1991. **147**(10): p. 3507-13.
428. Lee, D.C., et al., *p38 mitogen-activated protein kinase-dependent hyperinduction of tumor necrosis factor alpha expression in response to avian influenza virus H5N1.* J Virol, 2005. **79**(16): p. 10147-54.
429. Mok, C.K., et al., *Differential onset of apoptosis in influenza A virus H5N1- and H1N1-infected human blood macrophages.* J Gen Virol, 2007. **88**(Pt 4): p. 1275-80.
430. Si, Y., et al., *Entry properties and entry inhibitors of a human H7N9 influenza virus.* PLoS One, 2014. **9**(9): p. e107235.
431. Glinsky, G.V., *Genomic analysis of pandemic (H1N1) 2009 reveals association of increasing disease severity with emergence of novel hemagglutinin mutations.* Cell Cycle, 2010. **9**(5): p. 958-70.
432. Belser, J.A., et al., *Effect of D222G mutation in the hemagglutinin protein on receptor binding, pathogenesis and transmissibility of the 2009 pandemic H1N1 influenza virus.* PLoS One, 2011. **6**(9): p. e25091.
433. Nunthaboot, N., et al., *Evolution of human receptor binding affinity of H1N1 hemagglutinins from 1918 to 2009 pandemic influenza A virus.* J Chem Inf Model, 2010. **50**(8): p. 1410-7.
434. Gamblin, S.J., et al., *The structure and receptor binding properties of the 1918 influenza hemagglutinin.* Science, 2004. **303**(5665): p. 1838-42.
435. Pan, D., et al., *Molecular mechanism of the enhanced virulence of 2009 pandemic influenza A (H1N1) virus from D222G mutation in the hemagglutinin: a molecular modeling study.* J Mol Model, 2012. **18**(9): p. 4355-66.
436. Reading, P.C., J.L. Miller, and E.M. Anders, *Involvement of the mannose receptor in infection of macrophages by influenza virus.* J Virol, 2000. **74**(11): p. 5190-7.
437. Eierhoff, T., et al., *The epidermal growth factor receptor (EGFR) promotes uptake of influenza A viruses (IAV) into host cells.* PLoS Pathog, 2010. **6**(9): p. e1001099.
438. Sorkin, A., et al., *Epidermal growth factor receptor interaction with clathrin adaptors is mediated by the Tyr974-containing internalization motif.* J Biol Chem, 1996. **271**(23): p. 13377-84.
439. Alexander, A., *Endocytosis and intracellular sorting of receptor tyrosine kinases.* Front Biosci, 1998. **3**: p. d729-38.
440. Lanzetti, L., et al., *Rab5 is a signalling GTPase involved in actin remodelling by receptor tyrosine kinases.* Nature, 2004. **429**(6989): p. 309-14.

441. Brindley, M.A., et al., *Tyrosine kinase receptor Axl enhances entry of Zaire ebolavirus without direct interactions with the viral glycoprotein.* Virology, 2011. **415**(2): p. 83-94.
442. Wang, X.S., et al., *[Clinical characteristics and molecular epidemiology of the novel influenza A (H1N1) infection in children in Shanghai].* Zhonghua Er Ke Za Zhi, 2013. **51**(5): p. 356-61.
443. Oliveira, M.J., et al., *Molecular findings from influenza A(H1N1)pdm09 detected in patients from a Brazilian equatorial region during the pandemic period.* Mem Inst Oswaldo Cruz, 2014. **0**: p. 0.
444. Ye, J., et al., *Variations in the hemagglutinin of the 2009 H1N1 pandemic virus: potential for strains with altered virulence phenotype?* PLoS Pathog, 2010. **6**(10): p. e1001145.
445. Melidou, A., et al., *Molecular and phylogenetic analysis of the haemagglutinin gene of pandemic influenza H1N1 2009 viruses associated with severe and fatal infections.* Virus Res, 2010. **151**(2): p. 192-9.
446. Suphaphiphat, P., et al., *Mutations at positions 186 and 194 in the HA gene of the 2009 H1N1 pandemic influenza virus improve replication in cell culture and eggs.* Virol J, 2010. **7**: p. 157.
447. Galiano, M., et al., *Evolutionary pathways of the pandemic influenza A (H1N1) 2009 in the UK.* PLoS One, 2011. **6**(8): p. e23779.
448. Centers for Disease, C. and Prevention, *Estimates of deaths associated with seasonal influenza --- United States, 1976-2007.* MMWR Morb Mortal Wkly Rep, 2010. **59**(33): p. 1057-62.
449. Beare, A.S. and R.G. Webster, *Replication of avian influenza viruses in humans.* Arch Virol, 1991. **119**(1-2): p. 37-42.
450. Horimoto, T. and Y. Kawaoka, *Pandemic threat posed by avian influenza A viruses.* Clin Microbiol Rev, 2001. **14**(1): p. 129-49.
451. Munster, V.J., et al., *Pathogenesis and transmission of swine-origin 2009 A(H1N1) influenza virus in ferrets.* Science, 2009. **325**(5939): p. 481-3.
452. van den Brand, J.M., et al., *Severity of pneumonia due to new H1N1 influenza virus in ferrets is intermediate between that due to seasonal H1N1 virus and highly pathogenic avian influenza H5N1 virus.* J Infect Dis, 2010. **201**(7): p. 993-9.
453. Li, C.C., et al., *Correlation of pandemic (H1N1) 2009 viral load with disease severity and prolonged viral shedding in children.* Emerg Infect Dis, 2010. **16**(8): p. 1265-72.
454. Blazejewska, P., et al., *Pathogenicity of different PR8 influenza A virus variants in mice is determined by both viral and host factors.* Virology, 2011. **412**(1): p. 36-45.
455. Josset, L., et al., *Increased viral loads and exacerbated innate host responses in aged macaques infected with the 2009 pandemic H1N1 influenza A virus.* J Virol, 2012. **86**(20): p. 11115-27.
456. Launes, C., et al., *Viral load at diagnosis and influenza A H1N1 (2009) disease severity in children.* Influenza Other Respir Viruses, 2012. **6**(6): p. e89-92.

457. Delirezh, N., et al., *Comparison the effects of two monocyte isolation methods, plastic adherence and magnetic activated cell sorting methods, on phagocytic activity of generated dendritic cells.* Cell J, 2013. **15**(3): p. 218-23.
458. Delirezh, N. and E. Shojaeefar, *Phenotypic and functional comparison between flask adherent and magnetic activated cell sorted monocytes derived dendritic cells.* Iran J Immunol, 2012. **9**(2): p. 98-108.
459. Bodet, C., F. Chandad, and D. Grenier, *Modulation of cytokine production by Porphyromonas gingivalis in a macrophage and epithelial cell co-culture model.* Microbes Infect, 2005. **7**(3): p. 448-56.
460. Fritz, R.S., et al., *Nasal cytokine and chemokine responses in experimental influenza A virus infection: results of a placebo-controlled trial of intravenous zanamivir treatment.* J Infect Dis, 1999. **180**(3): p. 586-93.
461. Baskin, C.R., et al., *Early and sustained innate immune response defines pathology and death in nonhuman primates infected by highly pathogenic influenza virus.* Proc Natl Acad Sci U S A, 2009. **106**(9): p. 3455-60.
462. Seo, S.H. and R.G. Webster, *Tumor necrosis factor alpha exerts powerful anti-influenza virus effects in lung epithelial cells.* J Virol, 2002. **76**(3): p. 1071-6.
463. Srivastava, V., et al., *Resolution of immune response by recombinant transforming growth factor-beta (rTGF-beta) during influenza A virus infection.* Indian J Med Res, 2012. **136**(4): p. 641-8.
464. Fadok, V.A., et al., *Macrophages that have ingested apoptotic cells in vitro inhibit proinflammatory cytokine production through autocrine/paracrine mechanisms involving TGF-beta, PGE2, and PAF.* J Clin Invest, 1998. **101**(4): p. 890-8.
465. Myles, P.S., et al., *Risk of respiratory complications and wound infection in patients undergoing ambulatory surgery: smokers versus nonsmokers.* Anesthesiology, 2002. **97**(4): p. 842-7.
466. Delgado-Rodriguez, M., et al., *A prospective study of tobacco smoking as a predictor of complications in general surgery.* Infection control and hospital epidemiology : the official journal of the Society of Hospital Epidemiologists of America, 2003. **24**(1): p. 37-43.
467. Roman, J., et al., *Nicotine and fibronectin expression in lung fibroblasts: implications for tobacco-related lung tissue remodeling.* FASEB J, 2004. **18**(12): p. 1436-8.
468. Wu, W., et al., *Cigarette smoke extract suppresses the RIG-I-initiated innate immune response to influenza virus in the human lung.* Am J Physiol Lung Cell Mol Physiol, 2011. **300**(6): p. L821-30.
469. Doyle, I., et al., *Differential gene expression analysis in human monocyte-derived macrophages: impact of cigarette smoke on host defence.* Mol Immunol, 2010. **47**(5): p. 1058-65.

APPENDIX

In this appendix, the co-authorship statements and acknowledgments for the previously-published chapter (chapter 3) and for the manuscript in preparation (Chapter 4). This information includes author names, affiliations, and complete citation information.

CHAPTER 2

Authorship: Rachael L. Gerlach[a], Jeremy V. Camp[a], Yong-Kyu Chu[b], Colleen B. Jonsson[a,b]

Author Affiliations: Department of Microbiology and Immunology[a] and Center for Predictive Medicine for Biodefense and Emerging Infectious Diseases[b], University of Louisville, Louisville, Kentucky, USA

Citation: Gerlach RL, Camp JV, Chu Y-K, Jonsson CB (2013) Early Host Responses of Seasonal and Pandemic Influenza A Viruses in Primary Well-Differentiated Human Lung Epithelial Cells. PLoS ONE 8(11): e78912. doi:10.1371/journal.pone.0078912

Editor: Andrew Pekosz, Johns Hopkins University – Bloomberg School of Public Health, United States of America

Received: July 8, 2013; **Accepted:** September 23, 2013; **Published:** November 14, 2013

Funding: Funding support was provided in part by the Commonwealth of Kentucky as a Clinical and Translational Science Pilot Project Program at the University of Louisville to CBJ. The funders had no role in study design, data collection and analysis, decision to publish, or preparation of the manuscript. No additional external funding was received for this study.

Competing interests: The authors have declared that no competing interests exist.

Author contributions: Conceived and designed the experiments: RLG JVC YC CBJ. Performed the experiments: RLG JVC YC. Analyzed the data: RLG JVC YC CBJ. Contributed reagents/materials/analysis tools: RLG JVC YC CBJ. Wrote the paper: RLG JVC YC CBJ.

Acknowledgements: We thank Dr. Carl Bruder for helpful discussions during the design of the experiments and for helpful discussions regarding our findings. We thank Dr. Mawadda Alnaeeli for review of the manuscript.

CHAPTER 3

Authorship: Rachael L. Gerlach[a,b], Jeremy V. Camp[a,b], Mawadda Alnaeeli[a], Amar D. Parvate[c], Jason K Lanman[c], , Jill Suttles[a], Colleen B. Jonsson[a,b,d]

Author Affiliations: Department of Microbiology and Immunology[a] and Center for Predictive Medicine for Biodefense and Emerging Infectious Diseases[b], University of Louisville, Louisville, Kentucky, USA; Department of Biological Sciences, Purdue University, West Lafayette, Indiana, USA[c]; Department of Microbiology, University of Tennessee-Knoxville, Knoxville, Tennessee, USA [d]

Citation: In preparation for submission to the Journal of Virology, May 2015

Acknowledgements: We thank Jessica L. Kosanovich at the University at Buffalo, Buffalo, NY for assistance with IDO1 activity assays and Dr. Nejat K. Egilmez at the University of Louisville, Louisville KY for helpful discussions during design of our experiments.

CURRICULUM VITAE

Rachael (Lask) Gerlach

Department of Microbiology and Immunology
University of Louisville School of Medicine
Louisville, KY 40202
Phone: 502-314-1994
E-mail: rachael.lask@gmail.com

Education:

2010-present	Ph.D. candidate Microbiology and Immunology; University of Louisville, Louisville, KY Anticipated graduation May 2015
2012	M.S. Microbiology and Immunology University of Louisville, KY
2009	M.S.P.H. Public Health Microbiology and Emerging Infectious Diseases George Washington University School of Public Health Washington, DC
2007	B.S. Biology, minor Chemistry, graduated Cum Laude Murray State University, Murray, Kentucky

Research Experience:

2010-present *Graduate Student,* Department of Microbiology and Immunology, University of Louisville School of Medicine, Louisville, KY

Mentor: Colleen Jonsson, Ph.D.

Investigation of the early host responses of closely related clinical isolates of influenza A 2009 H1N1 pandemic viruses in primary human cell culture models.

2009-2010 *Training Fellow,* APHL/CDC Emerging Infectious Disease Training Fellowship Program, Florida Bureau of Laboratories, Tampa, FL

Mentor: Lillian Stark, Ph.D.

Developed a multiplex microsphere-based immunoassay for detection of sentinel chicken serum antibodies for surveillance of arboviruses in the state of Florida. Rotated in the departments of Microbiology, Parasitology at the Bureau of Laboratories, and in Epidemiology at the Hillsborough County Health Department

2008-2009 *Graduate Research Intern*, Department of Immunology, George Washington University, Washington, DC.

Mentor: Stephanie Constant, Ph.D.

Investigated the role of extracellular cyclophilins in leukocyte recruitment during asthma-mediated lung inflammation in C57BL/6 Mice.

Teaching Experience:

November 2014 Guest Scientist

Beer with a Scientist program at a local brewery to educate the public on science topics (monthly series) Louisville, KY

Title: Ebola! What is it, how is it treated and should we be worried?

January 2014 *Lecturer,* Department of Microbiology and Immunology, University of Louisville, Louisville, KY

Lecture title: “Introduction to the Orthomyxoviridae”

Course: MBIO 618 Cell Biology of Viruses

Publications:

Junling L., R. Gerlach, C. Jonsson, B. Gray, K.Pak, C.Ng. (2014) Characterization of 18F-dipicolylamine (DPA) derivatives in cells infected with influenza virus. *Nuclear Medicine and Biology.*

Gerlach R, J. Camp, Y-K. Chu, C. Jonsson (2013) Early Host Responses of Seasonal and Pandemic Influenza A Viruses in Primary Well-Differentiated Human Lung Epithelial Cells. PLoS ONE 8(11): e78912

Camp, J., Y-K. Chu, D-H. Chung, R. McAllister, R. Adcock, R. Gerlach, T. Wiemken, P. Peyrani, J. Ramirez, J. Summersgill, C. Jonsson (2013) Phenotypic Differences in Virulence and Immune Response in Closely Related Clinical Isolates of Influenza A 2009 H1N1 Pandemic Viruses in Mice. PLoS ONE 8(2): e56602.

In Preparation:

Gerlach, R., J. Camp J, M. Alneeli, J. Kosanovich, J. Suttles, N. Egilmez, C. Jonsson. (2015) Entry-dependent Innate Signaling of Influenza H1N1 viruses in human macrophages. *Journal of Virology*. Manuscript in prep

Oral Presentations:

2014 American Society of Virology Conference, Fort Collins, CO.

Gerlach, R., J. Camp J, M. Alneeli, J. Kosanovich, J. Suttles, N. Egilmez, C. Jonsson. Influenza A (H1N1) Virus Isolate-Specific Differences in Human Monocyte-derived Macrophage Immune Responses.

2013 American Society of Virology Conference, State College, PA.

Gerlach, R., J. Camp, J. Suttles and C. Jonsson. Early Host Responses of Seasonal and Pandemic Influenza A Viruses in Well-Differentiated Primary Human Lung Bronchial Epithelial Cells.

2012 American Society of Virology Conference, Madison, WS.

Gerlach, R., P.Mardhanan, J.Camp, and C. Jonsson. Replication kinetics and chemokine signaling distinguish two pandemic H1N1 influenza viruses in primary epithelial cell culture models that show different disease severity in mice and humans.

Webinar Presentations:

2009 MatTek Corporation, Ashland, MD

Hayden, P., C. Mankus, R. Gerlach. Organotypic in vitro Human Respiratory Models of the Tracheobronchial and Alveolar Epithelium- EpiAirway™ and EpiAlveolar™

Poster Presentations:

2012 Research Louisville Conference, University of Louisville, Louisville, KY

Gerlach R, J. Camp, Y-K. Chu, S. Adcock, C. Jonsson. Isolate-Specific Differences in Human Host-Influenza Virus interactions.

2011 Research Louisville Conference, University of Louisville, Louisville, KY

Gerlach, R., P.Mardhanan, J.Camp, and C. Jonsson. Viral Replication and Innate Immune Responses in Primary Human Bronchial Epithelial Cells Infected with Pandemic H1N1 Influenza Viruses Isolated from Patients in Kentucky Hospitals

2010 International Conference on Emerging Infectious Diseases (ICEID) Atlanta, GA.

Lask, R., L. Stark, J. Basile, Multiplex Microsphere-Based Immunoassay for Detection of Sentinel Chicken Serum Antibodies for Surveillance of Arboviruses in the State of Florida.

Memberships and Service:

2014-2015 *Member*, University of Louisville School of Business Entrepreneurship Academy, Louisville, KY

2013-present *Board member and grant writer*, Golden Retriever Rescue (GRRAND) in Louisville, KY

2012-present *Member*, American Society of Virology

2012-present *Volunteer judge,* Louisville area middle (St.Patricks) and high school (Dupont Manual) annual science fairs, Louisville, KY

2012-2013 *President*, Microbiology and Immunology Student Organization, University of Louisville, Louisville, KY

2011-2012 *Treasurer*, Microbiology and Immunology Student Organization, University of Louisville, Louisville, KY

2010-present *Member*, Microbiology and Immunology Student Organization, University of Louisville, Louisville, KY

2009-2010 *Public Health Technician License*, in Microbiology and Chemistry through the Florida Board of Clinical Laboratory Personnel

2007-2009 *Assistant Division I Women's Tennis Coach*, George Washington University, Washington, DC.

2007-2009 *Tennis Professional*, Mount Vernon Tennis Center, Washington, DC

2007-2009 *Volunteer*, Alexandria Health Department- Medical Reserve Corps Alexandria, VA

2008-2009 *Track Representative*, Public Health Student Association (PHSA), George Washington University, Washington, DC

2006-2007 *Vice president,* Student Athletic Advisory Council (SAAC) for the Ohio Valley Athletic Conference, Nashville, TN

2006-2007 *President*, Student Athletic Advisory Council (SAAC) for Murray State University, Murray, KY

2005-2006 *Member*, Pre-professional Health Club, Murray State University, Murray, KY

2005-2006 *Member,* Tri Beta Biological Honor Society, Murray State University, Murray, KY

Honors and Awards:

2014 *University of Louisville Travel Award*, Award funded travel to the annual meeting of the American Society of Virology, Fort Collins, CO

2013 *Society of Virology Travel Award*, Award funded travel to the annual meeting of the American Society of Virology, State College, PA

2012 *Society of Virology Travel Award*, Award funded travel to the annual meeting of the American Society of Virology, Madison, WS

2003-2007	*Athletic Scholarship*, 4-year Division I scholarship to play tennis at Murray State University, Murray, KY
2007	*2nd most winningest tennis player* at Murray State University
2007	*Tennis Team Champion* Ohio Valley Athletic Conference
2003-2007	*Intercollegiate Tennis Association All-Academic Scholar Athlete*
2003-2007	*Commissioners Honor Roll* Ohio Valley Athletic Conference